Thirteenth International Conference on
Time-Resolved Vibrational Spectroscopy

Freising, Germany

May 19-25, 2007

PROCEEDINGS

Edited by Alfred Laubereau, Karl-Heinz Mantel and Wolfgang Zinth

TRVS XIII Meeting in Review

The thirteenth meeting in a long-standing series of "Time-Resolved Vibrational Spectroscopy" (TRVS) conferences was held May 19th to 25th at the Kardinal Döpfner Haus in Freising, Germany, organized by the two Munich Universities - Ludwig-Maximilians-Universität and Technische Universität München. This international conference continues the illustrious tradition of the original in 1982, which took place in Lake Placid, NY. The series of meetings was initiated by leading, world-renowned experts in the field of ultrafast laser spectroscopy, and is still guided by its founder, Prof. George Atkinson (University of Arizona and Science and Technology Advisor to the Secretary of State). In its current format, the conference contributes to traditional areas of time resolved vibrational spectroscopies including infrared, Raman and related laser methods. It combines them with the most recent developments to gain new information for research and novel technical applications. The scientific program addressed basic science, applied research and advancing novel commercial applications.

The thirteenth conference on Time Resolved Vibrational Spectroscopy promoted science in the areas of physics, chemistry and biology with a strong focus on biochemistry and material science. Vibrational spectra are molecule- and bond-specific. Thus, time-resolved vibrational studies provide detailed structural and kinetic information about primary dynamical processes on the picometer length scale. From this perspective, the goal of achieving a complete understanding of complex chemical and physical processes on the molecular level is well pursued by the recent progress in experimental and theoretical vibrational studies.

These proceedings collect research papers presented at the TRVS XIII in Freising, Germany

Alfred Laubereau and Wolfgang Zinth

Conference Organizers

Wolfgang Zinth, CoChair
Lehrstuhl für BioMolekulare Optik
Ludwig-Maximilians-Universität München
Oettingenstraße 67
D-80538 München
Germany
Tel.: +49-89-21809201
Wolfgang.Zinth@physik.uni-muenchen.de

Alfred Laubereau, CoChair
Physik Department E11
Technische Universität München
James-Franck-Straße
D-85748 Garching
Germany
Tel.: +49-89-289-12841
Alfred.Laubereau@ph.tum.de

Local Organizers

Alfred Laubereau   Technische Universität München
Wolfgang Zinth   Ludwig-Maximilians-Universität München
Peter Gilch   Ludwig-Maximilians-Universität München
Karl-Heinz Mantel   Ludwig-Maximilians-Universität München
Hristo Iglev   Technische Universität München

Proceedings compiled by: K.H. Mantel, Cord Elsner

Participants in TRVS XIII
Freising, May 2007

Sponsors

Ludwig-Maximilians Universität München
Geschw.-Scholl Platz 1
D-80539 München
Tel: +49 (0) 89 2180-0
www.lmu.de

Technische Universität München
Arcisstrasse 21
D-80333 München
Tel: +49 (0) 89 289-01; Fax: -22000
www.tum.de

The Munich-Centre for Advanced Photonics
Am Coulombwall 1
D-85748 Garching b. München
Tel: +49 (0) 89 289-14078; Fax: -14072
www.map.uni-muenchen.de

Deutsche Forschungsgemeinschaft
Kennedyallee 40
D-53175 Bonn
Tel: +49 (0) 228 885-1; Fax: -2777
www.dfg.de

Bruker Optik GmbH
Rudolf-Plank-Str. 27
D-76275 Ettlingen
Tel: +49 (0) 7243 504-650; Fax: -698
www.brukeroptics.com

HORIBA Jobin Yvon GmbH
Neuhofstr. 9
D-64625 Bensheim
Tel: +49 (0) 6251 8475-0; Fax: -20
www.jobinyvon.de

BFI OPTILAS GmbH
Boschstr. 12
D-82178 Puchheim / München
Tel: +49 (0) 89 890135-0; Fax: +49 (0) 89 8002461
www.bfioptilas.com

Previous Time-Resolved Vibrational Spectroscopy Meetings

The following list encompasses the last two decades of recorded meetings since 1982. The origin of the conference was in 1982, organized and chaired by Prof. George Atkinson.

Dates	Title	Location	Chair(s)
June 1982	TRVS I	Lake Placid, NY USA	G. Atkinson
July 1985	TRVS II	Bischofsgrün, Germany	A. Laubereau and M. Stockburger
August 1987	TRVS III	Amersfoort, Netherlands	J.D.W. van Voorst
May 1989	TRVS IV	Princeton, NJ, USA	T. Spiro
May 1991	TRVS V	Tokyo, Japan	H. Takahashi
May 1993	TRVS VI	Berlin, Germany	A. Lau, F. Siebert and W. Werncke
June 1995	TRVS VII	Santa Fe, NM, USA	W. Woodruff
April 1997	TRVS VIII	Oxford, UK	A. W. Parker
May 1999	TRVS IX	Tuscon, AZ, USA	G. Atkinson
May-June 2001	TRVS X	Okazaki, Japan	H. Hamaguchi and T. Kitagawa
May 2003	TRVS XI	Castiglione, Italy	A. Califano and R. Righini
May 2005	TRVS XII	Washington, USA	T. Heilweil and T. L. Gustafson

Names and Addresses of the International Organizing Committee TRVS XIII – 2006

George H. Atkinson	University of Arizona, Department of Chemistry, Tucson, USA
Salvatore Califano	LENS, University of Florence, Italy
Paul M. Champion	Physics Department, Northeastern University, Boston, USA
Thomas Elsaesser	Max-Born-Institute, Berlin, Germany
Mostafa A.El-Sayed	Georgia Institute of Technology, School of Chemistry & Biochemistry, Atlanta
Marloes Groot	Vrije Universiteit, Faculty of Science, Biophysics, Amsterdam, Netherlands
Terry L. Gustafson	Department of Chemistry, The Ohio State University, Columbus, USA
Hiro-O Hamaguchi	The University of Tokyo, Japan
Peter Hamm	Universität Zürich, Physikalisch Chemisches Institut, Switzerland
Edwin J. Heilweil	Optical Technology Division, National Inst. of STDS & Technology, Gaithersburg, USA
Robin Hochstrasser	University of Pennsylvania, Department of Chemistry, Philadelphia, USA
Takayoshi Kobayashi	The University of Tokyo, Dept. of Physics, Faculty of Science, Japan
Yasushi Koyama	Kwansei Gakuin University, Faculty of Science, Japan
Alfred Laubereau	Technical University of Munich, Physik – Department E11, Germany
Jean-Louis Martin	Ecole Polytechnique INSERM, France
Stephen Meech	University of East Anglia, School of Chemical Sciences and Pharmacy Norwich, UK
R.J. Dwayne Miller	Departments of Chemistry and Physics, Toronto, ONT, Canada
Shaul Mukamel	Department of Chemistry, University of California, USA
Anne B. Myers-Kelley	School of Natural Sciences, University of California, USA
Anthony Parker	Rutherford Appleton Laboratory, Central Laser Facility, UK
Roberto Righini	LENS, University of Florence, Italy
Friedrich Siebert	Institut für Molekulare Medizin und Zellforschung, Albert-Ludwigs-Universität Freiburg, Germany
Thomas G. Spiro	Department of Chemistry, Princeton University, USA
Andrei Tokmakoff	Department of Chemistry, Massachusetts Institute of Technology, USA
Siva Umapathy	Inorganic and Physical Chemistry, Indian Institute of Science, Bangalore, India
Larry Ziegler	Boston University, Dept. of Chemistry, Metcalf Center for Science and Engineering, USA
Wolfgang Zinth	Lehrstuhl für BioMolekulare Optik, Department für Physik, Universität München, Germany

Table of Contents

COHERENT CONTROL

AND

COHERENT MULTIDIMENSIONAL SPECTROSCOPY

TRVS XIII

Freising 2007

Ultrafast N-H vibrational dynamics in the DNA model base pair 7 azaindole dimer

Jason R. Dwyer[1], Jens Dreyer[1], Erik T. J. Nibbering[1], Thomas Elsaesser[1]

[1]Max-Born-Institut für Nichtlineare Optik und Kurzzeitspektroskopie, Max-Born-Strasse 2A, D-12489, Berlin, Germany. E-mail: dwyer@mbi-berlin.de

Hydrogen bonds are ubiquitous in nature and provide structural flexibility critical for biochemical function[1]. N–H hydrogen bonds are a particularly compelling subject for study, with perhaps their most prominent biological role as key players in genetic encoding through the complementarity of DNA base pairs. While O–H hydrogen bonds have been studied in detail using a variety of techniques, N–H hydrogen bonds have been less-well characterized. Infrared spectroscopic studies of N–H hydrogen bonds in native DNA are hampered by spectral overlap with the O–H stretching absorption of the aqueous solvent. An additional difficulty is that native base pairs free of the DNA backbone are not guaranteed to adopt exclusively Watson-Crick pairing, but can interact through Hoogsteen base pairing. To circumvent these problems we perform IR pump-probe measurements on the 7-azaindole dimer, a widely studied model nucleic acid base pair which is soluble in nonpolar solvents and adopts a single, well-defined dimer geometry at the concentrations used in the experimental studies. This model system has the added advantage of being computationally tractable, thereby permitting theoretical investigations of experimentally measured vibrational dynamics.
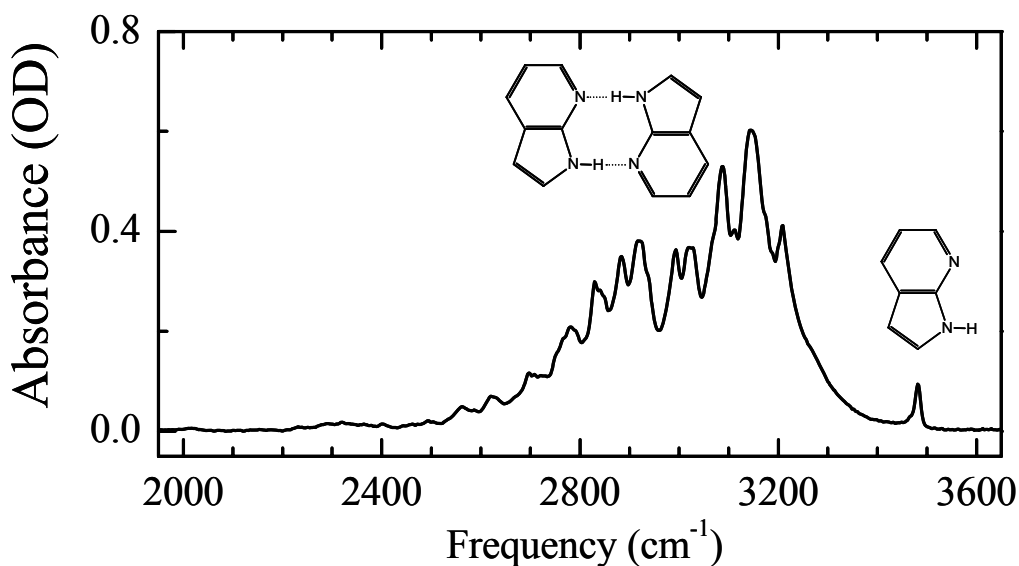
Figure 1. The figure shows the linear infrared spectrum of 7-azaindole dissolved in CCl_4. The peak at ~3500 cm^{-1} belongs to the fraction of molecules present as monomers, while the broadened, structured and red-shifted band belongs to the dimers present in the solution.

Recent efforts in ultrafast vibrational spectroscopy have revealed a large body of detailed information on the nature of the vibrational dynamics of hydrogen bonds[1], in particular for geometrically well-defined molecular systems with medium-strong hydrogen bonds, such as acetic acid dimers[2,3]

Fermi resonances and low-frequency dimer modes to both the linear and transient spectra[4]. Combined experimental and theoretical studies reveal the important pathways for vibrational energy redistribution in the well-defined O–H bonded dimers, and the prominent role of multiple low-frequency motions observed through stimulated ground state wave packet motion in transient infrared spectroscopic experiments[3].

The IR-active N–H stretching band of 7-azaindole dimer exhibits a frequency downshift on the order of 400 cm^{-1} upon formation of the medium-strong hydrogen-bonded dimer with a pronounced substructure (Figure 1). These overall characteristics are consistent with the acetic acid dimer spectrum and are indicative of significant anharmonic couplings with fingerprint and low-frequency modes. We used two-colour femtosecond infrared pump-probe spectroscopy to investigate the role of these anharmonic couplings in 7-azaindole dimers[5]. The N–H stretching vibration displays a 10 ps lifetime in the monomer. The lifetime upon dimer formation, however, is significantly shortened to ~100 fs (Figure 2). This lifetime shortening upon dimerization had previously been observed in chemically modified base pairs[6], and we undertook density functional calculations to reveal the underlying mechanism for this lifetime shortening in azaindole[5,7].
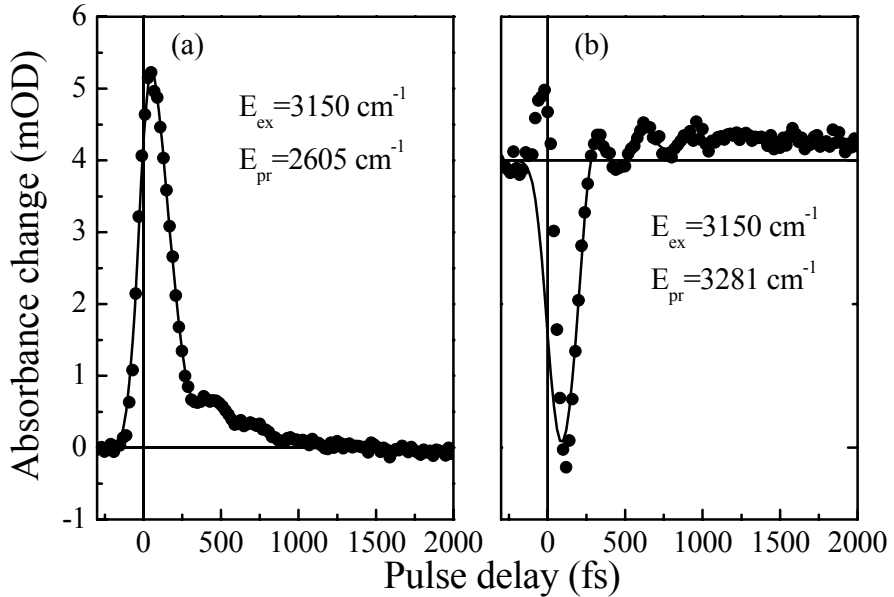
Figure 2. Panel (a) shows the extremely fast decay, with time constants of 100 and 300 fs, when the N–H $v = 1 \rightarrow v = 2$ transition is probed. Panel (b) shows a blue-shifted absorption that appears with the same time constant as the excited state lifetime decay. This feature is the hot ground state absorption after relaxation of the N–H oscillator. Superimposed on this feature is an oscillation of 100 cm^{-1} which arises from stimulated ground state wave packet motion in a different subset of dimers.

Fermi resonances play a significant role in the structure of the N–H stretching band. Density functional calculations of anharmonic couplings reveal similar coupling strengths between vibrational modes in the monomer and in the dimer, but the pronounced diagonal anharmonicity of the N–H stretching vibration in the dimers brought about by hydrogen bonding leads to a small energy mismatch between the $v = 1$ state and combination tones. This creates an efficient relaxation pathway and is the reason for the dramatic N–H lifetime shortening upon dimer formation.

In addition to the ultrafast population dynamics, we observed coherent modulations of the spectrally integrated pump–probe signals of 7-azaindole dimer (Figure 2). These underdamped signals with a 110 cm^{-1} frequency are due to resonantly enhanced coherent Raman excitation by the pump pulse of the dimer in-plane hydrogen bond stretching mode

strongly coupled to the N–H stretching vibration (Figure 3). Wave packet motion in the $v = 1$ N–H stretching state is rapidly damped by the ultrafast population decay whereas the wave packet in the $v = 0$ N–H stretching state oscillates for several picoseconds and modulates the N–H stretching absorption.
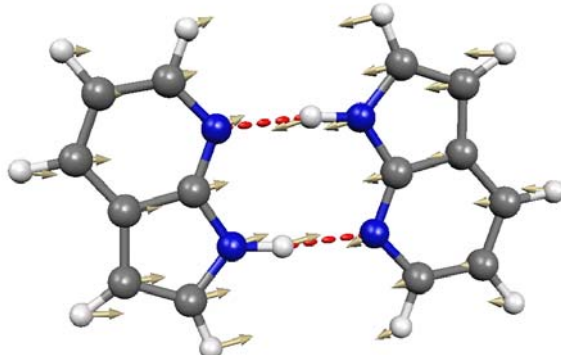
Figure 3. Excitation of the N-H stretching vibration with femtosecond infrared pulses gives rise to coherent underdamped motions of the dimer at a frequency of 110 cm^{-1}. The figure illustrates this mode, calculated using density functional theory.

The observation of significant N–H lifetime shortening upon 7-azaindole dimer formation and the prominent role of a single low-frequency mode in the stimulated ground state wave packet can be explained by detailed density functional theory calculations of 7-azaindole vibrational spectra that account for anharmonic couplings between vibrational modes. The resulting understanding of the linear spectrum, the population and coherent dynamics is one that is qualitatively consistent with previous experimental and computational studies of O–H hydrogen bonds in acetic acid dimers, but applicable to a system with more degrees of freedom. More importantly, this study of azaindole yields insight relevant to understanding hydrogen bond dynamics in DNA base pairs.

[1] E.T.J. Nibbering, T. Elsaesser, Chem. Rev., **2004**, 104, 1887-1914.
[2] K. Heyne, N. Huse, J. Dreyer, E. T. J. Nibbering, T. Elsaesser, S. Mukamel. J. Chem. Phys., **2004**, 121, 902-913.
[3] N. Huse, B. D. Bruner, M. L. Cowan, J. Dreyer, E. T. J. Nibbering, R. J. D. Miller, T. Elsaesser, Phys. Rev. Lett., **2005**, 94, 147402.
[4] J. Dreyer, J. Chem. Phys., **2005**, 122, 184306.
[5] J. R. Dwyer, J. Dreyer, E. T. J. Nibbering, T. Elsaesser, Chem. Phys. Lett., **2006**, 432, 146-151.
[6] S. Woutersen and G. Cristalli, J. Chem. Phys. **2004,** 121, 5381.
[7] J. Dreyer, J. Chem. Phys., *in press*.

Coherent Control of Population Transfer and Vibronic Coherence

T .Buckup[1], J. Hauer[1], C.Serrat[2], M. Motzkus[1]

[1] Physikalische Chemie, Fb Chemie, Philipps-Universität Marburg, Hans-Meerwein-Straße, D-35043 Marburg, Germany. [2] Departament de Fisica, Universitat Politécnica de Catalunya, 08222 Terrasa, Spain. buckup@staff.uni-marburg.de

Wave packet phenomena in molecules are a clear manifestation of the wave nature of matter. The manipulation of molecular vibrations has been a long term goal of coherent control, especially because it may represent motion along a reaction coordinate. It has been applied to a wide range of systems, reaching from atomic systems[1] to complex biomolecules[2]. Pulse shapes for manipulating vibrations can be predicted to be trains of pulses with temporal spacing between the sub-pulses equal to an integer multiple of the vibrational period.[3] Mukamel and co-authors[4] showed theoretically that an excitation with a pulse train under non-resonant excitation conditions is just able to select vibrational frequencies, depending on the sub-pulse spacing. Under this condition, no enhancement of the amplitude of the vibrational mode can be achieved if the total excitation energy of the multipulse does not exceed the energy of the Fourier-limited pulse.[5] Mode enhancement as required for efficiently controlling chemical reactions is therefore only to be expected for pulses more in resonance with an electronic level. Here we present a control scenario for vibrational motion and population transfer on a prototype molecular system: transient absorption of Nile Blue.

The experiment was carried out with laser pulses generated by a noncollinear optical parametric amplifier (nc-OPA), with typical pulse durations around 15 fs. The excitation pulse in the transient absorption experiment had energies below 80 nJ and was shaped with a liquid crystal mask (LCM) with 128 pixels in a 4f arrangement. Nile Blue was selected as prototype system since its strong oscillatory feature in transient absorption spectra are well known in literature.[6] Figure 1 shows the linear absorption of Nile Blue and the 5 different pump pulse spectra used to investigate the dependence of population transfer to the excited state and vibronic coherence on the excitation spectra. The wavelength at 550 nm was selected as probe for the excited states absorption (ESA), and thus as a measure for the population transfer.
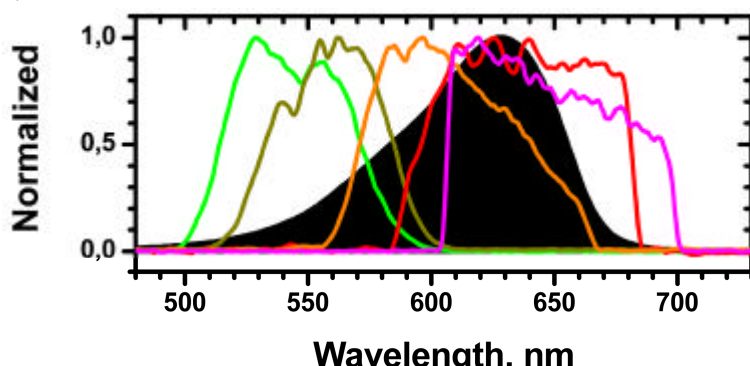
Fig.1 – Absorption spectrum of Nile Blue (LD 6900) in methanol (solid black spectrum) as well as 5 different spectra of the excitation pulse (coloured lines).

[1] D.Meshulach and Y.Silberberg, Nature **1998**, 396, 239-242.

[2] J.L.Herek, W.Wohlleben, et al, Nature **2002**, 417, 137-1319.

[4] Y.J. Yan and S.Mukamel, J.Chem.Phys. **1991**, 94, 997-1005.

[5] J.Hauer, H.Skenderovic, et al, Chem.Phys.Lett. **2006**, 421, 523-528.

[6] F.W.Wise, M.J.Rosker, et al, J.Chem.Phys. **1987**, 86, 2827-2832.

Figure 2 compares the transients and FFT spectra acquired with Fourier-limited and trains of pulses with equal total energy for the excitation spectrum centred at about 560 nm (dark green spectrum of Fig.1). The exclusion of the shaping window, where the phase modulated pump pulse and the probe pulse overlap, was performed equally for all measurements.[7] In Fig.2(E), the amplitude of the oscillation is increased by a factor of 1.5 in the shaped case compared to the unshaped one (Fig.2(D)). This proves that by the application of pulse trains, the vibrational coherence can be enhanced compared to unshaped excitation of equal energy. The amplitudes of the oscillation and the transient absorption signal scaled linearly with the energy of the excitation pulses in the regime of intensity the experiment was conducted in. Furthermore and independent thereof, pulse trains also optimize the population transfer to the excited state. The comparability between the case of shaped and unshaped excitation is assured by carefully keeping the excitation energy constant in each case. The increase in population transfer is illustrated by the amplified excited state absorption signal of the shaped transient in Fig.2(B). After t=0.5 ps, the shaped red transient is in average 3.5 mOD above the unshaped blue data set (Fig.2(A)). In the employed experimental set up, the statistical uncertainty for each data point is 1 mOD. If the temporal spacing between the pulse train's sub pulses is chosen to be out of phase with a molecular vibration, the latter can be dramatically suppressed as shown in Fig.2(F). Accordingly, no oscillation or improvement of population transfer is detectable with an out-of-phase pulse train, i.e., the level of the transient in Fig.2(C) is the same as in Fig.2(A).
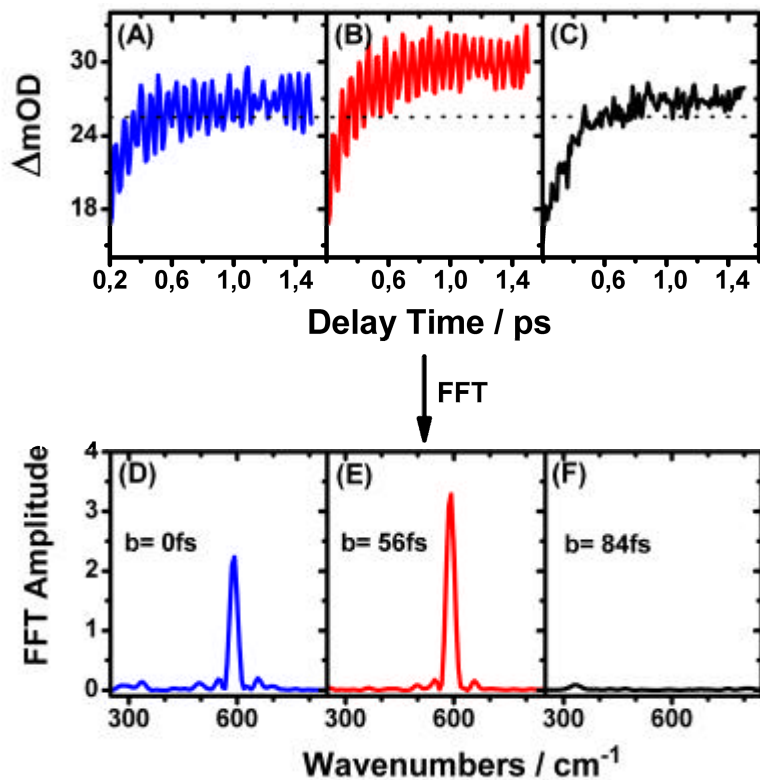
Fig.2 – Transients (A to C) and the respective Fourier spectra (D to F) at 550 nm probed wavelength after excitation at 550 nm[7]. The transferred population (B) as well as the amplitude of the induced oscillation (E) are optimized when excited by a pulse train (subpulse spacing b=56fs) compared to a Fourier-energy (A) and (D), respectively. Note that the optimized pulse train for 600 cm^{-1} is mode selective. The mode near 330 cm^{-1} is suppressed for this particular multipulse. A transient after excitation with a pulse train out of phase with the 600 cm^{-1} (b=84fs) mode is depicted in (C). This mode is completely suppressed in (F) while the transferred population remains unaffected (see level of dotted line in (A) to (C)).

---

[7] J.Hauer, T.Buckup, et al, J.Chem.Phys. **2006**, 125, art.no. 061101.

When the same procedure is performed for other excitation spectra shown in the Fig.1, a clear dependence of the enhancement factor for population transfer and vibronic coherence on the excitation wavelength can be seen in Fig.3. Using multipulses (b =56 fs) with equal total energy as the respective Fourier-limited pulses, the population transfer to the excited state can be enhanced when the excitation spectra is blue detuned from Nile Blue's absorption maximum by about 10% (Fig. 3A). No enhancement can be achieved when the excitation is totally resonant or red-detuned ($\lambda > 620$ nm). On the other hand, enhancement of vibronic coherence can be obtained for near-resonant excitation for blue as well as for red-detuned excitation spectra (Fig.3B). For totally resonant excitation with a pulse train, no enhancement can be achieved when the total energy is kept the same as the Fourier-limited pulse. The vibronic coherence enhancement curve mirrors the linear absorption of Nile Blue (compare Fig.1 with spline guide for the eyes of Fig.3B).
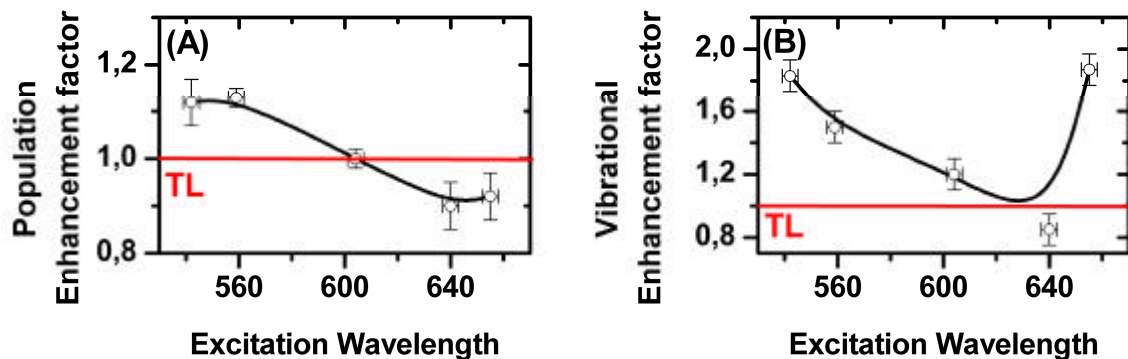
Fig.3 – (A) Excited-state absorption signal and (B) Fourier-spectra amplitude obtained at 550 nm probe wavelength for different excitation spectra (see Fig.1) using pulse trains (b = 56 fs) normalized by the respective signals obtained with Fourier-limited pulse with equal total energy (red line). The continuous black line (a spline fitting) in both graphs is just a guide to eyes.

The experimental findings can be well modelled by a four-level density matrix simulation, composed of two pairs of vibrational levels separated by the electronic transition gap. In particular, the simulation describes qualitatively the wavelength dependence of the enhancement for the population transfer as well as the vibronic coherence.[8]

In this work we showed that totally resonant pulses, which are in exact resonance with the two electronic states, are not suitable to enhance either population transfer to the excited state or vibronic coherence. On the other hand, near resonant multipulse excitation can achieve a high degree of enhancement and at the same time high selectivity. These effects cannot be attributed to a sheer macroscopic enhancement due to the fact that the total energy of the shaped and unshaped (Fourier-limited) was kept the same. We describe the observed amplification by a modulation of the absorption probability of individual molecules due to the multipulse excitation. The ability to enhance molecular vibrations opens a new perspective on the long standing aim of mode selective chemistry.

---

[8] T.Buckup, J.Hauer, C.Serrat, M. Motzkus, to be published.

Wavepacket motion of ultrafast proton transfer in the gas phase

S. Lochbrunner, C. Schriever, and E. Riedle

Lehrstuhl für BioMolekulare Optik, Physics Department, Ludwig-Maximilians-Universität München, Oettingenstr. 67, 80538 München, Germany.

Ultrafast molecular processes are governed by intramolecular motions at the speed of skeletal vibrations as well as the interaction with the surrounding medium. In particular only little is known about the influence of the environment on the coherent wavepacket motion and how environment induced variations of the wavepacket motion change the outcome of the process. To understand this interplay we investigate the ultrafast intramolecular excited state proton transfer (ESIPT) of 2-(2'-hydroxyphenyl)benzothiazole (HBT) in the gas phase and compare the dynamics to the ones found in solution[1,2].

It is crucial to use the same probe process for both experiments; otherwise the probe process projects the wavefunction onto different manifolds of final states, resulting in different signatures even if there are no changes in the molecular dynamics. We choose transient absorption as probe signal since it has proven in solution experiments that it provides a rich amount of spectroscopic information revealing detailed insight into the dynamics and it allows for a time resolution superior to most other techniques. To measure the transient absorption of low vapor pressure molecules like HBT in the gas phase requires to adopt to samples with very low particle densities. A focusing geometry with an interaction length of 50 mm is applied and a heatable gas cell was developed, to increase the vapor pressure. A 30 fs time resolution, achieved by using noncollinear optical parametric amplifiers[3] as pulse sources, allows us for the first time to compare directly the coherent wavepacket motion of molecules in the gas phase and in solution.
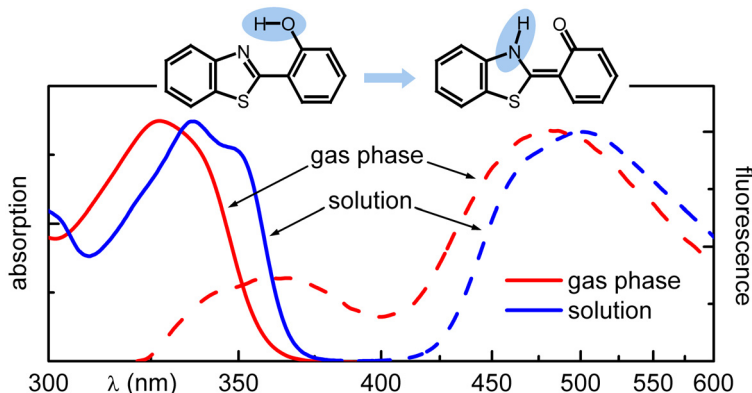
Fig. 1: Steady state absorption (solid lines) and fluorescence spectra (broken lines) of HBT in the gas phase (red traces) and dissolved in cyclohexane (blue traces).

ESIPT is a prototypical process for very fast chemical reactions since it leads to the breaking of the bond between the reactive hydrogen atom and the donating oxygen atom and the simultanous formation of a new bond, in the case of HBT between the reactive hydrogen atom and the accepting nitrogen atom (see Fig. 1). The transfer takes less than 50 fs and is associated with a pronounced wavepacket motion[1,2]. The electronically excited keto form populated by the ESIPT shows fluorescence in the visible spectral range which is Stokes shifted by about 8000 cm^{-1} compared to the ground state absorption of the original enol form. The absorption and emission spectra measured in the gas phase are slightly blue shifted compared to the spectra measured in a cyclohexane solution of HBT (see Fig. 1). The dominant emission band of the gas phase fluorescence shows also the large Stokes shift

charakteristic for ESIPT and the electronic structure seems to be the same in solution and in the gas phase. A second emission band in the near UV is observed in the gas phase. It can probably be ascribed to aggregates of HBT with water molecules which block the acceptor site and the corresponding HBT molecules cannot undergo ESIPT. The excited state lifetime of the keto form populated by the ESIPT is short (see below) which results in a small fluorescence yield. HBT molecules which do not exhibit ESIPT and stay in the enol form have a much higher fluorescence yield. It can be concluded that the fraction of HBT molecules with an intermolecular hydrogen bond is very small even though their contribution to the steady state fluorescence signal is significant. Accordingly, the mayority of the HBT molecules in the gas phase exhibits ESIPT.

We measured the evolution of the transient HBT absorption at various probe wavelengths after photoexcitation at 325 nm in the gas phase as well as in a cyclohexane solution. Figure 2 shows the time dependent transmission change at 490 nm and the Fourier transformation of the oscillatory components obtained for HBT in solution. The trace shows a transmission increase with a delay of several 10 fs followed by oscillations that are characteristic for the coherent excitation of vibrational modes. The delayed transmission rise results from the emission that occurs when the electronically excited keto form is populated by the ESIPT. The delay of 35 fs is therefore identified with the transfer time[2]. The transmission decrease at time zero is caused by the excited state absorption (ESA) from the S_1 state to higher electronic states and occurs immediately after the pump pulse has promoted the molecule to the S_1 state. The ultrafast ESIPT proceeds as a ballistic wavepacket motion and results in a coherent excitation of modes in the keto form that contribute strongly to the reaction coordinate. Comparing the frequencies of the two dominant modes at 113 cm^{-1} and 255 cm^{-1} (see Fig. 2)[1,2] to *ab-initio* calculations[4] reveals that the modes are in-plane deformations of the molecular skeleton which reduce the donor acceptor distance in the H-chelate ring[2,4]. This contraction dominates the reaction path since it reduces the distance between the reactive hydrogen and the accepting nitrogen atom without increasing the potential energy due to an elongation of the OH-bond. It allows for a barrier less reaction path and an efficient mixing between the electronic configurations of the enol and the keto form[5].
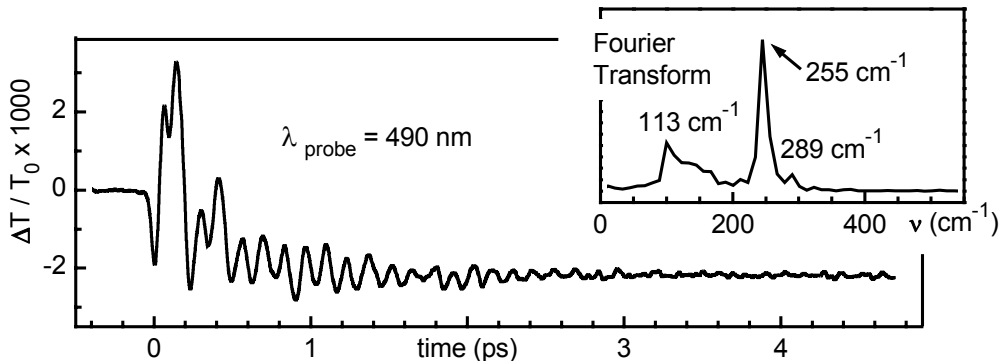
Fig. 2: Transient absorption probed at 490 nm after exciting HBT in a cyclohexane solution at 325 nm. The depicted Fourier transformation is obtained after subtracting the exponential contributions from the transients.

In solution the decay of the stimulated emission occurs with a time constant of about 100 ps. It reflects the internal conversion (IC) back to the electronic ground state. The rate observed with the excitation at 325 nm is somewhat faster than the decay found for an excitation at 347 nm[2]. This agrees with other ESIPT compounds in which the IC also accelerates with increasing excess energy[6]. It indicates that contrary to the ESIPT, a significant energy barrier has to be overcome for the IC.

The transient absorption of HBT in the gas phase exhibits also a transmission rise due to stimulated emission from the keto form populated by the proton transfer and strong oscillatory signal contributions[7]. We observe, however, that the emission decays with a time constant of 1.4 ps. The time dependence of the emission rise is identical in the gas phase and in the solution. A comparison with a precision of better than 5 fs shows that it occurs in both enviroments with a delay of 35 ± 5 fs. In both cases the oscillatory signal contributions are dominated by coherently excited modes at 113 cm^{-1} and 255 cm^{-1}. From the similarity of the signal signatures which result from the coherent wavepacket motion during and after the proton transfer we conclude that the ESIPT proceeds in the same way in the gas phase and in solution and the environment has only a negligible influence on the transfer itself. However, the gas phase traces exhibit an additional low frequency component at about 44 cm^{-1}. Since HBT has no in-plane modes in this frequency range (the in-plane mode with the lowest frequency is at 113 cm^{-1}) the component is assigned to an out-of-plane mode, tentatively to a torsional motion. In solution the friction induced by the interaction with the solvent molecules probably overdamps this motion. Surprisingly, the oscillatory signal contributions at higher frequencies are somewhat less pronounced and slightly faster damped in the gas phase than in solution. We presume that in solution part of the excess energy is already lost to the solvent during the initial motion. The motion is associated with a large amplitude bending of the entire molecular skeleton and should be subject to frictional forces which cause a significant dissipation of kinetic energy. This notion is supported by the observation that in solution the damping of the bending mode at 113 cm^{-1} is much faster than the damping of the other coherently excited modes[2]. In the gas phase friction does not occur and the product molecules are formed with roughly 4.000 cm^{-1} of vibrational excess energy. Higher vibrational levels are populated in the product potential, that are not equally spaced in energy due to the anharmonicity of the potential and that lead to an efficient broadening of the wavepacket without the need for additional dephasing processes.

The IC occuring after the ESIPT is much faster in the gas phase than in solution according to the measured emission decays. This was also observed for the ESIPT compound o-hydroxybenzaldehyde[6]. One reason is that the IC rate depends on the excess energy (see above) and friction induced energy dissipation as well as cooling by the solvent result in a smaller amount of excess energy for HBT in solution. However, this effect seems not to be sufficient to account for the extraordinary large difference in the IC rates. Since the low frequency mode, which is attributed to a torsional mode, occurs only in the gas phase we think that both phenomena are coupled. The torsional motion might bring the molecule to a region with strong coupling between the S_0 and the S_1 state, maybe even to a conical intersection. This motion is suppressed in solution resulting in a slowing down of the IC.

In conclusion, the ESIPT and the associated wavepacket motion are very similar in the gas phase and in solution indicating that the influence of the enviroment on this process is negligble. The opposite is true for the IC which is strongly accelerated in the gas phase probably due to the higher excess energy and the reduced damping of a torsional motion.

[1] S. Lochbrunner, A. J. Wurzer, and E. Riedle, J. Chem. Phys., **2000**, 112, 10699 - 10702.
[2] S. Lochbrunner, A. J. Wurzer, and E. Riedle, J. Phys. Chem. A, **2003**, 107, 10580 - 10590.
[3] E. Riedle, M. Beutter, S. Lochbrunner, J. Piel, S. Schenkl, S. Spörlein, and W. Zinth, Appl. Phys. B, **2000**, 71, 457 - 465.
[4] R. de Vivie-Riedle, V. De Waele, L. Kurtz, and E. Riedle, J. Phys. Chem. A, **2003**, 107, 10591 - 10599.
[5] S. Lochbrunner, C. Schriever, and E. Riedle, "Direct Observation of the Nuclear Motion during Ultrafast Intramolecular Proton Transfer" in Hydrogen-Transfer Reactions, J. T. Hynes, J. P. Klinman, H.-H. Limbach, and R. L. Schowen, eds. (Wiley-VCH, Weinheim, Germany, 2006), 349 - 375.
[6] K. Stock, T. Bizjak, and S. Lochbrunner, Chem. Phys. Lett., **2002**, 354, 409 - 416
[7] C. Schriever, S. Lochbrunner, and E. Riedle, in preparation.

Excited state vibrational dynamics near the S_2-S_1 conical intersection in all-*trans*-β-carotene

J. Hauer, T. Buckup, M. Motzkus

[1] Physikalische Chemie der Philipps - Universität Marburg, Hans – Meerwein- Straße, D - 35043 Marburg, Germany. hauer@staff.uni-marburg.de

Time resolving structural dynamics on short lived molecular excited states presents a challenging yet wide ranging field of ultrafast spectroscopy. Wide spread methods like transient absorption and Four-Wave-Mixing (FWM) techniques offer valuable insights. A common drawback however is the non-trivial assignment of the observed modes to the electronic ground or excited state. In the experiment discussed here, we present a method to not only unambiguously detect excited state structural dynamics in the time domain but also to observe the population dynamics between the concerned electronic states. [1,2]

The problem of differentiating between ground and excited state dynamics is resolved by introducing an additional pump beam prior to the four wave mixing sequence as depicted in figures 1a and 1c. The system under investigation is β carotene,[3] which belongs to a class of molecules playing an important role in photosynthetic light harvesting.
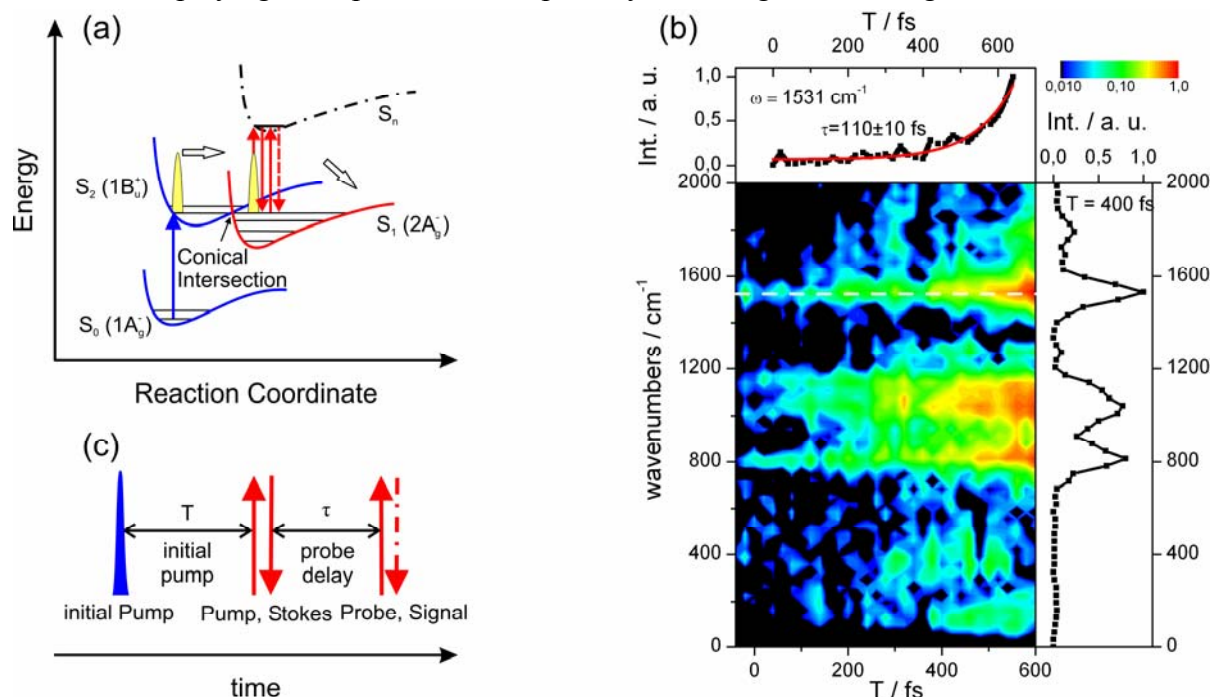
The initial pump promotes the system to its first optically allowed state S_2. Since the Degenerate-Four-Wave-Mixing sequence (DFWM) is set resonant with an excited state transition, the signal will we dramatically enhanced only if the initial pump is on. This first

[1]   Hauer, J.; Buckup, T., Motzkus, M. submitted to Journal of Physical Chemistry A

[2]   Hornung, T.; Skenderovic, H.; Motzkus, M. *Chemical Physics Letters* **2005**, *402*, 283.

[3]   Polivka, T.; Sundstrom, V. Chemical Reviews, **2004**, 104, 2021-2071

pulse can be periodically blocked by a chopper wheel. Due to this set up, there are two different time scales to be considered. The first is the initial pump delay T between the initial pump pulse and the DFWM-sequence's pump and Stokes pulses. Along this axis, the evolution of the excited state can be monitored. The other time axis along the probe delay τ is spanned between the simultaneously arriving pump and Stokes pulses and the probe pulse. If τ is varied, the molecular vibrations are detected as fast oscillations superimposed on the slowly decaying DFWM-signal. After Fast Fourier Transformation of these oscillations at different values of T, the structural dynamics of the system can be visualized as seen in figure 1b. Interestingly, the observed excited state modes show individual growth times. This can be explained by the fact that the first excited state S_2 decays towards its successor state S_1 within 180 fs via a conical intersection. The exponential growth rate of the observed modes is a sign for this mode specific ultrafast internal conversion between S_2 and S_1.

The data in figure 1b were all taken at a detection wavelength of 610 nm. Variation of this parameter reveals the different wavenumber regimes of the observable structural dynamics. Figure 2a shows a spectrally dispersed Pump-DFWM signal at $T = 1$ ps against the axis of the probe delay τ.
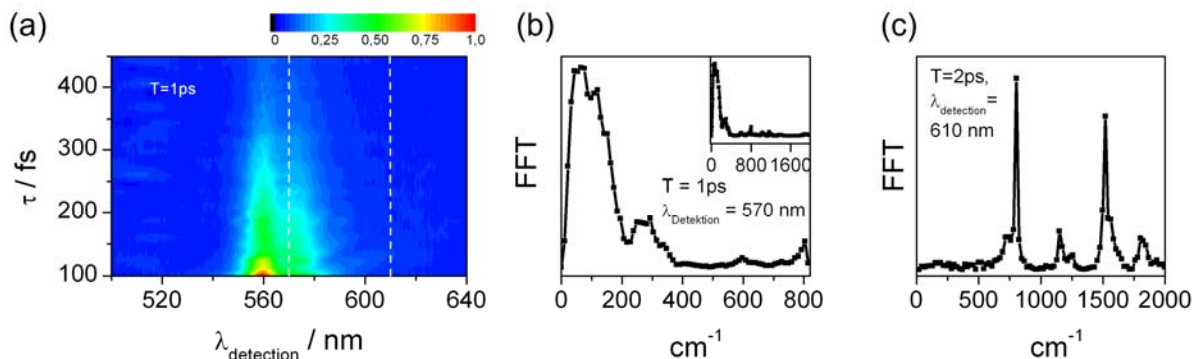
Figure 2. A typical spectrum of the Pump-DFWM signal against the probe delay τ is shown in figure 2a. The initial pump delay T was set to 1 ps. The vertical dashed lines mark two different detection wavelengths, where slices are taken at to be analyzed by a Fast Fourier Transformation (FFT) in figures 2b and 2c. The properties of the obtained spectra vary greatly depending on their respective detection wavelength.

The signal in figure 2a is strongest at the central wavelength of the incoming DFWM-beams which were centred around 560 nm to coincide with an electronic transition from the S_1 state. When taking transients at different spectral positions and performing an FFT-analysis, the influence of the detection wavelength becomes obvious. When stemming from a spectral region close to the DFWM-signal's maximum (figure 2b), the dominant features in the FFT-spectrum appear in the lower wavenumber region. Such low frequency modes were found to be playing a fundamental role in the energy relaxation pathway of carotenoids in protein matrices.[4] However, if the detection takes place at large detunings (figure 2c), modes up to 1800 cm^{-1} appear in the FFT-spectrum. This dependence on the detection wavelength can be understood intuitively by assuming that at low detunings from the central wavelength of the DFWM-pulses, frequency pairs spanning lower Raman transitions are present, leading to excitation of modes lower in energy. With the pulse lengths of 15 fs employed in the experiment this means that by choosing an appropriate detection wavelength, vibrational spectra up to almost 2000 cm^{-1} are within the experimental range. The ability to investigate the signal's dependence on the detection wavelength is an important intrinsic advantage of Pump-DFWM over frequency domain and related Raman-gain methods.[5] In the latter,

[4]   Herek, J. L.; Wohlleben, W.; Cogdell, R. J.; Zeidler, D.; Motzkus, M. **2002**, Nature, <u>417</u>, 533-535.

[5]   Kukura, P.; McCamant, D. W.; Mathies, R. A. **2007** Annual Review of Physical Chemistry, **2007**, <u>58</u>. 461-488

vibrational features appear as net gains at spectral positions characteristically shifted from the frequency of the scattered light. Pump-DFWM being a transient technique however bears an additional spectral axis (dashed vertical lines in figure 2a), along all of which the molecular oscillations may occur.

Besides the fast molecular oscillations, the DFWM-signal also consists of a slow mono-exponential decay. Since this response is dependent on the resonance conditions, the variation of this slow signal part against T is a measure for the electronic population dynamics as depicted in figure 2.
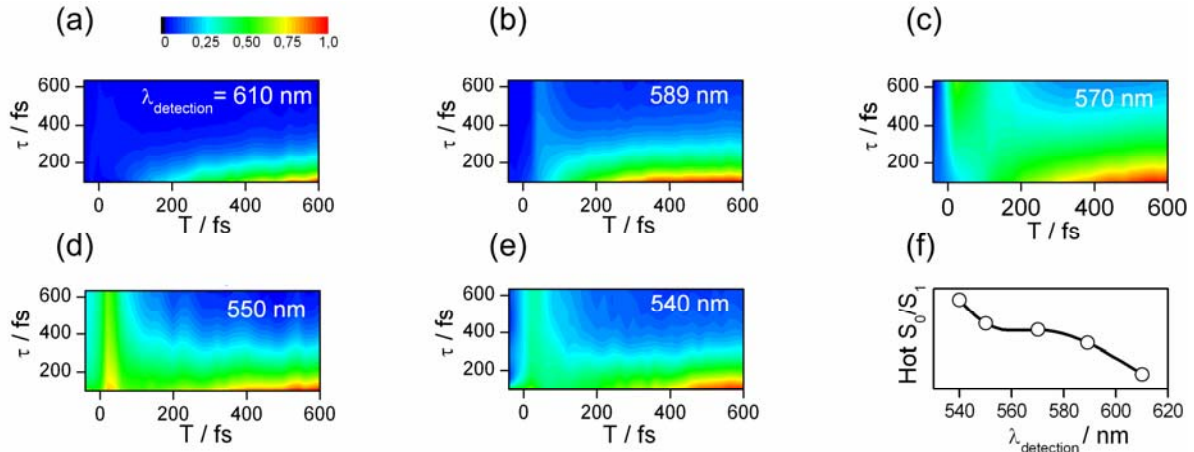
Figure 3. The slowly decaying part of the Pump-DFWM signal is plotted against the probe delay τ for different values of the initial pump delay T. The electronic population dynamics is thus visualized. In figures 3a to e, the dependence on the detection wavelength is shown. The increase of the signal with T is due to population of the resonantly excited S_1 state. The color code is set relative to the maximum in each plot. The long lived component for initial pump delay $T < 100$ fs is attributed to a vibrationally hot ground state as argued by the contribution of this component at differnt detection wavelengths shown in 3f.

Figures 3a to 3e show mono-exponential fits to the Pump-DFWM signal at different detection wavelengths. The axis of the probe delay τ within the DFWM sequence is plotted against the initial pump delay T. This perspective allows one to observe the change in electronic structure of the investigated molecule. A common feature of figures 3a to 3e is the slow increase of the signal along the T-axis after $T > 160$ fs. This is again due to the population build-up on S_1. Hence, the increase of the signal along the T-axis is explained by the electronic population sliding into the Franck-Condon window of detection defined by the spectral properties of the DFWM sequence. For early initial pump delays T when S_2 is still populated however, a signal with a long life time along the τ-axis occurs. Considering that the relative intensity of this signal increases when detected closer to the $S_0 \rightarrow S_2$ resonance (see figure 3f), we propose that for $T < 180$ fs the DFWM sequence dumps the excited state population back to a vibrationally hot ground state. A similar mechanism has been exploited in the frequency domain for stimulated emission pumping DFWM (SEP DFWM).[6]

In summary, Pump-DFWM presents a valuable tool for the detection of excited state dynamics. The combination of high spectral resolution of around 10 cm^{-1} and a temporal resolution of below 20 fs offers new possibilities for studying the interplay between structural and electronic dynamics. Since the method is a pure time domain technique, coherent control of these phenomena poses an intriguing option. Studying the influence of certain parameters of the spectral phase offers a new perspective on the topic of ultrafast vibrational cooling on electronically excited states.

---

[6]   Vaccaro, P. H. "Advanced Series in Physical Chemistry: Molecular Dynamics and Spectroscopy by Stimulated Emission Pumping"; World Scientific Publishers: New York, **1994**.

Coherent Optical Phonons in Diamond and Graphite

K. Ishioka[1], M. Hase[1], M. Kitajima[1], H. Petek[2]*

[1] Advanced Nano-characterization Center, National Institute for Materials Science, Sengen 1-2-1, Tsukuba, 305-0047 Japan. [2] Department of Physics and Astronomy, University of Pittsburgh, Pittsburgh, Pennsylvania 15260, USA.

Diamond is a quintessential covalently-bonded crystal with the widest band gap among the group IV elemental crystals, and thus serves as an ideal insulator with excellent optical properties. Graphite, in contrast, possesses highly anisotropic crystal structure, with strong covalent bonding of atoms within and weak van der Waals bonding between the hexagonal symmetry graphene sheets, which translates to a primarily 2D semi-metallic electronic structure. Recent development of materials science and nanotechnology cast a new light on carbon materials such as carbon nanotubes, single-layer graphene, and superconducting diamonds. Electronic and phononic properties in these novel carbon materials, especially their ultrafast dynamics, will dominate their functionality in future electrical and electro-optical devices. In the present study, we present transient reflectivity measurements on synthetic single-crystal diamond[1] and graphite excited with sub-10 fs laser pulses, and demonstrate that the simple one-color pump-probe technique can be a powerful tool to probe the ultrafast dynamics of high-frequency phonons in the carbon materials.

The samples used are synthetic type IIa and Ib diamond single crystal plates, from Sumitomo Electric Hardmetal, oriented to expose the (100) surface, and highly oriented pyrolytic graphite (HOPG). Pump-probe reflectivity measurements are performed using optical pulses with <10 fs duration, 395 nm wavelength, and 64 MHz repetition rate. Linearly polarized pump and probe beams are focused to a nominally 10 μm spot on the sample with angles of 20° and 5° from the surface normal, respectively. Pump power is varied between 5 and 50 mW (pulse energy 0.1 and 1mJ/cm^2), while probe power is kept at 2 mW. The probe beam is 45° polarized with respect to the optical plane, while the pump beam is vertically polarized. The detection is carried out in the "electro-optic (EO) sampling" configuration.[2] After reflection from the sample, the probe beam is analyzed into *s* and *p* components, and detected with matched photodiodes.   The difference between the two photocurrents $\Delta R_{eo} = \Delta R_p - \Delta R_s$ is recorded as a function of the pump-probe delay *t*. The time
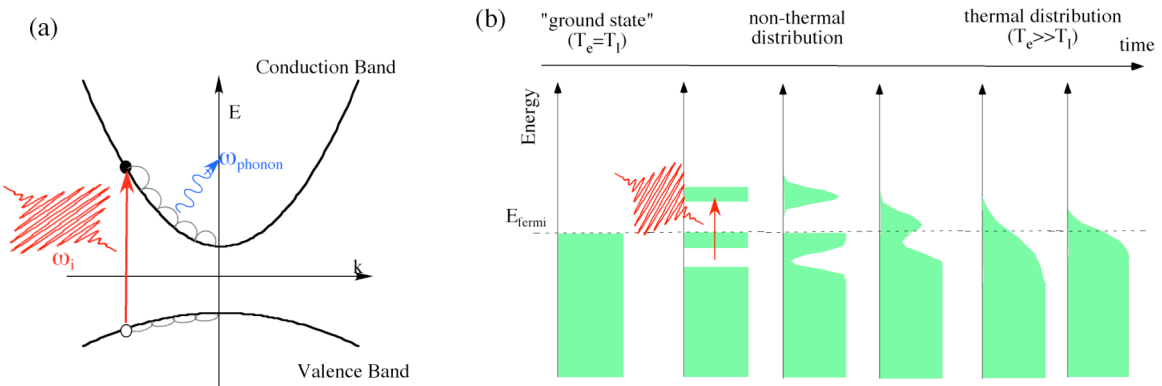
Fig. 1   Schematic illustrations of (a) excitation and relaxation of electron-hole pairs in semiconductors by phonon emission, and of (b) thermalization of photo-excited electrons to be followed by equilibration of electronic (T_e) and lattice (T_l) temperatures.

[*] Present address: Graduate School of Pure and Applied Sciences, University of Tsukuba.
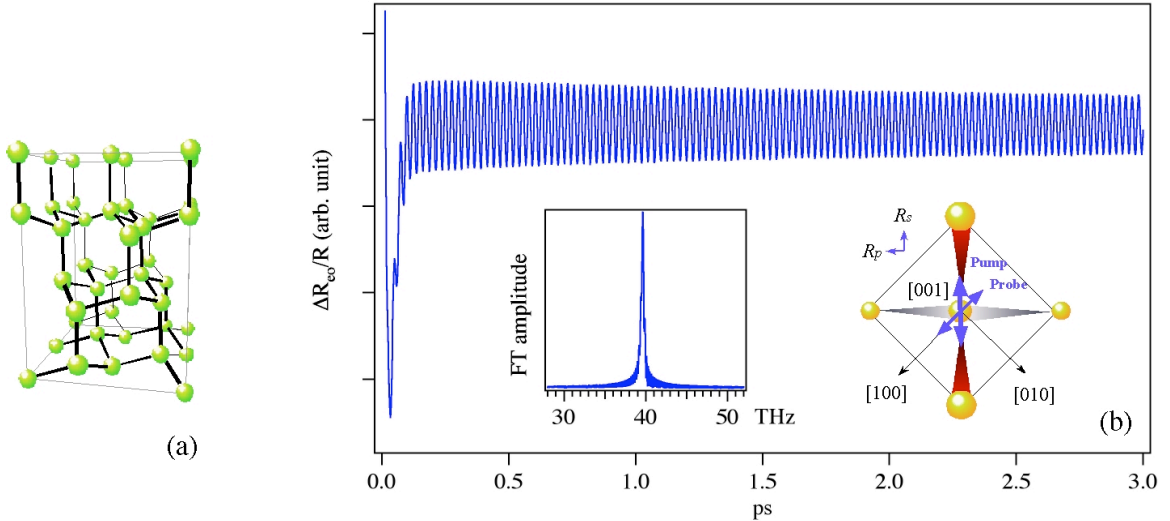
Fig. 2 (a) Crystalline structure of diamond, and (b) transient anisotropic reflectivity $R_{eo}/R = (\Delta R_p - \Delta R_s)/R$ of the (001) surface of single crystal diamond (type IIa). Pump and probe polarizations are illustrated with respect to the crystal in the right inset of (b). Fourier transform of the reflectivity signal after t=0 is shown in the left inset of (b).

delay between pump and probe pulses is scanned at a 20 Hz rate to enable accumulation up to 25,000 times.

Anisotropic reflectivity of diamond features an oscillation with a period of 25 fs, as shown in Fig. 2(b). The frequency of 40 THz, or 1330 cm^{-1}, agrees well with the Raman active optical phonon of diamond. The oscillations persist significantly long, for more than 300 cycles before dephasing on 8 ps time scale. The coherent phonon signal essentially vanishes after rotating the sample by 45° within the surface plane, being consistent with the off- diagonal $\Gamma_{25'}$ symmetry Raman tensor, confirming the stimulated Raman generation of the coherent phonon. With increasing pump power, the amplitude of the coherent phonon increases linearly. Since our excitation photon energy of 3.14 eV is too low for the one-photon indirect (5.48 eV) or direct (7.3 eV) band gap excitation, the linear power-dependence indicates the off-resonant nature of the coherent phonon generation, *i.e.*, the coherent phonons are driven by the electric-field via their deformation potential.   We emphasize that the linear power dependence of the phonon amplitude, described above, is observed both in type Ib and IIa diamond samples, which have strong absorption for 3.14 eV light and nominally no absorption, respectively. Indeed, the coherent phonon amplitude in type Ib (yellow) diamond is noticeably smaller than that for type IIa (colorless) diamond. This propensity also is observed for the Raman peak height of the optical phonon, and indicates that the localized electronic levels of N-impurities do not directly couple with the delocalized optical phonons.

Graphite exhibits coherent oscillations with a period of 21 and 770 fs in the anisotropic reflectivity, as shown in Fig. 3(c). The oscillations are assigned to the Raman active E_{2g2} (in-plane C-C stretching) and E_{2g1} (interlayer shear[3]) of graphite, respectively. The amplitude of the both E_{2g} phonons shows $\cos 2\theta$ dependence on the pump polarization angle θ with respect to the optical plane, which indicates, like in diamond, a stimulated Raman generation of the coherent phonons in graphite. Contrary to other materials under intense excitation, the E_{2g2} phonon frequency upshifts with increasing pump power. Time-windowed analysis shows that the frequency is highest at *t*=0 and relaxes to a lower frequency within 0.5 ps. The time scale is in good agreement with the thermalization time of electrons obtained from time-resolved THz spectroscopy.[4] We therefore attribute our observation to the transient stiffening of the C-C bonds in the presence of non-thermal occupations of photo-

14
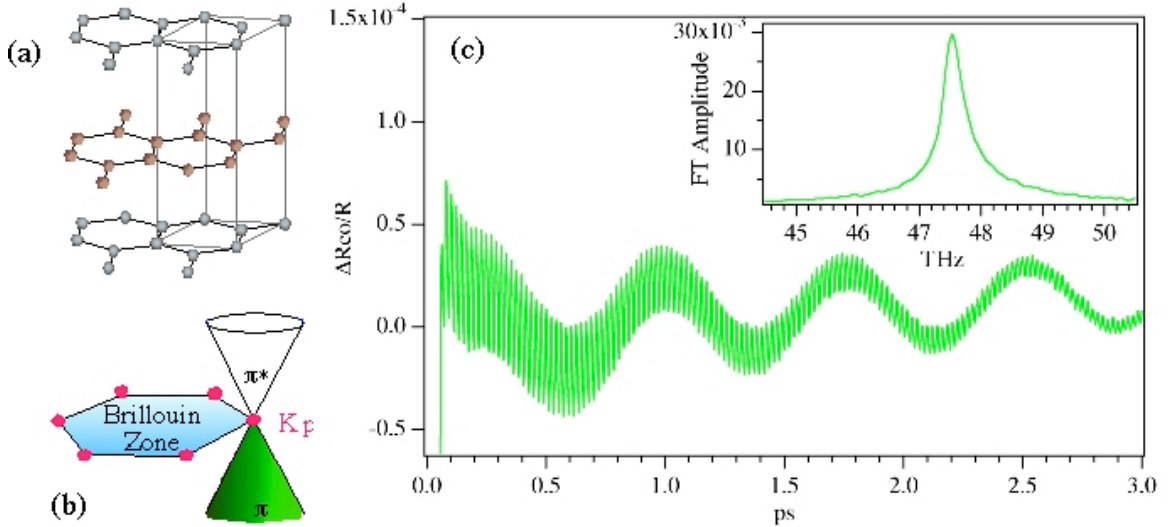
Fig. 3 (a) Crystalline structure of graphite, (b) its schematic -band structure, and (c) anisotropic reflectivity change of graphite at 50 mW. Fourier transform of the reflectivity signal after t=0 is shown in the inset in (c).

excited electrons, as schematically illustrated in Fig. 1(b), which is essentially weakening of the carrier screening (Kohn anomaly) dominating the Γ phonon frequency.[5]

In summary, sub-10 fs, 395-nm laser pulses excite 40-THz coherent phonons with an extremely small damping rate (0.15-ps^{-1}) in diamond. Linear power dependence of the phonon amplitude under off-resonant excitation condition gives a direct evidence for an

electric field-driven generation mechanism. The 47-THz coherent E_{2g2} phonon of graphite exhibits a frequency upshift upon photoexcitation, which relaxes within 0.5 ps to a stationary value through electron-phonon scattering. The phonon stiffening is attributed to the interaction of the lattice with the non-thermal electron-hole plasma.

[1] K. Ishioka, M. Hase, M. Kitajima, and H. Petek, *Appl. Phys. Lett.*, **89**, 231916 (2006).
[2] M. Hase, M.. Kitajima, A.M. Constantinescu, and H. Petek, Nature **426**, 51 (2003).
[3] T. Mishina, K. Nitta and Y. Masumoto,, Phys. Rev. **B62**, 2908 (2000).
[4] T. Kampfrath, L. Perfetti, F. Schapper, C. Frischkorn, and M. Wolf, *Phys. Rev. Lett.* **95**, 187403 (2005).
[5] S. Piscanec, M. Lazzeri, F. Mauri, A.C. Ferrari, and J. Robertson, *Phys. Rev. Lett.* **93**, 185503 (2004).

2D-IR spectroscopy of Fermi resonances in benzene

Paul M. Donaldson,[1] Rui Guo,[1] Frederic Fournier,[1] Elizabeth M. Gardner,[1] Laura M.C. Barter,[1] D. Jason Palmer,[2] Chris J. Barnett,[1] Keith R. Willison,[3] Ian R. Gould[1] and David R. Klug[1]

[1]*Department of Chemistry, Imperial College London, SW7 2AZ, UK*

[2]*European Laboratory for Non-Linear Spectroscopy, University of Florence, Polo Scientifico Via Nello Carrara 1, I-50019-Sesto-Fiorentino (FIRENZE), Italy.*

[3]*Cell and Molecular Biology, Institute of Cancer Research, London, SW3 6JB, UK*

Fermi resonances of vibrational states are common features in the spectra of complex molecules. Being a mixture of two or more vibrational states and involving multiple anharmonic terms, the energies and intensities of Fermi resonance states are sensitive reporters on structure and environment. Identification and assignment of Fermi resonances in IR absorption or Raman spectra is difficult because such bands have no special features to distinguish them from others. Cross peaks of Fermi resonance states in 2D-IR spectra however have a characteristic splitting pattern which uniquely identifies them.[1,2,3]
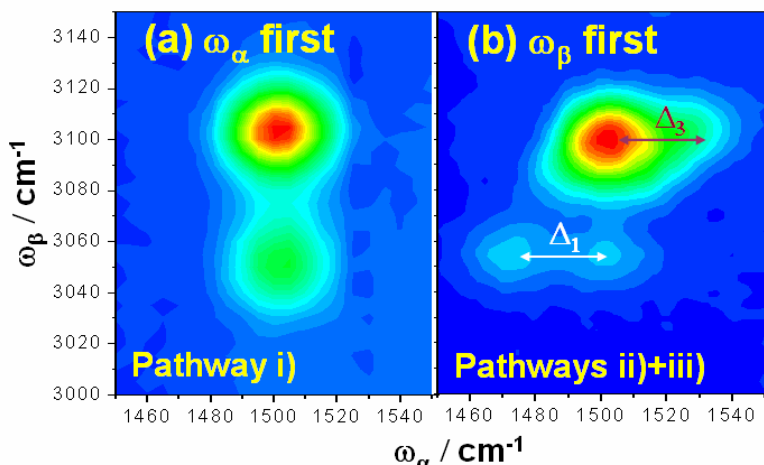
Figure 1. Experimental 2D-IR DOVE-FWM spectra of Fermi resonances in benzene demonstrating the switching on and off of features that identify Fermi resonances. When the lowest frequency IR pulse ω_α is pulse 1, a single coherence pathway is selected giving single cross peaks of the Fermi resonance states. When the highest frequency IR pulse ω_β is pulse 1, two coherence pathways occur simultaneously, each having different resonance frequencies along ω_α, revealing red and blue shifts Δ characteristic of Fermi resonances.[1]

We show that by using 2D-IR DOVE–FWM, the characteristic splitting pattern in the 2D spectrum can be turned on and off by altering the pulse sequence used to generate the 2D-IR spectrum.[1] The splittings naturally appear in 2D-IR pump probe and photon echo experiments however the ability to remove them makes the identification of Fermi resonances unambiguous and can also decongest the 2D-IR spectrum, a feature useful when looking at complicated bandshapes and in analytical applications of 2D-IR such as protein fingerprinting. Choosing benzene as a model system for a 2D-IR DOVE-FWM study revealed these effects clearly (see figure 1) and allowed for straightforward spectral modelling by ab inito methods, serving as a platform for calculations on more biologically relevant systems.

DOVE-FWM is usually performed as a mixed frequency/time domain experiment.[4] Two picosecond infrared pulses ~1 ps (20 cm^{-1}) fwhm and frequencies ω_α and ω_β ($\omega_\beta > \omega_\alpha$) are mixed in the sample with a picosecond visible pulse ω_γ. A third order nonlinear signal is observed that radiates at $\omega_\beta - \omega_\beta + \omega_\delta$, its intensity peaking when ω_α and ω_β are resonant with two coupled vibrational modes. figure 3 shows the three coherence pathways which give rise to the third order signal. Pathway i) can be uniquely selected if

pulse 1 is E_α (see figures 1 and 2). This gives single cross peaks when ω_α is tuned to the **g-a** resonance frequencies of the analyte (**g**=ground state, **a**=vibrational excited state). If pulse 1 is E_β, coherence pathways ii) and iii) occur simultaneously. Referring to figure 3 it can be seen that pathway ii) has identical ω_α resonance frequencies to pathway i). In pathway iii) however, E_α is removing a quantum of the **a** mode from the combination band/Fermi resonance **c** and the ω_α resonant frequency for this step is shifted relative to pathway ii) by the anharmonic shifts Δ associated with **c**. Pathways ii) and iii) destructively interfere, however in the presence of an anharmonicity Δ, their separation along ω_α allows them to be observed. As can be seen in figure 1 (b), this gives two sets of cross peaks.
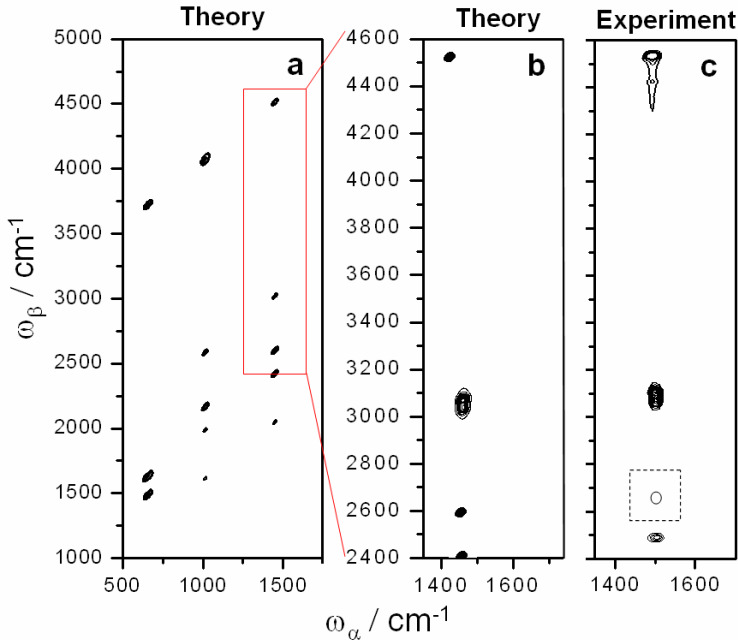
Figure 2. Experimental and theoretical benzene DOVE-FWM cross peaks. Plots (a) and (b) show the cross peaks calculated theoretically. (a) uses Gaussian lineshapes to show positions/intensities. (b) is a zoom into the region accessed experimentally and uses response function lineshape modelling and a rigorous treatment of Fermi resonances. Plot (c) shows experimental DOVE-FWM spectra of the three sets of cross peaks. Pulse ordering was used to select the single coherence pathway i). To suppress the many competing nonlinear processes the spectra were collected with delays of T_{12} and T_{23}=2-3 ps. [1]
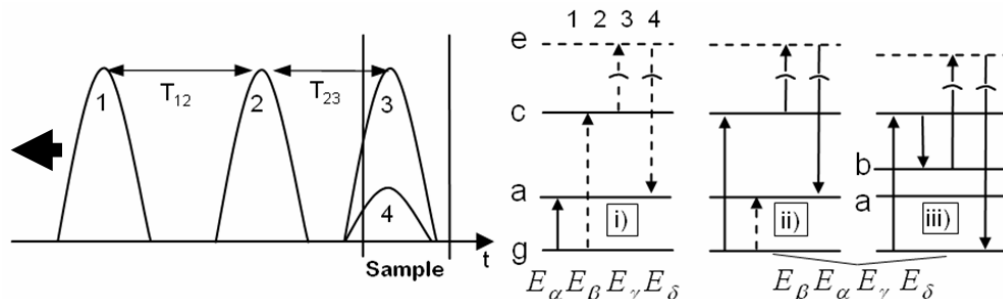
Figure 3. 2D-IR DOVE-FWM pulse ordering schemes and coherence pathways i), ii) and iii).

Calculations of benzene's second order electrical and third order mechanical anharmonicities were performed (Gaussian 03 DFT B3LYP 6-311++G(p,d) basis set). A comparison between the theoretical and experimental 2D-IR DOVE-FWM spectra is shown in figure 3. Experimentally, six cross peaks of the 1480 cm^{-1} ring breathing mode ν_{13} (Herzberg notation) with a range of combination bands and Fermi resonances were observed, spanning a region of 2300-4550 cm^{-1}. The 4400 cm^{-1} cross peak seen in the experiment is due to the $\nu_3+\nu_{13}+\nu_{16}$ combination band and therefore not described by the calculations. The Fermi resonances states were constructed using the unperturbed state energies and the calculated mechanical anharmonicities to rediagonalise the Hamiltonian matrix of the states involved. Response function lineshape simulations were able to describe most aspects of the unique cross peak

shapes that were seen. A comparison between theory and experiment is shown in Table I, demonstrating that for the relative intensities and energy splitting of the Fermi resonance states, theory and experiment are in agreement to within 35% of one another. Having rigorously compared benzene 2D-IR DOVE-FWM theory and experiment, using the same calculational framework, substituted aromatic compounds were examined. Figure 4 shows how toluene and p-methyl phenol serve as good analogues for understanding the cross peaks of phenylalanine and tyrosine.

	E_{1-3} / cm^{-1}	Fermi resonance peak amplitudes		
		1	2	3
Expt	45	1	0	2.6
Theory	65	1	0.04	1.7

Table I. Benzene Fermi resonance peak splittings and relative amplitudes. Comparison between theory and experiment.[1]
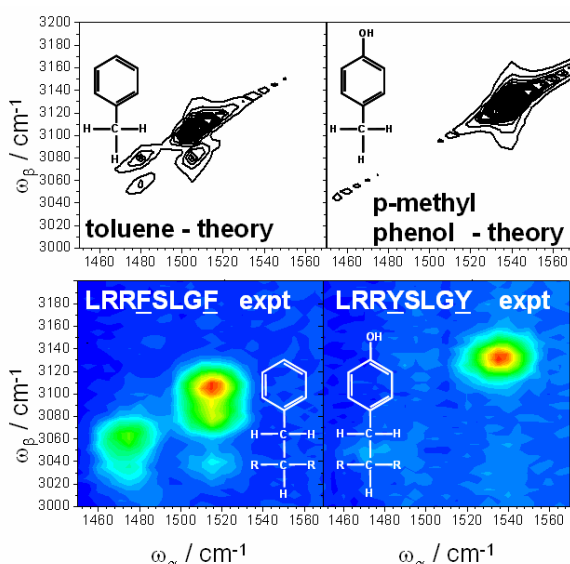
Figure 4. Comparison between theoretical 2D-IR spectra of aromatic amino acid analogues and experimental 2D-IR spectra of peptides containing phenylalanine (left) and tyrosine (right).

Conclusions:

The 2D-IR DOVE-FWM methodology has a useful type of coherence pathway selection, allowing anharmonic cross peak splittings to be revealed or removed. Using benzene as a model system we have demonstrated and modelled this feature and in the process acquired a robust methodology which we are now applying to our work in fingerprinting peptides and proteins.

References:

1) Donaldson P.M. et al, Journal of Chemical Physics (2007)
2) Edler J. and Hamm P., Journal of Chemical Physics **119** (5), 2709 (2003)
3) Zheng J.R. et al, Journal of Chemical Physics **123** (16) (2005)
4) Wright J.C., International Reviews in Physical Chemistry **21** (2), 185 (2002)

Acknowledgements

Nonlinear Vibrational Response of Coupled Anharmonic Systems — Towards the 2D IR Spectrum of H₂O

A. Paarmann,[1] T. Hayashi,[2] S. Mukamel,[2] and R. J. D. Miller[1]

[1] Institute for Optical Sciences and Departments of Physics and Chemistry, University of Toronto, Toronto, ON, M5S 3H6, Canada [2] Department of Chemistry, University of California, Irvine, California 92697-2025, USA. Email: alexis@lphys.chem.utoronto.ca, URL: http://lphys.chem.utoronto.ca

The recent experimental observation of extremely fast memory loss in pure water[1] is still pending a full understanding of the underlying mechanisms and theoretical description, mainly due to difficulties in treating the resonant energy transfer in the pure liquid. We present a new method of numerical propagation of the vibrational dipole moments that allows for nonlinear signal calculations, fully treating the coupled fluctuating Hamiltonian and Non-Condon effects. This approach will, for the first time, allow us to calculate two-dimensional infrared (2D IR) spectra of the OH-stretching vibration in pure water.

We use molecular dynamics (MD) simulations in combination with an ab initio electrostatic map[2] to gain the fully anharmonic, fluctuating vibrational Hamiltonian and transition dipole moments. We then numerically propagate initially excited dipole moments in the molecular basis according to the different Liouville pathways necessary to calculate the 3rd order signal.[3,4]

As a first application, we studied the effect of intermolecular coupling on nonlinear vibrational response using the OH stretching mode in pure HOD as a model system. A constant volume SPC/E water MD trajectory of N = 64 molecules with 0.5 fs time steps at room temperature is generated using the GROMACS-3.3.1 program.[5] We employ the following Hamiltonian as a function of the MD time step τ for N coupled local modes, using the electrostatic map[2] of HOD to extract transition frequencies and dipole moments of the OH stretch.

$$\hat{H}(\tau) = \sum_m \varepsilon_m(\tau)\hat{B}_m^\dagger \hat{B}_m + \sum_{m \neq n} J_{mn}(\tau)\hat{B}_m^\dagger \hat{B}_n +$$
$$\sum_{mn,m'n'} V_{mn,m'n'}(\tau)\hat{B}_m^\dagger \hat{B}_n^\dagger \hat{B}_{m'}\hat{B}_{n'} + \int dr \hat{P}(r) \cdot E(r,\tau) \tag{1}$$

The first two terms describe the free Boson system, where ε_m is the transition frequency of mode m. The intermode coupling J_{mn} is calculated using resonant dipole-dipole coupling. The last term describes the interaction with the optical fields. The third term contains both diagonal (intramolecular) and off-diagonal (intermolecular) anharmonicities. The off-diagonal anharmonicities, in this model, arise from anharmonicities in the transition dipole moments (see Equ. 2) affecting the resonant dipole dipole coupling.

$$\hat{\mu}(\tau) = \sum_m \mu_m(\tau)(\hat{B}_m^\dagger + \hat{B}) + \sum_m \Delta\mu_m(\tau)\hat{B}_m^\dagger(\hat{B}_m^\dagger + \hat{B}_m)\hat{B}_m \tag{2}$$

Here, μ_m is the 0→1 fundamental transition dipole moment and $\Delta\mu_m$ is the anharmonicity of the 1→2 transition dipole moment. The propagation of initially excited dipole moment is performed using numerical integration of the Schrödinger equation ($\hbar = 1$).

$$\hat{G}(\tau_2,\tau_1) = -i\Theta(\tau_2 - \tau_1)\prod_{\tau=\tau_1}^{\tau_2-\Delta\tau} \exp(-i\hat{H}(\tau)\Delta\tau) \tag{3}$$

$\hat{G}$ propagates the system from τ_1 to τ_2, $\theta(\tau)$ is the usual Heaviside function, $\Delta\tau = 1\,\text{fs}$. The nonlinear vibrational signal is calculated in the impulsive limit by dipole interactions (Equ. 2) and propagations (Equ. 3) following the six necessary Liouville pathways.[3,4]

The matrix exponential in Equ. 3 is calculated exactly for single particle excitations. Propagation of the two-particle excitations needed for the excited state absorption diagrams,[4] however, poses some difficulties. The large size of the symmetrized two-particle basis being N(N+1)/2 makes the calculation of the matrix exponentials in Equ. 3 computationally extremely expensive. On the other hand, the two-particle diagram contains all the anharmonicities and a very high precision for this propagation is required. We propose a new method of calculating these matrix exponentials. We split the two-particle Hamiltonian into harmonic and anharmonic part and employ the split-operator method[6] to calculate the total propagator.

$$\exp\left(-iH^{(2)}\Delta\tau\right) = \exp\left(-iH_0^{(2)}\Delta\tau\right)\exp\left(-iV\Delta\tau\right) \qquad (4)$$

Here, $H^{(2)}$ denotes the full two-particle Hamiltonian, and $H_0^{(2)}$ is the harmonic part (first two terms in Equ. 1) and V is the anharmonic part (third term in Equ. 1) of $H^{(2)}$. The harmonic exponential can be calculated exactly from factorization of the single-particle propagators, and $V\Delta\tau$ is small enough to allow 1st order Taylor expansion of the exponential with good accuracy. The split operator method gives good accuracy provided small enough time steps.[7] The calculated 3rd order response functions were averaged over 200 trajectories for each required combination of excitation pulse polarizations.

In Figure 1 (a), we show the impulsive pump probe signal for parallel and crossed polarization of the pump and probe pulses, with and without intermolecular coupling. The signal was spectrally integrated over the whole OH band. In Figure 1 (b), we plot the polarization anisotropy, calculated from these pump probe transients. The signal of the uncoupled system shows two contributions, an early damped oscillation (oscillation period ~ 70 fs, damping constant ~ 35 fs, amplitude ~ 0.025) due to librational modulation, and a slower reorientation of the transition dipoles with a time constant of ~ 950 fs. Switching on the intermolecular coupling, we observe these two processes to become negligible and the signal is now dominated by intermolecular energy transfer.

The main interest of this study is the effect of the intermolecular coupling on the nonlinear signal, and in particular the 2D spectra, when entering the coupling regime observed for pure H_2O.[1] Therefore, we adjusted the one free parameter in the model, that is the dielectric constant ε in the resonant dipole dipole coupling, to reproduce the anisotropy decay of ~ 80fs observed in H_2O.[1,8] The resulting ε is ~ 40 which is about two times smaller than the value expected for water.[9] This, however, can be well understood from single-mode character of our HOD model system that provides only half as many accepting modes per unit volume. For this value of ε, we extract an average next neighbor coupling of 25 cm^{-1}.
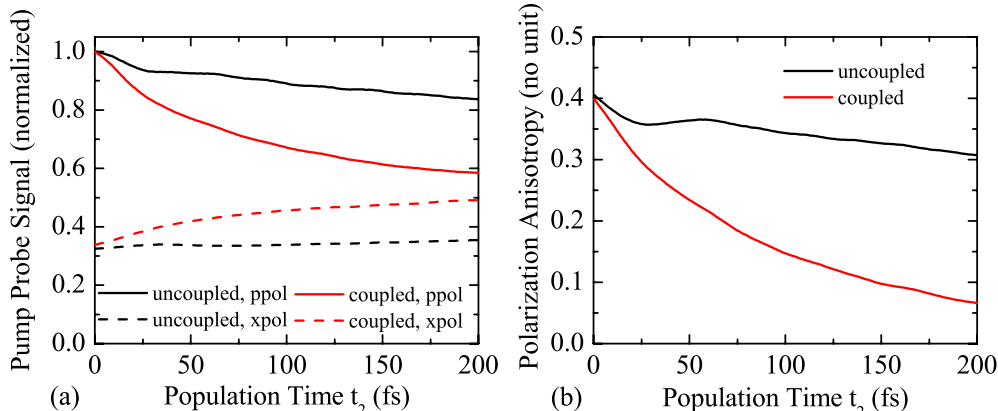
Figure 1. (a) Spectrally integrated, impulsive pump probe signal, parallel (solid) and crossed (dashed) polarization for the uncoupled (black) and coupled (red) system. (b) Transient polarization anisotropy of the OH-stretching vibration. Upon coupling (red), resonant energy transfer dominates the signal decay, librational modulation and reorientation dynamics become negligible.
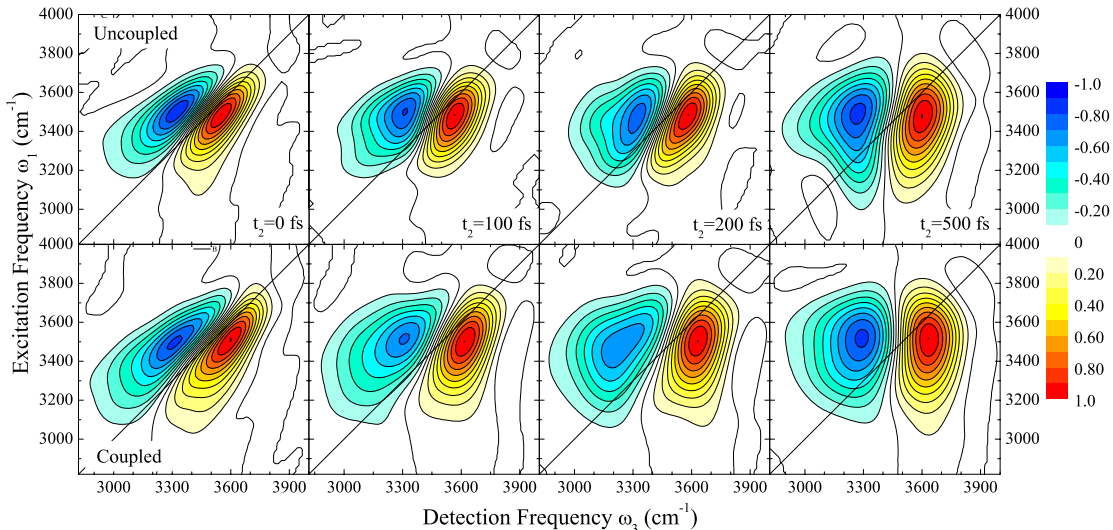
Figure 1. 2D IR spectra of the OH stretch in pure HOD at population times t_2 = 0, 100, 200, 500 fs. The coupled system shows slightly broader spectral response, as well as moderately faster decay of frequency correlations.

In Figure 2, we compare the 2D IR spectra of the uncoupled and coupled system for population times t_2 = 0, 100, 200, and 500 fs. For both systems, we see an initial inhomogeneity corresponding to an initial distribution of molecular environments. The spectra of the uncoupled system evolve with t_2, exhibiting an averaging of sites on a ~ 500 fs time scale. This agrees well with the intermediate time scales observed in experimental studies system of isolated OH or OD oscillators in a water environment.[10,11] Upon coupling, we observe two effects. (1) All spectra broaden slightly. This effect is already observed in the linear spectra (not shown) where the coupling leads to an additional broadening of ~ 80 cm^{-1}. (2) The spectral diffusion dynamics speed up moderately. We observe ~ 300 fs spectral diffusion time. Therefore, we conclude that the resonant energy transfer, even though it contributes, does not dominate the extremely fast spectral diffusion observed in 2D IR spectra of pure water systems.[1]

In conclusion, we present a new method of calculating nonlinear vibrational signal of moderately sized, fluctuating anharmonic molecular systems by numerical propagation, fully treating intermolecular coupling and non-Condon effects. This approach allows us to estimate the effect of intermolecular coupling on the nonlinear vibrational response. For a pure HOD model system, we observe 80 fs resonant energy transfer for an average next neighbor coupling of ~ 25 cm^{-1}. This intermolecular coupling leads to moderate decrease in spectral diffusion time scales. The new method will allow us to calculate the nonlinear vibrational response of H_2O treating all the above effects for the first time. S. M. gratefully acknowledges the support of NIH (Grant # GM59230) and NSF (Grant # CHE-0446555).

[1] M. L. Cowan, et al., Nature 434, 199-202, **2005**.

[2] T. Hayashi, et al., J. Phys. Chem. A 109, 64-82, **2005**.

[3] S. Mukamel, *Principles of Nonlinear Optical Spectroscopy,* Oxford University Press, New York, **1995**.

[4] T. l. C. Jansen and J. Knoester, J. Phys. Chem. B 110, 22910-22916, **2006**

[5] H. J. C. Berendsen, D. van der Spoel, and R. van Drunen, Comput. Phys. Commun. 91, 43, **1995**.

[6] R. Kosloff, J. Phys. Chem. 92, 2087-2100, **1988**.

[7] We tested for convergence by reducing the time step from 1.0 fs to 0.5 fs which showed no detectable difference in the nonlinear signal.

[8] H. Torii, J. Phys. Chem. A 110, 9469-9477, **2006**.

[9] J. N. Murrell, A. D. Jenkins, *Properties of Liquids and solutions,* 2nd Ed., John Wiley & Sons, Chichester, England, **1994**.

[10] J. B. Asbury, et al., J. Phys. Chem A 108, 1107-1119, **2004**.

[11] J. D. Eaves, et al., Proc. Nat. Acad. Sci. 102, 13019-13022, **2005**.

Mid-infrared time resolved polarization study of vibrationally excited Mn(CO)$_5$Br in the liquid phase

E.A.Torres and K.L.Kompa

Max-Planck-Institut für Quantenoptik, Hans-Kopfermann-Str. 1, 85748 Garching bei München. elva.torres@mpq.mpg.de

Time domain vibrational spectroscopy has driven structure and dynamics studies of complex systems, as well as prompted the application of coherent control methods to achieve various aims such as controlled population transfer[1] and the implementation of molecular-level computing schemes.[2] Additionally, time resolved anisotropy studies in liquid environments have been used to yield significant insight into various molecular processes including reaction mechanisms and energy transfer processes. Here we present a model system in which the vibrational relaxation process has been investigated via the measurement of anisotropy decay.

We use one color mid-infrared femtosecond pump-probe spectroscopy in order to study the ground state vibrational relaxation dynamics of a mono-substituted metal carbonyl complex Mn(CO)$_5$Br in solution, a recent candidate for molecular computation studies.[2b] In particular, we excite the two infrared active carbonyl stretches, the A$_1$ and E normal modes, which are separated by 50 cm^{-1}. A schematic diagram of these carbonyl stretches is shown in figure 1a where the equatorial E state vibration is doubly degenerate and the axial non-degenerate A$_1$ state vibration is found opposite to the bromine atom. Since both of these states lie within the bandwidth of our 130 fs pump and probe pulses, we are able to excite and monitor them simultaneously. The inset in fig.1a shows the probe pulse spectra transmitted through the sample flow cell. The pulse frequency is centered between the fundamental transitions $(\upsilon = 0 \rightarrow 1)$ of the two modes at 2018 cm^{-1}. A spectrograph with a 3.2 cm^{-1} resolution using a 2x32 pixel array MCT detector is used to spectrally resolve the probe pulse as a function of pump-probe delay time.
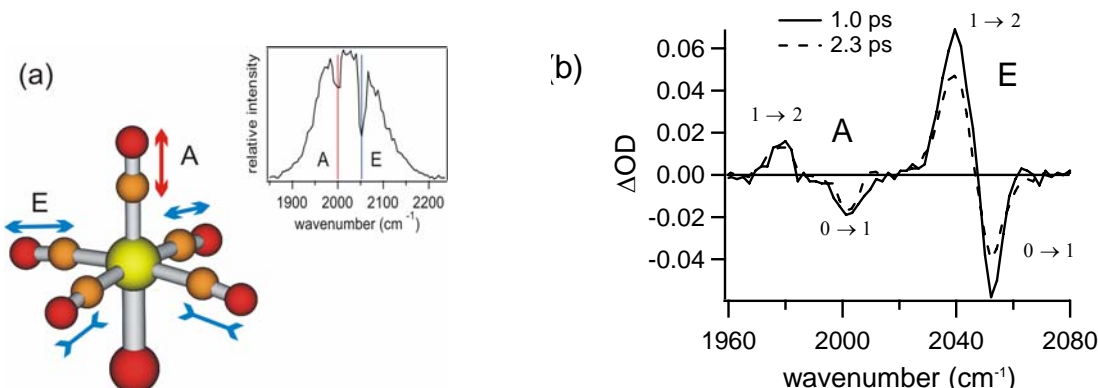
Figure 1. (a) Schematic representation of Mn(CO)$_5$Br infra-red active carbonyl stretches. (b) Transient absorption spectra of Mn(CO)$_5$Br in CCl$_4$ at 1.0 and 2.3 ps delay times. The complex is excited with 2.6 μJ at 2018 cm^{-1}. The absorption for the fundamental $\Delta\nu_{10}$ and the first excited state transitions $\Delta\nu_{21}$ are indicated.

[1] T.Witte, J.S.Yeston, M.Motkus, E.J.Heweil, K.L.Kompa, Chem.Phys.Lett. 392 (2004) 152. C. Ventalon, J.M. Fraser, M. H.Vos, A.Alexandrou, J. Martin and M. Joffre, PNAS 101 (2004) 13216

[2] (a) F. Remacle and R.D. Levine, Appl. Phys. Sci., 101 (2004) 12091 (b) B.M.R Korff, U. Troppmann, K.L. Kompa and R. De Vivie-Riedle, J. Chem. Phys. 123 (2005) 244509 (c) C.Gollub, B.M.Korff, K.L.Kompa and R.deVivie-Riedle, Phys.Chem.Chem.Phys., 9 (2007) 369

Figure 1b shows a time dependent transient absorption spectra at delay times of 1.0 ps and 2.3 ps from which state anharmonicities (χ_e) are extracted for each infrared active carbonyl stretch. We find $\chi_e = 21$ cm^{-1} for the more red-shifted A_1 state as compared to $\chi_e = 14$ cm^{-1} for the E state. Not surprisingly, the measured E state anharmonicity corresponds more closely to the anharmnonicity found in the triply degenerate T_{1u} vibration of various hexacarbonyl metal complexes.[3] These measured anharmonicities have been use to correct calculated *ab initio* potential energy surfaces used in various coherent control schemes for this molecule.[2c]
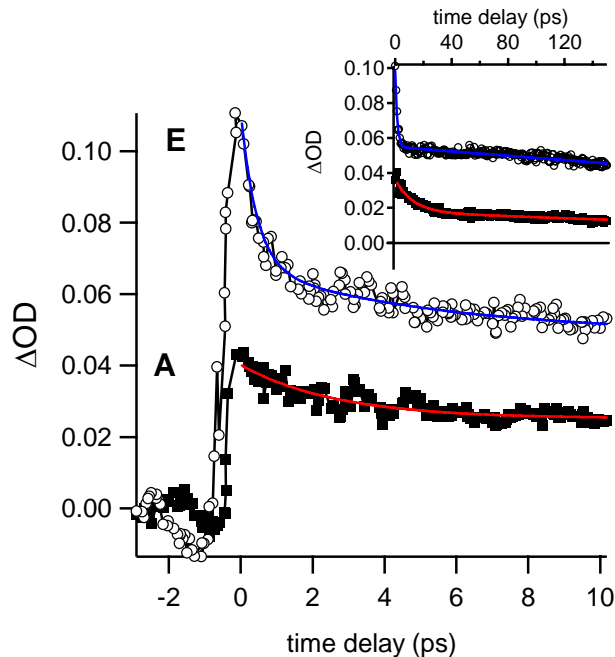
Figure 2. Time dependent transient absorption profiles of Mn(CO)$_5$Br for the first excited state transitions $\Delta \nu_{21}$ of the E (○) and A_1 (□) infrared active modes. A single exponential fit is applied to A state and a double exponential fit is applied to the E state.

Furthermore, time profiles mapping the temporal evolution of the population distribution reveal very different early time relaxation dynamics for these two vibrations. In figure 1b we can clearly see that the E state has a very fast initial relaxation component that is not present in the A_1 state. The A_1 state remains essentially unchanged after 2.3 ps while the E state $\nu = 1$ population has already decreased by 32%. Figure 2 shows the time dependent transient absorption profiles for the first excited state transition $\Delta \nu_{21}$. Similar behavior is found in the corresponding ground state bleaching signals. Indeed, a sub-picosecond component is measured in the E state relaxation that is not found to be present in the A_1 state relaxation. The inset in figure 2 shows the long time state evolution.

In order to gain more insight into the observed vibrational relaxation, the anisotropy decay $r(\tau)$ was measured, where $r(\tau) = S_\parallel(\tau) - S_\perp(\tau) / S_\parallel(\tau) + 2S_\perp(\tau)$. Figure 3 displays the measured anisotropy decay for the fundamental and first excited state transitions after

[3] K.Nakamoto, Infrared Spectra of Inorganic and Coordination Compounds. (John Wiley & Sons, Inc., New York. 1963)
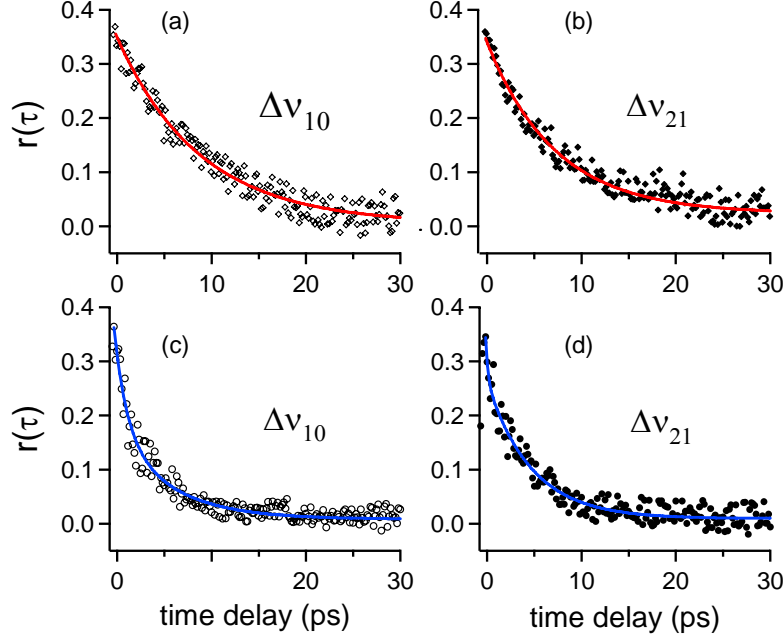
Figure 3. Experimental anisotropy decay $r(\tau)$ and exponentially fitted (solid line) for the A_1 (–) and E (–) state transitions of $Mn(CO)_5Br$ in CCl_4.

excitation of the $Mn(CO)_5Br$ with 2.6 μJ. The initial anisotropy is found to be nearly identical for both modes, $r(0) = 0.34 \pm 0.03$. The E state anisotropy, however, exhibits a bi-exponential decay with a very fast decay component which is not present in the A_1 state anisotropy. Fitting the E state anisotropy for the $\Delta\nu_{21}$ transition with a double exponential function yields decay times of $\tau_1^E = 1.02 \pm 0.48$ ps and $\tau_2^E = 5.40 \pm 0.74$ ps (fig. 3d). A single exponential decay is found for the non-degenerate A_1 state anisotropy yielding $\tau^A = 9.27 \pm 0.32$ ps for the $\Delta\nu_{21}$ transition (fig. 3b). Similar decay times are found for the corresponding ground state bleaching: $\tau^A = 9.92 \pm 0.55$ ps for the A_1 state (fig. 3a) and $\tau_1^E = 1.01 \pm 0.35$ ps and $\tau_2^E = 5.71 \pm 0.85$ ps for the E state (fig. 3c). Attempts to fit the A_1 state anisotropy with double exponential functions gave unacceptably poor and erroneous fits.

In conclusion, molecular relaxation dynamics and excitation transfer is of long and continuing interest. In the present case, we observe three distinct time regimes in the vibrational relaxation process for the doubly degenerate E state and two for the A_1 state. In the long time regime (>50ps) both of these states seems to reflect the damping of a simple harmonic oscillator in a dilute environment. In this time scale we have a completely depolarized system where the anisotropy is found to be zero. However, in the very short time regime we find varying relaxation dynamics for these states which is also manifested in the measured anisotropy. Since both of these carbonyl stretches belong to the same molecular entity, we can clearly state that the fast anisotropy decay found in the E state is not due to rotational diffusion. If this had been the case both states should have the same depolarization rates due to molecular rotational diffusion. Instead, the fast decay component observed in the anisotropy decay and lifetime (τ~600 fs) of the E state is attributed to solvent induced *intramolecular* relaxation between the degenerate states of the E mode. Whereas the measured A_1 state anisotropy appears to indeed reflect the expected loss of polarization due to rotational diffusion.

Real-time monitoring of biological processes inside a living cell
by functional CARS microspectroscopy

A. Kovalev[1], P. Nandakumar[1,2], A. Volkmer

[1] 3rd Institute of Physics, University of Stuttgart, Pfaffenwaldring 57, 70550 Stuttgart, Germany.
[2] Physics Group, Birla Institute of Technology and Science Pilani, Goa Campus, NH 17B, Byepass Road, Zuarinagar, Goa-403726, India.
Email: a.volkmer@physik.uni-stuttgart.de, URL: http://www.pi3.uni-stuttgart.de/ags/volkmer/

A subject of wide interest in the physical and life sciences is the noninvasive characterization of chemical species or biological components within a complex heterogeneous system, i.e. a living cell, through optical microscopy. In the last years, coherent anti-Stokes Raman scattering (CARS) microscopy has emerged as a very promising tool in both the life and material sciences. Its potential to employ vibrational signatures as contrast parameter - not requiring any exogenous labels! - and to visualize both chemical composition and physical state with high detection sensitivity is unprecedented. Because of its coherent nature the CARS signal is several orders of magnitude more sensitive than spontaneous Raman scattering. In addition, CARS microscopy has been demonstrated to exhibit three-dimensional sectioning capability with high spatial resolution and to provide a deep penetration depth for imaging through thick tissues or cells with negligible photo-damage[1].
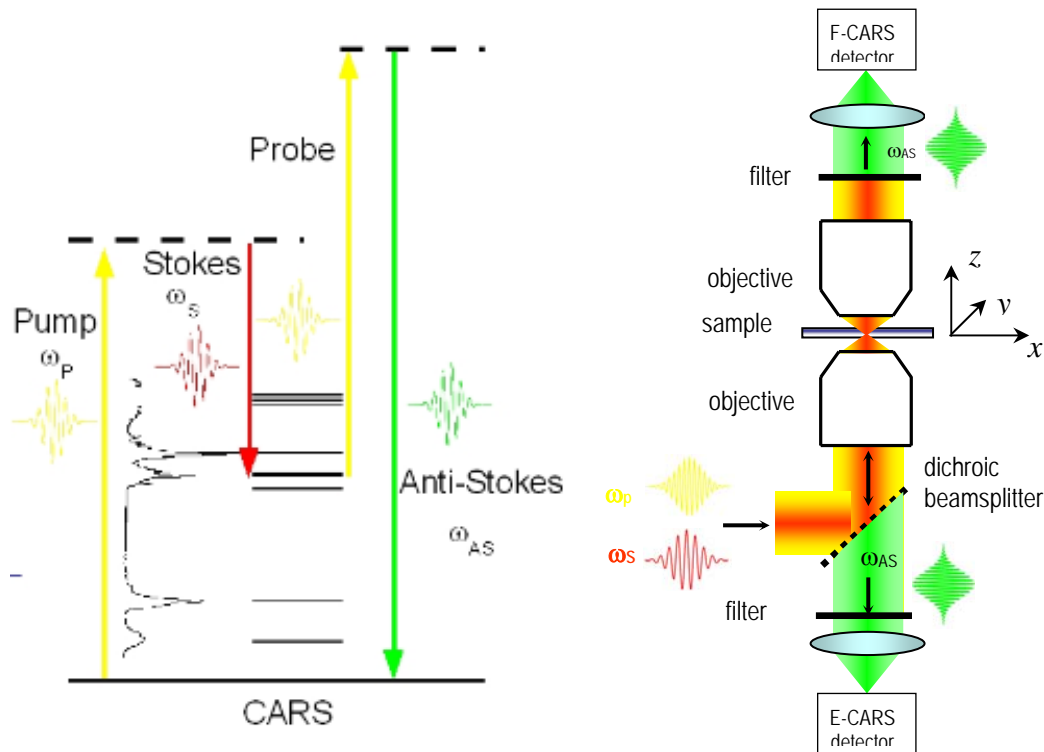
Left: Energy level diagram for the Raman-resonant contribution to the CARS process. Right: Schematic configuration for collinear F-CARS and E-CARS microscopy.

---

[1] For a Topical Review see : A. Volkmer, J. Phys. D: Appl. Phys., **2005**, 38, R59-R81.

By going beyond vibrational imaging that has been the predominant realization of CARS microscopy to date, our efforts have been focused on the application of high-sensitivity multiplex CARS microspectroscopy, which offers the possibility for space- and frequency-resolved vibrational spectroscopy, thus providing access to the full wealth of the spectroscopic information content of macromolecular objects on the sub-micron length scale with typical data acquisition times below 100 ms. Combined with a detailed CARS spectral analysis, this vibrational microspectroscopy allows the noninvasive and quantitative chemical examination of slow dynamical processes inside a living cell occurring on time scales of seconds to hours. In order to demonstrate the feasibility of CARS microspectroscopy for the non-invasive chemical analysis inside a living cell, we have performed experiments on live differentiated NIH 3T3-L1 fibroblast cells in the spectral region where the C-H stretch vibrations reside.
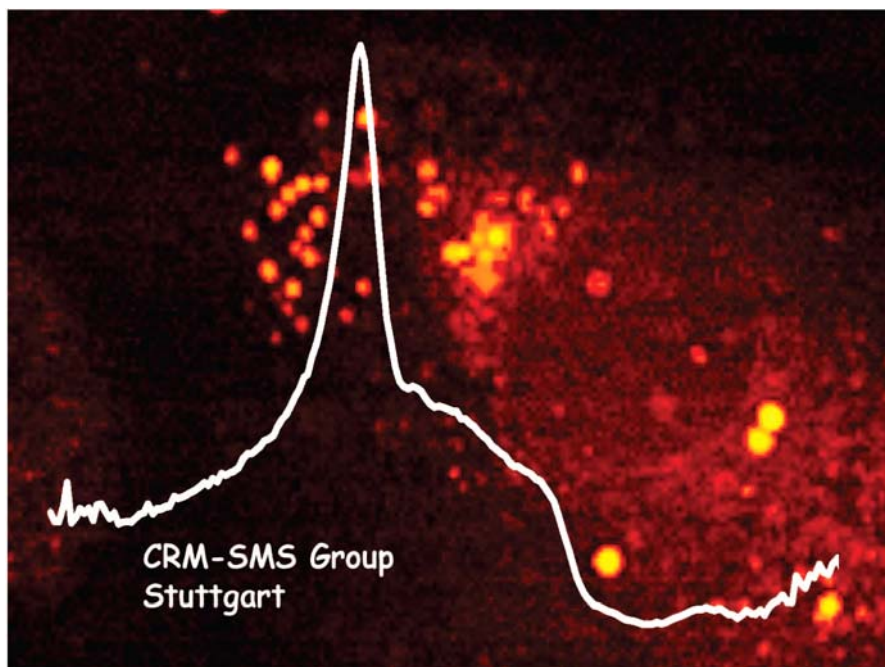
Noninvasive intracellular CARS imaging and microspectroscopy of individual lipid droplet organelles inside a living NIH 3T3-L1 fibroblast cell.

As shown in the above Figure, where a single cell is imaged by recording the spectrally integrated CARS signal, the sub-cellular distribution of constituents with high densities of lipids is visualized. Besides the membrane envelope of the nucleus, intracellular lipid droplet (LD) organelles are imaged with very high contrast. Different image locations of interest were selected for subsequent chemical analysis by means of multiplex CARS microspectroscopy. This is exemplified by the CARS spectrum recorded for a single LD organelle. Despite an integration time of 100 ms, which is significantly shorter than typical acquisition times in conventional confocal Raman microspectroscopy, a high signal-to-noise

ratio for the LD CARS spectrum is achieved. Based on this spectrum, the following conclusions can already be drawn without further data processing:

(i) The spectrum of a single LD is dominated by the symmetrical CH_2 stretch vibration at 2845 cm^{-1}, which suggest that its composition is dominated by neutral lipids.

(ii) The thermodynamic state of the lipids inside the organelle resembles that of a liquid crystalline state.

With the reconstructed Raman spectrum extracted, a quantitative interpretation of the linear Raman response from this single LD is now possible. This information content allows the *in vivo* functional analysis of lipolysis involved in lipid droplet metabolism in real time. The latter is currently not possible to address with conventional techniques in a non-destructive manner.

A novel imaging system:

Femtosecond Stimulated Raman Microscopy (FSRM)

E. Ploetz[1], S. Laimgruber[1], P. Gilch[1]

[1] LS für BioMolekulare Optik, Department für Physik, Ludwig-Maximilians-Universität, Oettingenstr. 67, 80538 München, Germany, evelyn.ploetz@physik.uni-muenchen.de   http://www.bmo.physik.uni-muenchen.de

Modern microscopy often relies on spectroscopy for contrast enhancement. Vibrational spectroscopy is of particular interest since IR and Raman spectra feature a good correlation between spectroscopic signatures and molecular structures. So, vibrational microscopy can yield maps of the distribution of substances in a microscopic object, for instance a cell. IR microscopy suffers from the strong IR absorption of water and relatively long wavelength of mid IR radiation which results in a low spatial resolution. Raman microscopy offers a better spatial resolution and signal contributions from water are comparatively weak. Yet, low Raman cross sections result in long acquisition times which can hamper "real time" monitoring of biological processes. Applying non-linear Raman techniques can strongly increase the effective Raman cross section. The approach presently favoured is coherent anti-Stokes Raman scattering (CARS)[1]. CARS is a four wave mixing process which occurs if a Raman resonance condition is fulfilled. In addition to this resonant contribution off-resonance four wave mixing mediated by the electronic non-linearity takes place. The recorded signal is a superposition of resonant and off-resonant contributions. Due to this superposition CARS spectra often strongly differ from conventional Raman spectra and the molecular information is obscured. To get rid of this drawback elaborate methods to reduce the non-resonant background have been introduced. They rely, for instance, on different polarization[2] or temporal properties[3] of the CARS signal and the non-resonant background. These methods commonly increase the complexity of the CARS microscope and decrease its sensitivity.
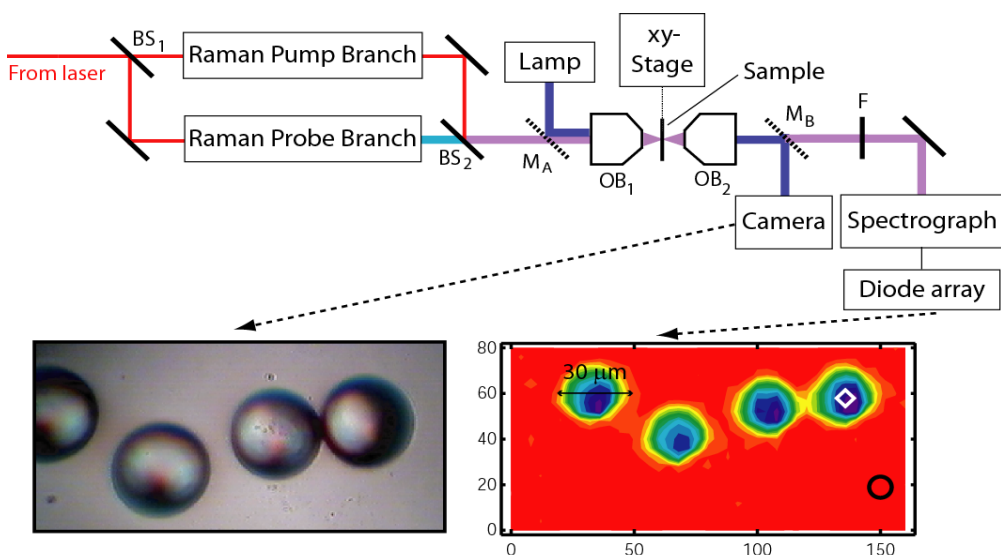
Figure 1: Schematic of the FSRM set-up. The picture on the left shows a conventional micrograph of polystyrene beads dispersed in water. The false color image on the right is based on a two-dimensional array of Raman spectra. Spectral integrals covering the C-H stretch region are indicative for the polystyrene concentration and are contour-plotted here.

[1] J.-X. Cheng, X.S. Xie, J. Phys. Chem. B, **2004**, 108, 827-840
[2] D. Oron, N. Dudovich, Y. Silberberg, Phys. Rev. Lett. **2003,** 90, 213902
[3] A. Volkmer, L.D. Book, X.S. Xie, Appl. Phys. Lett. **2002**, 80, 1505-1507

A different non-linear Raman technique, stimulated Raman spectroscopy, usually does not suffer from these signal distortions. In a stimulated Raman experiment two light fields with frequencies ω and $\omega_{s,a}$ interact in the sample. If these two frequencies fulfill the Raman condition $|\omega_p-\omega_{s,a}|=\omega_R$ (ω_R is the frequency of a Raman transition) a stimulated Raman process takes place which results in an amplification ($\omega_p-\omega_s > 0$) or an attenuation ($\omega_p-\omega_a < 0$) of the $\omega_{s,a}$ light field. For small effects the field changes depend only on the imaginary part of the non-linear Raman susceptibility[4]. So as one scans the frequency $\omega_{s,a}$ one records the intensity changes of the $\omega_{s,a}$ light field which match the conventional Raman spectrum. A particularly appealing method of stimulated Raman spectroscopy is femtosecond stimulated Raman spectroscopy (FSRS)[5]. An intense picosecond laser pulse (Raman pump, frequency ω_p) and a weaker white light continuum pulse (Raman probe, frequency components ω_c) interact in the sample. The Raman probe pulse is spectrally broad enough to cover all Raman resonances of the sample simultaneously. In combination with a multi-channel detector this allows for multiplex stimulated Raman spectroscopy.

FSRS has mainly been used to record time dependent data[5]. Recently, we have introduced FSRS into microscopy and presented femtosecond stimulated Raman microscopy (FSRM)[6]. In our prototype set-up (see Figure 1) a Raman probe and Raman pump pulse both derived from the output of a 1 kHz CPA system are coupled into a scanning microscope. At the focus stimulated Raman interaction modulates the white light spectrum. Chopping the Raman pump light at 500 Hz allows to record these modulation and retrieve the Raman spectrum of the focus. Multi-channel detection yields the complete spectrum simultaneously. The retrieved spectrum matches the spontaneous Raman spectrum and is free from distortions. (As an example the FSRS spectrum of polystyrene film is depicted in Figure 2.)
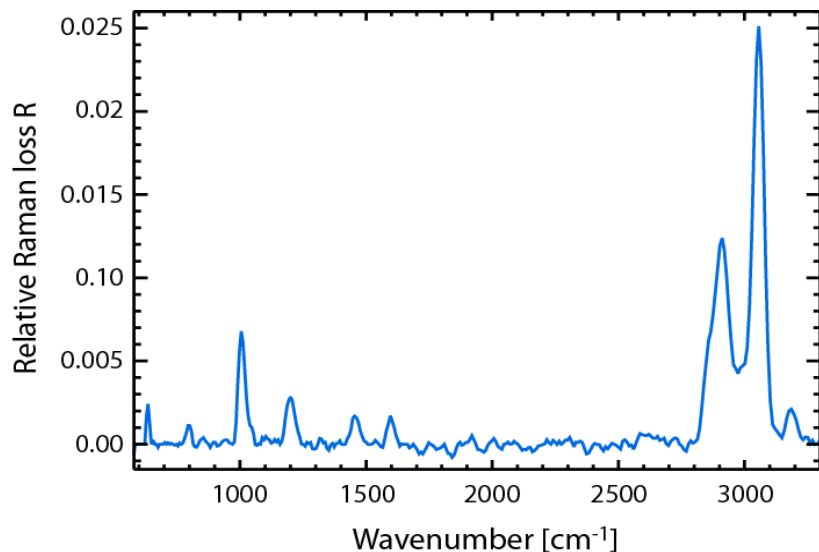
Figure 2: Raman spectrum of polystyrene recorded with the set-up depicted in Figure 1. For the acquisition of this spectrum 1000 laser shots (500 Raman pump on) have been averaged. The energy of the Raman pump pulse was ~ 100 nJ.

By raster-scanning the sample, complete Raman spectra of each point of the sample are recorded and converted into chemical maps. To demonstrate the feasibility of the approach "chemical" maps of polystyrene beads suspended in water have been recorded (see Figure 1).

---

[4] W. Zinth, W. Kaiser, Opt. Comm. **1980**, 32, 507-511
[5] P. Kukura, D. McCamant, R.A. Mathies, Annu. Rev. Phys. Chem. **2007**, 58, 461-488
[6] E. Ploetz, S. Laimgruber, S. Berner, W. Zinth, P.Gilch, Appl. Phys. B, **2007**, 87, 389-393

Contrast can be achieved by spectrally integrating the CH stretch region around 3000 cm^{-1} or the aromatic breathing mode around 1000 cm^{-1}. For the maps depicted in Figure 1 the spatial resolution was ~ 5 μm and limited by the Cassegrainian objective used.

The Cassegrainian (reflective microscope objective) has one important advantage over conventional objectives. When employing a Cassegrainian all relevant frequency components of the Raman probe light arrive at the focus within the duration of the Raman pump pulse. This is necessary to record complete Raman spectra simultaneously. In comparison to Cassegrainians conventional objectives offer higher transmission, compactness, and most important higher spatial resolution. However, they impose group delay onto the Raman probe pulse, which can obstruct the simulataneous recording of FSRS spectra. By means of Kerr gating experiments this group delay has been recorded for some refractive microscope objectives (see Figure 3).
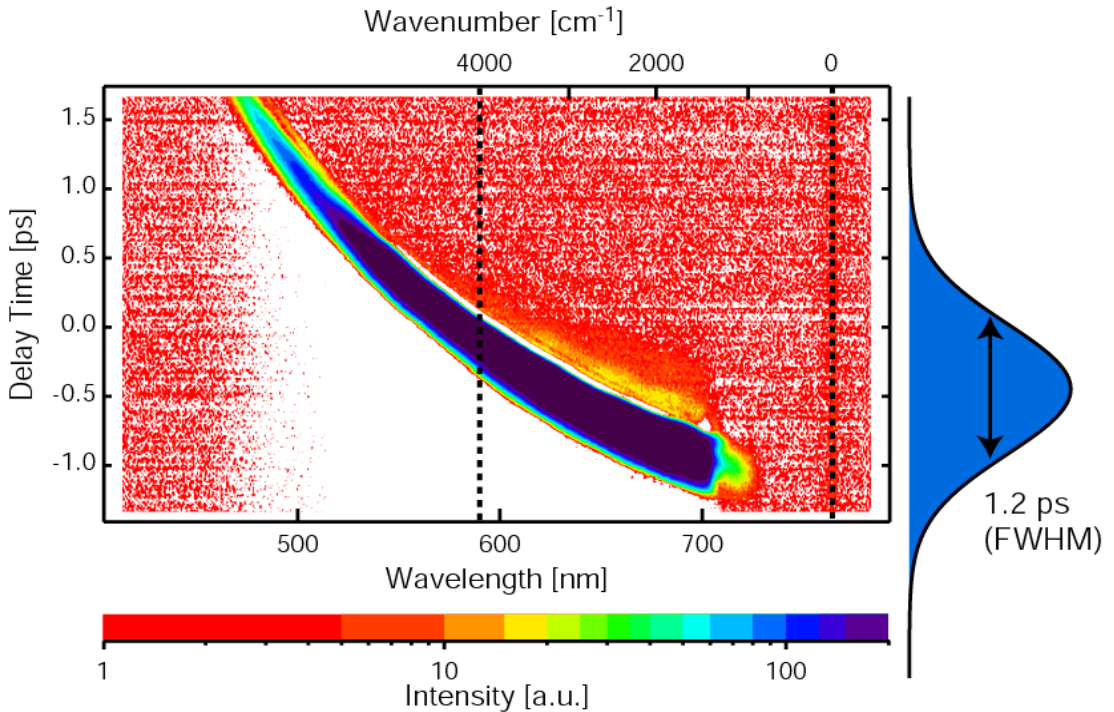
Figure 3: Group delay of the Raman probe light after passing a microscope objective (Leitz 20x, NA 0.4). The spectral range required for Raman spectroscopy and the temporal envelope of the Raman pump pulse are marked.

In the spectral range which needs to be covered for Raman spectroscopy, the group delay induced by the objective is around 1 ps. A bandpass filter with a bandwidth of 15 cm^{-1} generates Raman pump pulses long enough to cover this delay. Using such a filter the acquisition of complete spectra has recently been demonstrated. The signal qualitiy can further be improved by pre-chirping the Raman probe pulse and thereby compensate for the group delay imposed by the objective. We will address this issue in the near future and then seek to record first FSRM images of biological tissue.

BIOLOGY

Gauging excited state dynamics of retinal proteins with impulsive spectroscopy

A. Kahan[1], O. Bismuth[1], N. Friedman[2], M. Sheves[2], and S. Ruhman[1]

[1] Department of Physical Chemistry and the Farkas center for light induced processes, Hebrew University, Jerusalem 91904, Israel. [2] Department of Organic Chemistry, Weizmann Institute, Rehovot 76100, Israel. E-mail: sandy@fh.huji.ac.il.

Bacteriorhodopsin (BR) is a light energized proton pump, embedded in the purple membrane of the photosynthetic Halobacterium. The absorbing chromophore is a retinal molecule covalently linked to the protein. Early in the BR photocycle, the retinal selectively isomerizes from *all-trans* to the *13-cis* form, and the protein undergoes a series of structural changes leading to ejection of one proton from the cytoplasm. Previous studies have demonstrated that photon absorption leads to the appearance of a fluorescent state coined (I_{460}) exhibiting stimulated emission and excited state absorption bands peaking at 850 and 460 nm respectively. These features decay concertedly within ~1 psec, to form a red shifted intermediate coined "J", thought to be in the ground electronic state. Fundamental questions concerning excited state dynamics in BR remain unresolved. Resonance Raman spectroscopy shows that numerous retinal degrees of freedom are activated by BR photoexcitation aside from double bond torsion – particularly double bond stretches[1]. Mounting evidence suggests that the decay of I_{460} reflects the stage of retinal isomerization / internal conversion (IC)[2], yet remarkably it is accompanied by negligible spectral evolution, and the contours of transient absorption changes reveal little of the underlying structural changes.

Vibrational spectroscopies such as transient Raman or IR can provide multimode structural information concerning short lived intermediates, but in the case of BR have not clarified the questions above[3]. An alternative based upon stimulated Raman probing with ultrafast time resolution has been employed to study excited state dynamics in retinal proteins[4]. Here early photoinduced BR dynamics are covered with impulsive vibrational spectroscopy (IVS). The wave packets formed along the active vibrations in both the ground and excited states evolve and can be read out as modulations in probe transmission, and through their delineation, excited state dynamics can be deduced. Low frequency spectral modulations (~160 cm^{-1}) observed in I_{460} stimulated emission have been assigned to excited state coherent torsions[5]. However, coverage of all relevant frequencies requires sub 10 fsec time resolution. Two previous studies by Shank, Mathies, and coworkers[6] and more recently by the Kobayashi lab[7] have led to conflicting interpretations concerning the source of modulation. Here we investigate BR and its isolated chromophore the retinal protonated Schiff base (RPSB) with ~6 fsec IVS to separate S_0 and S_1 coherences, and from them understand photon energy storage in BR.

Experiments were conducted with a one stage NOPA peaking at ~550 nm, and ranging from 500 to 700 nm. Compression was performed with a deformable mirror pulse shaper, and verified by polarization FROG. Pump and probe were derived from the NOPA and the later were either interference filtered, detected in silicone photodiodes, and averaged either in a lock in amplifier for BR data, or dispersed in a CCD spectrometer in the case of RPSB. The results for BR at five probing wavelengths above and below the peak absorption are shown in figure 1. The inset to panel B depicts a typical pulse spectrum along with the absorption spectrum of BR. The signals at 540, 570, and 600 nm all show an enhanced transmission since this range is dominated by ground state bleach. Probe wavelengths farther to the red are

increasingly influenced by excited state absorption and exhibit shallower ΔOD. Superimposed on all the signals are rapid intensity modulations that observably decay within the depicted first 1.5 psec of pump-probe delay.
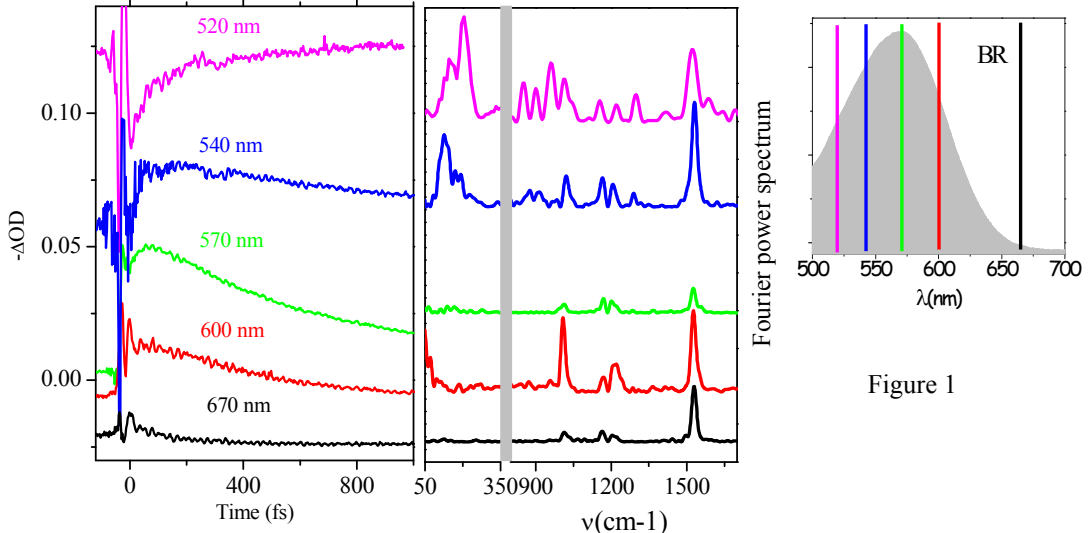
Figure 1

Once subtracted from the slower background, DFT power spectra of these modulations over the first 2 psec of delay are shown in panel B. Three spectral features are observable in all – two prominent peaks at 1530 and 1008 cm^{-1}, along with a doublet centered at 1180cm^{-1}. The former two are assigned to C=C stretching and methyl rocking respectively, while the doublet falls in the C-C stretching frequency range. These are precisely the features presented by Dexheimer et.al[6]., and resemble the BR Raman peaks both in central frequency and in line widths. Contrary to that early report, all of these features are weakest when probed at the peak of the ground state absorption (570 nm) and increase in amplitude for probing wavelengths above and below. To aid in the assignment of the observed spectral features to S_0 or

Figure 2

S_1, results of excitation with pulses positively and negatively chirped pulses were compared with the data above, as shown in figure 2. Clearly the modulations observed with transform limited excitation pulses is strongly accentuated with negative chirp, but almost washed out with a frequency sweep in the opposite direction.
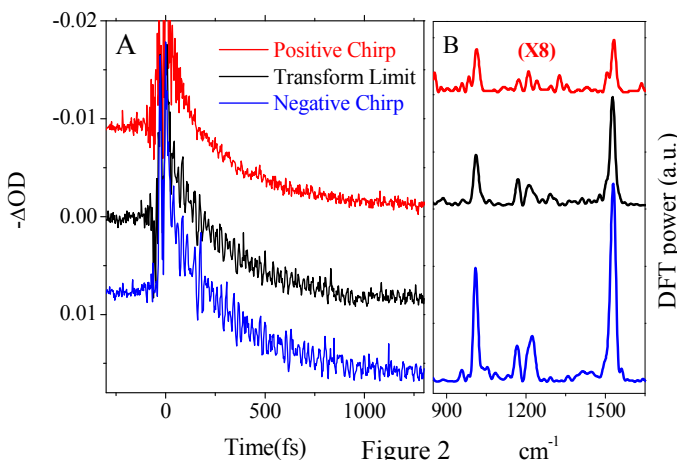
Fourier analysis of the resulting spectral modulations demonstrate that transient transmission at dispersed probe wavelengths $\lambda_{probe} \geq 570$ nm are predominantly influenced by RISRS induced ground state vibrational coherences[8]. This conclusion is based upon the frequencies of spectral modulations, their decay rates, and the variation in their amplitudes with shifts in the dispersed probing wavelength. It is bolstered by linear chirp effects in the pump pulse on the amplitudes and spectra of the observed modulations[9]. At probing wavelengths of 540 and 520 nm new vibrational features were observed consisting of high and low frequency shoulders adjacent to the strong C=C stretching and methyl

rock modes respectively, which have ground state frequencies of 1008 and 1530 cm^{-1}, a strong mode at 1290 cm^{-1}, and brief activity centered at ~900 cm^{-1} which is characteristic of ground state HOOP vibrational modes. Along with the variations at the high frequency end, activity below 200 cm^{-1} also appears only in this range. Since 540 nm is the red edge of an intense absorption band assigned to the reactive excited state, these new features are tentatively assigned to wavepacket motions along excited state displaced normal vibrational coordinates. While the shoulders may reflect mild frequency variations of the active vibrations in the excited state, the HOOP mode activity is not easily explained in view of the inactivity of these modes in the resonance Raman spectrum. It is intriguing since motions along these coordinates have been implicated in the IC reaction coordinates of rhodopsin[10], and also of BR[11].

While the onset of steep excited state absorption is a plausible explanation of the abrupt change in IVS below 540nm, the extensive overlap of S_0 and S_1 bands in BR over the probed spectral range casts doubts on this assertion. To clarify this, a closely related model system suffering less from such overlap, the retinal protonated Schiff base (RPSB) in solution, was addressed. Before IVS experiments, a broadband multichannel pump-probe experiment was conducted on this system. Our objectives were to uncover kinetic signatures of conformational inhomogeneity in the reactants, and also to discover where the analogous RPSB excited state absorption band is centered. Previous studies show that excited RPSB absorbs intensely just below the ground state absorption in photon energy – appearing to peak at 500 nm[12]. Whether that absorption involved the levels giving rise to the 460 nm band in BR or that

Figure 3

centered at ~720 nm which partially cancels the stimulated emission was unclear. The figure to the left gives transient spectra collected at various pump-probe delays following 400nm irradiation. The prominent absorption feature referred to, and the ground state bleach above, are clearly discernable, as is the excited state emission to the red of 600 nm. The choice of this model is also apparent, as S_0 absorption overlaps only the blue edge of the NOPA spectrum. The inset compares RPSB absorption in ethanol with that of BR, and demonstrates the large discrepancy in absorption widths of the two. The data also indicate for the first time that stimulated emission extends deep into the near IR (NIR), and exhibits a double humped structure with a minimum near 770 nm. Concentrating here on the absorption features, we assign the double humped emission to an overlapping low energy absorption band as in BR, identifying peak at 500 nm as the analogue of I_{460}'s intense absorption at the onset of which the modulation spectrum changed abruptly.
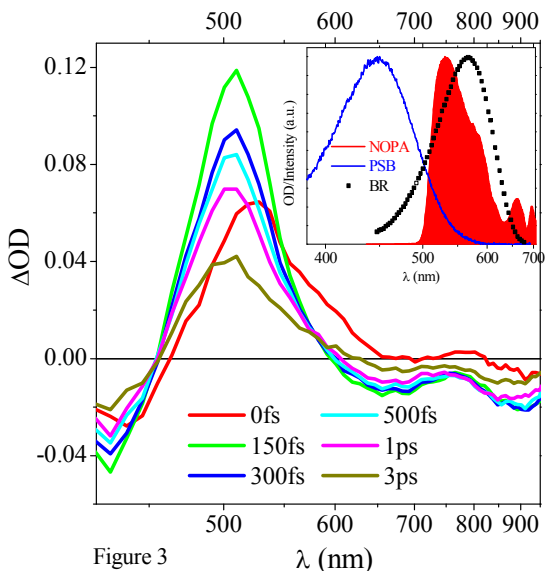
The RPSB solution was then subjected to degenerate NOPA pump–probe investigation, after spectral tuning to the blue so as to enhance spectral overlap with S_0 absorption in RPSB. Probe and reference pulses were collected in a multi-track fiber bundle and dispersed in an imaging CCD spectrograph providing a full $\Delta OD(t,\omega)$ record. A 2 dimensional cut at 630 with Fourier analysis is presented in figure 4. Aside from the long lived solvent vibrations designated by asterisks, the

clearest RPSB peaks are the broad low frequency activity centered at ~190 cm^{-1}, and a relatively short lived intense peak at 1560 cm^{-1}. The former resembles the low frequency activity reported in figure 1 below 540 nm, and assigned to torsional coherences in BR excited state[5]. The latter poses a challenge of interpretation. Its central frequency matches that of the symmetric C=C stretching mode in ground state RPSB to within 2 cm^{-1}, but its lifetime is more than twice too short. Lines in the power FFT should match in width to the same features measured with Raman spectroscopy, and indeed such a match is found for the solvent features collected in the same data. It stands to reason therefore that we are measuring, at least in part, excited state vibrational dynamics, and therefore that in the RPSB the C=C symmetric stretching vibration has nearly the same central frequency in S_0 and S_1. The fact that this feature is discernable deep into the red with respect to ground state absorption bolsters this view. These encouraging preliminary results suggest that the IVS of RPSB will allow us to perfect our methods of separating excited and ground state activity, and allow us to appreciate how primary events in BR are reflected IVS modulation spectra.
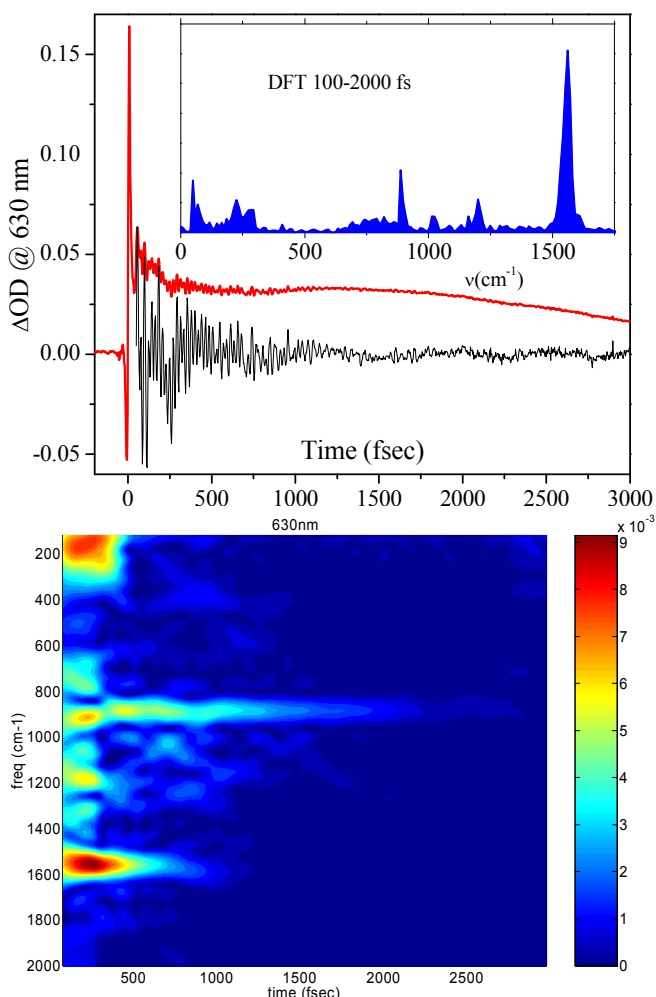
[1] A. B. Myers, R. A. Harris, R. A. Mathies, *J. Chem. Phys.,***79**,60 (1983).

[2] T. Ye, N. Friedman, Y. Gat, G. H. Atkinson, M. Sheves, M. Ottolenghi, S. Ruhman, , *J. Phys. Chem. B*, **103**, 5122 (1999).

[3] J. Herbst, K. Heyne, R. Diller, *Science* **297**, 823 (2002).

[4] D. W. McCamant, P. Kukura, R. A. Mathies, *J. Phys. Chem. B*, **109**, 10449 (2005).

[5] B. Hou, N. Friedman, M. Ottolenghi, M. Sheves , S. Ruhman, *Chem. Phys. Lett.*, **381**, 549 (2003).

[6] Pollard, W.T.; Dexheimer, S.L.; Wang, Q.; Peteanu, L.A.; Shank, C.V.; Mathies, R.A. *J. Phys. Chem.* **96**, 6147(1992).

[7] T. Kobayashi, T. Saito, H. Ohtani, *Nature*, **414**, 531 (2001).

[8] A.Kahan, O. Nahmias, N. Friedman, M. Sheves, S. Ruhman, JACS. 129 (2007) 537.

[9] Lanzani, G.; Zavelani-Rossi, M.; , G.; Comoretto, D.; Dellepiane, G. *Phys. Rev. B* **2004**, *69*, 134302; Malkmus, S.; Du1rr, R.; Sobotta, C.; Pulvermacher, H.; Zinth, W.; Braun, M. *J. Phys. Chem. A* **2005**, *109*, 10488.

[10] P. Kukura, D. W. McCamant, S. Yoon, D. B. Wandschneider, R. A. Mathies, *Science*, **310**, 1006 (2005).

[11] A. C. Terentis, L. Ujj, H. Abramczyk, G. H. Atkinson, *Chemical Physics,* **313**, 51 (2005).

[12] P. Hamm, M. Zurek ,T. Roschinger ,H. Patzelt, D. Oesterhelt, W. Zinth, Chem.Phys.Lett. 263 (1996) 613.

A setup for time-resolved step-scan spectroscopy of samples with irreversible photo reaction: first results on rhodopsin

D. Winter and F. Siebert

Daniel Winter and Friedrich Siebert, Institut für Molekulare Medizin und Zellforschung, Hermann Herder Str. 9, Albert-Ludwigs-Universität Freiburg, 79104 Freiburg, email: daniel.winter@biophysik.uni-freiburg.de

The method of step-scan FTIR spectroscopy has been developed over 15 years ago[1]. It combines the excellent signal to noise ratio of FTIR measurements with a time resolution of nano seconds. To achieve this, the movable mirror of the spectrometers' Michelson interferometer is not moving continuously back and forth. Instead it is capable of performing a step-wise movement. As usual, the IR radiation from the interferometer is guided through the sample and focused onto the MCT detector. Two transient recorder cards measure the reaction-induced changes of the IR light intensity (i.e. changes of the interferogram) with a sampling rate of up to 200 MHz. After a transient is recorded the movable interferometer mirror is moved stepwise to the next position as determined by the Nyquist theorem. At each position another transient data set is taken. 540 mirror positions with a step-spacing of 4*633 nm are needed to cover the IR interferogram for the spectral range up to 1975 cm^{-1} with a spectral resolution of 8 cm^{-1}. Finally, Fourier transformation of the difference interferogram and of the static interferogram renders difference absorbance spectra for each time slice the transient recorders have measured after the reaction was triggered.

Step-scan spectroscopy has been successfully applied to a variety of photoactive systems in the past. All these samples have one property in common: the photoreaction is reversible, i.e. the system undergoes a photo-cycle after light excitation. In order to obtain a sufficient signal to noise ratio the sample is excited and measured several times at each fixed mirror position and signal averaging is performed. The same sample is usually excited at least 5000 times for one single step scan measurement to be complete. These experiments can only be performed with samples that show the same reaction kinetics even after 5000 flash excitations.

One possibility to overcome the limitation of reversible systems is the replacement of the sample after each excitation. A setup with a micro-illuminator and an x-y translation stage has been described, including test measurements on ATP hydrolysis[2]. It is clear that larger amounts of protein are required.

In order to reduce the protein quantity, one has to balance the number of triggering events against the loss in IR intensity. A satisfactory compromise is a micro-illuminator based on parabolic mirrors with a focus of 1 mm, and a sample area of 7 cm^2 which is scanned via an
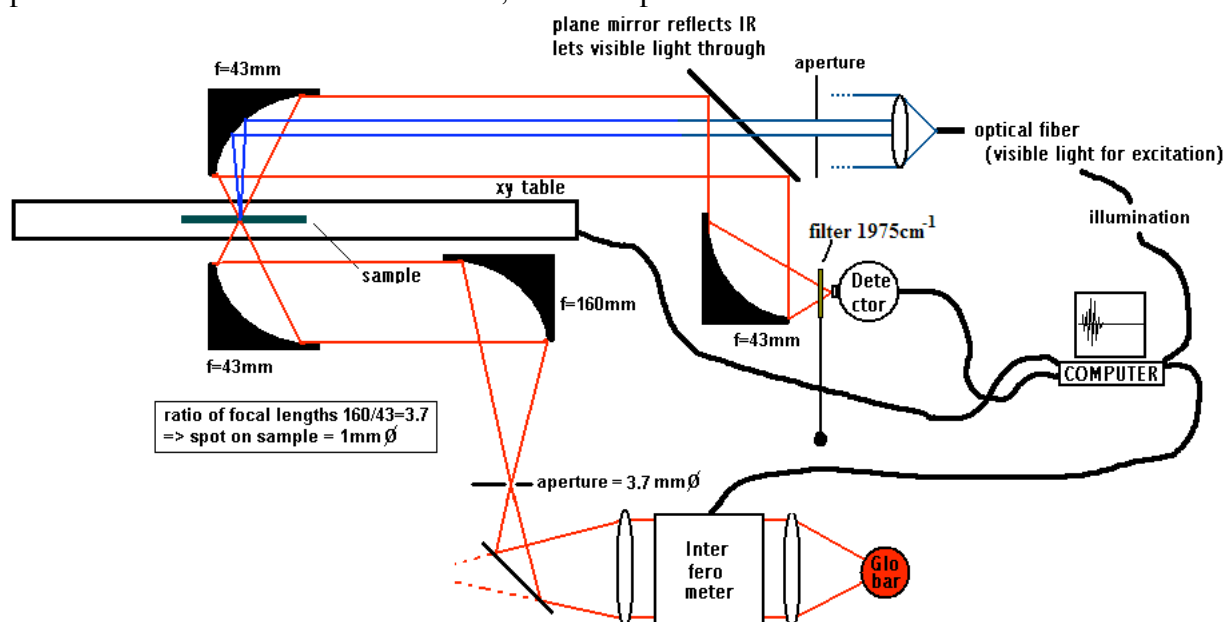
Figure 1: Schematic setup for step-scan FTIR spectroscopy of irreversible photo reactive samples

xy translation table. With this arrangement, the number of possible sample excitations is somewhat larger than the minimum number of sampling positions required for one complete step-scan measurement. See figure 1 for a schematic of the this setup.

The success of the new method is demonstrated for the case of the visual pigment rhodopsin which bleaches irreversibly after excitation. The complete step-scan measurement procedure is performed and coordinated by self-developed software. A self-made high precision automatic offset correction device subtracts the background IR intensity from the signal before each scan is performed. The tool enables dc amplification of the signal. Approx. 20 nMol of rhodopsin are required to cover the 7 cm^2 sample area. In order to improve the quality of the spectra, the laser flash induced signals are corrected for variations in flash energy. Also changes in protein concentration at all sample positions are measured with the conventional opus software and the flash-induced signals are corrected for. The noise in the spectra is further reduced by averaging 16 measurements. The 3D image shown in figure 2 shows the rhodopsin
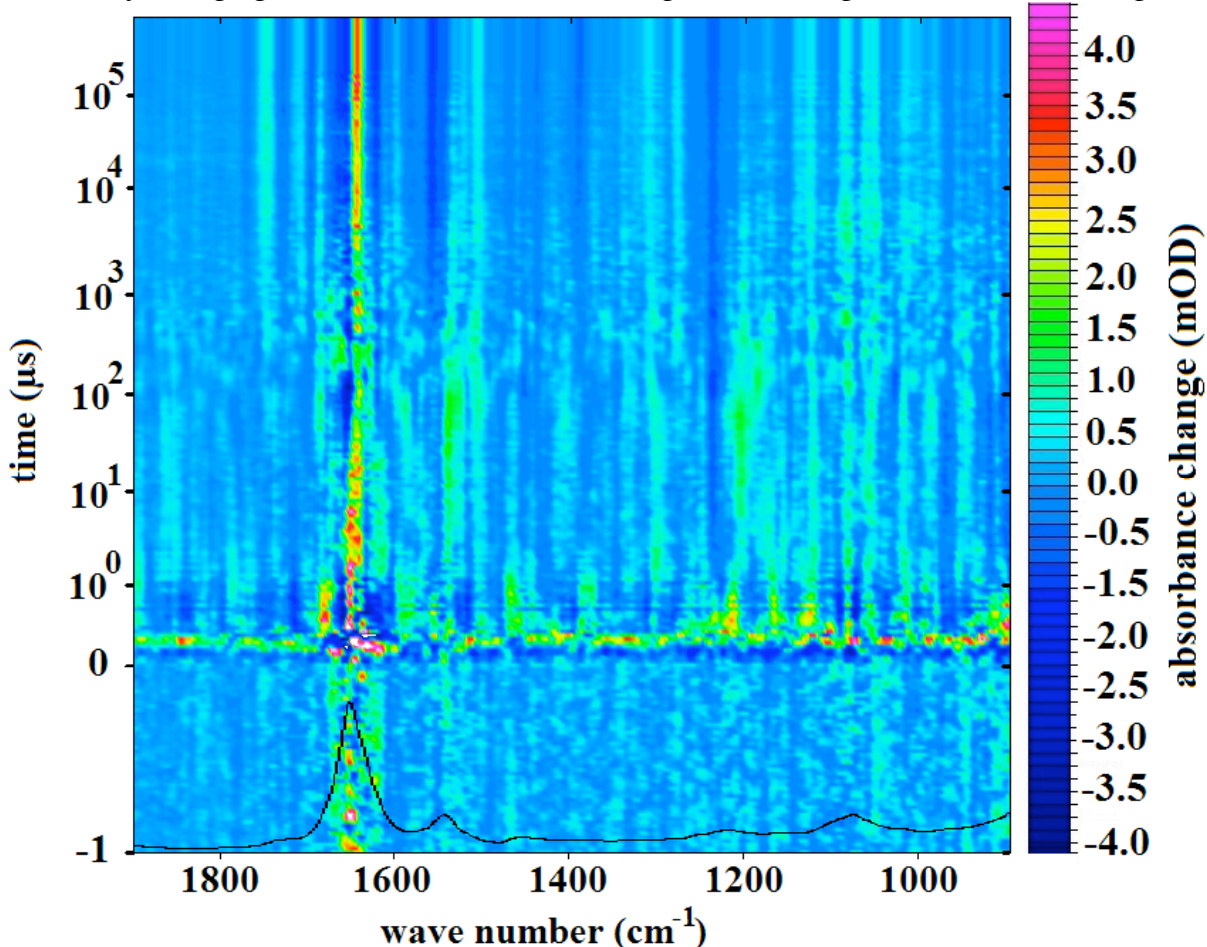
Figure 2: Average of 16 step-scan measurements on rhodopsin, 20 °C, pH 5.

kinetics for the spectrum between 900 – 1900 cm^{-1} and between 1 μs before and 629 ms after flash excitation of the sample spots at 480 nm. The color bar at the side denotes the absorbance change amplitudes in mOD. The graph shows the first time-resolved measurements of rhodopsin in the infrared covering the μs to ms time regime at ambient temperature. The absorbance changes due to the formation of the intermediate states lumi, meta I and meta II can be clearly identified. The spectral region > 1800 cm^{-1} is a reference for the noise since no absorption changes are expected for this region. The noise level is quite substantial before 1 ms which has to be taken into account when interpreting the results. The spectral distribution of the noise is indicated by the black line superimposed on the pretrigger time range. It is based on the inverse of the IR transmission spectrum through the sample. Between 0 to 1 μs the spectra are heavily distorted by laser-induced rf noise in the amplification system. Around 1 ms mirror fluctuations cause baseline distortions and after 10 ms a 50 Hz noise caused by the power

supply of the preamplifier is seen.

Despite of the high noise level the spectral features of the intermediates lumi, meat I and meta II can be readily identified. The average spectra of certain time slices reveal the intermediate states by comparison with temperature stabilized spectra[3], see figure 3.
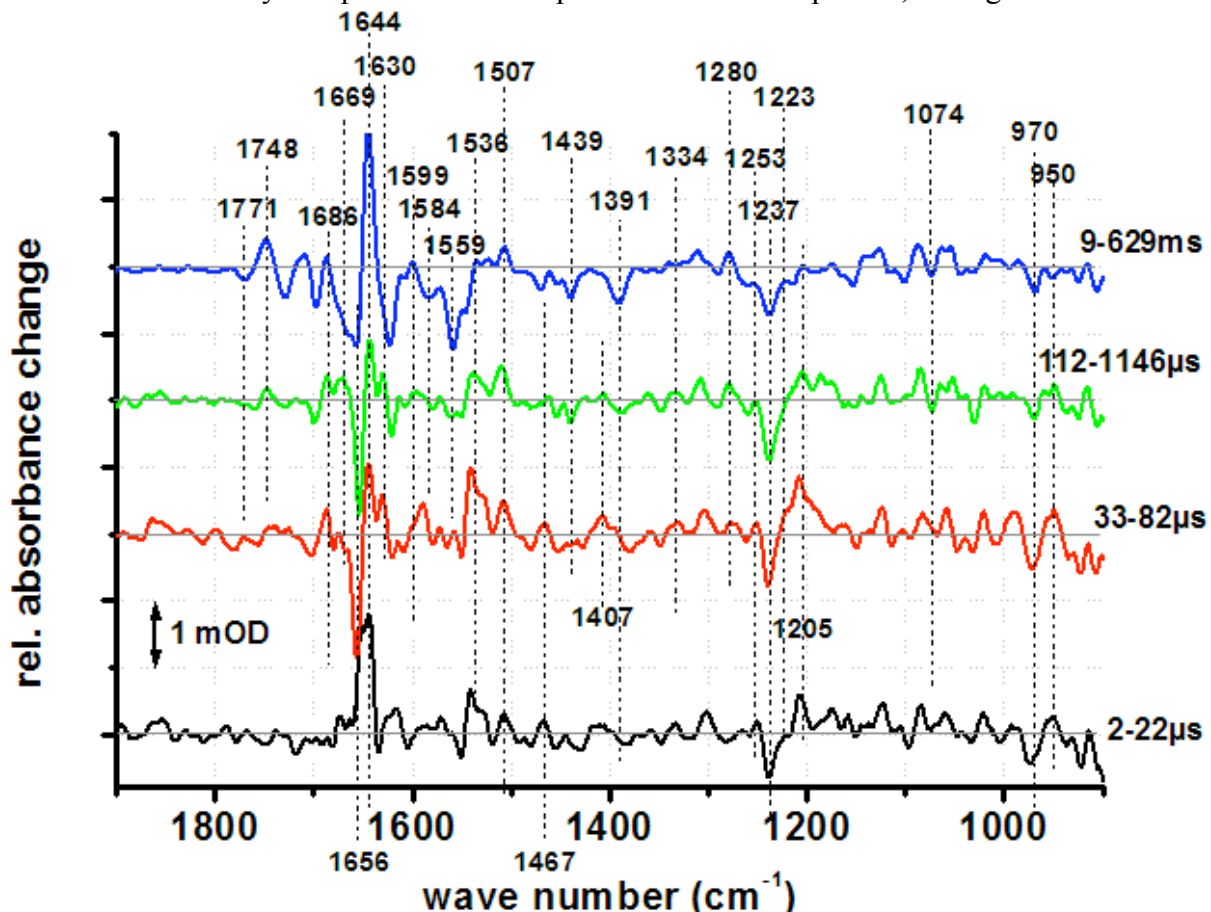
Figure 3: Intermediate state formation within the specified time windows belonging to figure 2.

The spectrum from 2 – 22 µs remains uncharacterized. At this early time the noise influence is very large. The spectrum resembles a mixture of the batho and lumi intermediates. From 3 – 82 µs the lumi intermediate is seen. Most characterizing for the meta I state is the peak at 1669 cm^{-1} showing up from 112 to 1146 µs. The meta II spectrum for the time after 9 ms is an almost perfect reproduction of the temperature stabilized spectrum and proves the functioning of the developed measurement method.

Time slices of certain spectral regions are also analyzed. Very interesting is the transition of lumi to meta I as it seems to occur earlier in the fingerprint region around 1219 cm^{-1} than in the amide I region at 1665 cm^{-1}.

The found transition times of 60 -120 µs for lumi – meta I and 5 – 12 ms for the meta I – meta II transition are in agreement with time-resolved UV-vis absorption measurments[4]. The number of spectra available for averaging has to be increased to 60 – 80 in order to get a sufficiently good signal to noise ratio before further interpretations become possible.

1:   W. Uhmann, A. Becker, C. Taran, F. Siebert, Applied Spectroscopy, **1991**, <u>45</u>, 390-397
2:   R. Rammelsberg, S. Boulas, H. Chorongiewski, K. Gerwert, Vibrational Spectroscopy, **1999**, <u>19</u>, 143-149
3:   F. Siebert, Israel Journal of Chemitry, **1995**, <u>35</u>, 309-323
4:   I. Szundi, J. W. Lewis, D. S. Kliger, Biophysical Journal, **1997**, <u>73</u>, 688 - 702

Save and submit your contribution as a pdf-file. Do not forget to embed the fonts in your file (If you have any doubt about the quality of your pdf-file, please also submit the doc-file). Please send your contribution to

trvsxiii@physik.uni-muenchen.de

The deadline for the submission of your contribution is **June 25th, 2007**.

The proceedings will be posted on the web server of the LMU München as a searchable document.

Ultrafast infrared spectroscopy of a versatile nanomachinery:

Photoinduced processes in retinal proteins

R. Groß[1], R. Diller[1], C. Schumann[1], M. Wolf[1], O. Trentmann[2], E. Neuhaus[2], J.P. Klare[3], M. Engelhard[3], J. Tittor[4]

[1] Fachbereich Physik, Technische Universität Kaiserslautern, Erwin-Schrödinger-Straße, 67663 Kaiserslautern, Germany. [2] Fachbereich Biologie, Technische Universität Kaiserslautern, Erwin-Schrödinger-Straße, 67663 Kaiserslautern, Germany. [3] Max-Planck-Institut für Molekulare Physiologie, Otto-Hahn-Straße 11, 44227 Dortmund, Germany. [4] Max-Planck-Institut für Biochemie, Am Klopferspitz 18, 82152 Martinsried, Germany. diller@physik.uni-kl.de

Protein function is often mediated by protein conformational changes. Systems incorporating an intrinsic chromophore which excerts a perturbation on the protein upon photoexcitation offer the opportunity to study ultrafast protein dynamics. Important prototypes in this regard are proteins exhibiting cis-trans photoisomerization of a bound cofactor, as e.g. bilin binding phytochromes and retinal binding proteins. Here, the steric part of the perturbation is realized by the torsional movement of the isomerizing chromophore moiety. Prominent examples are the primary photoreactions of bilin-binding phytochromes (cp. contribution by C. Schumann et al. in this volume) and of retinal proteins.

Bacteriorhodopsin (BR), halorhodopsin (HR), sensory rhodopsin I and II (SRI/II) are transmembrane proteins in archaeal organisms, e.g. *Halobacterium salinarum*. BR is a light driven outward proton pump, HR acts as an inward chloride pump and SRI and II are photoreceptors that enable the organisms to avoid harmful light conditions. The retinal chromophore in its all-trans configuration (Fig. 1) binds via a protonated Schiff base to the ε-amino group of a lysine residue in the G-helix. Whereas the primary, light induced all-trans to 13-cis isomerization reaction occurs within a few picoseconds, the respective photocycles are completed on the time scale of up to hundreds of milliseconds via a series of thermally activated intermediate states. Thereby, the photoreaction is coupled to protein conformational changes and to the specific biological function.
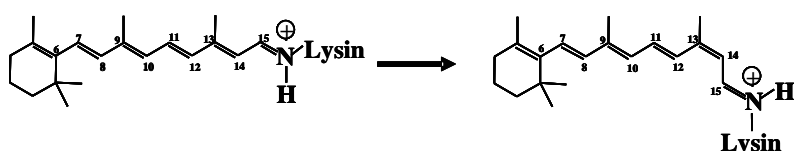
Fig.1: All-trans to 13-cis isomerization of the retinal chromophore in SR, HR and BR.

Sub-picosecond time resolved infrared (IR) spectroscopy has revealed the chromophore vibrational dynamics along the retinal isomerization reaction in BR[1] and HR[2] and recently in SRII (*Natronomonas pharaonis*)[3]. Fig. 2a shows absorbance transients of SRII in the visible (VIS) using a hydrated protein film on a CaF$_2$ window. They reproduced the time constants observed earlier using a sample of protein suspension[4], proving the integrity of the sample. Fig. 2b,c show selected absorbance transients in the fingerprint (C-C - stretch) region and decay associated spectra (DAS) of a global analysis in this region, using a sum of exponentials as a fit function. Corresponding datasets were obtained for the ethylenic (C=C) stretch - and the Schiff-base (C=NH) stretch region. A reaction scheme was suggested[3,4] very

[1] J. Herbst, K. Heyne, R. Diller, Science **2002,** 297, 822-825
[2] F. Peters, J. Herbst, J. Tittor, D. Oesterhelt, R. Diller, Chem. Phys., **2006,** 323, 109-116
[3] R. Diller, R. Jakober, C. Schumann, F. Peters, J.P. Klare, M. Engelhard, Biopolymers **2006,** 82, 358-362
[4] I. Lutz, A. Sieg, A. A. Wegener, M Engelhard, I. Boche, M. Otsuka, D. Oesterhelt, J. Wachtveitl, W. Zinth, Proc. Natl. Acad. Sci. USA **2001,** 98, 965-967

similar to that of BR, i.e. a branching reaction from the S_1-state, with one channel repopulating the all-trans ground state and the second channel leading to the isomerized 13-cis ground state with a time constant of 0.5 ps, followed by energy and conformational relaxation of the chromophore within ca. 4 ps (Fig.3).
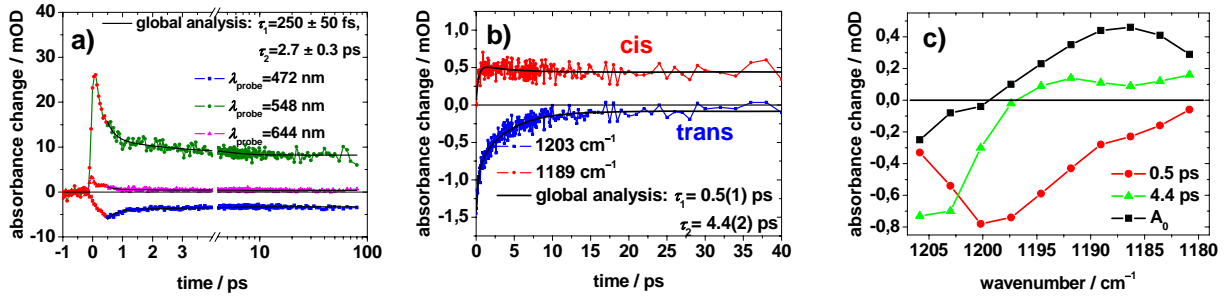
Fig. 2: a) Absorption transients in the visible; b) Absorption transients at marker bands for all-trans- and 13-cis-retinal in the fingerprint region; c) DAS of a global analysis in the fingerprint region.
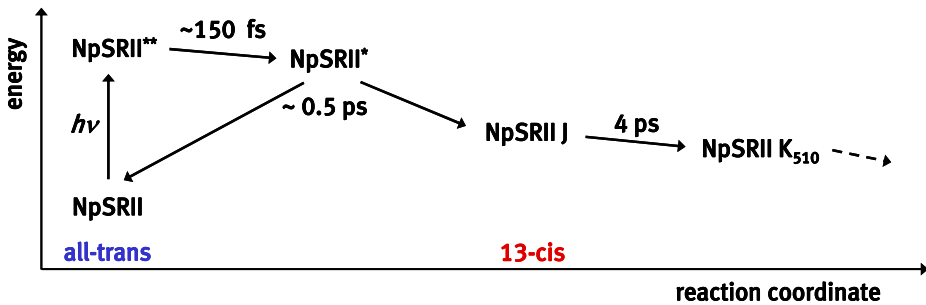
Fig. 3: Suggested reaction scheme corresponding to data from the visible and IR transient spectra.

In addition to these kinetic components that are observed similarly in analogous transient absorption spectra in the visible[4], IR transient spectra of SRII in the amide II region show a slow component, i.e. a DAS of ca. 12 ps (Fig. 4).
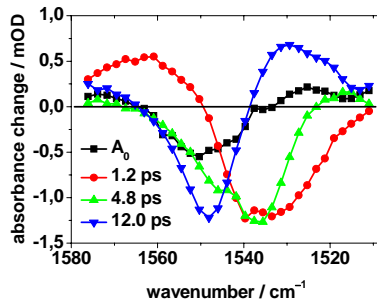
Fig. 4: DAS in the ethylenic stretch region in D_2O buffer showing a large amplitude of the 12 ps time constant.

It consists of a negative lobe at around 1550 cm^{-1} and a positive lobe at around 1539 cm^{-1} and partly overlaps with the DAS describing the (known) chromophore dynamics. A similar slow kinetic component is observed around 1660 cm^{-1} in the amide I region of SRII as well as in specific parts of the amide I & II region of BR and HR (Fig. 5). Upon H_2O/D_2O - exchange of the sample buffer, in the amide II region of SRII no changes of the slow kinetics are observed (Fig.4 and DAS in H_2O, data not shown). In the amide I region of BR and SRII,

as expected, the C=NH - stretch vibration shifts down from 1640 cm^{-1} to 1627 cm^{-1} in BR and from about 1650 cm^{-1} to 1630 cm^{-1} in SRII. However, the slow component around 1660 cm^{-1} disappears in D$_2$O in both BR and SRII (Fig. 5a and Fig. 6). Since the C=NH-stretch is the chromophore mode with highest frequency in this region, the participating modes must be assigned to protein vibrations or the bending vibration of protein bound water molecules. Note, that in contrast to BR in SRII a bleach signal remains at 1660 cm^{-1}, whereas in BR a positive band appears.
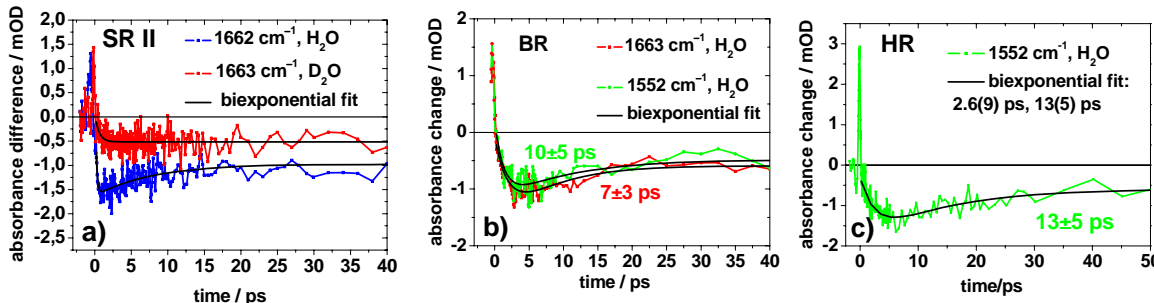
Fig. 5: Absorption transients in specific parts of the amide I and II region of a) SRII, b) BR and c) HR showing a slow kinetic component.
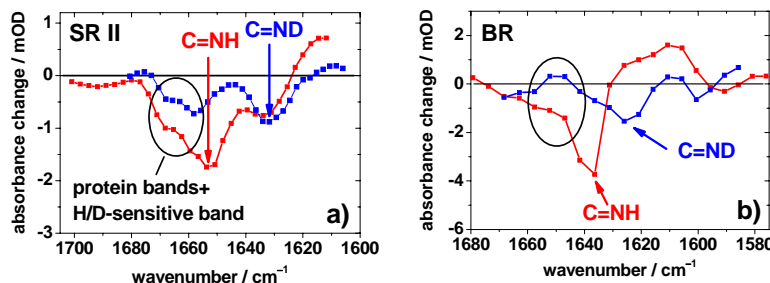
Fig. 6: Absorption difference spectra at 12 ps of a) SRII and b) BR in H$_2$O and D$_2$O buffer in the amide I region.

These observations concerning protein contributions in the transient IR spectra can be related to results on the same subject obtained by other methods. First, fast FTIR-experiments (30-100 ns time resolution) of the K-state of SRII (H$_2$O/D$_2$O) suggested a larger distortion of the protein backbone as compared to BR[5]. Second, a low-temperature FTIR study on stretching modes of protein bound water molecules in the K-state of SRII revealed a considerable distortion of the pentagonal water cluster in the Schiff-base region of the chromophore[6]. Third, the X-ray structure of the SRII ground state and the K-state revealed the rearrangement of both the amino acids forming the retinal binding pocket and of the water cluster as well as the formation of disordered water molecules[7].

In summary, in addition to those kinetic components that reflect processes observable in transient VIS experiments, the IR experiments reveal additional dynamics in the amide I and II region of BR, HR and SRII. These signals appear rapidly on the time scale of the isomerization and decay partly with a time constant between 8 and 13 ps. The H/D effect observed implies that a mode with an exchangeable proton must be involved. The results strongly suggest ultrafast protein response to the isomerization in retinal proteins.

[5] M. Hein, A. A. Wegener, M. Engelhard, F. Siebert, Biophys. J., **2003**, *84*, 1208-1217

[6] M. Shibata, H. Kandori , Biochem., **2005**, *44*, 7406-7413

[7] R. Moukhametzianov, J. P. Klare, R. Efremov, C. Baeken, A. Göppner, J. Labahn, M. Engelhard, G. Büldt, V. I. Gordeliy, Nature, **2006**, *440*, 115-119

Events in the Photocycle of Proteorhodopsin: an Infrared Study

M.-K. Verhoefen , K. Neumann[1], I. Weber[2], C. Glaubitz[2] and J. Wachtveitl[1]

[1] Institut für Physikalische und Theoretische Chemie, Johann Wolfgang Goethe-Universität Frankfurt, Max-von-Laue-Straße 7, 60438 Frankfurt, Germany. [2] Institut für Biophysikalische Chemie, Johann Wolfgang Goethe-Universität, Max-von-Laue-Straße 9, 60438 Frankfurt, Germany. wveitl@theochem.uni-frankfurt.de http://www.theochem.uni-frankfurt.de/femtochem

Proteorhodopsin (PR) is a new member of the type I retinal binding protein family[1] and was suggested to function as a light-driven ion-pump. Upon excitation the protein undergoes a photocycle with a series of distinguishable intermediates similar to that of bacteriorhodopsin (BR)[2]. Measurements of the pumping activity via BLM techniques showed that the pumping direction can be inverted by lowering the pH. However, the issue of variable vectoriality is still under discussion, since the inversion of H^+ pumping could not be confirmed by photocurrent measurements of oriented membranes[3]. For BR it was demonstrated that the control of the deprotonation and reprotonation steps during the photocycle are important for the overall pumping activity of the protein.

To gain information about the vectoriality of the photocycle, low temperature difference spectroscopy at pH 9, 7, 5 and 4 was performed similar to protocols reported before for PR[4] or BR[5]. Spectra were taken both in the IR (1300 cm^{-1} – 1900 cm^{-1}) and the UV-visible range (380 nm – 650 nm).
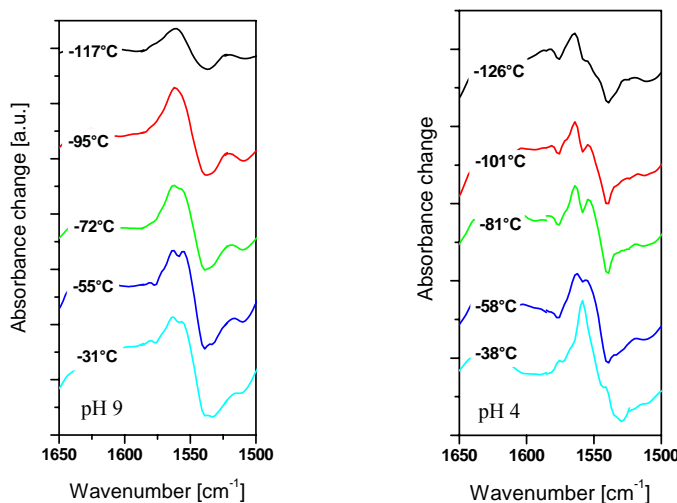
Figure 1: IR difference spectra of PR at pH 9 (left) and pH 4 (right), respectively.

Under alkaline conditions we observed three different intermediates being in equilibrium with each other. The first difference signal belongs to the K intermediate also observed in ultrafast spectroscopy. The evolution of several marker bands (1756 cm^{-1}, 1742 cm^{-1}, 1555 cm^{-1}, 1541 cm^{-1} and 1516 cm^{-1}) represents the conversion to M. With rising temperatures, the appearance of a signal at 1556 cm^{-1} is assigned to the formation of a later intermediate. Under acidic conditions the spectral characteristics of the same three intermediates could be identified, however with different temperature characteristics than for pH 9. In contrast to kinetic studies[2,6,7] the M intermediate could be clearly observed in these cryo trapping experiments. Low temperature experiments thus prove as useful tool to unravel spectroscopically silent photocycle intermediates. The appearance of a M intermediate at acidic conditions is a further indication of the variable vectoriality of PR.

Further on, we studied the primary dynamics of PR via ultrashort vis-pump infrared-probe spectroscopy by monitoring the marker bands between 1500 cm^{-1} and 1580 cm^{-1}, which correspond to C=C stretching vibrations reflecting the π-electron delocalization in the polyene part, and between 1590 cm^{-1} and 1680 cm^{-1}, which is the region of the C=N stretching vibrations. This mode is sensitive to the environment of the Schiff base linkage between the chromophore and the lysine[8]. Figure 2 indicates that the spectral positions of the difference bands are almost equal for pD 9.2 and pD 6.4. Interestingly, the temporal evolution of the difference bands does not exhibit a significant difference between the pD 6.4 and pD 9.2 sample. Looking in detail at the bands in the C=C stretching region, directly after excitation two pronounced bands appear at 1540 cm^{-1} (-) and at 1510 cm^{-1} (+). The negative band at 1540 cm^{-1} is assigned to the depopulation of the C=C stretching vibration of the ground state PR. The positive band in the region of 1500 cm^{-1} to 1530 cm^{-1} can be attributed to the C=C stretching vibrations of vibrationally excited molecules in the S_1 and in the S_0 state. The spectra at long delay times indicate the formation of the J and K intermediate, respectively.
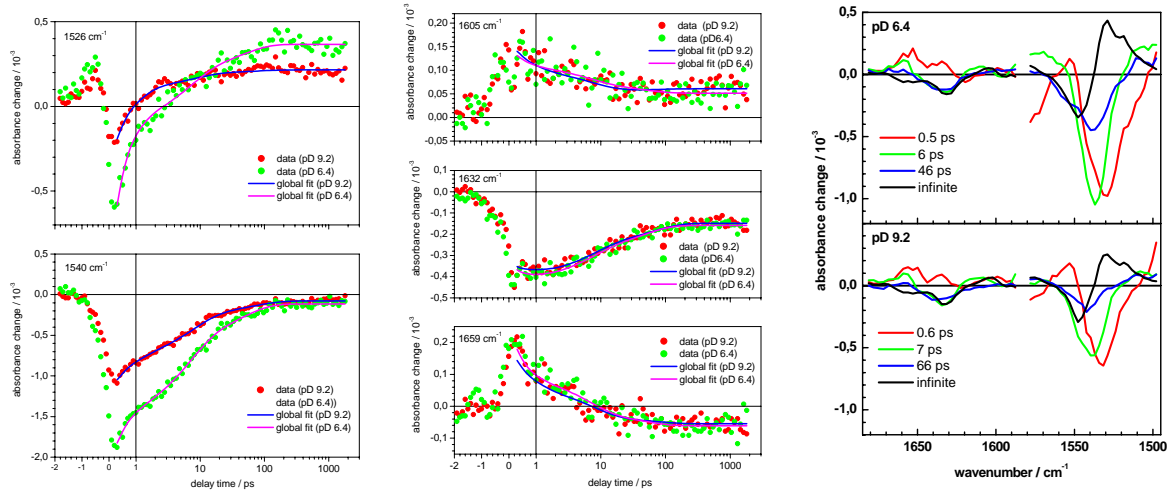
Figure 2: Left and middle: Transients displaying the temporal evolution of the C=C stretching and the C=N stretching vibration. Right: DAS of the global fit analysis of PR at pD 6.4 and PR at pD 9.2 in the mid-IR spectral range.

Analyzing the data using a global fit procedure shows that four decay time constants were necessary for an optimal fitting of all channels. The decay associated spectra (DAS) of the short time constant τ_1 (0.5 ps for pD 6.4 and 0.6 ps for pD 9.2) shows a minimum at 1529 cm^{-1} which is closely related to the formation of the positive band in the DAS of the infinite time constant. This can also be seen in the transient at 1526 cm^{-1}, because this is near the isosbestic point of the instantaneous signals and hence their decay will not obscure this component. The formation of negative contributions is not observable due to the dominant initial bleach of the ground state vibrational bands. The DAS of τ_2 (6 ps for pD 6.4 and 7 ps for pD 9.2) and τ_3 (46 ps for pD 6.4 and 66 ps for pD 9.2) exhibit a band around 1540 cm^{-1} (-). Their spectral position and shape is very similar to the transient spectra observed immediately after excitation, where the negative signal represents the instantaneous bleach of ground state vibrations due to the $S_0 \rightarrow S_1$ transition. We can therefore assign these time constants to a biphasic recovery of the PR ground state vibrations. The most prominent signals in the spectral region of the C=N stretching vibration are a strong negative band at 1632 cm^{-1} and a smaller positive band at around 1605 cm^{-1}. Around 1660 cm^{-1} a positive band decays and turns into a negative contribution within 20 ps. Following the band

assignment for PR , the positive band observed at long delay times around 1600 cm^{-1} should represent a contribution of the K intermediate. The DAS can be interpreted as follows: the infinite time constant mainly represents the contribution of the K-state, as monitored by other methods. The inverted amplitude of the shortest time (τ_1) indicates, that this process is related to the formation of the photoproduct. As in the C=C spectral range, τ_2 and τ_3 time constants describe a biphasic recovery of the bleached PR ground state. The negative band appearing at 1660 cm^{-1} at long delay times is assigned as amide I contribution of the protein. Here, the negative contribution at long delay times is clearly resolved in the DAS of the infinite time constant as in the transients. As before, the τ_3 DAS shows a positive amplitude corresponding to a formation of the negative signal. In contrast to the results in the C=N and C=C region, the τ_2 component unambiguously contributes to the formation of this negative signal, whereas the DAS of τ_3 exhibits a small positive amplitude and is therefore hardly contributing to the photoproduct spectrum in this region.

Comparing the results with UV-vis experiments[9,10] one more time constant is needed to fit the data in the mid-IR range accurately. In case of PR steady state FTIR spectra at low temperature conditions show that protonation of Asp97 has almost no influence on the position of the difference bands of C=C stretching and C=N stretching vibrations. These bands therefore seem not to be sensitive for the altered H-bonding pattern or changed electrostatic interactions at different pH values in PR, whereas these differences are clearly seen in other regions. This perfectly fits our finding that in contrast to UV-visible results the reaction rates of pD 9.2 and pD 6.4 sample are equal for C=C stretching and C=N stretching vibration. It shows that the branching into two different reaction pathways is not observed by the vibrational bands examined in this study. The isomerization of the retinal therefore does not have to be directly connected to these vibrations, which is in agreement with fs-IR studies on other retinal proteins. So the energy redistribution after excitation seems not to proceed through C=C stretching and C=N stretching vibrations. This implies that the two main features monitored in this infrared study are no essential coordinates governing the different isomerization pathways in PR at acidic and alkaline pH values.

[1] O.Béjà, L. Aravind, E.V. Koonin, M.T. Suzuki, A. Hadd, L.P. Nguyen, S. Jovanovich, C.M. Gates, R.A. Feldman, J.L. Spudich, E.N. Spudich and E.F. DeLong, Science, **2000**, 289,1902–1906

[2] T. Friedrich, S. Geibel, R. Kalmbach, I. Chizhov, K. Ataka, J. Heberle, M. Engelhard and E. Bamberg, J. Mol. Biol., **2002**, 321,821–838

[3] A.K. Dioumaev, J.M. Wang, Z. Bálint, L.S. Brown, G.Váró and J.K. Lanyi. Biochemistry, **2003**, 42, 6582–6587

[4] V. Bergo, J.J. Amsden, E.N. Spudich, J.L. Spudich, K.J. Rothschild, Biochemistry, **2004**, 43, 9075-9083

[5] F. Siebert, W. Mäntele, Eur. J. Biochem., **1983**, 130, 565-573

[6] M. Lakatos, J.K. Lanyi, J. Szakács and G. Váró, Biophys. J, **2004**, 84, 3252-3256

[7] G.Váró, L.S. Brown, M. Lakatos and J.K. Lanyi, Biophys. J., **2003**, 84, 1202-1207

[8] J. Herbst, K. Heyne, R. Diller, Science, **2002**, 297, 822-825

[9] R. Huber, T. Köhler, M.O. Lenz, E. Bamberg, R. Kalmbach, M. Engelhard and J. Wachtveitl, Biochemistry, **2005**, 44, 1800–1806

[10] M.O. Lenz, R.Huber, B. Schmidt, P. Gilch, E. Bamberg, R. Kalmbach, M. Engelhard and J. Wachtveitl, Biophys. J., **2006**, 91, 255-262

Primary charge separation in PS2 core from *Synechocystis*: a comparison of femtosecond visible/mid-IR pump-probe spectra of wild type and two P$_{680}$ mutants.

M. Di Donato[1], R. O. Cohen[2], B. A. Diner[2], J. Breton[3], R. van Grondelle[1] and

M. L. Groot[1]

[1] Department of Physics, Vrjie Universiteit Amsterdam, de Boelelaan 1081, 1081 HV Amsterdam, The Netherlands. [2] E. I. Du Pont de Nemours & Co, Wilmington, Delaware. [3] CEA Saclay, 91191 Gif-sur-Yvette Cedex, France. E-mail : didonat@few.vu.nl

Photosystem II (PSII) is a pigment-protein complex located in the thylakoid membrane of plants and cyanobacteria, able to convert solar light into electro-chemical energy by promoting a sequence of electron transfer events coupled to proton translocation across the membrane. The PSII core is composed by three main protein-complexes, the two core antennas CP43 and CP47 and the D1D2-Reaction Centre (RC).[1] Absorption of light by the antenna proteins induces fast and multi-exponential intra-antennas energy transfer and energy trapping from the RC. Once the excitation reaches the reaction centre a sequence of electron transfer events occurs, ultimately leading to the formation of a long living charge separated state. On the analogy of non oxygenic bacterial reaction centres, it was initially proposed that the primary donor in PSII would be a special pair of chlorophyll (Chl) molecules, P$_{680}$, which once excited would transfer an electron to a pheophytin (H) molecule, generating the primary radical pair P$_{680}^{+}$H^{-}. Recent time resolved vis-pump/Mid-IR probe experiments performed on isolated RC[2] however showed that charge separation in PSII predominantly starts not from P$_{680}$, but from the monomer chlorophyll B$_A$, located on the D1 protein subunit. The identification of the primary donor was based on the observation that characteristic absorption signals of H^{-} were visible in the spectrum after ~1 ps, while marker bands indicating the formation of P$^{+}_{680}$ only appeared after 6 ps. In this experiment it was however not possible to definitely assign specific absorption bands of B$_A$. In order to further investigate the dynamics of primary charge separation in intact PSII cores and to identify specific infrared signatures of the monomer chlorophyll B$_A$, we have compared the femto-IR pump-probe spectra of the wild type (WT) PS2 core with those of two mutants, in which the histidine residue coordinated to P$_B$ (D2-H197) has been changed to alanine or glutamine. Since the mutated histidine is indirectly H-bonded to B$_A$ through a water molecule, the mutation is expected both to perturb the vibrational properties of B$_A$, possibly by displacing the H-bonded water molecule, and to modify the electronic properties and the cation localization on P$_{680}$.

The samples were excited with a 100 nJ, 680 nm laser beam and probed in the Mid-IR spectral region between 1800 and 1600 cm^{-1} were absorption from the 9-keto and 10-ester groups of chlorophylls are expected. This spectral region is particularly informative since both carbonyl and ester vibrations are very sensitive to the environment in which the pigment is located and shifts of several wavenumbers are expected, with respect to the absorption measured for isolated chlorophylls in a non polar solvents, due to the formation of H-bonds or variation in the polarity of the environment.[2,3] The time resolved traces collected for both PSII wild type and the two mutants were globally analyzed with a sequential kinetic scheme with increasing life times. The resulting evolution associated difference spectra (EADS) are shown in figure 1.

---

[1] Loll, B. *et al*, Nature, **2005**, <u>438</u>, 1040; Ferreira, K. N. *et al,* Science*, **2004**, <u>303</u>, 1831

[2] Groot M.L. *et al*, Proc. Natl.Acad. Sci. U.S.A.*, **2005***, <u>102</u>**, 13087

[3] Groot M. L. *et al*, J. Phys. Chem. B., **2004**, <u>108</u>, 8001; Di Donato, M. *et al*., J. Phys, Chem. B, **2007**
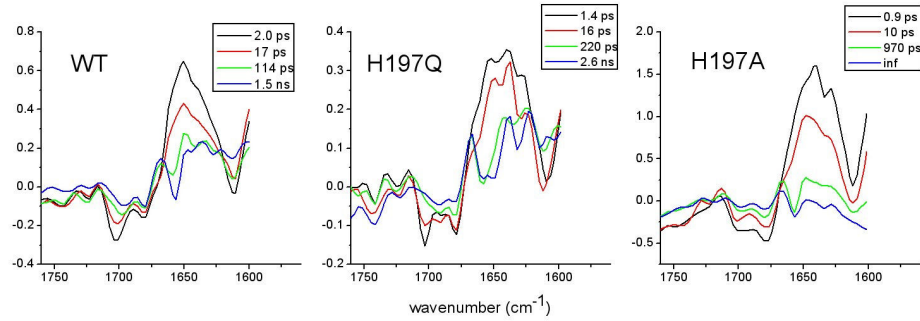
Figure 1: Evolution associated difference spectra resulting from a global analysis with increasing lifetime for vis/Mid-IR pump-probe measurements on wild type PSII core and the two mutants H197Q and H197A.

In all the spectra bleaching signals are evident in region between 1700-1650 cm^{-1}, due to the absorption of 9-keto groups of chlorophylls contained both in the antennas and in the RC. Ester group absorption is visible at ~1750 cm^{-1}. In the excited state both ester and keto absorptions downshift, the 9-keto giving rice to the intense and broad induced absorption band centred around 1650 cm^{-1}, while charge separation, and localization of a positive charge on chlorophyll induce an upshift of the absorption. The comparison of the wild type EADS with those of the mutants shows significant differences, particularly in the carbonyl bleaching region. In the case of WT two bleaching signals are evident in all the spectral components, an intense one at 1702 cm^{-1} and less pronounced one at 1680 cm^{-1}, while for the H197Q an additional small bleaching at ~1690 cm^{-1} appears in the first spectral component and becomes more evident in the following spectral evolution. In the case of the H197A mutant again two bleaching signals are present, whose position is similar to that observed for the WT, but the intensity ratio between them is reversed, and in this case the bleaching at 1680 cm^{-1} is the most intense. The dynamics of the charge separation process is slightly affected by the mutation, in higher amount for the H197A mutant, where the first two components are faster than the WT, while the third one is significantly slower. Spectral differences between the three set of measurements are already evident in the fastest time component, which possibly imply that the mutation also affects the dynamics of energy transfer between the minor antennas CP43 and CP47 and the RC, because of a variation of the electronic levels of P_{680}/B_A, determining a different distribution of the initial excitation between the D1D2-RC and the antennas.

Although spectral differences can be evidenced by analyzing the EADS obtained by global analysis, it is difficult to assign from these spectra the signals pertaining to the primary donor and to disentangle energy transfer and primary charge separation processes. The EADS are not representative of a particular state of the system, but, especially in the case of the fastest components, they can represent a mixture of excited states and charge separated states. In order to extract more 'pure' spectra it is necessary to apply a kinetic model to the time resolved data and to analyze them by means of a target or compartmental analysis. Given the complexity of the system and the high number of pigments contained in PSII core (approximately 15/17 Chls for each antenna and 8 chlorins per RC) it is necessary to apply a simplified scheme, which however has to give a satisfactory description of the dynamics of the system. Here we applied the kinetic scheme represented in figure 2, in which the species associated difference spectra (SADS) obtained for the wild type are also shown. The kinetic scheme used in our target analysis contains five compartments: the two antenna compartments CP43 and CP47, a RC*/RP1 compartment, representing the excited state of the reaction center and the first radical pair $B_A^+H^-$, and two following radical pair compartments, both

representing the final state reached by the system in our experimental conditions, namely $P^+_{680}H^-$.
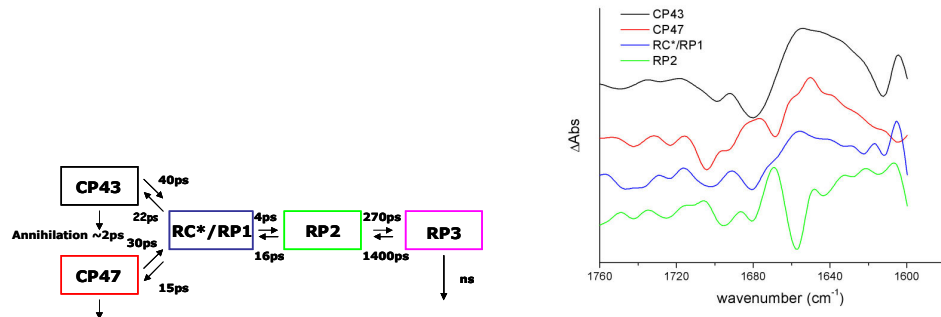
Figure 2: Kinetic scheme used for target analysis and the resulting SADS obtained for the wild type.

Although it was not possible to obtain from our analysis a pure RP1 spectrum, the comparison of the RC*/RP1 SADS of the wild type to those obtained by performing a target analysis applying the scheme of figure 2 to the kinetic traces collected for the mutants, allowed us to propose a possible assignment for the 9-keto absorption band of B_A. The comparison of the RC*/RP1 SADS of wild type with those of the H197A and H197Q mutants is shown in figure 3.
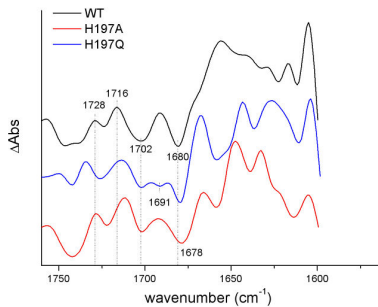
Figure 3: Comparison between the RC*/RP1 SADS of wild type and the two mutants H197Q and H197A

The three SADS differ significantly in the carbonyl bleaching region. The wild type spectrum shows two bleaching signals at 1702 and 1680 cm^{-1}, the H197Q SADS exhibits an additional small bleaching at 1691 cm^{-1} and for the H197A the intensity ratio of the two bleaching signals is inverted with respect to the wild type. Previous light-induced FTIR measurements of triplet formation in PSII assigned a bleaching signal at 1670 cm^{-1} to B_A, on which the triplet is mostly localized at low temperature.[4] In agreement with such interpretation we conclude that in the case of WT the 1670 cm^{-1} signal is hided by the induced absorption band, while the absorption of B_A becomes visible for the mutants, where we expect it to up-shift because of the perturbation of the H-bond on B_A. According with this interpretation we assign the small bleaching seen at 1691 cm^{-1} for the H197Q mutant to the up-shifted 9-keto carbonyl of B_A and we suggest that in the case of the mutant H197A this signal is shifted to ~1680 cm^{-1}, determining the increasing of intensity of this band with respect to the wild type.

---

[4] Noguchi, T. *et al*, Biochemistry, **2001**, <u>40</u>, 2176

Watching DNA Get "Sunburned"

P. Gilch[1], W.J. Schreier[1], T.E. Schrader[1], F. O. Koller[1], W. Zinth[1],

C. E. Crespo-Hernández[2,3], B. Kohler[2]

[1]Department für Physik, Ludwig-Maximilians-Universität München, Oettingenstr. 67, D-80538 München, Germany, e-Mail: peter.gilch@physik.uni-muenchen.de, URL: http://www.imo.physik.uni-muenchen.de/~gilch/
[2]Department of Chemistry, The Ohio State University, 100 West 18th Avenue, Columbus, OH 43210, USA
[3]Current address: Department of Chemistry, Case Western Reserve University, 10900 Euclid Avenue, Cleveland, OH 44106, USA

DNA, the carrier of genetic information, is constantly subject to internal and external hazards. One of the external hazards is the UV light to which one is exposed when sunbathing. UV light is absorbed by the DNA bases and can induce hazardous photoreactions. Among the various photoproducts the CPD (cyclobutane pyrimidine dimer) lesion is the most abundant. It can form if two thymine (T) bases are adjacent in a DNA strand. These combine in a [2+2] photoaddition to yield the CPD (see Figure 1). The formation of this lesion has been reported more than forty years ago[1]; yet, its kinetics has only been resolved very recently[2].
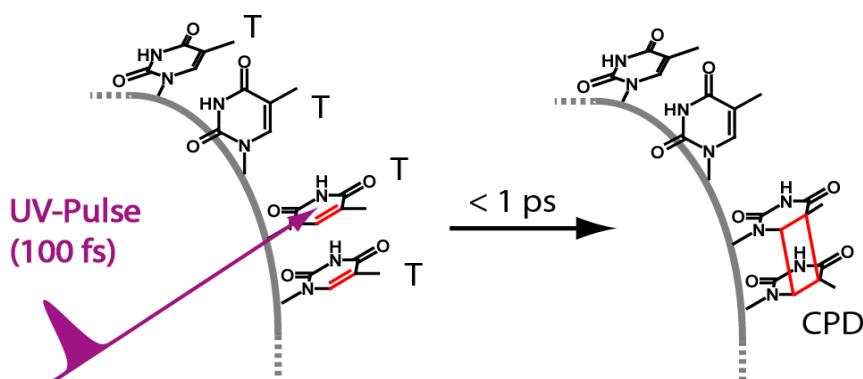
Figure 1 Schematic of the formation of the CPD lesion between thymine bases in a DNA single strand. Only thymines with a suitable conformation, in this case the lower two bases are reactive.

In (over-)simplified form, CPD formation can be regarded as a bimolecular photo-reaction. So the following recipe should yield the rate constant k_r of the dimer formation. One determines the decay constant k_{int} of "the" excited state of an isolated thymine and the constant k_q of (at least) two thymine bases in proximity (for instance on a DNA strand). The dimer formation constant k_r should be given by $k_r = k_q - k_{int}$. and the reaction yield should equal $\varphi = k_r/k_q$. For various reasons the determination of k_r for the CPD formation is more involved. The excited state lifetime of isolated thymine (k_{int}^{-1}) is very short (~ 500 fs)[3] and the yield of the dimer φ is rather low (on the order of one percent for adjacent bases in DNA[4]). So one would have to measure k_q with better than one percent precision to determine k_r. Even if one had done so the determined value might be irrelevant. The excited state lifetime of a DNA base depends on the surrounding bases even in the absence of any photochemistry[5]. Further, the photo-excitation of thymine results in the consecutive population of several electronically excited

[1] R. Beukers, W. Berends, Biochim. Biophys. Acta **1960,** <u>41</u>, 550-551
[2] W.J. Schreier et al. Science **2007,** <u>315</u>, 625-629
[3] Crespo-Hernandez, C. E., Cohen, B., Kohler, B. **2004** Chem. Rev. 104, 1977-2019
[4] Douki, T., Court, M., Sauvaigo, S., Odin, F., Cadet, J. **2000** J. Biol. Chem. <u>275</u>, 11678-11685
[5] Crespo-Hernandez, C. E., Cohen, B., Kohler, B. **2005** Nature <u>436</u>, 1141-1144
6 Hare, P. M., Crespo-Hernandez, C. E., Kohler, B. **2007** Proc. Nat. Acad. Sci. USA <u>104</u>, 435-440

singlet and triplet states[6], e.g. $\pi\pi*$ and $n\pi*$ states, which all might function as precursors for the CPD. Furthermore, in the UV/Vis spectral range no clear spectroscopic marker for dimer formation exists[5].
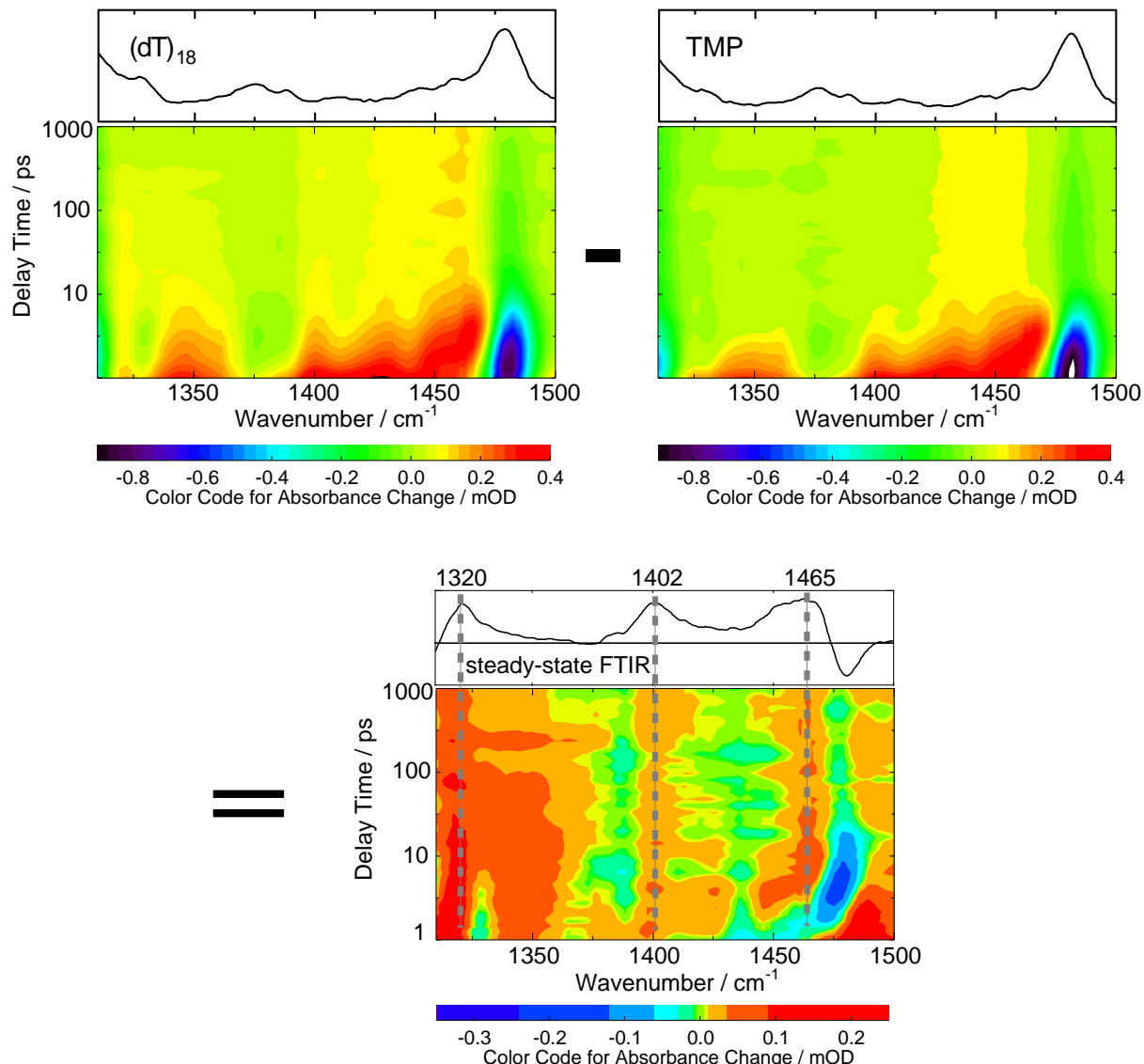
Figure 2 Steady-state and time resolved difference IR spectra of $(dT)_{18}$ and TMP in buffered D_2O solution. The spectra focus on the finger print region where characteristic marker bands of the CPD lesion are observed. In the contour representation of the femtosecond IR data red coloring stands for positive absorption changes induced by a 100 fs UV (272 nm) pulse, blue coloring represents bleaches. The two graphs in the upper panel show the femtosecond IR measurements for the two samples. The graph in the lower panel represents the difference of the two. The differences are indicative for CPD formation in the Oligomer. The dashed lines in the difference plot indicate the correspondence to the steady state experiment referred to in the text.

In the IR range such marker bands exist. We studied a DNA single strand containing 18 thymine bases (dT_{18}). Similar systems are known to feature a relatively high dimerization yield of a few percent[7]. Steady-state illumination of a buffered solution (pH 7) of $(dT)_{18}$ in D_2O accumulates CPD lesions and its IR signature can be recorded. The corresponding IR difference spectrum (Figure 2) features three pronounced bands in the fingerprint region. Comparison of this difference spectrum with a model compound[8] containing the CPD motif unequivocally assigns these bands to the CPD. In the femtosecond UV/IR probe experiments

described below we relied on these marker bands to determine the CPD formation time. Since the CPD quantum yield amounts to only a few percent one expects the dominant time-resolved signature to arise from the non-reactive channel. To separate these contributions from the CPD signature the femtosecond IR data of thymidine 5'-monophosphate (TMP) and $(dT)_{18}$ were recorded under the same experimental conditions. As expected the spectral dynamics are very similar (Figure 2). After UV excitation the $\pi\pi^*$ state decays on a sub picosecond time scale. The $\pi\pi^*$ depletion predominately results in the formation of a vibrationally excited ground state. The strong induced absorption adjacent to the low frequency side of the 1480 cm^{-1} bleach is a manifestation of this vibrational excitation. As the vibrational excess energy is transferred to the solvent within a few picoseconds this feature vanishes. Weak spectroscopic signatures evolving on the 100 ps time scale are most likely due to a singlet $n\pi^*$ state populated in a yield of about 10 %. In the representation depicted in the upper part of Figure 2 the signature of CPD formation cannot be clearly discerned. To unravel this signature the TMP data set was subtracted from the (dT_{18}) set. The resulting difference data have a magnitude of only $\sim$ 10 μOD. Still, the CPD marker bands at 1320, 1402, and 1465 cm^{-1} and the bleach at 1480 cm^{-1} present in the steady state difference spectrum are seen (Figure 2, lower part). The magnitude of the signal in comparison to the initial bleach matches the reported CPD quantum yield[7] of $\sim$ 3 %. The marker bands can be observed as early as $\sim$ 1 ps and do not rise thereafter. From this we conclude that the CPD lesion is formed in less than 1 ps.

The observed short formation time is of the order of the decay time of the excited singlet $\pi\pi^*$ state. So this state is the precursor of the CPD lesion and not the singlet $n\pi^*$ state or the triplet state. Since an isolated thymine base already features a sub picosecond lifetime ($= k_{int}$) one may *not* immediately conclude from the above that the reaction rate k_r is ultrafast. Two limiting kinetic scenarios might apply. (i) The dT_{18} sample is "homogenous", i.e. all thymine pairs on the strand have the same reaction propability. In that case the low quantum yield φ implies that the time constant of the reaction is of the order of 10 ps. (ii) The dT_{18} sample is "heterogeneous", meaning that a small fraction of adjacent thymines react with high probability. Such pairs are expected to adopt a relative arrangment that closely resembles that in the CPD lesion (see Figure 1). Several experimental findings favor the second scenario. The overall structure of the investigated oligomer is known to be strongly disordered[9]. It is highly unlikely that all of the thymines in a single strand adopt a reactive conformation. CPDs kept in a frozen solution can be split into two thymines by UV light. Those two thymines have a very high dimerization yield close to unity since the frozen liquids keeps them in an arrangement favorable for reaction[10]. Similarly, for thymine hydrate crystals in which the thymine molecules are stacked, high quantum yields of dimerization are observed[11].

From these experiments, and our recent femtosecond work[5], we can conclude that the CPD lesion is formed in an ultrafast photoreaction, provided that the the two thymines adopt a relative conformation favorable for dimerization. Because larger conformational changes occur on the time scale of 10 ps, a reactive conformation has to be adopted prior to photo-excitation. Based on these findings we propose that the helical twist of native DNA suppresses such conformations and is responsible for the low quantum yields in this system. In this sense the double helix therefore has a UV-protective effect.

_____

7 Marguet, S., Markovitsi, D. **2005** J. Am. Chem. Soc. <u>127</u>**,** 5780-5781
8 Butenandt, J., Eker, A. P. M., Carell, T. **1998** Chem. Eur. J. <u>4</u>, 642-654
9 Mills, J. B., Vacano, E. & Hagerman, P. J. **1999** J. Mol. Biol. <u>285</u>, 245-257
10 Lamola, A. A., Eisinger, J. **1968** Proc. Nat. Acad. Sci. USA <u>59</u>, 46-51
11 Lisewski, R., Wierzchowski K.L. **1970** Photochem. Photobiol. <u>11</u>, 327-347

Ultrafast Infrared-Spectroscopy on Flavin Systems

M. Wolf[1], R. Groß[1], C. Schumann[1], T. Domratcheva[2], B. Person[3], J. Heberle[3], R. Diller[1]

[1] Fachbereich Physik, TU Kaiserslautern, D-67663 Kaiserslautern [2] Max-Planck-Institut für medizinische Forschung, D-69120 Heidelberg [3] Fakultät für Chemie, Universität Bielefeld, D-33615 Bielefeld.

The function of blue light receptors, like the BLUF proteins or the LOV domains, is based on the photochemistry of diverse flavin chromophores in their respective protein environment. Although these proteins bind similar chromophores, the respective reaction mechanisms differ significantly and range from covalent adduct formation to solely perturbation of H-bonded networks. Transient time resolved vibrational spectroscopy is highly suited to characterize changes in chromophore structure upon photoexcitation that initiate the subsequent chemical or physical processes[1].

Here we present for the first time ultrafast IR vibrational spectroscopy of riboflavin and flavin adenine dinucleotide (FAD) in solution, together with a quantum chemical vibrational analysis of riboflavin.

In addition we present first measurements of the flavin mononucleotide (FMN) binding domain LOV1 (mutant C57S) of the phototropin 1 of the green algae *Chlamydomonas Reinhardtii*.

Riboflavin and FAD (Sigma) samples were prepared as 13 mM solution in dimethyl sulfoxide (DMSO, Fluka) as well as in DMSO-d6 (Euriso-top) to avoid the strong solvent absorption between 1300 and 1450 cm^{-1}. The LOV1[2] protein was prepared as a humidified film on a CaF_2 window. All experiments were performed at room temperature. The sample window was rotated through the laser beams, to exchange the irradiated volume between laser shots.

The transient absorption experiments were performed as describes earlier[3]. For the pump pulse, the 775 nm, 150 fs output of a CPA-2001 (Clark-MXR) kHz-amplifier system was frequency doubled to 387.5 nm. Probe pulses were generated by means of a two stage
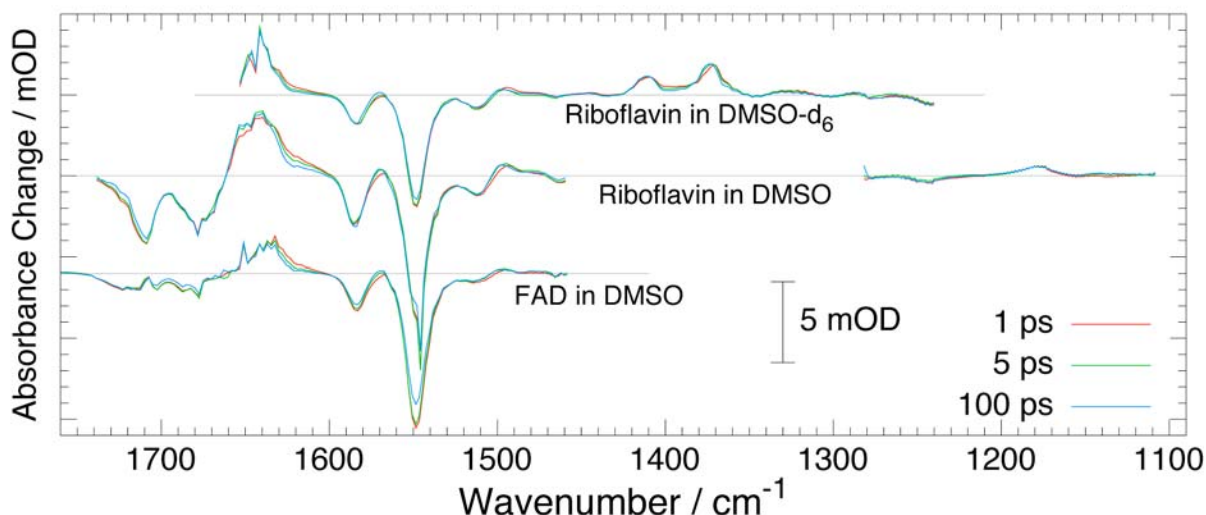
Figure 1: Difference spectra of riboflavin and FAD solved in DMSO and DMSO-d$_6$ for selected delay times.

[1] J. Herbst, K. Heyne, R. Diller, Science, **2002**, 297, 822-825
[2] T. Kottke, J. Heberle, D. Hehn, B. Dick, P. Hegemann, Biophysical Journal, **2003**, 84, 1192-1201
[3] F. Peters, J. Herbst, J. Tittor, D. Oesterhelt, R. Diller, Chemical Physics, **2006**, 323
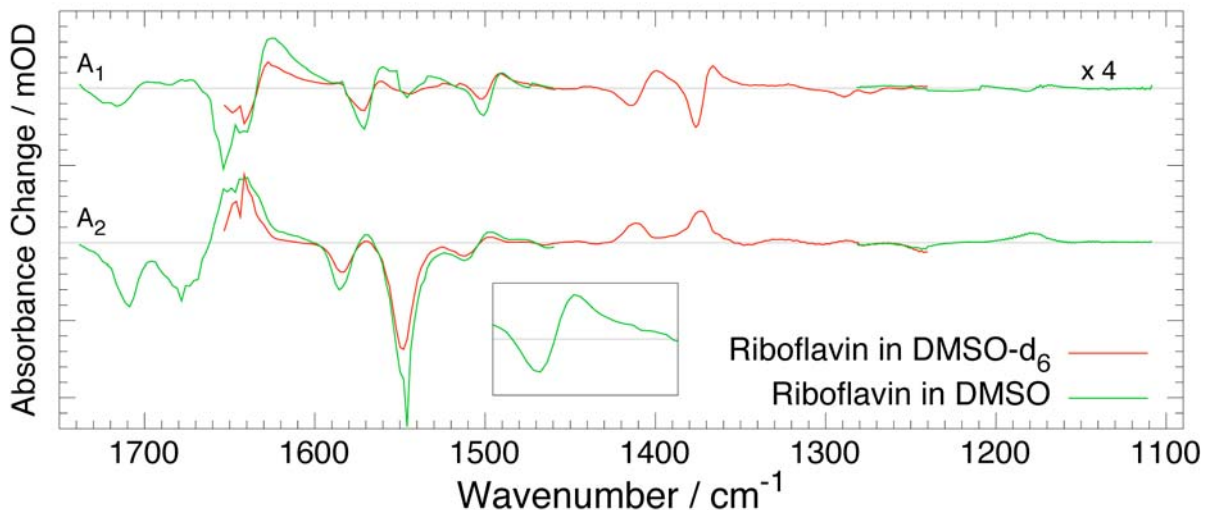
Figure 2: Decay associated spectra A_1 and A_2 of riboflavin in DMSO and DMSO-d_6. The inset shows the characteristic pattern of vibrational cooling as repeatedly observed in A_1.

optical parametric amplifier with consecutive difference frequency generation tuneable through a wide mid infrared range. A pump/probe cross correlation of 300 fs (FWHM) was achieved.

As seen in Figure 1 riboflavin in both solvents and FAD in DMSO show essentially the same difference spectra in the covered spectral region. All measurements show two distinct kinetic components: A slow decay of all bleaching (neg.) and product (pos.) bands on a nanosecond timescale (data not shown) and a fast component within a few picoseconds.

As depicted in Figure 2 a global kinetic analysis with a sum of two exponentials yields two distinct time constants and their decay associated spectra (DAS) A_1 and A_2. The slow component τ_2 of several nanoseconds is assigned to the decay of the excited state, as it has previously been observed via fluorescence measurements (3.18 ns for riboflavin in DMSO[4]). The fast component τ_1 was determined to 4.0 ± 0.2 ps for riboflavin in DMSO, 4.8 ± 0.2 ps for riboflavin in DMSO-d_6 and 7 ± 0.6 ps for FAD. The respective DAS A_1 shows a characteristic pairing of negative and positive bands, indicating a blue shift of all product bands within 4-5 ps (cp. Figure 2). Therefore these dynamics are assigned to cooling of the excited electronic state vibrational modes, and vice versa, allow an identification of excited state vibrations that would otherwise not or hardly be visible in the transient absorption difference spectra.

Thus we derived a set of electronic ground and excited state vibrational frequencies from the A_1 and A_2 component of the DAS as listed in Table 1. An assignment of both sets was performed by quantum-chemical calculations employing Hartree Fock (HF) and configuration interaction single excitations (CIS) methods. A scaling factor of 0.87 was derived by comparison of the calculated and experimentally observed S_0 frequencies and was then applied to the calculated S_1 frequencies.

As seen a good assignment of both ground and excited state vibrations could be accomplished. This also corroborates the assignment of the excited state populated after photoexcitation to the lowest lying S_1 ($\pi\pi^*$) state in contrast to the neighbouring S_2 ($n\pi^*$) state (calculated frequencies not shown).

---

[4]   P. Drössler, W. Holzer, A. Penzkofer, P. Hegemann, Chemical Physics, **2003**, <u>286</u>, 409-420

Experimental			Calculated		
S_0 cm^{-1}	S_1-cold cm^{-1}	S_1-hot cm^{-1}	S_0 cm^{-1}	S_1 ($\pi\pi^*$) cm^{-1}	Putative assignment
1711	1716	1698	1761	1713	ν(C=O$_4$)
1676	1652	1625	1713	1694	ν(C=O$_2$)
1584	1571	1560	1579	1538	
1547	1546	1534	1522	1522	ν(C=C, C=N) in the ring system
1511	1501	1491	1506	1469	
1464 [†]	1454 [†]	1440 [†]	1456	1443	
	1413 [†]	1400 [†]		1362	δ(H–N$_3$–C)
1427 [†]	1376 [†]	1368 [†]	1429	1395, 1385	ν(C-C, C-N), δ(H-C-H) in CH$_3$
1345 [†]			1318		ν(N$_1$-C$_2$, N$_1$-C$_{10}$)
1302 [†]			1284		δ(H-C-N$_{10}$)
	1290 [†]	1281 [†]		1337	ν(C-C, C-N), δ(H-C-C) ring I, δ(H-O-C) in ribityl tail
1278			1241		δ(H-O-C) in ribityl tail
1245			1226		ν(N$_5$-C$_{5a}$)
	1225	1208		1224	ν(C$_{4a}$-C$_{10}$, N$_{10}$-C$_{10a}$, C$_{5a}$-C$_6$), δ(H-C-C, H-O-C, H-C-N$_{10}$)
	1182	1169		1168	ν(N$_3$-C$_2$, N$_3$-C$_4$, C$_4$-C$_{4a}$, C$_{4a}$-C$_{10}$)

[†]: Derived from measurements in DMSO-d$_6$ ν: streching-mode

δ: bending-mode
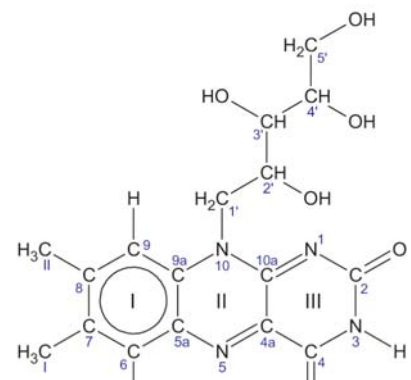
Table 1: Vibrations in the ground and first excited state of riboflavin in DMSO and DMSO-d$_6$ with a putative assignment as determined by HF and CIS calculations.

For the first time we also performed preliminary experiments on the LOV1/C57S domain of phototropin 1 on a sub-ps time scale. As shown in Figure 3 a product band at about 1420 cm^{-1} is observed and is assigned to a precursor state of the long lived LOV1-715 intermediate[2].

In summary, the vibrational analysis of Riboflavin in DMSO and the first experimental results of LOV1 give a solid basis for elucidation of flavo-protein photochemistry.
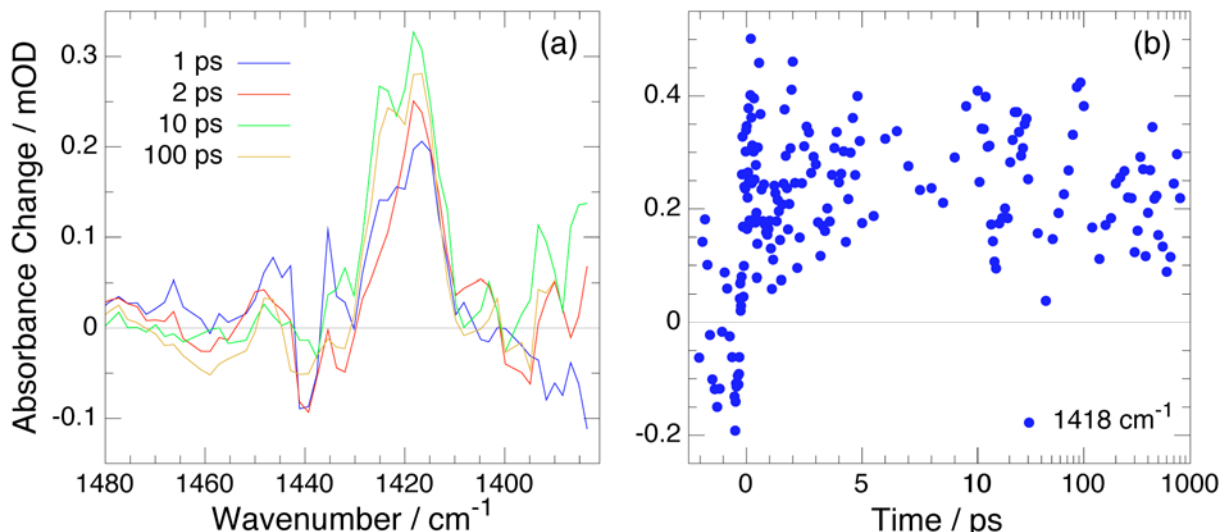
Figure 3: a) Transient absorption difference spectra of the LOV1 domain of phototropin 1 of the green algae *Chlamydomonas Reinhardtii*. A product band at ~1420 cm^{-1} is clearly visible. **b)** Time dependency of the product band. Besides the instantaneous rise of the signal, its further temporal evolution is obscured by the current signal to noise ratio.

Solvent Effects on Vibrational Cooling: Differences Between Cytidine and para-Nitroaniline

T. E. Schrader[1], A. Sieg[1], W. J. Schreier[1], F. O. Koller[1], B. Kohler[2], P. Gilch[1], W. Zinth[1]

[1] Lehrstuhl für BioMolekulare Optik, Ludwig-Maximilians-Universität München, Oettingenstr. 67, 80538 München. [2] Department of Chemistry, The Ohio State University, 100 West 18th Avenue, Columbus, OH 43210. E-mail: tobias.Schrader@physik.uni-muenchen.de, URL: http://www.bmo.physik.uni-muenchen.de/

Many aromatic and heteroaromatic molecules undergo rapid internal conversion (IC) after electronic excitation. The IC process converts several 10,000 cm^{-1} of electronic excitation energy into vibrational energy. In the gas phase this strong vibrational excitation can induce chemical reactions. In solution phase energy transfer to the solvent usually prevents such ground state reactions and thus is crucial for the photostability of these molecules. This stabilizing effect of the solvent of course depends on the time scale of vibrational relaxation. We report here on time-resolved IR measurements which explore the time scales and the mechanism of this relaxation.
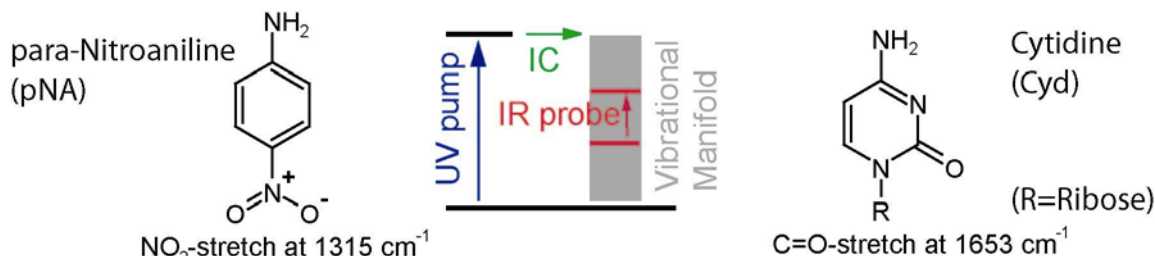
Figure 1: After photoexcitation para-Nitroaniline (pNA) and Cytidne (Cyd) both show a rapid internal conversion to the electronic ground state in less than 1 ps. After internal conversion these molecules exhibit a non-equilibrium vibrational manifold. In this study the relaxation of the vibrational excitation is probed by transient fs-IR spectroscopy.

In this study we compare two molecules undergoing rapid internal conversion, pNA and cytidine, see Figure 1. For pNA subpicosecond IC time constants for various solvents have been reported[1]. Cytidine, as all other DNA bases, undergoes rapid IC; time constants of ~1 ps have been observed[2]. Vibrational relaxation (energy transfer to the solvent) following the rapid IC has been studied by femtosecond UV/VIS spectroscopy[3].
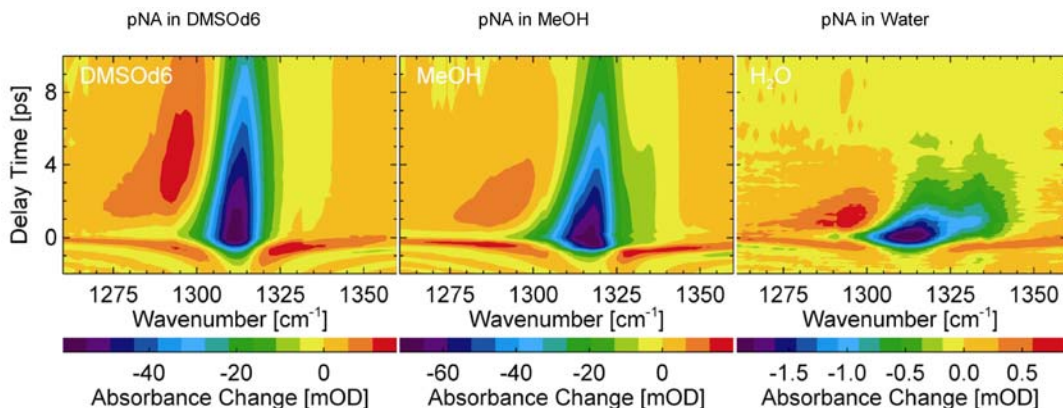
Figure 2: Time dependent absorption changes after photoexcitation of pNA with pulses centered at 407 nm in the spectral region of the NO_2 stretch mode were measured in three different solvents: perdeuterated dimethylsulfoxide (DMSO-d6), methanol and water. The coloring blue indicates a decrease in absorption (bleaching) and the red regions show induced absorption.

The technique used here to follow the vibrational cooling and redistribution processes is UV-pump/IR-probe spectroscopy[4]. For the nucleoside cytidine the excitation pulse was centered at 267 nm, whereas for pNA pulses at 407 nm were used. Figure 2 shows the time-dependent absorption changes for pNA after photoexcitation in three different solvents. The vibrational mode under investigation is the symmetrical NO_2-stretch mode around 1315 cm^{-1}. An induced absorption is observed, which is red-shifted with respect to the ground state absorption. This is the typical signature of vibrational cooling. Combined with the ground state bleach the transient difference spectra acquire a sigmoidal shape[5]. One can correct for the bleaching signal by adding a properly scaled infrared absorption spectrum of pNA. This delivers positive signals with an asymmetric skewed Gaussian line shape representing the illuminated molecules. The amplitudes of these bands approach the continuous wave value with time constants of 0.7 ps in water, 4.4 ps in methanol and 7.5 ps in deuterated dimethylsulfoxide (DMSO-d_6). The spectral integral over the skewed Gaussian bands is not constant in time but rises with time constants of around 3 ps for DMSO-d_6 and Methanol and 0.7 ps in water. Probably the best metric for the relaxation processes observed is the peak shift which has a time constant of 3.4 ps in DMSO-d_6, 1.9 ps in methanol and 1.5 ps in water. These energy relaxation time constants agree well with ones inferred from UV pump/visible probe spectroscopy[1].
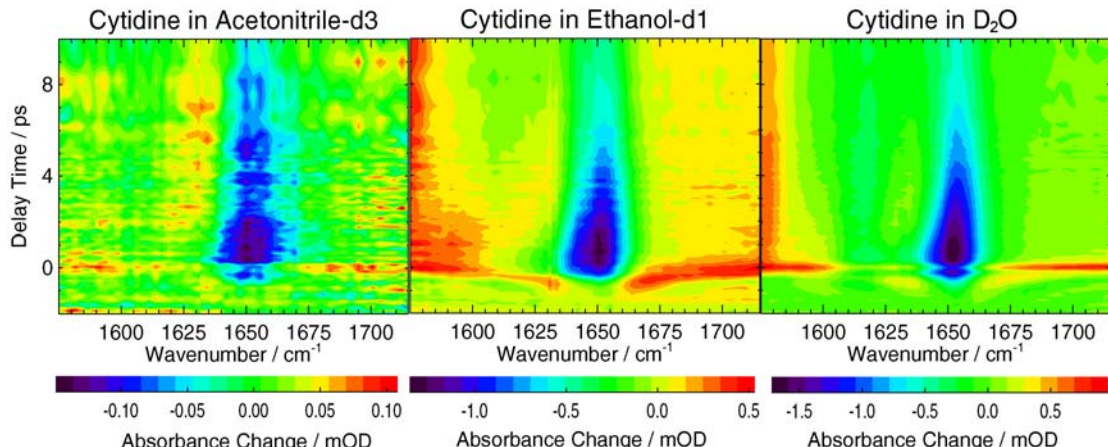
Figure 3: Two dimensional plots of the time dependent absorption changes after excitation with a pump pulse centered at 267 nm probed in the range of the C=C and C=O stretch modes of cytidine in three different solvents.

Figure 3 shows the transient data after photoexcitation for cytidine in three different solvents in the range of the CO-stretch mode at 1653 cm^{-1}. The dominant signal is the bleaching of the ground state absorption. Almost no absorption increase is observed. The typical red-shifted increased absorption might be partially compensated by the bleach of the C=C-stretch vibration at 1612 cm^{-1}.
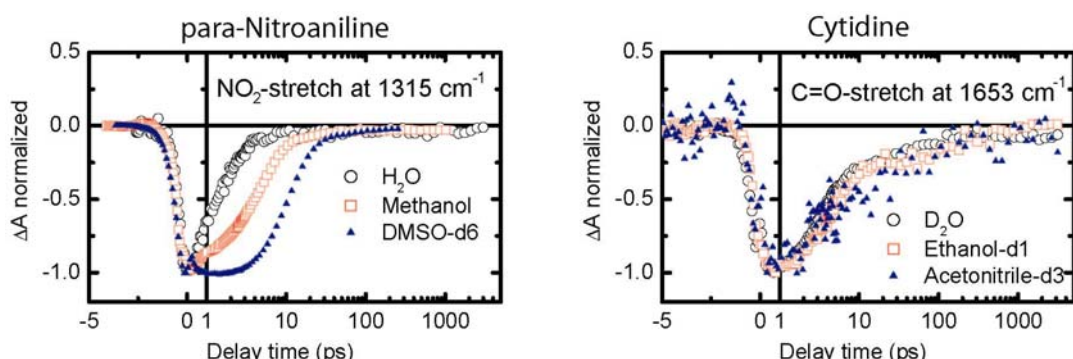
Figure 4: (left) Transient absorption changes of pNA in three different solvents detected in the bleach recovery region of the NO_2-stretch mode at 1315 cm^{-1}. (right) Transient absorption changes of cytidine in three different solvents observed at 1653 cm^{-1}.

Figure 4 compares transients at the wavelengths for the maximum bleaching signals of pNA and cytidine in the different solvents. For pNA a strong influence of the solvent on the bleach recovery time constant is observed, whereas for cytidine this influence of the solvent is negligible within experimental error. The two time constants for the bleach recovery of cytidine are 3 ps and 70 ps. These time constants were determined from a double exponential fit to the transient data shown in Figure 4 (right).

From experiments on pNA one knows that along the symmetric NO_2-stretch coordinate the potential is in good approximation harmonic[4]. It is only through its off-diagonal anharmonic coupling to other modes that an infrared difference signal is observable. Figure 5(A) provides a visualization of this situation. After internal conversion and partial intramolecular vibrational redistribution of the excitation energy. The temperature of the molecule can be estimated to be around 1600 K. Thus low frequency modes are excited. Due to anharmonic coupling the observed high frequency modes change their frequency. This change is present until the decay of the low frequency excitations. Thus the high frequency mode can be used as a sensor for the excitation of low frequency modes. Their de-excitation depends on the solvent which explains the solvent dependence of the bleach recovery of the high frequency mode.
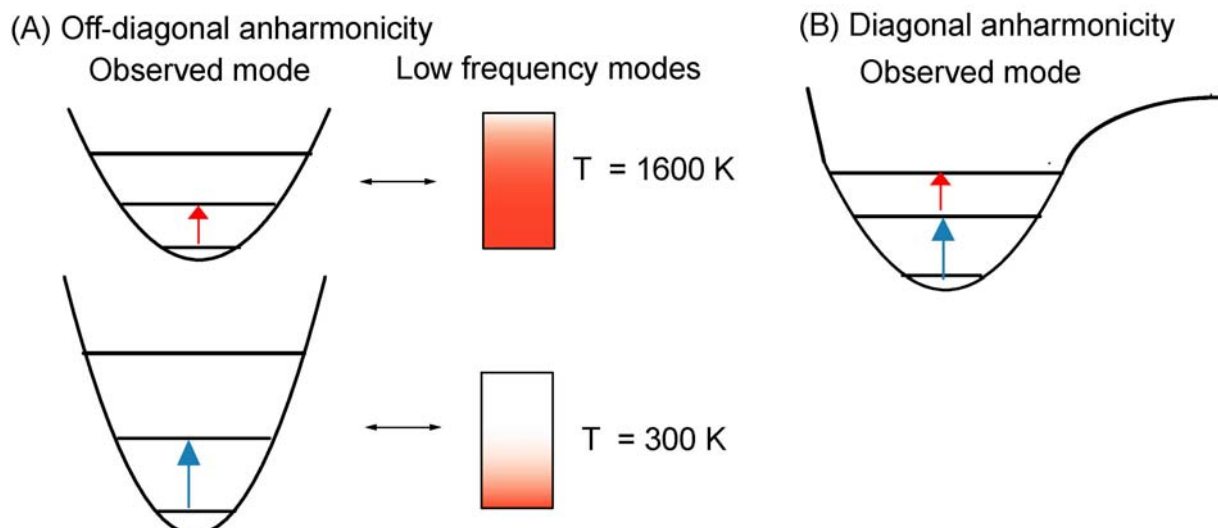
Figure 5: (A) Model for the observed red-shift of the absorption of the NO_2-stretch vibration in pNA after IC: In the electronic ground state low frequency modes are excited after IC. Due to anharmonic coupling this changes the frequency for the observed mode. Therefore one observes a difference signal even though the observed mode itself is not excited. (B) If only the observed vibrational mode is excited one observes a difference signal in IR absorption spectroscopy only when the observed mode itself is anharmonic (diagonal anharmonicity).

For cytidine little is known about the diagonal anharmonicity of the CO-stretch vibration. Assuming that the diagonal anharmonicity is not negligible, the observed signals can be explained by excitation of the CO-stretch vibration via internal conversion (Figure 5B). Internal vibrational redistribution then leads to de-excitation of this mode which causes the signal decay seen in Figure 4 (right). Apparently its coupling to low frequency modes is weak and thus would explain the solvent independent de-excitation. According to this model, the CO-stretch of cytidine is a localized mode which senses vibrational energy transfer to the solvent less effectively than the NO-stretch mode of pNA.

[1] S. A. Kovanlenko, R. Schanz, H. Hennig, N. P. Ernsting, J. Chem. Phys., **2001**, 115, 3256-3273
[2] C. E. Crespo-Hernández, B. Cohen, P. M. Hare, B. Kohler, Chem. Rev., **2004**, 104, 1977-2019
[3] R. J. Malone, A. M. Miller, B. Kohler, Photochemistry and Photobiology, **2003**, 77,158-164
[4] T. Schrader, A. Sieg, F. Koller, W. Schreier, Q. An, W. Zinth, P. Gilch, Chem. Phys. Lett., **2004**, 392, 358-364
[5] P. Hamm, S. M. Ohline, W. Zinth, J. Chem. Phys., **1997**, 106,519-529

Sub-picosecond time-resolved infrared spectroscopy of phytochrome

C. Schumann[1], R. Groß[1], N. Michael[2], R. Diller[1], T. Lamparter[2,3]

[1] Fachbereich Physik, TU Kaiserslautern, Erwin-Schrödinger-Str. 46, 67663 Kaiserslautern, Germany. [2] Institut für Pflanzenphysiologie, FU Berlin, Königin-Luise-Str. 12-16, 14195 Berlin, Germany. [3] present address: Universität Karlsruhe, Botanik 1, Kaiserstraße 12, 76128 Karlsruhe, Germany.

Phytochromes are a class of biological photoreceptors incorporating a linear tetrapyrrole bilin chromophore. In green plants they regulate seed germination, flowering and shade avoidance, whereas their physiological function in most bacteria is still unclear. To trigger signal transduction, phytochromes employ two thermally stable and photochemically interconvertible forms. Upon absorption of red light, the so-called P_r form (λ_{max} = 655 to 700 nm) is converted to the so-called P_{fr} form (λ_{max} = 700 to 750 nm). Depending on the phytochrome, either P or P_{fr} can be the physiologically active form. The primary reaction of the P_r to P_{fr} photoconversion is a Z-E isomerization of the $C_{15}=C_{16}$ double bond between pyrrole rings C and D (Fig. 1). The P_{fr} to P_r back conversion is also light-triggered by the absorption of far red light and includes an E-Z isomerization of the same double bond as primary process.

P_r chromophore configuration   P_fr chromophore configuration
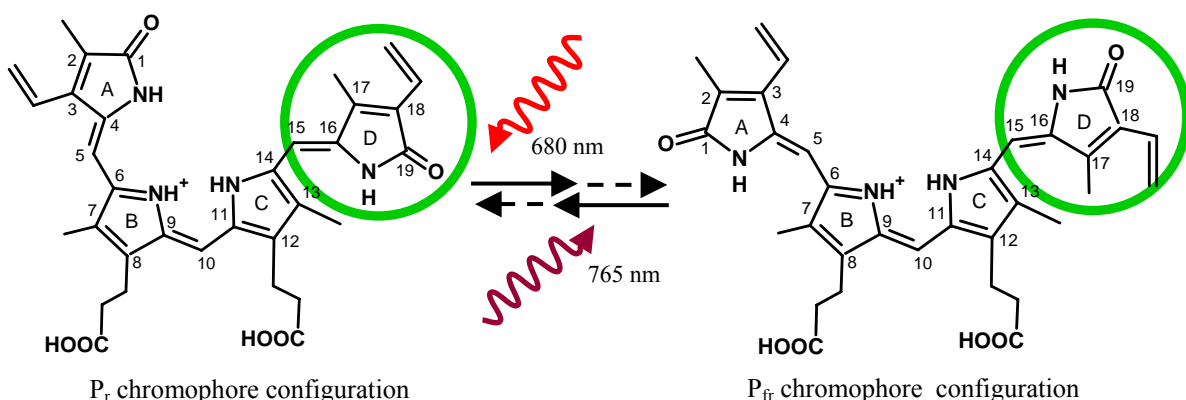
Figure 1: Biliverdin chromophore configuration and photoisomerization of the $C_{15}=C_{16}$ double bond in the primary processes of P_r and P_{fr} reaction.

The photocycle of phytochromes has been subject to numerous spectroscopic investigations including FTIR[1] and Raman[2] spectroscopy using low-temperature trapping techniques as well as time-resolved UV-VIS spectroscopy[3]. The chromophore configurations in the P_r and P_{fr} states have been identified using locked chromophores[4] and a three-dimensional structure of the chromophore binding domain of the bacterial phytochrome *Dr*BphP in the P_r form has recently been determined[5].

[1] H. Foerstendorf, E. Mummert, E. Schäfer, H. Scheer and F. Siebert, Biochemistry **1996** 35, 10793-10799

[2] A. Remberg, I. Lindner, T. Lamparter, J. Hughes, C. Kneip, P. Hildebrandt, S. E. Braslavsky, W. Gärtner and K. Schaffner, Biochemistry **1997** 36, 13389-13395

[3] K. Heyne, J. Herbst, D. Stehlik, B. Esteban, T. Lamparter, J. Hughes and R. Diller, Biophys. J. **2002** 82, 1004-1016

[4] K. Inomata, M. A. S. Hammam, H. Kinoshita, Y. Murata, H. Khwan, S. Noack, N. Michael and T. Lamparter, J. Biol. Chem. **2005** 280, 24491-24497

[5] J. R. Wagner, J. S. Brunzelle, K. T. Forest and R. D. Vierstra, Nature **2005** 438, 325-331

Here we study the primary reactions of the P_r as well as the P_{fr} form of the biliverdin-binding phytochrome Agp1-BV[6] from *Agrobacterium tumefaciens* using sub-picosecond time-resolved infrared and VIS spectroscopy[7]. The protein samples in H_2O and D_2O buffer solution were disposed between two CaF_2 windows. In order to avoid accumulation of P_{fr} (P_r) in the P_r (P_{fr}) experiments, short pulse excitation on the blue (red) edge of the absorption spectrum was accompanied by background illumination in the absorption spectrum of P_{fr} (P_r).

Investigation of the P_r reaction shows the bleach of ground state absorptions in the carbonyl stretch region at 1712 cm^{-1}. This can be assigned to the C_{19}=O stretching vibration whose oxygen is H-bonded to a histidine residue in the binding pocket and thus responds sensitively to the isomerization state of the methine bridge between rings C and D (Fig. 2). Another marker band is the C=C stretch vibration at 1585 cm^{-1}, which is sensitive to the isomerization state via the delocalized π-system of the chromophore pyrrole chain (Fig. 3). This spectral range shows numerous chromophore vibrations with dominant C=C stretching character.
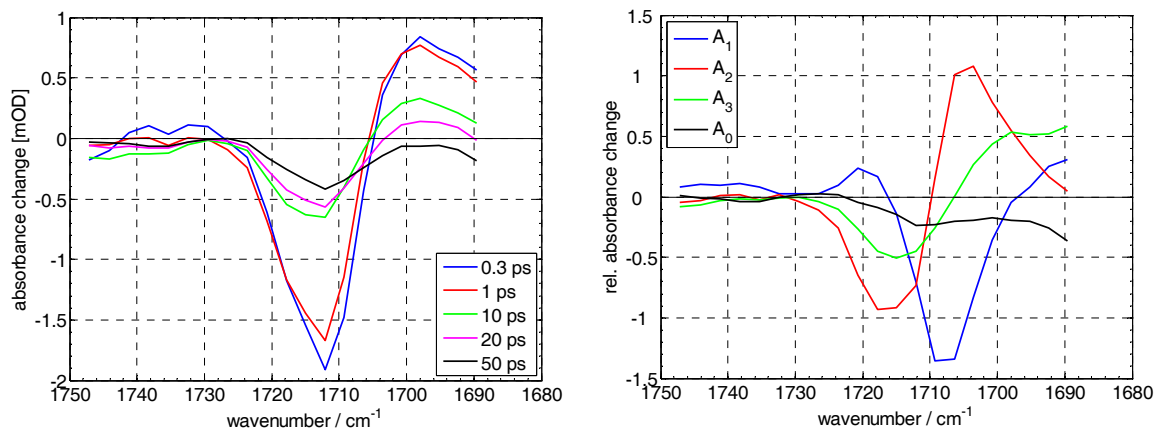
Figure 2: Difference spectra (left) and decay associated spectra (right) of the carbonyl stretch region after photoexcitation of Agp1-BV-P_r at λ_{exc}=680 nm. (H_2O buffer)
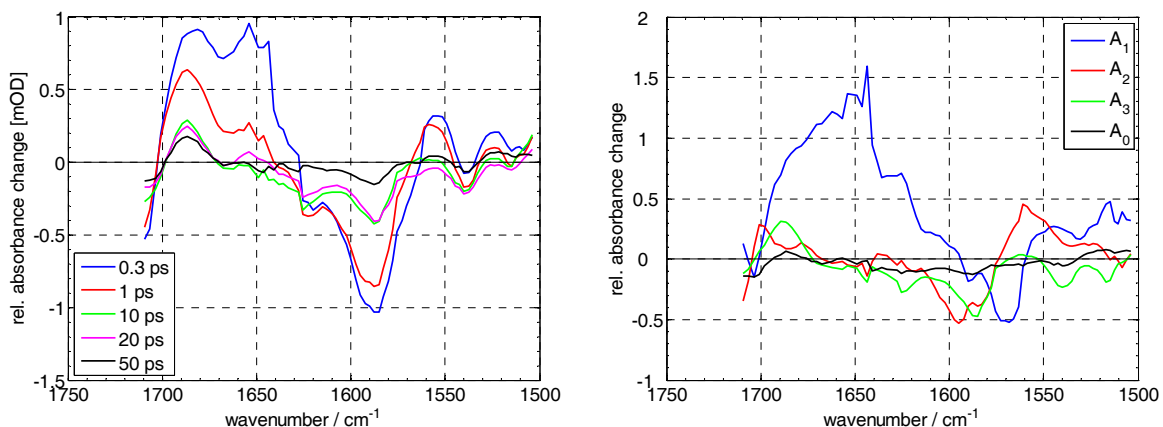
Figure 3: Difference spectra (left) and decay associated spectra (right) of the ethylenic stretch region after photoexcitation of Agp1-BV-P_r at λ_{exc}=680 nm. (D_2O buffer)

[6] T. Lamparter, N. Michael, F. Mittmann and B. Esteban, Proc. Natl. Acad. Sci. **2002** 99, 11628-11633
[7] C. Schumann, R. Groß, N. Michael, T. Lamparter and R. Diller, submitted to ChemPhysChem **2007**

A global analysis of the time-resolved data from the P_r reaction shows three time constants of τ_1=0.7 ps (DAS A_1), τ_2=3.3 ps (DAS A_2) and τ_3=33.3 ps (DAS A_3). Previous time-resolved fluorescence experiments on oat phytochrome PhyA have shown a biphasic decay of the excited electronic state[8] and suggest two states on the S_1 potential energy surface as general feature of the P_r reaction of phytochromes. Combining the results from our time-resolved IR experiments and accompanying sub-picosecond VIS spectroscopy with these previous findings we can construct a reaction scheme for the primary process of the P_r reaction (Fig. 5, left). In addition, the quantum yield of the primary reaction could be determined to 0.094, which, by comparison to data for complete P_{fr} formation[6], shows that the (low) quantum yield of the P_{fr} formation is already determined in the primary process.
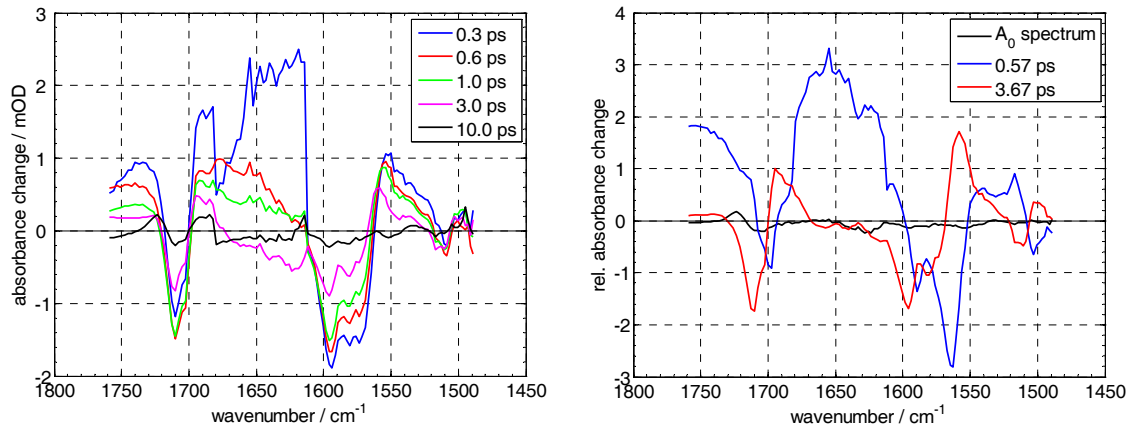
Figure 4: Difference spectra (left) and decay associated spectra (right) of Agp1-BV-P_{fr} after photoexcitation at λ_{exc}=765 nm. Samples were in D_2O buffer.

Sub-picosecond time-resolved infrared (Fig. 4) and UV-VIS investigation of the P_{fr} reaction shows only two time constants in a global analysis, as reflected by our proposed reaction scheme (Fig. 5, right). Here, we attribute the time constant of τ_2=3.7 ps to the lifetime of a vibrationally excited ground state, analogous to the P_r reaction. Thus, the E-Z isomerization of the C_{15}=C_{16} methine bridge is strongly suggested to take place within the decay time of the excited electronic state of τ_1=0.6 ps.
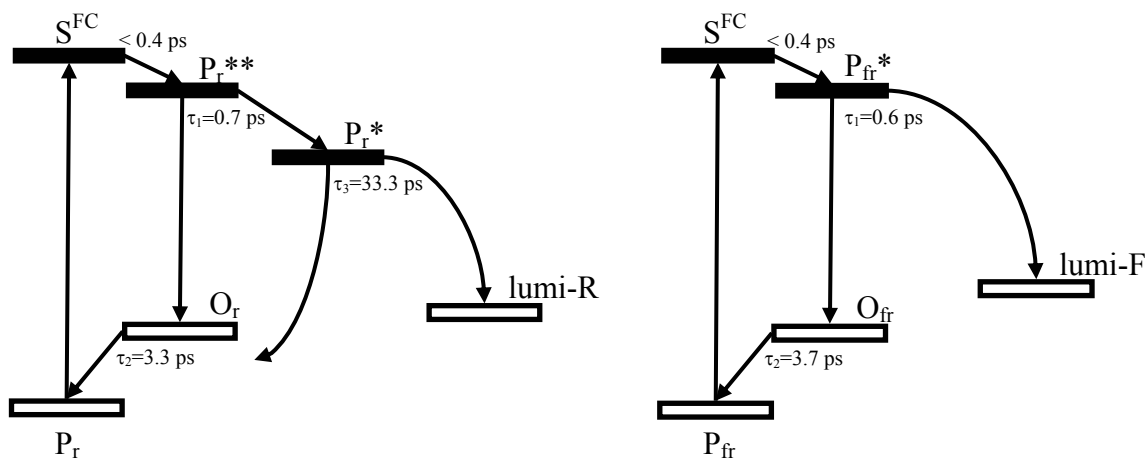
Figure 5: Proposed reaction schemes for the primary processes of the P_r (left) and P_{fr} (right) reactions of Agp1-BV. FC: Franck-Condon, O_r/O_{fr}: vibrationally excited electronic ground state.

[8] A. R. Holzwarth, E. Venuti, S. E. Braslavsky and K. Schaffner, Biochimica et Biophysica Acta **1992** 1140, 59-68

Ultrafast Structural dynamics in BLUF Domains: Transient infrared Spectroscopy of AppA and its Mutants

Allison Stelling,[1] Peter J. Tonge,[1]* Kate L. Ronayne,[2] Jerome Nappa[3] and Stephen R. Meech[3]*

[1]Department of Chemistry and the Biochemistry and Structural Biology Graduate Program, Stony Brook University, Stony Brook, New York 11794-3400, USA, Rutherford Appleton Laboratory, [2]Central Laser Facility, CCLRC, Didcot, Oxon, OX11 0QX UK, [3]School of Chemical Sciences and Pharmacy, University of East Anglia, Norwich NR4 7TJ, UK.

Presenter e-mail : s.meech@uea.ac.uk (http://www1.uea.ac.uk/cm/home/schools/sci/cap/people/faculty/srm)

In this paper we describe ultrafast time resolved IR (TRIR) studies of the dynamics underlying the operation of the blue light sensing using FAD (flavin adenine dinucleotide) (BLUF) proteins. The BLUF domain of AppA, a transcriptional antirepressor from the photosynthetic bacterium *Rhodobacter sphaeroides* will be studied as an example. Under low light conditions, the dark state of AppA binds to PpsR forming an AppA-PpsR$_2$ complex that is unable to bind DNA. Upon blue light photoexcitation, AppA dissociates from PpsR, allowing formation of the repression-competent PpsR tetramer which then binds to DNA and inhibits gene transcription.

AppA is unusual among photoactive proteins. In many of the known photoactive proteins (e.g. photoactive yellow protein, rhodopsin etc.) electronic excitation leads to a fast structural change in the excited state which acts as the trigger for formation of the signaling state of the protein. In contrast for FAD in AppA there is no apparent excited state structure change. All that is seen is a ca 10 nm red shift in the absorption spectrum between the dark adapted (dAppA) and light adapted (lAppA) states. Structural studies point to changes in the interaction between FAD and the protein, probably through modified H-bonding interactions.[1]

TRIR spectra were recorded at the Central Laser Facility. The pump pulse at 400 nm was of < 200 fs duration, had an energy of < 1 µJ and a repetition rate of 1 kHz. The IR probe pulse was generated by difference frequency mixing of the outputs of an OPA. The apparatus has been described elsewhere.[2] The protein samples (concentration 1mM in a 25 µm pathlength flow cell) were raster scanned in the beam to avoid accumulation of lAppA photoproducts. The lAppA samples themselves were generated by illumination of dAppA by the filtered output of a Xe arc lamp around 400 nm. The aqueous solution of FAD (20 mM in a 6 µm static cell) was simply rastered.

In figure 1 the TRIR spectra for dAppA are compared with those for an aqueous
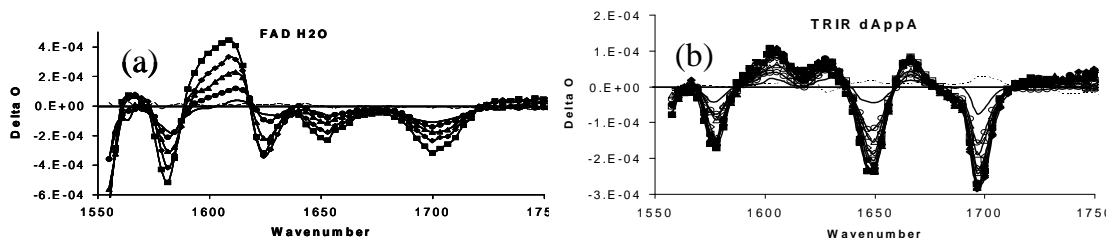
Figure 1: *(a) TRIR spectra of FAD in D2O measured with delay times of 1 (squares) 5 (diamonds) 10 (triangles) 20 (disc) and 50 ps (line) after excitation. (b) TRIR for dAppA recorded 1 (filled squares) 5 (filled diamonds) 10 (filled triangles) 20 (filled circle), 50 (open square) 100 (open diamond) 300 (open triangle) 500 (open circle) and 2000 ps (line) after excitation. Note that data for 1,5,10 ps are overlapped indicating the slow initial decay.*

[1] A. Jung et al*., J. Mol. Biol*., **2006**, *362*, 717
[2] M. Towrie et al., *Appl. Spectrosc*. **2003**, *57*, 367

solution of FAD. The spectra in this window are dominated by four transient bleach modes which are formed instantaneously on excitation. These were assigned to FAD on the basis of DFT calculations as (from the highest wavenumber down, using the atomic labels for the isoalloxazine ring of lumiflavin – see scheme) the C4=O and C2=O carbonyl stretches, which are accompanied by an NH wag, a phenyl ring mode and a C4aN5 stretch.[3] In addition there is a strong transient absorption for both species around 1600 cm^{-1} which has been assigned to the C=O modes in the excited electronic state. Critically there is an additional transient absorption in dAppA which is absent in FAD at 1666 cm^{-1}. One other noticeable difference in the spectra is the width of lines, which are narrower for FAD bound in the protein. This is assigned to a narrower distribution of longer lived H-bond interactions in the protein compared with aqueous solution. Turning to the dynamics, the ground state recovery in FAD in solution is much faster than in the protein. The rapid recovery in FAD reflects the quenching interaction between the adenine ring and the excited isoalloxazine ring, which is supressed in the bound state because the adenine is spatially separated from the chromophore. The TRIR spectral profile for dAppA is essentially independent of time, showing that no spectrally distinct state is formed in the first nanosecond after excitation.

Lumiflavin (Lf)

Scheme 1 Atom numbering used

In figure 2 the TRIR spectra for dAppA are contrasted with those for lAppA. Two major differences are apparent. First the carbonyl bleach modes have broadened and that for C4=O has developed into a doublet. Polarisation analysis[4] shows this to be due to modes with distinct orientations rather than a Fermi doublet. This behaviour is tentatively assigned to light induced disorder in the location of the FAD chromophore. The second major difference in the spectra is the loss of the transient absorption seen in dAppA at 1666 cm^{-1} in lAppA. This transient has no corresponding mode in FAD, so is assigned to a protein mode instantaneously perturbed on excitaion of the FAD.[4] Its absence in lAppA suggests that it is a marker mode for protein chromophore configurations which are capable of going on to form the signalling state. This assignment has been confirmed through a study of photoactive and photoinactive mutants of AppA in which the 1666 cm^{-1} mode is only recovered in the photoactive form.[4] These studies also suggest that the protein mode may be associated with residue Q63 which is known to rotate between light and dark adapted structures. These ideas are being investigated through TRIR studies of isotopically edited AppA and further mutants.

Figure 2. *(a) TRIR for dAppA recorded 1 (filled squares) 5 (filled diamonds) 10 (filled triangles) 20 (filled circle), 50 (open square) 100 (open diamond) 300 (open triangle) 500 (open circle) and 2000 ps (line) after excitation. Note that data for 1,5,10 ps are overlapped indicating the slow initial decay. (b) TRIR in lAppA 1 (filled squares) 5 (filled diamonds) 8 (filled triangles) 15 (filled circle), 20 (open square) 50 (open diamond) 200 (open triangle) and 1000 ps (open circle) after excitation.*

[3] M. Kondo et al., *J. Phys. Chem. B*, **2006**, *110*, 20107
[4] J. Nappa et al., Submitted for publication

Structural Dynamics of the Organic Pigment Yellow 101

K. Neumann[1], T. Köhler[1], H. Staudt[1], M.-K. Verhoefen[1], J. Wachtveitl[1]

[1] Institut für Physikalische und Theoretische Chemie, Johann Wolfgang Goethe-Universität, Max-von-Laue-Straße 7, 60438 Frankfurt am Main, Germany, wveitl@theochem.uni-frankfurt.de, http://www.theochem.uni-frankfurt.de/femtochem

Pigment Yellow 101 (P.Y. 101) was first synthesized in 1899 and is industrially used since decades in various fields, for example: coloration of viscose, printing inks, artist's colors, non destructive material testing and fluorescence marker. It belongs to the group of aldazine pigments with a characteristic central bisazomethine substructure and two naphthol rings (Figure 1a). It is the only commercially available organic yellow pigment which fluoresces in the solid state.

P.Y. 101 exhibits unusual photochemical and photophysical properties, since it fluoresces even though it has OH-groups and despite the short intramolecular distances in solid state. In contrast 1,1′-Naphthaldazine, a derivative lacking the OH-groups, is not fluorescent. Therefore, the hydrogen bonds between OH and N seem to be essential for the fluorescence behavior.

Experiments employing fs vis-pump/vis-probe spectroscopy gave rise to a complicated excited state dynamics with several competing relaxation pathways. Five time constants are necessary to describe the sub-ns excited state kinetics. The combination with quantum chemical calculations using time dependent density functional theory (TD-DFT) allowed to propose a molecular mechanism that explains the unusual fluorescence behavior of P.Y. 101 and its derivatives[1,2,3], which is depicted in Figure 1.

Enol ("A","B")   Keto ("C")   twistet Keto, ground state ("E")

a)   **b)**
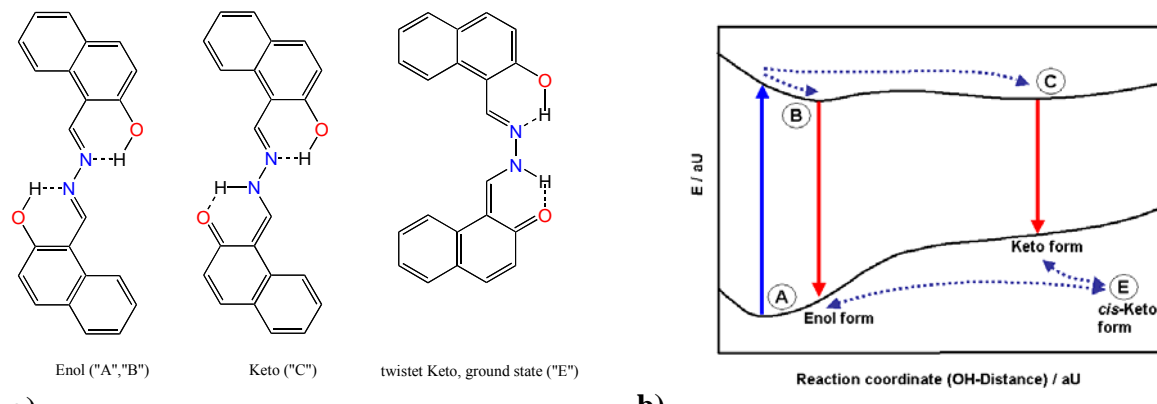
Figure 1: a) Structures of P.Y. 101 according to the model in b ; b) Simplified reaction model derived by the pump probe experiments in the visible spectral range and the quantum chemical calculations . Only those processes and states which are observed in the vis-pump/IR-probe experiment are shown.

Pigment Yellow 101 is optically excited in the S_1 state. An excited state intramolecular proton transfer (ESIPT) causes the formation of a keto-form. Fluorescence is the main decay path of most of the excited state population, which occurs probably out of the enol-form of P.Y. 101 (*B*) and only to a minor extent out of the keto-form (*C*). Isomerization of the central bisazomethine subunit leads to a long-lived cis-keto ground state structure (*E*). An ultrafast enol-keto tautomerism was also observed in structurally related molecules[4,5,6].

In this study we investigated the structural dynamics of P.Y. 101 by vis-pump/IR-probe spectroscopy. P.Y. 101 is hardly soluble in most solvents, thus it was practically impossible to dissolve it in sufficiently high concentration for IR spectroscopy. Instead all fs vis-pump/IR-probe measurements were performed in a highly concentrated dispersion of P.Y. 101 in CCl_4. We used a flow cell with 200 μm thickness and the sample was pumped through the cuvette via a closed cycle flow system by means of a peristaltic pump. The flow rate was high enough to exchange the probed sample volume within two successive laser shots. Continuous stirring in the reservoir guaranteed a homogeneous dispersion and steady conditions during the experiment. The sample was excited at 390 nm with 6 μJ pump energy and probed in the range of 1050 cm^{-1} to 1650 cm^{-1}.
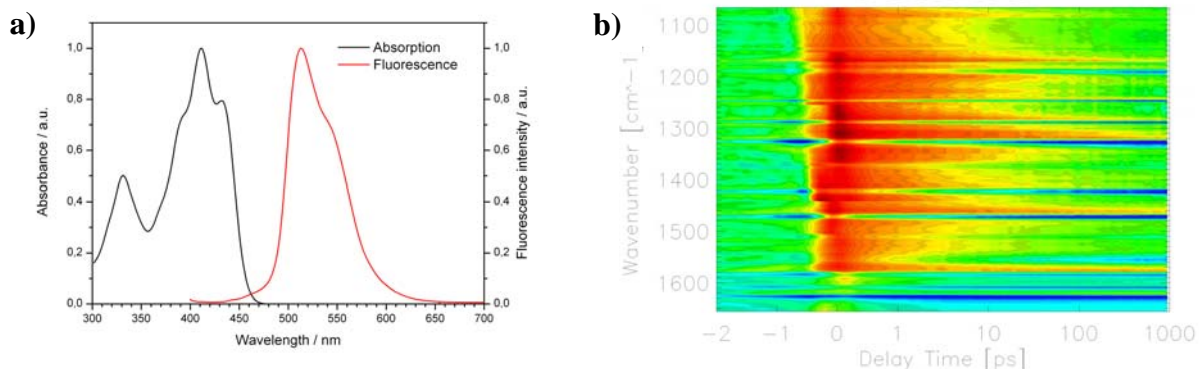
Figure 2: a) Absorption and fluorescence spectra of P.Y. 101 dissolved in CH_2Cl_2; b) Photoinduced transient absorbance changes of P.Y. 101 dispersed in CCl_4, red: positive, blue: negative, green: no absorbance change. The timescale is linear in the range of –2 ps to 1 ps and logarithmic for longer delay times.

The resulting transient absorbance changes are shown in Figure 2b. At negative delay times the perturbed free induction decay, at positive delay times a broad positive absorbance change and a redshift of all vibrational bands is observed. These signals rise within the time resolution of the setup. The broad positive signals decay on a 10 ps timescale, whereas the redshifted photoproduct is stable on the timescale of our experiment.

The data were analyzed with a global fit analysis using 4 decay times (Figure 3c), confirming earlier results from experiments in the range from 1530 cm^{-1} to 2535 cm^{-1} (data not shown). The 0.8 ps time constant is most likely associated with a vibrational cooling and isomerization on the S_1 potential energy surface. The 10 ps and 200 ps time constants are in agreement with those found in pump probe experiments in the visible spectral range of pigments dispersed in a film. Therefore, they can be assigned to a biexponential decay of the S_1 state. According to the model depicted in Figure 1, we assign this decay to two different populations on the S_1 surface, the enol and the keto configuration. The spectrum associated with the infinite time constant corresponds to a photoproduct living much longer than the maximum delay time of 1.8 ns in our fs setup. Its lifetime has been determined by ns laser flash photolysis spectroscopy to be approx. 50 μs (Figure 3d). Positive signals at 1620 cm^{-1} might be associated with vibrational bands of the keto group.

Summarizing the results, we identified a ground-state intermediate of P.Y. 101, which corresponds most likely to the cis-keto-form (*E* in Figure 1) of the proposed reaction model. The spectral signatures of this intermediate appear immediately after excitation and its lifetime was determined to be 50 μs. The bleach signals and the rise of positive bands around 1620 cm^{-1} are not assigned yet, but they might be associated with the formation of the keto-form (*C* in Figure 1). The ESIPT model derived from previous calculations and fs transient absorption experiments in the visible spectral range fit our results nicely, which fully supports the reaction model depicted in Figure 1.
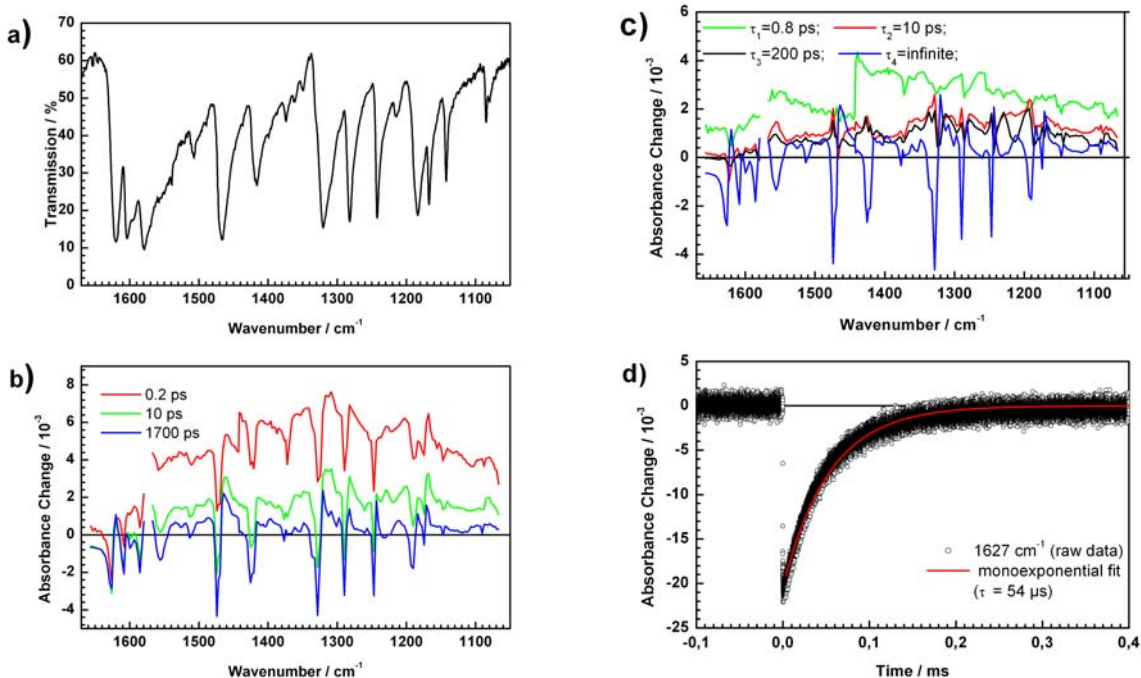
Figure 3: a) FTIR spectrum (transmission) of the P.Y. 101 dispersion in CCl_4; b) Transient spectra at selected delay times; c) Decay associated spectra (DAS) of the global fit with 4 decay times; d) Photoproduct observed with ns laser flash photolysis spectroscopy at 1627 cm^{-1}.

Although there is strong evidence for bands associated with the formation of a keto-group, an unambiguous assignment is still necessary. Analogous experiments with deuterated OH-groups will allow us to identify the IR bands, that are involved in the proposed ESIPT process.

[1] A. Dreuw, J. Plötner, L. Lorenz, J. Wachtveitl, J. E. Djanhan, J. Brüning, T. Metz, M. Bolte and M. U. Schmidt Ang. Chem. Int. Ed., **2005**, 44, 7783-7786

[2] J. Plötner and A. Dreuw, Phys. Chem. Chem. Phys., **2006**, 8, 1197-1204

[3] L. Lorenz, V.V. Matylitsky, J. Plötner, A. Dreuw and J. Wachtveitl, **2007**, submitted

[4] M. Rini, A. Kummrow, J. Dreyer, E. T. J. Nibbering and T. Elsässer, Faraday Discuss., **2002**, 122, 27-40

[5] M. Rini, J. Dreyer, E. T. J. Nibbering and T. Elsässer, Chem. Phys. Lett., **2003**, 374, 13-19

[6] M. Ziólek, J, Kubicki, A. Maciejewski, R. Nascręcki and A. Grabowska, Phys. Chem. Chem. Phys., **2004**, 6, 4682-4689

STRUCTURAL DYNAMICS OF HEMOGLOBIN ENCAPSULATED IN SILICA GELS

Atsushi Inagaki[1] and Yasuhisa Mizutani[2]

[1] Graduate School of Science and Technology, Kobe University, 1-1 Rokkodai, Nada, Kobe 657-8501, Japan

[2] Graduate School of Science, Osaka University, 1-1 Machikaneyama, Toyonaka 560-0043, Japan

E-mail: 068s203n@stu.kobe-u.ac.jp

Hemoglobin (Hb) controls oxygen affinity by tertiary and quaternary structural changes. Encapsulating of Hb in silica gels[1] makes its quaternary structural changes extremely slow. This allows us to investigate the tertiary structural changes without quaternary structure changes. We applied this technique to investigate structural dynamics of Hb fixed in R and T quaternary structures following CO dissociation by time-resolved resonance Raman (TR[3]) spectroscopy.

EXPERIMENTS

Three kinds of CO-bound Hb (HbCO) samples were prepared: Hb associated with CO before the encapsulation (denoted by *R* gel), Hb associated with CO after the encapsulation of deoxyHb (*T* gel) and HbCO in solution. Steady state resonance Raman spectra were obtained by using 410-nm CW laser for Soret enhancement of CO-bound state. Nanosecond TR[3] spectra were obtained by using 436-nm pulse for Soret enhancement of deoxy state after delay time from pumping by 532-nm pulse for CO photolysis. Picosecond TR[3] spectra were also obtained by using 540-nm pump and 442-nm probe pulses.

RESULTS

There was a small difference in steady state resonance Raman spectra of HbCO between R and T quaternary structures (Fig. 1). It is suggested that the frequency of ν_4 band observed in 1350-1380 cm^{-1} is proportional to that of Fe-histidine stretching [ν(Fe-His)] band[2], which is known to be sensitive to structure of proximal side of the heme pocket and is not observed for CO-bound form[3]. On the other hand, the frequencies of Fe-CO stretching [ν(Fe-CO)] band observed around 500 cm^{-1} and C-O stretching band [ν(C-O)] observed around 1950 cm^{-1} are known to be sensitive to structure of distal side of the heme pocket[4]. These results show that the structure of the heme pocket on both proximal and distal side of CO-bound heme is independent from quaternary structure.

Fig. 2 shows nanosecond TR[3] spectra upon CO photolysis. The temporal changes of four Raman bands were different between them: the ν(Fe-His) frequency downshift, the γ_7
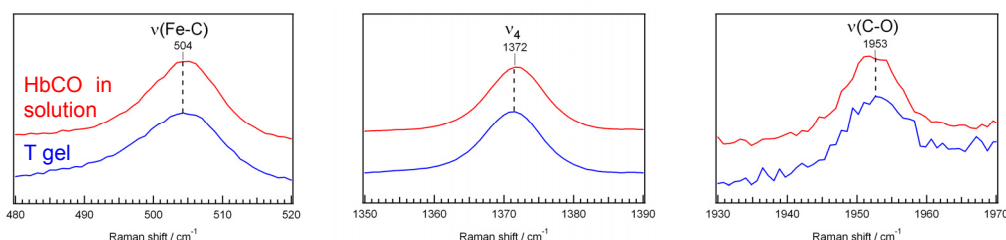
Fig. 1. Steady state resonance Raman spectra (410 nm excitation) of HbCO in solution (red) and *T* gel (blue). Iron-Carbon stretch band region (left), ν_4 band region (center) and carbon-oxygen stretch band region (right) are shown.

(methine wagging mode) frequency downshift, the ν_8 (pyrrole stretch and substituent bending mode) intensity increase and the $\delta(C_\beta C_c C_d)$ (propionate bending mode) intensity increase (Fig. 3). The observed downshift of ν(Fe-His) frequency is correlated with a development of Fe-His bond tension. This suggests that the F helix moves away from the heme in ns-μs time region, consistent to the observed downshift of the γ_7 frequency. It has shown that the band frequency shifts by isotopic substitution of central metal in case of NiOEP[5]. Thus, γ_7 frequency can be expected to correlate with the tension of axial ligand bond. The increase of ν_8 intensity is caused by the increase of degree of hydrogen bonding to the propionate as revealed by resonance Raman study of Hb in trehalose glass[6]. In HbA, the 6-propionate forms a hydrogen bond with an E helix residue or a water molecule that is hydrogen-bonded to E helix residues[7]. Thus, the observed intensity increase suggests that the E helix moves toward the heme. These results show that the transient structure around heme in ns-μs is different between R and T gels.

Fig. 4 shows picosecond TR^3 spectra upon CO photolysis. A 7-cm^{-1} frequency difference in ν(Fe-His) band between the R gel and T gel was observed in the time-resolved spectrum at 10 ps. This suggests that the structural difference around heme between the R gel and T gel has appeared within 10 ps after CO dissociation.

DISCUSSON

A model of the structural dynamics of the R and T gels are proposed as shown in Fig. 5, based on our present results and other groups' results.

CO-bound state. Resonance Raman spectra indicate that the E-F helix orientation toward CO-bound heme is nearly identical between R and T quaternary structure, although the liganded Hb in T quaternary structure is highly unstable. This result implies that there is a
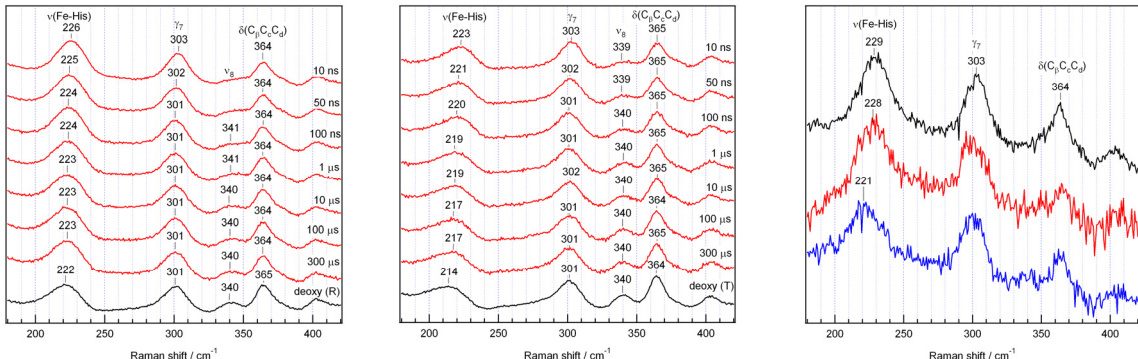
Fig. 2. Nanosecond TR^3 spectra of the R gel (left) and T gel (right) upon CO photolysis. Spectra of both deoxy states are shown at the bottom.
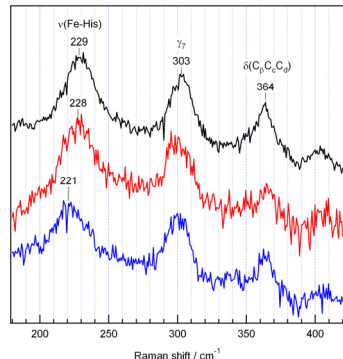
Fig. 4. Picosecond TR^3 spectra of 10 ps-transient species of HbCO in solution (black), R gel (red) and T gel (blue).
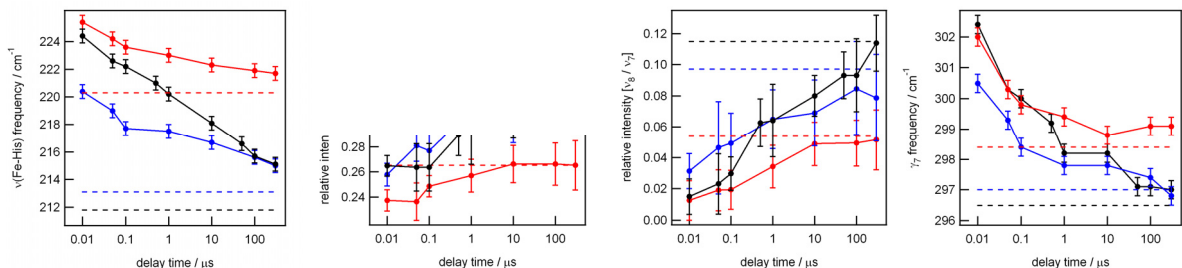
Fig. 3. Temporal changes of the Raman bands upon CO photolysis for R gel (red), T gel (blue) and HbCO in solution (black). Each dashed line shows the value of the corresponding deoxy form.

strong strain on the subunit interface in the *T* gel.

Picosecond structural changes after CO dissociation. Picosecond TR[3] investigation for HbCO in solution has showed that there were little structural changes around heme in ps region. According to this result, it is expected that there are also little structural changes around heme in the *R* gel in picosecond region. On the other hand, in the *T* gel, the iron-histidine bond tension from F helix increase within 10 ps as revealed by observation for lower ν(Fe-His) frequency at 10 ps in the *T* gel than in the *R* gel. Taking account of the interface strain in the *T* gel, such rapid structural change may result from a cooperative motion of the E-F-G helix to reduce the interface strain. These ideas are consist of crystallographic study, which has showed that the movement of the E-F-G helix following CO photolysis at low temperature is much larger in the T quaternary structure than in the R quaternary structure[8].

Nanosecond structural changes after CO dissociation. Nanosecond TR[3] spectra of both *R* and *T* gels suggest that the E and F helices move toward and away from the heme in nanosecond after CO photodissociation, respectively. This idea is consistent to the TR[3] study of Hb in solution, which indicated that a cooperative motion of E-F helix occurs at ~65 ns with releasing photolysis-induced strain which is stored in porphyrin ring and Fe-His bond[9]. According to this study, the nanosecond E and F helical motion of the *R* and *T* gel is also induced by the photolysis-induced strain.

In conclusion, we demonstrated that the structural changes around heme after CO dissociation in the *T* gel is faster than that in the *R* gel. This may result from the expected strain on the subunit interface in the *T* gel.
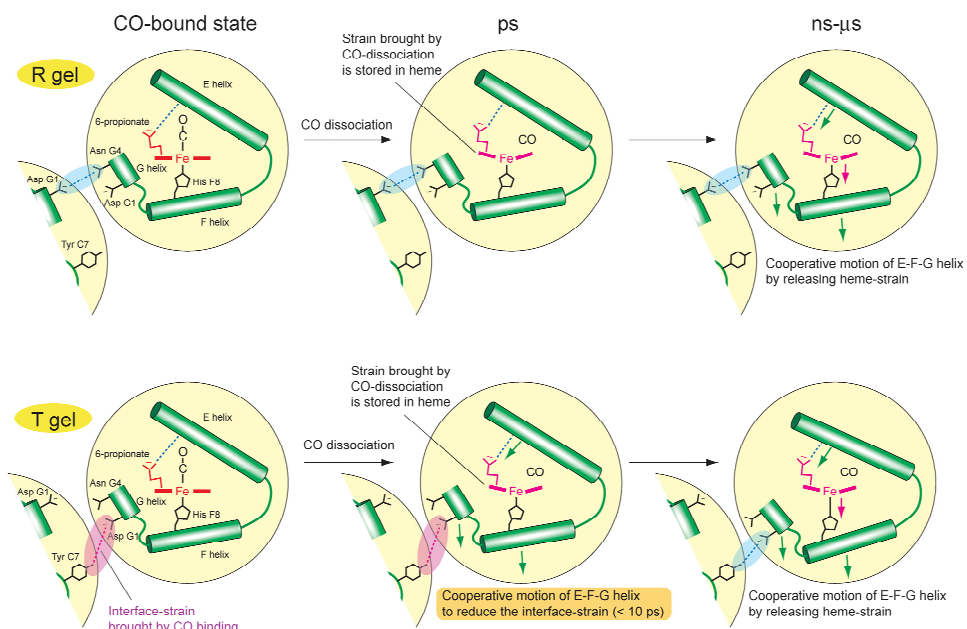
Fig. 5. A model of structural dynamics of the *R* gel and *T* gel.

[1] N. Shibayama and S. Saigo, J. Mol. Biol., **1995**, *251*, 203-209.
[2] M. R. Ondrias et al., Biochemistry, **1982**, *21*, 3428-3437.
[3] T. Kitagawa, "In Biological Applications of Raman Spectroscopy" Vol Ш, p 97, **1987.**
[4] T.G. Spiro and I. H. Wasbotten, J. Inorg. Biochem., **2005**, *99*, 34-44.
[5] X.-Y. Li et al., J. Am. Chem. Soc., **1989**, *111*, 7012-7023.
[6] D. S. Gottfried et al., J. Phys. Chem., **1996**, *100*, 12034-12042.
[7] G. Fermi et al., J. Mol. Biol., **1984**, *175*, 159-174.
[8] S. Adachi et al., Proc. Natl. Acad. Sci. USA, **2003**, *100*, 7039-7044.
[9] G. Balakrishnan et al., J. Mol. Biol., **2004**, *340*, 843-856.

Noninvasive Tissue Oxygenation Monitoring by Resonance Raman Spectroscopy

J. Terner[1,], K.R. Ward[2,3], R.W. Barbee[2,3], I.P. Torres Filho[2,4], M.H. Tiba[2], L.N. Torres[2,3], P.S. Reynolds[3], and R.N. Pittman[3]*

[1] Dept. of Chemistry, [2] Dept. of Emergency Medicine, [3] Dept. of Physiology, [4] Dept. of Anesthesiology, Virginia Commonwealth University, Richmond, VA 23284-2006, USA

* jterner@vcu.edu   http://www.has.vcu.edu/che/people/bio/terner.html

The determination of the state of tissue oxygenation is important to many medical fields, as a means to monitor the health of individual organs, or to determine the adequacy of whole body oxygenation during the course of traumatic shock that could result from injury or sepsis. The rational for a regional tissue measurement to assess whole body oxygenation lies in the premise that certain tissue beds, such as skeletal muscle or the gastric or oral mucosa, are metabolically sensitive to changes in blood flow. Blood volume in a given segment of tissue is proportioned as approximately 70% venous, 20% capillary, and 10% arteriole.   Sampling at this level is therefore an aggregate measurement but is dominated by venous blood. Examination of the tissue milieu for indicators of oxygenation will largely reflect the post-extraction compartment of the tissue, allowing for the assessment as to whether tissues are being adequately oxygenated.

Noninvasive optical methods for the determination of tissue oxygenation without the use of tracer compounds have long been sought. A method that has been under long term development is a technique termed near infrared absorption spectroscopy (NIRS), which make use of the differences in absorption between oxygenated and deoxygenated hemoglobin, or the oxidized and reduced states of cytochrome oxidase. Among the challenges faced by such differential absorption techniques, are to account for the interaction of the utilized wavelengths of light with heterogeneous media such as tissue, and to account for the effects of other chromophores on the composite absorption spectra. The now common diagnostic procedure known as pulsed oximetry discriminates against background signals, but is only able to register the oxygenation of arterial blood, which is not reflective of the post-arterial state of tissue oxygen utilization.

Methods currently used for the measurement of acute oxygen levels in tissue and venous blood include gastric tonometry and pulmonary artery catheterization. Gastric tonometry involves insertion of a naso-gastric tube down into the stomach.   Pulmonary artery catheterization involves threading a catheter through the chambers of the heart, and can be a risky procedure. It would be beneficial to replace such procedures with non-invasive methods that are as easy to implement as pulsed oximetry, a method which is now universally employed for the measurement of oxygen saturation levels in arterial blood.

We have initiated measurements of hemoglobin oxygen saturation in tissues using resonance Raman spectroscopy[1-3].   The resonance Raman effect is the enhancement of Raman signals that occurs when the excitation wavelength is in resonance with an electronic absorption.   Strong enhancement of hemoglobin is afforded by excitation in the deep violet. The percent saturation of tissue hemoglobin can be determined by interrogating an externally accessible mucosal surface that is metabolically active and is known to be sensitive to changes in blood flow. The limited tissue penetration of deep violet wavelengths avoids background signals from deep tissue components[2].   The clarity of the signals obtained from animal experiments, and the modest laser power levels required, support the potential for transferring the methodology from the hard-wired laboratory bench to portable clinical systems.
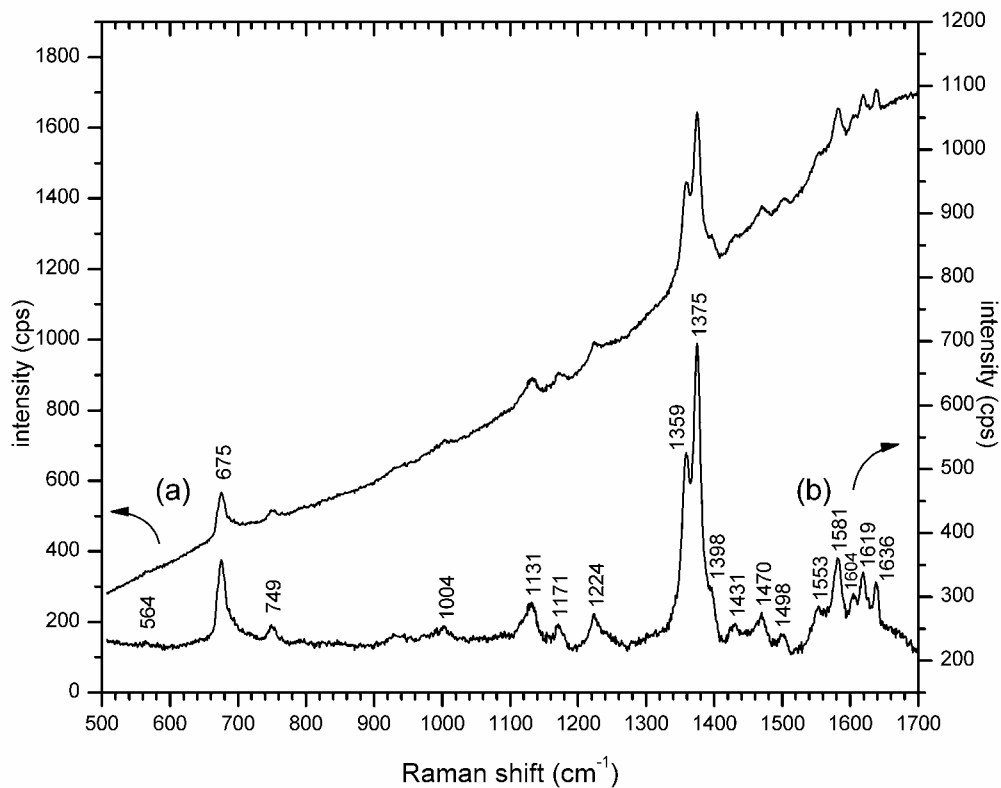
Figure 1. Resonance Raman spectra from the sublingual surface of a rat. (a) Unprocessed and (b) baseline leveled data are shown with the respective left and right vertical axes giving signal intensities. 5 mw, 406.7 nm excitation. No smoothing was performed. The fluorescence background did not significantly degrade signal quality.

Fluorescence is often cited as a major impediment to the utilization of visible lasers for biomedical applications of Raman spectroscopy, prompting the widespread implementation of longer wavelength excitation towards the near-infrared, despite the need for higher incident laser power at such wavelengths.   We have noted that though near-infrared excitation provides a lowering of background signals such as from fluorescence, this occurs at the expense of diminishment of signal intensity through the loss of the resonance enhancement that would have occurred at shorter wavelengths.   By contrast, we have found that shorter wavelength excitation of tissue in the visible range affords strong enhancement of signals from hemoglobin at low incident laser power.   The addition of potentially toxic reporter compounds is not required.   At optimal wavelengths the resonance Raman signals can be sufficiently strong that the fluorescence background does not significantly degrade the signal quality of the signals of interest (Figure 1).   With the current availability of miniaturized laser sources and fiber optic spectrometers at modest cost, it could become practical to adapt this methodology to the determination of tissue oxygen saturation in a clinical setting.

Figure 1 illustrates resonance Raman data obtained from the sublingual surface of a rat tongue. Animal experiments were approved in advance by the Virginia Commonwealth University Institutional Animal Care and Use Committee. Rats were instrumented for measurement of arterial and central venous pressure and blood gases at the femoral artery and right jugular vein, and were provided with supplemental oxygen. Animals were subjected to stepwise hemorrhage until 50% of the blood volume was removed. Blood withdrawal was

stopped intermittently at 10% increments of shed blood volume. Animals were resuscitated with shed blood after an equal volume of normal saline. Upon acquisition of Raman signals, central venous oxygen saturation was measured from blood samples from the jugular vein that were placed in sealed capillaries and subjected to traditional oximetry. Comparison of tissue oxygenation measured by resonance Raman with central venous and arterial saturation is shown in Fig. 2. Mucosal blood saturation on the underside of the tongue, as measured by resonance Raman, correlated with the saturation levels of central venous blood. The arterial blood saturation, that is ordinarily measured by pulse oximetry in human patients, was maintained at 98%.
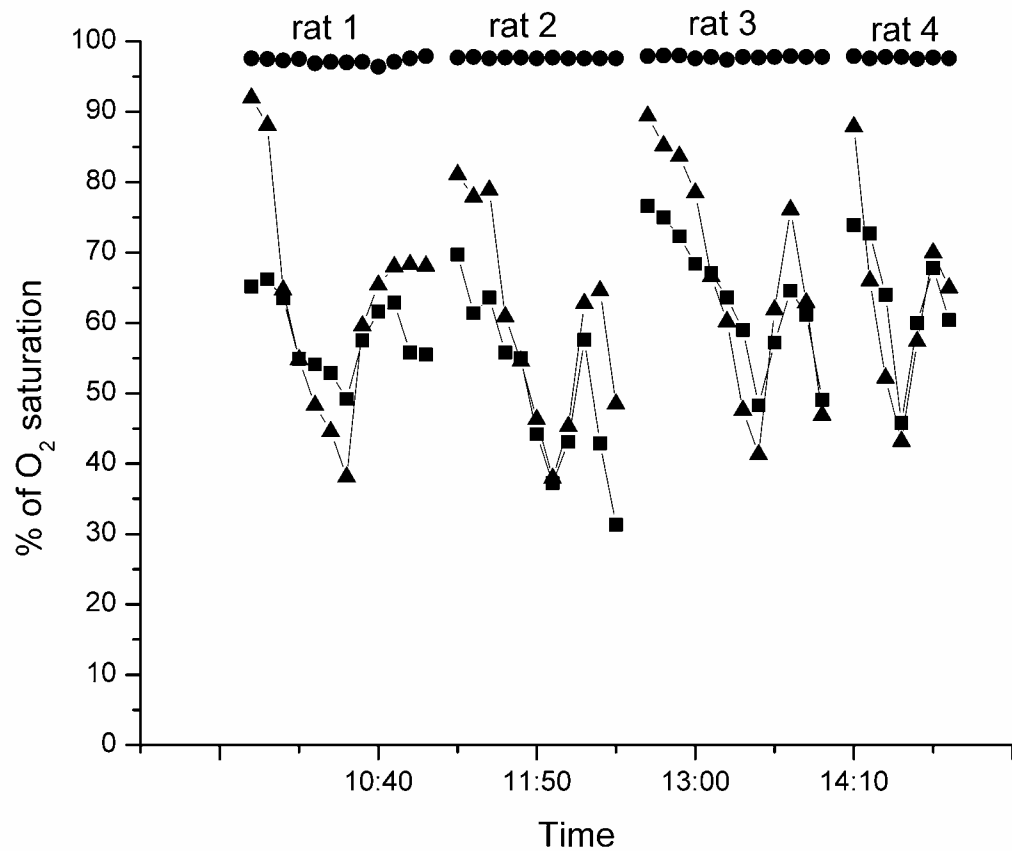
Figure 2. Comparison of the oxygen saturation of mucosal tissue on the sublingual surface of rats, measured by resonance Raman - ■ -, with saturation of arterial - ● - and central venous blood - ▲ -. The resonance Raman measurements correlated with central venous saturation.

---

[1] I. P. Torres Filho, J. Terner, R. N. Pittman, L. G. Somera, and K. R. Ward, Am. J. Physiol.- Heart Circ. Physiol. **289,** H488-H495 (2005).

[2] K. R. Ward, R. W. Barbee, P. S. Reynolds, I. P. Torres Filho, M. H. Tiba, L. Torres, R. N. Pittman, and J. Terner, Anal. Chem. **79,** 1514-1518 (2007).

[3] K. R. Ward, I. Torres Filho, R. W. Barbee, L. Torres, M. H. Tiba, P. S. Reynolds, R. N. Pittman, R. Ivatury, and J. Terner, Crit. Care Med. **34,** 792-799 (2006).

Femtosecond infrared spectroscopy of the anesthetic gas nitrous oxide in lipid-membranes

Logan Chieffo[1,3], Jason J. Amsden[2,3], Jeffrey Shattuck[1,3], M. K. Hong[2,3], Lawrence Ziegler[1,3], Shyamsunder Erramilli[2,3,4]

[1] Department of Chemistry, Boston University 590 Commonwealth Avenue, Boston, MA 02215, USA.
[2] Department of Physics, Boston University 590 Commonwealth Avenue, Boston, MA 02215, USA.
[3] Photonics Center, Boston University 8 St. Mary's Street, Boston, MA-02169, USA.
[4] Department of Biomedical Engineering, Boston University 44 Cummington Street, Boston, MA 02215, USA.
E-mail: shyam@bu.edu

More than 150 years after the discovery of anesthesia, the molecular mechanism of anesthetic action remains a mystery. General anesthesia is a complex phenomenon associated with the loss of consciousness, amnesia, suppression of spinal cord reflexes, reduced neuronal processing, alterations in the central nervous sytem and paralysis. The list of molecules that are known to form general anesthetics range from ether, halothane and other halogenated hydrocarbons, morphine, cocaine, but also include simple molecules like nitrous oxide and the inert gas Xenon. It is difficult to conceive of a single model that would explain the effect of this remarkable range of molecules. About 100 years ago, Meyer and Overton[1] discovered that the potency of anesthetics is correlated with solubility in the hydrophobic solvent olive oil. This suggested that, while individual anesthetic molecules may target different sites in lipid membranes or membrane proteins[2], the molecular level interaction may share common universal features. Conventional molecular methods like fluorescence spectroscopy have labels that are too perturbing. Vibrational infrared spectroscopy provides a label-free, nonperturbative method for the study of this important unsolved problem.

Nitrous oxide is a good model system for probing anesthetic-solvent interactions using femtosecond nonlinear infrared spectroscopy. Nitrous oxide (N-N-O) is a linear triatomic molecule. The two infrared active fundamental modes are the symmetric
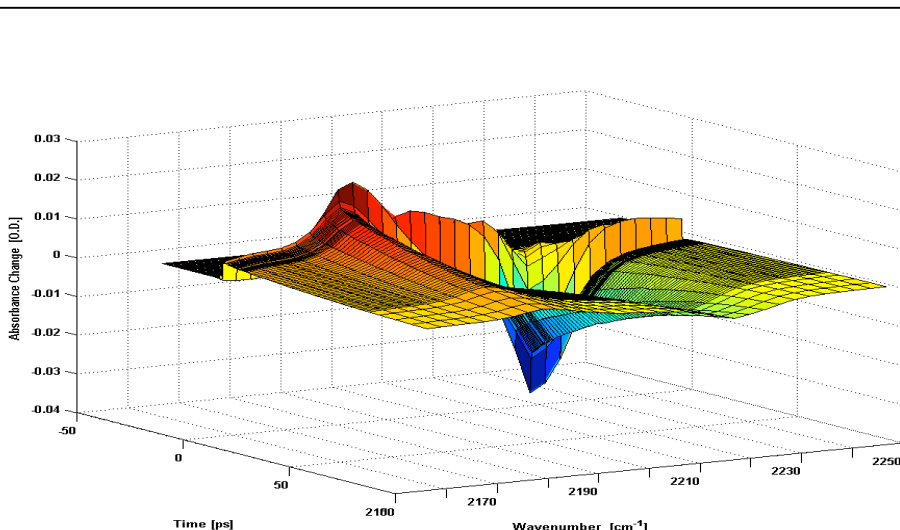
Figure 1. Array detector measurement of the vibrational dynamics of N_2O in octanol. Both ground nd excited state dynamics can be measured simultaneously, as a function of time, with a signal size limit of 10^{-5} OD on a 100 fs time scale, over a spectral range 2180cm^{-1}-2240 cm^{-1}.

[1] A. S. Janoff, K. W. Miller, in *Biological Membranes* D. Chapman, Ed. (Academic Press, 1982) pp. 417-476.
[2] N. P. Franks, W. R. Lieb, *Nature* **300**, 487 (Dec 9, 1982).

stretching mode v_1 at 1285 cm^{-1} and a strong fundamental antisymmetric stretch v_3 centered at 2224 cm^{-1} in the gas phase. The antisymmetric stretch is especially attractive as it falls in a window that is removed from the crowded part of the "fingerprint" spectrum, where a large number of normal modes due to proteins, nucleic acids and other biomolecules are present, and where the absorption due to water is reduced. Studies by Caughey and co-workers have shown that the infrared absorption spectrum associated with v_3 is sensitive to the environment[3]. We have measured the extinction coefficient of the molecule dissolved in hydrophobic solvents and find a peak extinction coefficient of 1.5×10^3 M^{-1} cm^{-1}. The potential of femtosecond 1D- and 2D-IR spectroscopy on nitrous oxide in lipid membranes for studying the molecular mechanism of anesthetic action is unique and may help to unravel the molecular mechanism of anesthetic action.

We have measured the vibrational energy relaxation lifetime of the fundamental antisymmetric stretching mode v_3 centered at 2218 cm^{-1}
(^{14}N$_2$^{16}O) dissolved in octanol and olive oil, both model systems in use today for assessment of anesthetic potency[4]. A liquid nitrogen cooled HgCdTe (MCT) array detector system was used to measure the pump-probe spectra over the spectal range 2180cm^{-1} – 2240 cm^{-1}. We report here the first studies of the vibrational energy relaxation of nitrous oxide in a lipid-water model membrane system. The results are to be compared with the pump-probe studies using octanol where the vibrational energy relaxation time of $\tau_r = 52 \pm 1$ ps was observed. We have also measured the relaxation time of N$_2$O dissolved in bulk water, where we observe τ_r to be 9±1 ps. The relaxation of N$_2$O in the fully hydrated phospholipid system 1,2-Dimyristoyl-sn-Glycero-3-Phosphocholine (DMPC)-water was measured at a temperature of 303 K, where the lipid-water system is in the liquid crystalline lamellar L_α phase. Global analysis of decays over all the frequencies show that there are multiple components in the decay associated spectra from the lipid-water system. One component, with a peak frequency at 2218cm^{-1} has a lifetime that is nearly identical to the octanol or olive oil value. This component is assigned to N$_2$O bound to the
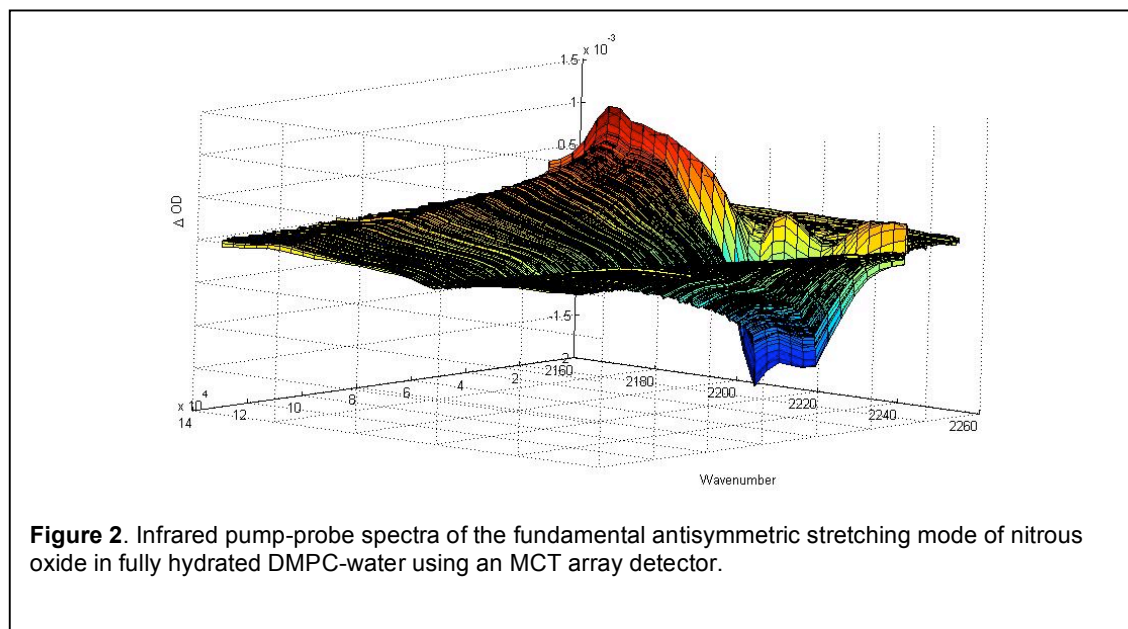
Figure 2. Infrared pump-probe spectra of the fundamental antisymmetric stretching mode of nitrous oxide in fully hydrated DMPC-water using an MCT array detector.

[3] A. Dong, P. Huang, X. J. Zhao, V. Sampath, W. S. Caughey, *J Biol Chem* **269**, 23911 (Sep 30, 1994).

[4] L. Chieffo, J. Amsden, J. Shattuck, M. K. Hong. L. Ziegler and S. Erramilli "Femtosecond infrared vibrational lifetime measurements of the anesthetic gas nitrous oxide in membranes." *Biophysical Reviews and Letters*, Vol. 1, 309-316 (2006). Web archive at arXiv:0705.0835v1

hydrocarbon tail region of the lipid water system. In the fully hydrated lipid-waer system, above the excess water point, there is another component with a lifetime of 9 ps, identical to the bulk water value. In addition to these two components, we find evidence for a third component with a lifetime in between these two values. The observations can best be explained by proposing that there is resonant energy transfer between the vibrationally excited N_2O and modes in its aqueous environment, which include continuum modes and the libration-stretch combination band that also occur in the same region of the infrared spectrum. The interesting role played by energy transfer to water molecules suggest a remarkable universal mechanism for anesthetic action, whether in lipid membranes or portein pockets.

PROTEIN AND PEPTIDE DYNAMICS

Time-domain theoretical analysis of the IR, polarized Raman, and 2D-IR spectra of peptide chains in aqueous solution

Hajime Torii

Department of Chemistry, School of Education, Shizuoka University, 836 Ohya, Shizuoka 422-8529, Japan
E-mail: torii@ed.shizuoka.ac.jp, URL: http://reve.ed.shizuoka.ac.jp/

For the purpose of elucidating the structures and dynamics of proteins and peptide chains in aqueous solution, there has been continuing interest in the analysis of their vibrational band profiles. To correctly analyze those band profiles, there are three important factors that should be taken into account: (i) diagonal frequency shifts of individual peptide groups induced by the interactions with surrounding peptide groups and solvent water molecules, (ii) off-diagonal couplings between the vibrations of the peptide groups, and (iii) the dynamics of the peptide–water system that modulate the distances and relative orientations of the peptide groups. Especially in the case of the amide I band, which is known to be sensitive to the secondary structures because of the large magnitude of the vibrational transition dipole, all these three factors are considered to be equally important. In the present study, by using a time-domain computational method (called the MD/TDC/WFP method)[1,2] combined with the Amber 8 program,[3] the profiles of the IR, polarized (isotropic and anisotropic) Raman, and 2D-IR spectra of the amide I mode are analyzed for $(Ala)_4$ (tetraalanine) and $(Ala)_{21}$ in aqueous solution.
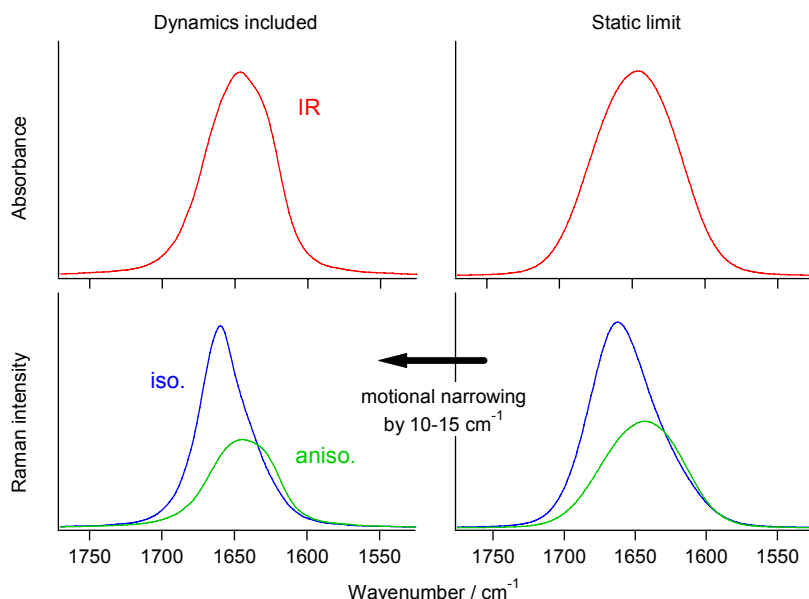
Figure 1. (Left) IR (red), isotropic Raman (blue), and anisotropic Raman (green) spectra in the amide I region calculated for tetraalanine in aqueous solution at 298 K by using the time-domain (MD/TDC/WFP) computational method. (Right) The spectra calculated with all the dynamics being frozen (static limit).

The IR and polarized Raman spectra in the amide I region calculated for tetraalanine in aqueous solution with the present computational method are shown on the left-hand side of Figure 1. It is seen that the isotropic Raman band is located at a higher frequency position than the IR and anisotropic Raman bands, i.e., there is a negative noncoincidence effect

[1] H. Torii, M. Musso, and M. G. Giorgini, *J. Phys. Chem. A* **2005**, <u>109</u>, 7797-7804.

[2] H. Torii, *J. Phys. Chem. A* **2006**, <u>110</u>, 4822-4832.

[3] D. A. Case et al., *Amber 8*, University of California, San Francisco, **2004**.

(NCE). This feature is in agreement with that of the observed spectra.[4] This negative NCE arises from the positive coupling between the vibrations of neighboring peptide groups and the negative scalar product between the transition dipoles of those vibrations, and is related to the structure of this peptide chain that is mainly in the polyproline II and β-type conformations. The IR and polarized Raman spectra calculated with all the dynamics of the system being frozen are shown on the right-hand side of Figure 1. Comparing the two sets of spectra, it is recognized that the vibrational bands are narrowed by 10–15 cm^{-1} by the modulations of the vibrational frequencies induced by the dynamics of the system.
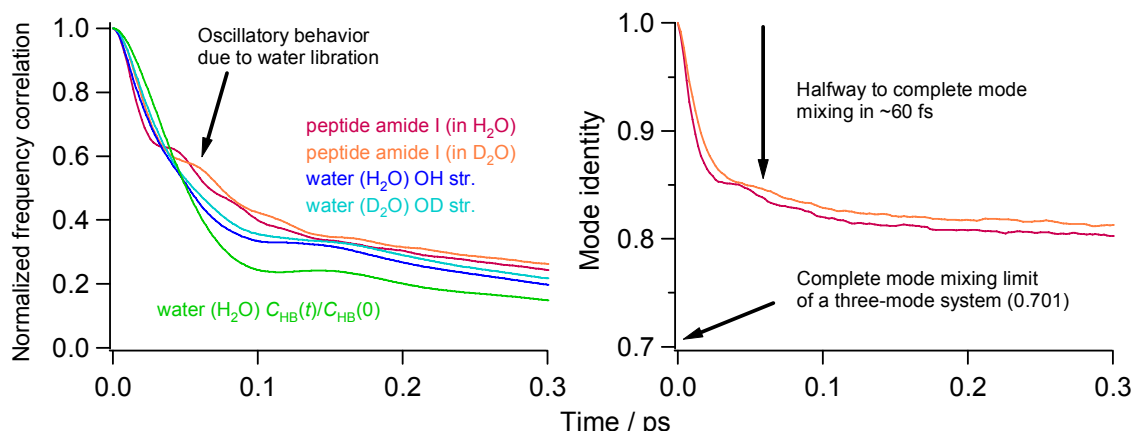
Figure 2. (Left) Normalized time correlation functions of the frequency modulations $C_L(t)/C_L(0)$ calculated for the amide I mode of tetraalanine in H_2O and D_2O solutions (red and orange), the OH stretching mode of neat liquid H_2O (blue), and the OD stretching mode of neat liquid D_2O (light blue) at 298 K. The normalized time correlation function of the hydrogen-bond length $C_{HB}(t)/C_{HB}(0)$ calculated for neat liquid H_2O is also shown. (Right) Time correlation functions of the mode identity $M(t)$ calculated for the amide I mode of tetraalanine in H_2O and D_2O solutions (red and orange) at 298 K.

To see the nature of the vibrational frequency modulations in more detail, the time correlation functions $C_L(t)$ of the frequency modulations are calculated. The result is shown on the left-hand side of Figure 2. It is seen that $C_L(t)$ decays rapidly in the first ~100 fs, giving rise to a motional narrowing effect on the band profiles, with an oscillation of the period of ~43 fs (corresponding to ~770 cm^{-1}). Because of this value of the oscillation period, and because it becomes longer by a factor of ~$\sqrt{2}$ when the solvent is changed to D_2O, it is suggested that the amide I frequencies of tetraalanine in aqueous solution are modulated by the librational motions of solvent water molecules. This is in contrast to the case of the OH and OD stretching modes of liquid H_2O and D_2O, whose frequencies are modulated by the changes in the hydrogen bond lengths.[5] The latter is clearly seen from the little isotopic effect in the form of $C_L(t)/C_L(0)$, and its similarity to that of the normalized time correlation function of the hydrogen-bond length $C_{HB}(t)/C_{HB}(0)$, as also shown on the left-hand side of Figure 2.

Since the amide I modes of peptide chains are delocalized to some extent, vibrational frequency modulations of individual peptide groups also give rise to changes in the eigenvectors, i.e., the vibrational patterns of the normal modes. This is called the non-adiabatic effect. To see this quantitatively, the time correlation function $M(t)$ of the mode identity[6] is calculated. The result is shown on the right-hand side of Figure 2. It is recognized

[4] R. Schweitzer-Stenner et al, *J. Am. Chem. Soc.* **2004**, 126, 2768-2776.
[5] H. Torii, *J. Phys. Chem. A* **2006**, 110, 9469-9477.
[6] H. Torii, *J. Phys. Chem. A* **2002**, 106, 3281-3286.

that $M(t)$ decays from unity to ~0.85 in the first ~60 fs. Considering that the limiting value of $M(t)$ upon complete mode mixing of a three-mode system is $(1+2\sqrt{3}/\pi)/3 \cong 0.701$, it may be said that the three-mode system of the amide I band of tetraalanine in aqueous solution proceeds halfway to complete mixing in ~60 fs. The similar time scales of the decays of $C_L(t)$ and $M(t)$ indicate the importance of the non-adiabatic effect in the calculations of the vibrational band profiles of peptide chains in aqueous solutions.
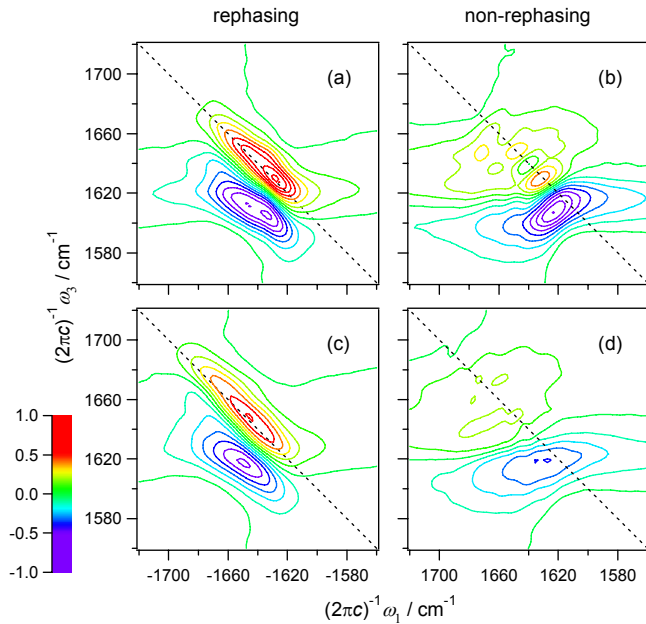
Figure 3. Rephasing and nonrephasing 2D-IR spectra (real part) in the amide I region calculated for tetraalanine in aqueous solution at 298 K by using the time-domain (MD/TDC/WFP) computational method. Parts a and b are calculated for the time interval where residues 2 and 3 are both in the region of the polyproline II or β-type conformation, and parts c and d are for the time interval where at least one of those residues is in a different conformation.

The rephasing and nonrephasing 2D-IR spectra (real part) in the amide I region calculated for tetraalanine in aqueous solution are shown in Figure 3. In this calculation, the whole simulation time is divided into two parts, the time interval where residues 2 and 3 are both in the region of the polyproline II or β-type conformation, and the time interval where at least one of those residues is in a different conformation. It is recognized that the intensity of the nonrephasing spectrum is weaker in the latter time interval than in the former. This is considered to arise from the strongly inhomogeneous situation in the latter time interval, where the two residues are located at significantly different positions on the Ramachandran map.

In the case of (Ala)$_{21}$ in the α-helical conformation, the calculated frequency difference between the IR and isotropic Raman bands (not shown) is smaller than that of (Ala)$_4$. However, this does not mean that the vibrational coupling is smaller. In the calculated rephasing 2D-IR spectrum of (Ala)$_{21}$ (not shown), a signature of strong vibrational coupling is seen as a weaker intensity of the negative band than the positive band.

Optical fingerprinting of peptides using two-dimensional infrared spectroscopy: Demonstration of principle.

Frédéric Fournier,[1] Elizabeth M. Gardner,[1] Rui Guo,[1] Paul M. Donaldson,[1] Laura M. C. Barter,[1] D. Jason Palmer,[2] Chris J. Barnett,[1] Keith R. Willison,[3] Ian R. Gould[1] and David R. Klug[1].

[1] Molecular Dynamics Research Group, Department of Chemistry, Imperial College London, Exhibition Road, London SW7 2AZ, United-Kingdom.

[2] European Laboratory for Non-Linear Spectroscopy, University of Florence, Polo Scientifico Via Nello Carrara 1, I-50019-Sesto-Fiorentino (FIRENZE), Italy.

[3] Institute of Cancer Research, Chester Beatty Laboratories, Cancer Research UK, Center of Cellular & Molecular Biology, London SW3 6JB, United-Kingdom.

f.fournier@imperial.ac.uk

Introduction

Multi-dimensional non-linear optical methods have in recent years become a practical and realizable approach to optical spectroscopy. Coherent multi-dimensional vibrational spectroscopy has in principle the power to decongest vibrational spectra and allow the fingerprinting of proteins without the need for significant sample manipulation.

Fingerprinting of peptides and proteins by two-dimensional infra red (2D IR) methods requires accessing a wide range of disparate coupled vibrational states. In order to access these, we have adopted a technique developed by Wright et al. In this article we apply this method to peptides and demonstrate its utility for fingerprinting aromatic amino acid side chains. We demonstrate the practicality of using an internal reference to achieve relative quantification of amino acid level, thereby providing a proof of principle for this particular fingerprinting strategy. The level of signal appears to be proportional to the square of the number of molecules excited; we propose to verify experimentally that a direct linear correlation can then be made between level of signal and number of molecules. The results are presented for eight peptide sequences having variable levels of phenylalanine and tyrosine.

Principle of 2D IR FWM spectroscopy

A complete description of this spectroscopic method, its principle and advantages can be found in the various publications from J. C. Wright's group. Briefly, the two-dimensional infrared four-wave mixing is a non-linear coherent optical technique giving two-dimensional vibrational spectra. Four-wave mixing is a third order process where three laser beams interact with the medium through the third order susceptibility tensor. By using two infrared (IR) beams (ω_α and ω_β) and a third visible beam (ω_γ), this technique becomes a powerful vibrational spectroscopic tool: the IR beams' wavelengths are scanned over vibrational resonances, the FWM signal appears multiplicatively enhanced when the IR beams are in resonance with coupled vibrational modes. This enhancement happens only if the vibrational modes excited by ω_α and ω_β are coupled by inter- or intra- molecular interactions or if they are composed of a fundamental mode and its overtone, or a fundamental mode and a combination band.

Results

Two-dimensional spectra of peptides

The two-dimensional vibrational spectra of the eight peptide samples are shown in figure 1.
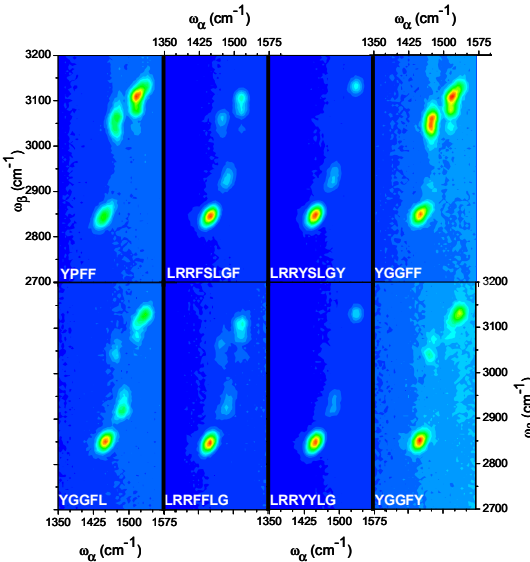
Figure 1. 2D IR FWM spectra of the eight samples studied. The amino acid sequence for each of the samples is indicated in each spectrum; F: phenylalanine, G: glycine, L: leucine, P: proline, R: arginine, S: serine, Y: tyrosine. For all spectra the delays are τ_{12}=1.5 ps and τ_{23}=1 ps. ω_α is scanned from 1350 to 1570 cm^{-1} and ω_β from 2700 to 3200 cm^{-1} both with a 5 cm^{-1} increment. The spectra are presented with the horizontal and vertical axis evenly scaled and the intensity linearly scaled; thus the peak line shapes are real. The peak at 1450/2850 common to all the spectra is attributed to aliphatic CH$_2$ vibrational modes, and is taken as an internal reference. The high frequency features are attributed to aromatic vibrational modes of tyrosine and phenylalanine.

The spectra have in common a strong peak at around 1450/2850. It has been identified as corresponding to CH$_2$ vibrational modes; this feature is used as an internal reference for the calculation of the ratio of the integrated intensities.

The identified peaks and the description of the modes are depicted in figure 2.
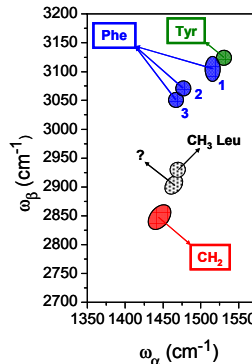
Figure 2. Identified spectral features in the peptide spectra. A spectral feature for leucine is identified, as well as a CH$_2$ peak which is present in all the peptide spectra and used as an internal reference for the fingerprinting. The peak at 1460/2900 was left unassigned: it could be a weak contribution from glycine. The CH$_2$ peak at 1450/2850 is assigned to δ CH$_2$ / ν_s CH$_2$. There are two vibrational ring stretching modes contributing to the aromatic peaks: CC+HCC in-plane (ν_{13}) and CC+HCC in-plane+CCC in-plane (ν_{16}). For phenylalanine, the peak 1 has mainly two identified contributions: 1515/3110 (ν_{13} / comb. ν_{13} & ν_{16}) and 1515/3080 (ν_{13} / comb. ν_{13} & δ CH$_2$+ν_{16}), the weaker peak at 1515/3040 being left unidentified; the peaks 2 and 3 (at 1480/3070 and 1470/3050) are attributed respectively to (δ CH$_2$+ν_{13} / comb. δ CH$_2$+ν_{13} & ν_{16}) and (δ CH$_2$+ν_{13} / comb. δ CH$_2$+ν_{13} & δ CH$_2$+ν_{16}). The tyrosine peak at 1530/3130 is only composed of the ring stretching modes: (ν_{13} / comb. ν_{13} & ν_{16}).

We focus on the phenylalanine's doublet, the most intense peak of the phenylalanine's triplet and the most intense tyrosine peak. We extract the FWHM and amplitudes, as well as the

frequencies of the aliphatic, tyrosine and phenylalanine peaks and their relative integrated intensities.

Quantification of amino-acids levels

Shown in figure 3 are the integrated intensity of the Phe and Tyr peaks relative to the CH_2 peak integrated intensity as a function of the number of Phe and Tyr present in each sequence relative to the total number of CH_2 groups.
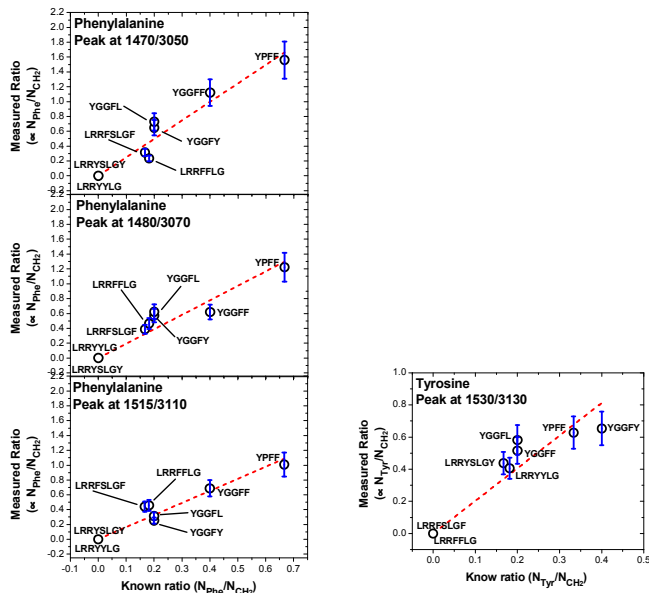
Figure 3. Correlation between the known phenylalanine(tyrosine) to CH_2 ratios and the ratios measured by 2D IR. The square root of the ratio of the integral of the peaks relative to the aliphatic peak integral ($Ratio_{Phe(Tyr)} \propto N_{Phe(Tyr)}/N_{CH_2}$) is plotted as a function of the known relative number of phenylalanine(tyrosine) compared to the number of CH_2 groups. Data points are shown by open circles and are labeled by the amino acid sequence of the corresponding sample. The dashed red line is the linear fit. The vertical error bars are the standard errors obtained from a reproducibility test performed on eight different YPFF samples (blue).

Conclusion

Two-dimensional spectra of peptide side chains have been measure and specific features corresponding to the aromatic vibrational modes of tyrosine and phenylalanine were identified as well as an aliphatic mode. Using the spectra obtained for different amino acid sequences containing different amounts of phenylalanine and tyrosine, it has been shown that the relative integrated signal strengths are proportional to the numbers of phenylalanine or tyrosine in the peptide relative to the number of methylene groups. The linear behaviour demonstrated here comforts the idea of using this technique as a proteins fingerprinting. Using established relationships like the ones shown in the figures 3, it is possible to determine a quantity ratio using a measured intensity ratio. Ultimately, the strategy will be to dispose of a database of amino acids quantity ratios determined from a database of known proteins. For a given unidentified protein, the intensity ratios will be measured for a certain number of identified peaks, each corresponding to a specific known amino acid. The quantity ratios corresponding will be compared to the proteins ratios database and then the corresponding protein will be identified. Preliminary tests made using such a database (30000 human proteins) have shown that if the mass of the unknown protein is initially measured with 5kDa, 5 amino acid quantity ratios measured within 10% accuracy would be enough to identify the protein.

Future work will identify fingerprint modes for other key amino acids and apply this knowledge to the fingerprinting of proteins.

Hydrogen Bond Dynamics in Complexes of Formic Acid with Amines

Christopher M. Cheatum, Kenan Gundogdu, Jogar Bandaria, Michael Nydegger, William Rock

Department of Chemistry, University of Iowa, Iowa City, Iowa. Christopher-cheatum@uiowa.edu, http://www.chem.uiowa.edu/faculty/cheatum/

Introduction Hydrogen bonding is among the strongest intermolecular interactions with important applications ranging from structural biology to the solvation properties of liquids. Strong hydrogen bonds in asymmetric complexes are interesting because of their relationship to proton-transfer reactions, which underlie many chemical phenomena including acid-base chemistry, biological energy transduction, and enzyme catalysis. Infrared absorption spectroscopy has long been used to characterize hydrogen bonds because of the distinct red shift and line broadening of the proton-stretching vibration of hydrogen-bonded complexes. These effects result in line shapes that span 1000 cm^{-1} or more, but, in spite of extensive experimental and theoretical study, the origins of these unusually broad absorption bands are not fully understood.[1]

We report a transient grating study of the vibrational dynamics of the proton-stretching vibration in complexes of formic acid with pyridine and pyrazine.[2] Formic acid forms strong hydrogen bonds to these bases as indicated by the broad, red-shifted absorptions for the proton-stretching bands of these complexes. We measured transient grating decays at four excitation wavelengths. The transients decay on two time scales consistent with a sequential relaxation model. We also observe oscillations of the transient grating signal whose amplitude and frequency depend on the excitation wavelength. We present a model incorporating these features that accurately reproduces the essential features of our grating measurements.

Results Figure 1 shows the infrared absorption spectra of the complexes of formic acid with both pyridine and pyrazine in CCl$_4$. These complexes have broad absorptions characteristic of strong hydrogen bonds.
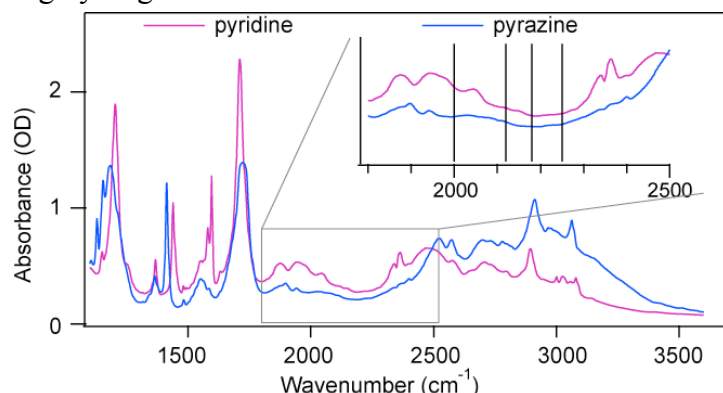
Figure 1. Infrared absorption spectra of complexes of formic acid with pyridine and pyrazine. The inset focuses on the region for our measurements with the experimental excitation energies indicated by vertical lines.

Figure 2 shows the transient grating decays for formic acid with pyridine (a) and pyrazine (b) along with fits to the model outlined below. For each base, we show transients at four excitation wavelengths: 2250 cm^{-1}, 2180 cm^{-1}, 2120 cm^{-1}, and 2000 cm^{-1} (top to bottom). These excitation wavelengths probe the deep, broad hole in the spectrum near 2200 cm^{-1}. The

---

[1] T. Elsaesser and H. J. Bakker, "Ultrafast Hydrogen Bonding Dynamics and Proton Transfer Processes in the Condensed Phase", Kluwer, Dordrecht, **2002**

[2] K. Gundogdu, J. Bandaria, M. Nydegger, W. Rock, C.M. Cheatum, J. Chem. Phys., (In Press)

large peak at time zero for each transient comes from the nonresonant response of the solvent which decays within 200 fs.
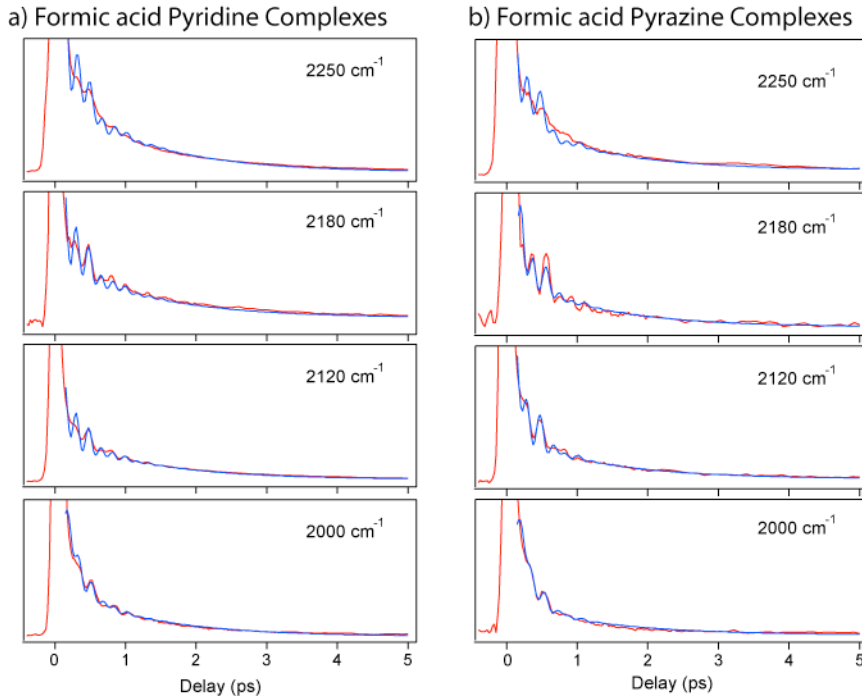
Figure 2. Transient grating decays (red) for formic acid with pyridine (a) and pyrazine (b) at four different excitation wavelengths and fits (blue) to the kinetic model outlined below.

Figure 3 illustrates the model we use to describe the data. We assume a model comprised of three, coupled, anharmonic oscillators. We model the population relaxation using an irreversible sequential kinetic scheme. Population in any of the one-quantum states relaxes first to an intermediate state that is weakly anharmonically coupled to the initially excited states and, ultimately, returns to the ground state.
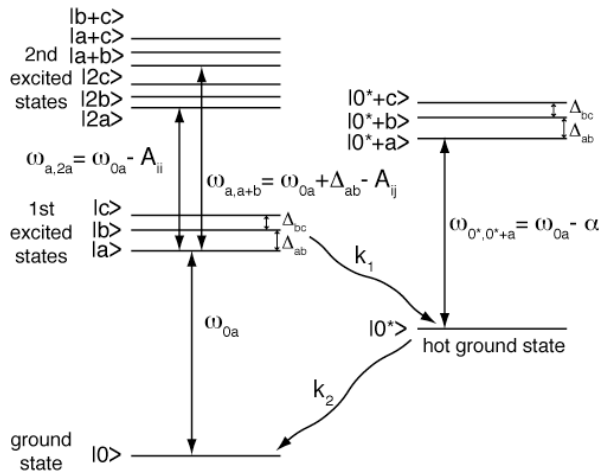
Figure 3. Schematic diagram of the model used to describe the transient grating decays. The model corresponds to three coupled oscillators whose population relaxation mechanism follows a sequential kinetic scheme through and intermediate hot ground state.

Table 1 gives the parameters used in the model to simulate the grating decays. These result from a global fit to the excitation wavelength dependent transients for each complex.

	ω_{0a} (cm^{-1})	Δ_{ab} (cm^{-1})	Δ_{bc} (cm^{-1})	μ_{0a}	μ_{0b}	μ_{0c}	$1/k_{deph}$ (fs)	$1/k_1$ (fs)	$1/k_2$ (fs)
Pyridine	2040	125	68	1	0.58	1.13	400	400	2560
Pyrazine	2040	123	60	1	0.79	1.21	370	370	2560

Discussion All of the transients we measure show coherent oscillations that depend strongly on the excitation wavelength and decay at a rate similar to the fast component of the population kinetics. The oscillations arise from the natural time evolution of a coherent superposition state prepared by the broadband excitation pulses that form the transient grating. Our model uses three one-quantum states and we observe oscillations with frequencies that correspond to the energy differences between each pair of these states. The vibrational character of these states is important because it relates to the molecular origins of the breadth observed in the infrared absorption spectrum. One possibility is that low-frequency motions of the hydrogen-bonded complex couple to the proton-stretching vibration leading to a Franck-Condon-like progression of states built upon the proton-stretching transition as proposed for some previously studied complexes.[3,4] Then, the coherence we excite in our experiment would involve superpositions of states in the low-frequency coordinates. Another possibility is that the strong hydrogen bond between formic acid and the base improves the coupling of the O-H stretch to nearby overtones and combination bands. If the state mixing is sufficiently large, the O-H stretching vibration will be Fermi-resonance coupled to many states across the spectrum. In this case, the coherences that we excite in our experiments will be superpositions of these Fermi-resonance-coupled overtone and combination states that gain oscillator strength by mixing with the bright O-H stretching vibration.

If low-frequency modes were responsible for the oscillations we observe, then the oscillations should decay on a time scale longer than the relaxation of the O-H stretch excited-state population. For the formic acid complexes we study, the oscillations decay with the same rate as the population decay for the initially prepared state. The absence of longer-lived oscillations from coherences in the ground state of the O-H stretch suggest that low-frequency motions do not contribute to the oscillatory dynamics we observe. In addition, the excitation-wavelength dependence of the oscillations should be rather weak for low-frequency coherences. Thus, the excitation-wavelength dependence of the oscillatory components we observe argues against low-frequency modes as the source of the oscillations. Finally, the frequencies of the oscillations for this mechanism should be different for the complexes of formic acid with pyridine and pyrazine because of the differences in hydrogen-bond strength. In contrast, we observe only a small difference in the oscillation frequencies for complexes with pyridine and pyrazine. Thus, although we cannot rule out their potential contribution, it seems unlikely that superpositions of low-frequency motions are the origin of the oscillatory contributions to our measurements.

Although our results indicate the character of the states we excite, the identity of these Fermi-resonance-coupled states remains uncertain. There are no distinguishable features in the absorption spectrum across the spectral region we probe in our measurements. On the red edge of this region there is some structure to the spectrum, but the states that underlie this structure do not give rise to coherent oscillations because we see only weak oscillatory contributions at the lowest excitation energies. These complexes require further study, both experimental and theoretical, to discern the character of the Fermi-resonance-coupled states that broaden the spectrum.

[3] K. Heyne, N. Huse, J. Dreyer, E.T.J. Nibbering, T. Elsaesser, J. Chem. Phys., **2004**, 121, 902-913
[4] J. Dweyer, J. Dreyer, E.T.J. Nibbering, T. Elsaesser, Chem. Phys. Lett., **2006**, 432, 146-151

Energy Transport in Peptide Helices

Ellen Backus[1], Virgiliu Botan[1], Rolf Pfister[1], Alessandro Moretto[2],
Marco Crisma[2], Claudio Toniolo[2], Phuong Nguyen[3], Gerhard Stock[3],
Peter Hamm[1]

[1] Physikalisch-Chemisches Institut, Universität Zürich, Winterthurerstrasse 190, CH-8057 Zürich, Switzerland. [2] Department of Chemistry, University of Padova, Via Marzolo 1, I-35131 Padova, Italy. [3] Institut für Physikalische und Theoretische Chemie, J. W. Goethe Universität, Marie-Curie-Strasse 11, D-60439 Frankfurt, Germany. E-mail: e.backus@pci.unizh.ch.

Proteins are the macromachines of life. They act for example as catalysts or transport small molecules (e.g. oxygen by hemoglobin) through living systems. As such they play a key role in the functioning of living organism. Protein action requires energy transport to the active site. On the other hand, as proteins only work in narrow temperature ranges, access energy has to be removed efficiently from the proteins active site. It has been suggested that vibrational energy transport is possible through the helical part of a protein. In order to study this, we have constructed a stable 3_{10}-helix of 8 amino acids (Aib, a less common but natural amino acid) which a chromophore (azobenzene) attached at one side (see figure 1). With only 8 residues stable 3_{10}-helices are formed.
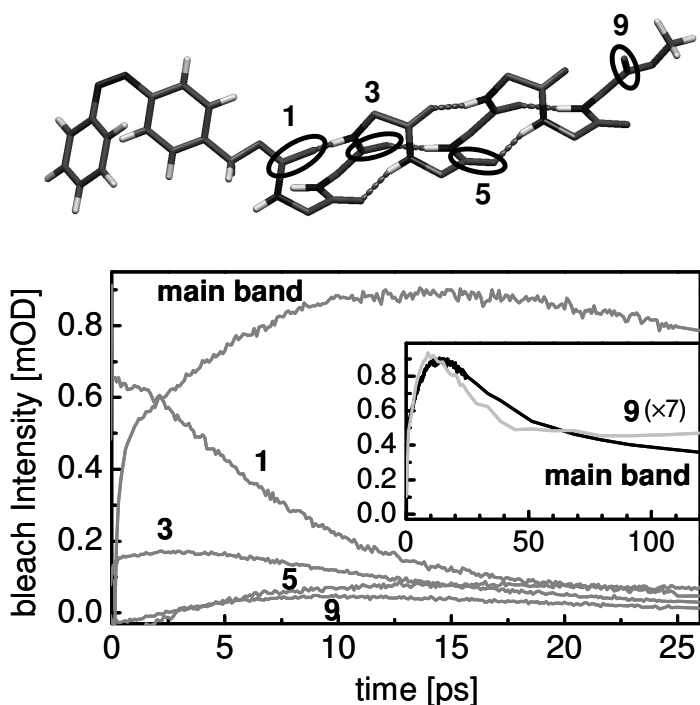
Figure 1: Chemical structure of the backbone of the helix and the attached chromophore and time dependencies of the bleach intensities of bands 1 to 9 and the main band (all other CO groups). The inset shows the recovery of the main band and band 9 on a longer timescale. The tags **1** to **9** label the CO groups.

Excitation of the azobenzene with a femtosecond laser pulse results in a large local temperature increase on short timescales (~200 fs) due to ultrafast isomerisation. The subsequent transport of energy through the helix is detected by molecular groups acting as

local thermometers at specific locations with a second, non-perturbing laser pulse at different times after exciting the azobenzene. The CO groups of the backbone of the peptide could be used as local thermometers, as vibrational band shifts in frequency upon heating its surrounding[1]. To be site selective we have used different molecules with an isotopically labeled C=O group at different locations along the helix (e.g. 3 and 5 in figure 1). As the C=O group at the start and end of the helix are chemical different from the others, we can use them as intrinsic labels (label 1 and 9).

With this approach we observed energy transport along the helix: the maximum of the bleach intensity of group 3 comes later then the one of group 1 (see figure 1). However, for label 5 and 9 we only observe a signal that is similar to the main band (all other CO's groups that are not labeled). Apparently, the transport along the helix has to compete with energy losses into the solvent. Another clear observation in the figure is the presence of a signal already at time zero for band 1 and 3. Apparently immediately after excitation heat has reached already these groups. As at t=0 the azobenzene isomerizes we assign this signal to ballistic transport, a shock wave, through the helix. This type of transport reaches only the helix part that is relative close to the chromophore, the part (apparently the first ~10 heavy atoms) where the chain is relative rigid.

To unravel whether the energy transport takes place via the backbone of the peptide or via the hydrogen bonds (e.g. between 1 and 3, see figure 1), we constructed a molecule with the label at position 2. Unfortunately the signal of this band is partly covered by the signal from the main band. Nevertheless we can conclude that the amount of heat in band 2 is higher than in band 3. The maximal temperature relative to the temperature of band 1 has been plotted in figure 2 as a function of the band number. Clearly, the energy first arrives at band 1, then at 2 and then at 3. So the energy travels via the backbone.
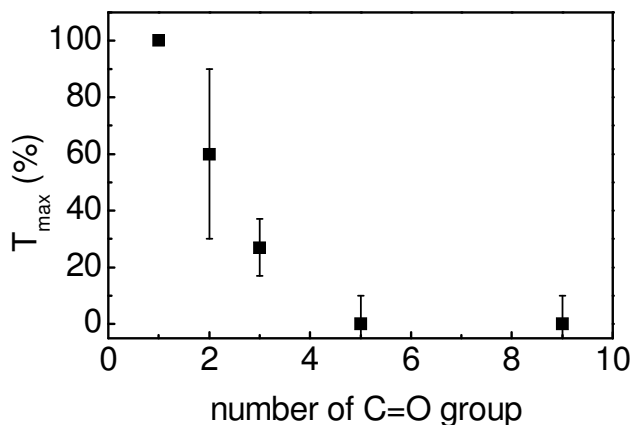
Figure 2: Maximal amplitude of the energy transferred to the C=O groups.

By modeling the data with a simple model of coupled differential equations we can describe our observation quite well with an energy transport time of 2 ps between neighboring amino acids and a cooling time to the solvent of ~7 ps. By relating the energy transport time

---

[1] P. Hamm, S.M. Ohline, and W. Zinth, J. Chem. Phys., **1997**, 106, 519-529

to the heat diffusivity $D=\Delta x^2/\tau$ (with $\Delta x \approx 2\text{Å}$ being the helical translation per residue for a 3_{10}-helix[2]), we obtain $D=2\ \text{Å}^2\text{ps}^{-1}$.

The cooling to the solvent results in an elevated temperature of the solvent. This is reflected in the increase of band 5, 9 and the main band (all other CO groups) on the 7 ps timescale. At this fast timescale only the solvent molecules in the neighboring of the peptide are hot. As time proceeds the heat is further equilibrated into the probe volume, resulting in a cooling of the solvent close to the peptide reflected in the decrease of the bleach for band 5, 9 and the main one.

The main conclusions of the work[3], instantaneously heat signal for group 1 and 3 and after that energy transfer along the backbone of the helix, are corroborated by MD simulations.

---

[2] C. Toniolo and E. Benedetti, Trends Biochem. Sci., **1991**, <u>16</u>, 350-353

[3] V. Botan, E.H.G. Backus, R. Pfister, A. MOretto, M. Crisma, C. Toniolo, P.H. Nguyen, G. Stock, and P. Hamm, Proc. Natl. Acad. Sci. USA, **2007**, accepted

α-helix formation on a photoswitchable peptide gathered by means of time-resolved IR spectroscopy

Janne Ihalainen[1], Jens Bredenbeck[1,2], Ellen Backus[1], Rolf Pfister[1], Peter Hamm[1]

[1] Institute of Physical Chemistry, University of Zürich, Winterthurerstrasse 190, CH-8057 Zürich, Switzerland. [2] Johann Wolfgang Goethe-University Institute of Biophysics Max-von-Laue-Str. 1, 60438 Frankfurt/Main, Germany. E-mail: jihala@pci.unizh.ch.

By using two synchronized femtosecond laser systems together with specially designed photo-switchable helices, we have recently established an experimental method which allows us to capture all timescales of the folding and unfolding processes, from picosecond motions of individual side chains to the final formation of the α-helix on a microsecond timescale [1-3].
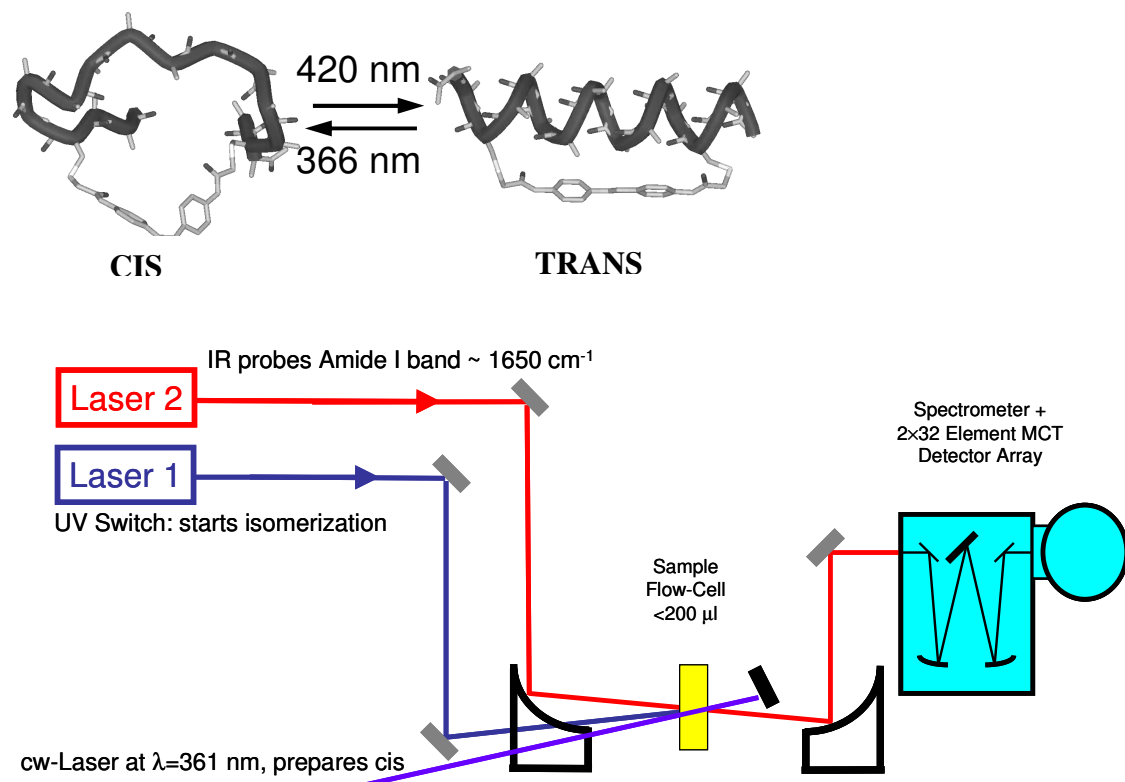
Figure1. Upper panel: Schematic drawing of the photoswitchable peptide in its cis (left) and trans (right) conformation. Lower panel: Schematic drawing of the experimental set up.

Briefly about the laser systems [3], the output of laser system 1 is frequency doubled to generate pulses which switches the azobenzene between the cis and the trans state. In order to initiate unfolding, the transition from trans (folded) to cis (unfolded) is initiated by a short (700 fs) laser pulse at 380 nm. To initiate folding, first the initial cis state is prepared by continuous UV irradiation with an Ar-Ion Laser (Coherent "Innova 100", 363 nm, 50 mW) or with a photodiode (Blue color illuminator, Marubeni) and the transition from cis to trans is then initiated by a (700 fs) laser pulse at 425 nm. The output of laser system 2 is used to pump an OPA to obtain IR probe pulses (100 fs, center frequency 1620 cm^{-1}, bandwidth 240 cm^{-1} FWHM) which detects the changes on the amide I' vibration (at around 1640 cm^{-1} with the other laser system) indicative to the dynamic changes of the peptide during the reaction (Figure 1).

By measuring folding and unfolding reactions of one and the very same molecule we observed that (i) both folding and unfolding show complex spectral kinetics at all time ranges from picoseconds up to microseconds, (ii) the kinetics of both folding and unfolding processes show strong temperature-dependence, (iii) different types of kinetics are obtained when one observes folding or unfolding process at different wavelengths within the amide I' band, (iv) the spectral responses are different in the folding and unfolding experiments (See Figure 2). We concluded that the low helical form of the peptide consists of a rather small number of mis-folded states [2], and suggested that the rate limiting step for folding is the escape from those mis-folded states (Figure 3).
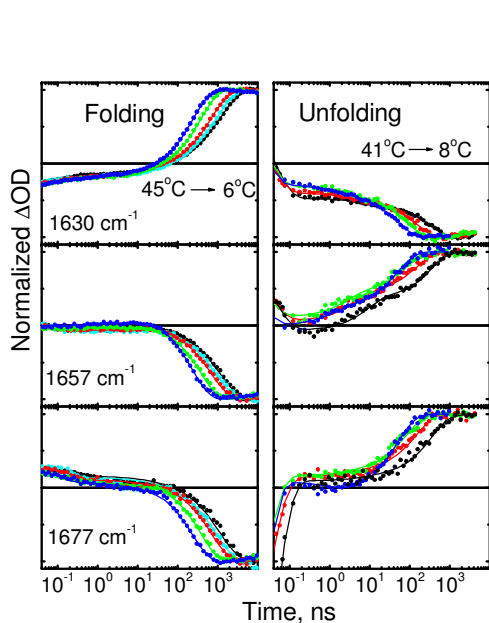
Figure 2. Kinetic traces at various wavelengths and temperatures in the folding (left panel) or unfolding (right panel) process.
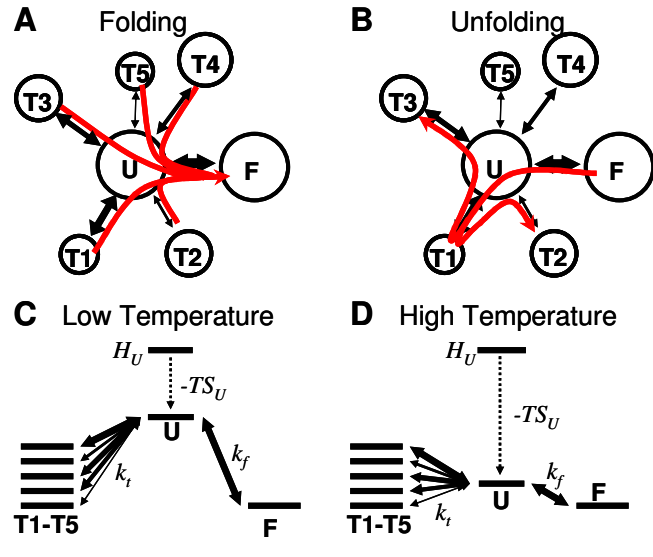
Figure 3. A proposed model (A and B) and the effect of temperature on the barrier heights, which in principle is the unfolded state U (C and D).

In order to get more insight on the kinetic behaviour of those mis-folded states we detected folding kinetics on a single amino acid level by utilizing ^{13}C=^{18}O labelled peptides. In this way single-amino acid resolution can be obtained as the frequency of a particular amino acid downshifts about 65 cm^{-1} from the main band. The usage of ^{13}C=^{18}O labelling has two advantages compared to ^{13}C=^{16}O. First, the amide I' frequency is further down-shifted from the main band and therefore easier to detect, and second, a possible small dipole-dipole coupling between the labelled group and the remainder of the peptide, leading to delocalization of the vibrational state, is considerably reduced. Any signal from a ^{13}C=^{18}O label reports therefore on the formation or breaking of a single hydrogen-bond.

In order to get isotope labelled peptides the alanine 1-^{13}C and H$_2$^{18}O were purchased from Cambridge Isotopes Laboratories. The ^{16}O to ^{18}O exchange in the Ala-carbonyl was performed as described in Ref. [4] and the FMOC-protection for the ^{13}C=^{18}O-labeled alanine was performed as described in Ref. [5]. IR together with mass spectroscopic analysis confirmed that the sample contained more than 90% FMOC-Ala-1-^{13}C=^{18}O-^{18}OH. Ac-AACAKAAAAKAAACKA-NH2 labelled at eight different positions were prepared using FMOC-based solid phase peptide synthesis (GL Biochem(Shanghai) Ltd.). The peptides were

then cross-linked with the photo-isomerizable linker [6] to obtain the photoswitchable peptide.

By measuring the folding rates of peptides with $^{13}C=^{18}O$ labelling at various positions we have been able to detect individual folding rates at each position of the peptide. We will show in the forthcoming publication that the complexity that exists in the peptide folding kinetics can be obtained only with techniques where resolution reaches a single amino acid level [7].

References:

1. Bredenbeck, J, Helbing, J, Kumita, J. R, Woolley, G. A, & Hamm, P. (2005) Proc. Natl. Acad. Sci USA 102, 2379-2384
2. Ihalainen, J. A, Bredenbeck, J, Pfister, R, Helbing, J, Chi, L, van Stokkum, I. H. M, Woolley, G, & Hamm, P. (2007) Proc. Natl. Acad. Sci. 104, 5383-5388
3. Bredenbeck, J, Helbing, J, & Hamm, P. (2004) Rev. Sci. Instrum. 75, 4462-4467
4. Murphy, R. C. and Clay, K. L. (1990) Meth. Enzymol. 193, 338-343
5. Bolin, D. R., Sytwu, I. I., Humiec, F., and J. Meienhofer, J. (1989) Int. J. Peptide Protein Res. 33, 353-359
6. Kumita, J. R., Smart, O. S., and Woolley, G. A. (2000) Proc. Natl. Acd. Sci. USA 97, 3803-3808
7. Ihalainen, J.A. Backus, E.H.G., Bredenbeck, J., Pfister, R., Woolley, G.A. & Hamm, P. Submitted

Investigation of the Z → E Isomerization of a Hemistilbene/Hemithioindigo Based Peptide-Switch with Ultrafast Infrared Spectrocopy

N. Regner[1], T. Cordes[1], B. Heinz[1], T. E. Schrader[1], C. Hoppmann[2],

K. Rück-Braun[2], and W. Zinth[1]

[1] Lehrstuhl für BioMolekulare Optik, Department of Physics, University of Munich, Oettingenstraße 67, 80538 Munich, Germany, email: nadja.regner.@physik.uni-muenchen.de

[2] Technical University Berlin, Institute for Chemistry, Straße des 17. Juni 135, 10623 Berlin
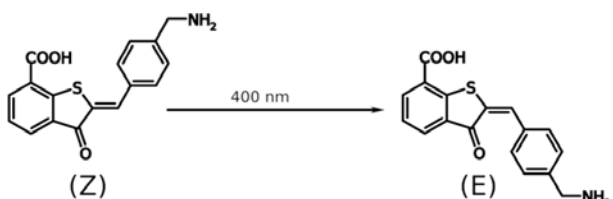
Figure 1: Structures of the Z and E-isomers of the investigated HTI ω-amino-acid.

Photoinduced Z/E isomerizations are prominant prototype reactions with high importance in chemistry and biology.[1] The photochromic compound HTI derived by combining a hemithioindigo and hemistilbene moiety can model a ω-amino acid. This molecule may act as a backbone switch in peptides and proteins.[2] Ultrafast photochemistry of Z/E isomerzations of HTI leads to a deeper understanding of the underlying molecular processes. The Z→E isomerzation of the HTI-ω-amino-acid shown in Figure 1 can be triggered by irradiation at 400 nm.

A variety of time resolved measurements has been performed to characterize the photochemical reaction course of the Z→E isomerization: Transient absorption experiments in the visible and infrared together with transient fluorescence.[3] Both visible experiments can be described by multi exponential analysis with three time constants of 200 fs, 4 ps, 30 ps . These results suggest a reaction course with three intermediate states.

These intermediates can be kinetically interconnected in various ways. A branched and a sequential scheme (see Figure 2, right part) are two reasonable models. In the branched scheme a relaxed state (RS) and a state with charge transfer character (CTC) are formed in parallel (200fs) out of the Franck-Condon state (FC*). The two states subsequently decay with 4 ps and 30 ps. Considering a sequential scheme the FC*-state relaxes into the RS state which then populates the CTC-state. To distinguish between these two possible schemes, fluorescence spectra of the intermediate states for both models are calculated and shown in the left part of Figure 2.
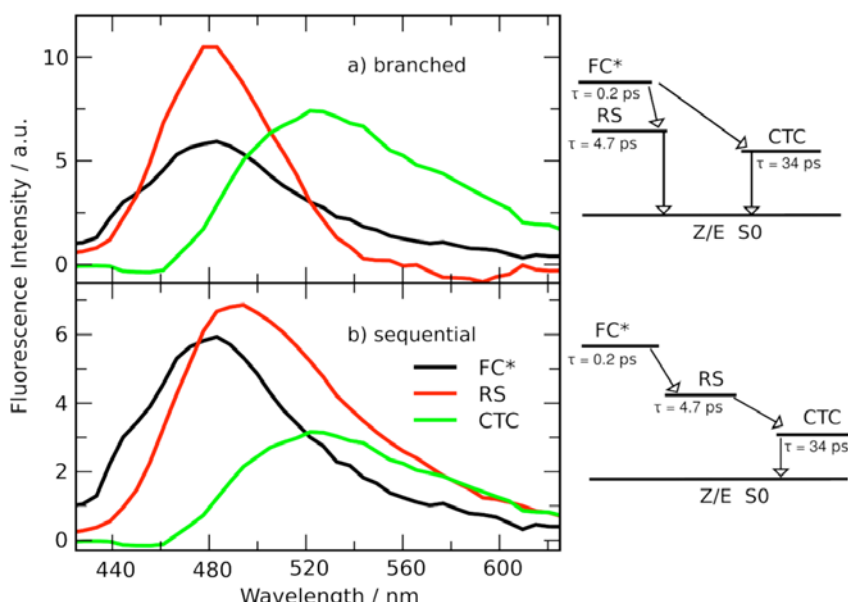
Figure 2: Calculated fluorescence spectra of the intermediate states associated to the models shown in the right panel of the figure. a: branched model; b: sequential model.
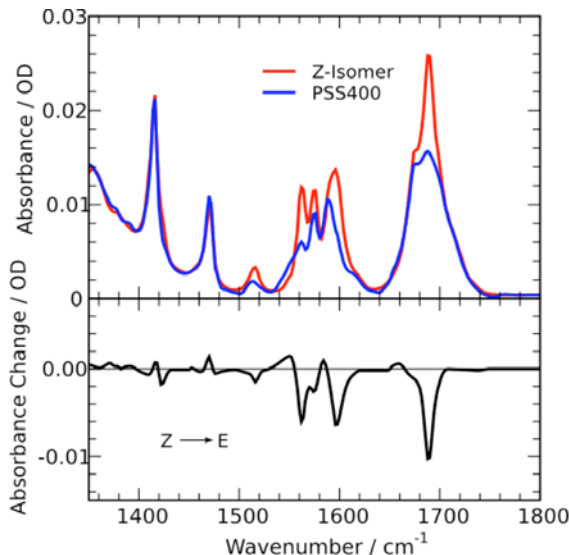
Figure 3: Upper panel: IR-spectra of the Z-Isomer and the PSS400 (ca. 85% E isomer) of the HTI-molecule. Lower panel: Difference of the spectra above.

The calculated FC* spectrum for both reaction models peaks at 480 nm with a long wavelength emission up to 650 nm. In case of the branched scheme (Figure 3a) a RS fluorescence spectrum with a higher amplitude as the FC* state is observed which additionally peaks at the same spectral position. However vibrational and solvent relaxation should be associated with the FC* → RS transition, hence the fluorescence intensity should be conserved and the peak maximum should be red-shifted. The CTC fluorescence shows an increase in oscillator strength and the expected red-shift of the maximum. The results obtained for the branched model are in contradiction to theoretical arguments.

The sequential model detailed in Figure 3b gives a better description of the molecular processes: the RS emission has approximately the same oscillator strength as the FC* emission and peaks at longer wavelength. The emission of the CTC state is decreased in comparison to FC*/RS with a strong red-shift.[4] The weakened and red-shifted emission supports the charge transfer character of this state. We now consider time-resolved infrared measurements to prove the assumption of a sequential model.

The IR spectrum of the Z-isomer (Figure 3, upper panel) of the HTI molecule shows an intense C=O mode at 1680 cm^{-1}. Isomerization (λ_{exc} = 400 nm) into the E-isomer reduces the intensity of this mode in the high frequency region (Figure 3, lower panel). As the C=O modes are strongly affected by the switching process, the time-resolved measurements focus on the corresponding spectral region from 1650 - 1720 cm^{-1} (Figure 4, upper part). The HTI-molecules (Z-form) were excited with ultrashort (190 fs) pulses centered at 402 nm with subsequent probing of the transient absorption changes in the infrared.[5]

At early delay times (t_D = 0.5 ps) a pronounced absorption decrease of the original C=O stretch absorption band around 1680 cm^{-1} is observed. Additionally a broad absorption increase at all other frequencies is present. These spectral features point to the population of an excited electronic state. The bleaching signal

Figure 4: Upper panel: Transient spectra at certain delay times. Lower panel: Amplitude spectra derived from a global fitting routine.

shows no significant change within the next 10 ps, the transient signal corresponding to the CO-mode recovers on slightly longer timescales. The transient data set can be fitted by a multi-exponential function with three time constants of 2.4 ps, 34 ps and 600 ps (Figure 4, lower panel). The amplitude spectrum of the 2.4 ps kinetic component shows no indications for recovery of the CO-band. The broad absorption increase related with this process can be interpreted as a rearrangement and relaxation of the HTI-molecule in the exited electronic state. The strongest amplitude is found for the 34 ps time constant. This process can be associated with the return of HTI-molecules into the electronic ground state and marks the end of the photoreaction. The 600 ps time constant shows a very broad spectral signature which is positioned in the range of the carboxy modes. Therefore this component may preliminary be assigned to a reorientation of the carboxy group and its surroundings. The infrared measurements clearly show that the rate limiting step of the photoreaction is associated with the 30 ps time constant. Additionally no indications of ground state return on the timescale of a few pico seconds (200 fs, 4 ps) are found.

These results are summarized in the sequential reaction model (Figure 5). After optical excitation of the Z-isomer a FC*-state relaxes with 200 fs into the RS-state. In the next process, which takes ca. 4 ps, the system populates the CTC with a strongly red-shifted emission. The final reaction is the transition into the ground state (Z or E isomer). From the CTC state the transition to the ground state of the photoproduct is only possible if the molecule considerably changes its shape to reach a critical geometry. Therefore a molecule in the CTC-state has to overcome a barrier. Subsequently the molecule reaches the ground state presumably via a conical intersection.[3]

Figure 5: Sequential model for the pathway of the Z→E reaction.

In conclusion we clearly demonstrated the sequential photochemical pathway of HTI-molecules. Alternative reaction pathways could be excluded by the use of time-resolved infrared spectroscopy and a theoretical modeling procedure.

[1]   C. Dugave, L. Demange, *Chem. Rev.* **2003**, 103, 2475-2532.
[2]   T. Cordes, D. Weinrich, S.Kempa, K. Riesselmann, S. Herre, C. Hoppmann, K. Rück-Braun, W. Zinth, *Chem. Phys. Lett.* **2006**, 428, 167-173.
[3]   T. Cordes, B. Heinz, N. Regner, C. Hoppmann, T. E. Schrader, W. Summer, K. Rück-Braun, W. Zinth. *ChemPhysChem,* **2007,** DOI 10.1002/cphc.200700223 .
[4]   W. Baumann, H. Bishcof, J. C. Frohling, C. Brittinger, W. Rettig, K. Rotkiewicz, *J. Photochem. Photobiol. A* **1992**, 64, 49-72
[5]   T. Schrader, A. Sieg, F. Koller, W. Schreier, Q. An, W. Zinth, P. Gilch, Chem. Phys. Lett. 392 (2004) 358.

Ultrafast β-Turn Opening Observed by Transient 2D–IR Spectroscopy

C. Kolano[1], J. Helbing[1], M. Kozinski[1], W. Sander[2], P. Hamm[1*]*

[1] Physikalisch-Chemisches Institut, University of Zürich, Winterthurerstrasse 190, CH-8057 Zürich, Switzerland.

[2] Lehrstuhl für Organische Chemie II, Ruhr-Universität Bochum, Universitätsstr. 150, D-44801 Bochum, Germany

c.kolano@pci.unizh.ch
http://www.pci.unizh.ch

Understanding biomolecular processes at the atomic level means determining the unique and highly organized functional three dimensional structure in which biomolecules fold, as well as dynamic interconversions between conformations. Our view of biomolecules is mainly based on the static architecture, probed by X–ray and neutron scattering methods and nuclear magnetic resonance (NMR). Changes in these architectures on ultrafast timescales, however, are very difficult or impossible to observe by these techniques. 2D–NMR spectroscopy, in contrast, is intrinsically very slow, in particular in the *non-equilibrium* regime. 2D–IR spectroscopy measures local contacts between molecular groups through the coupling between vibrational transitions, similar as 2D-NMR spectroscopy does for spins, however, it is many orders of magnitudes faster. Transient 2D infrared (T2D-IR)[1] spectroscopy can be understood as an extension of the 2D-IR experiment to the *non-equilibrium* regime, which allows to take full advantage of the high time resolution. Transient 2D-IR spectroscopy combines microscopic structural information with picosecond time resolution, providing an atomic view on dynamic processes that can directly be linked to molecular dynamic (MD) simulations**.**
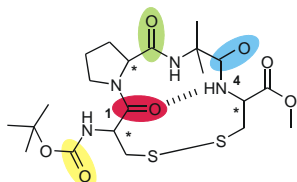
Scheme 1: Lewis structure of cyclo(Boc-Cys-Pro-Aib-Cys-OMe) (**1**). The dashed line indicates the intramolecular hydrogen bond.

We investigated the cyclic disulfide-bridged peptide cyclo(Boc-Cys-Pro-Aib-Cys-OMe) (**1**) in CD_3CN (Scheme 1).[2,3] Due to the stabilizing effect of the disulfide bridge and an intramolecular hydrogen bond, the peptide is very rigid and adopts one exclusive β–turn structure, according to NMR results.[2,3] Since the disulfide bridge is a weak covalent bond (dissociation energy ~65 kcal mol^{-1}), it can easily be cleaved by UV light providing a "predetermined breaking point", a photo–trigger introduced by *Volk et al.*.[4] The FTIR absorption spectrum (Fig. 1a) of the peptide shows well resolved bands in the amide I region related to individual C=O groups of the peptide backbone (Band assignment: see Scheme 1). We determined the dynamics of the peptide upon ultrafast cleavage of the disulfide bridge using time-resolved mid-IR spectroscopy (Fig. 1b).[5] The pulsed photolysis resulted in an instantaneous red shift of the amide I bands. Within the first 200 ps the initial red shifted signal has transformed into a blue shifted spectrum. This behavior can be observed independent of concentration ranging from 14 mM to 200 mM. Only at high concentrations (blue dotted spectra in Fig. 1b) the transient spectrum starts to alter again after approximately 1 ns. This effect is an artifact caused by aggregates/clusters formed via intermolecular hydrogen-bonds. The underlying dynamics can be described as follows:

a) Dissipation of excess energy to the solvent (20 ps); b) Blue shift of the C=O group of Cys(1) at 1654 cm^{-1}, suggesting a weakening of the hydrogen bond and conformational change (160 ps); c) Very slow decay of the liberated cysteinyl radicals.

To probe specifically the lifetime of the free cysteinyl radicals, we applied UV-pump-IR-probe experiments (Fig. 1c).[5] In the time-resolved IR spectra we observed no change on a μs timescale, which is in agreement with MD simulations (Fig. 1d). Time-resolved UV laser flash photolysis experiments (Fig. 1e)[5] showed that the concentration of the cysteinyl radical decays non-exponentially on a 100 μs timescale and about 50% are still present after 1 ms.
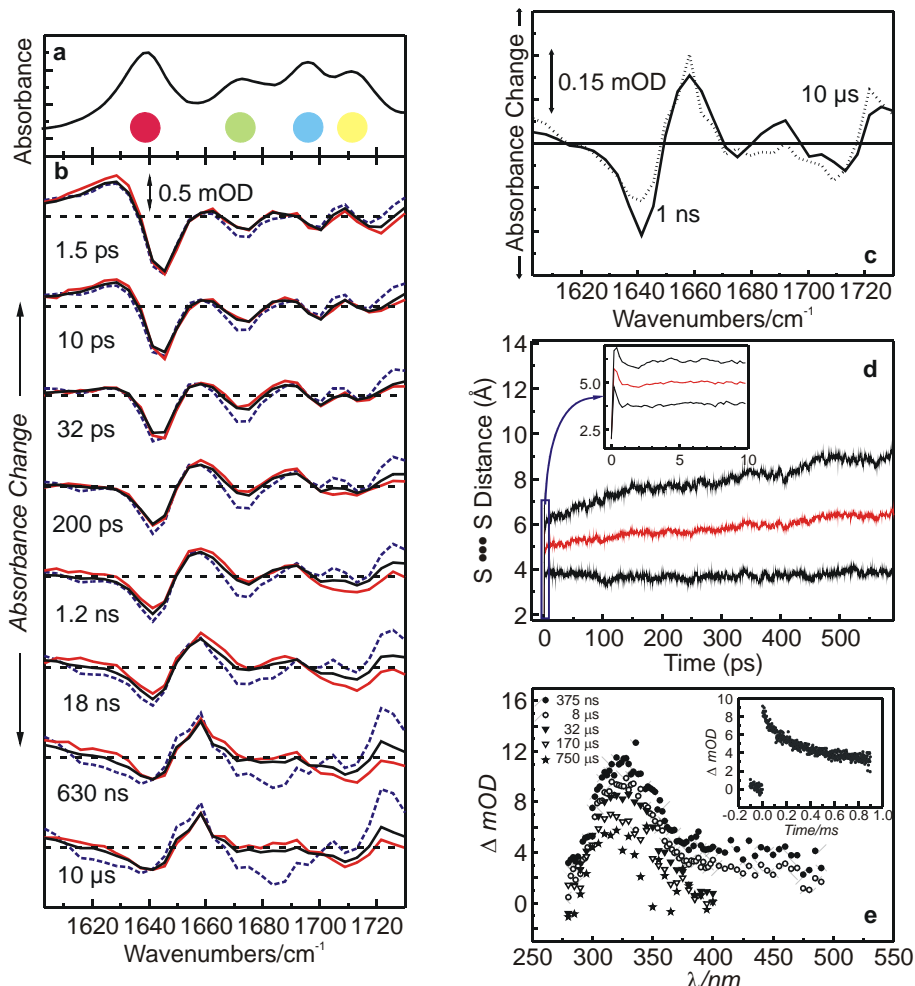
Figure 1: a: FTIR spectrum of **1**. Band assignments correspond to the highlighted regions in **1** (Scheme 1). **b:** Magic angle pump-probe spectra at different time delays after excitation $\lambda_{exc.}$ = 266 nm. Red spectra: Conc. 14 mM, black spectra: 53 mM, blue dotted spectra: 192 mM. **c:** Magic-angle pump-probe spectra (53 mM) at delay times of 10 ns (solid) and 10 ms (dotted) after excitation. **d:** Mean S•••S distance averaged over 120 *non-equilibrium* trajectories (red curve) together with ± one standard deviation of the distribution of distances (black curves). Inset: Magnification of the 0-10 ps time region. **e:** Transient absorption spectra following 266 nm excitation in argon purged acetonitrile displaying the photochemistry of **1**. Inset: Transient decay trace, recorded at λ = 330 nm, upon laser flash photolysis of **1** in degassed acetonitrile *[adapted from Ref. [2] and [5]]*.

The 2D-IR experiment was first performed under *equilibrium* conditions with the S-S bond still intact. Figure 2b shows various crosspeaks, most of which are caused by coupling of neighboring amide groups (dotted arrows). Of importance will be the additional crosspeak at 1654 cm^{-1}, which is caused by the interaction between Cys(1) and Aib (arrow between red and blue dot). The *non-equilibrium* structural dynamics of **1** were obtained using transient 2D-IR spectroscopy.[1] Figure 2d shows T2D-IR spectra at characteristic UV-pump-2D-IR

probe delay times of 3, 25 and 100 ps. The most important feature is a transient crosspeak, highlighted by the indicator (TC), which matches with the position of the crosspeak at 1654 cm^{-1} in the *equilibrium* 2D-IR spectrum of Fig. 2b. The intensity of the transient crosspeak grows as a function of time from 3 ps to 100 ps; both in absolute, but even more so in a relative sense compared to the corresponding diagonal signal. Since the crosspeak is caused by the interaction between Cys(1) and Aib, its change in time is direct evidence for a backbone dynamics, which is correlated to the strength and the distance of the intramolecular hydrogen bond. To complement the experimental results, we have performed *non-equilibrium* MD simulations, which show ring opening on a 200 ps timescale in good agreement of our data.
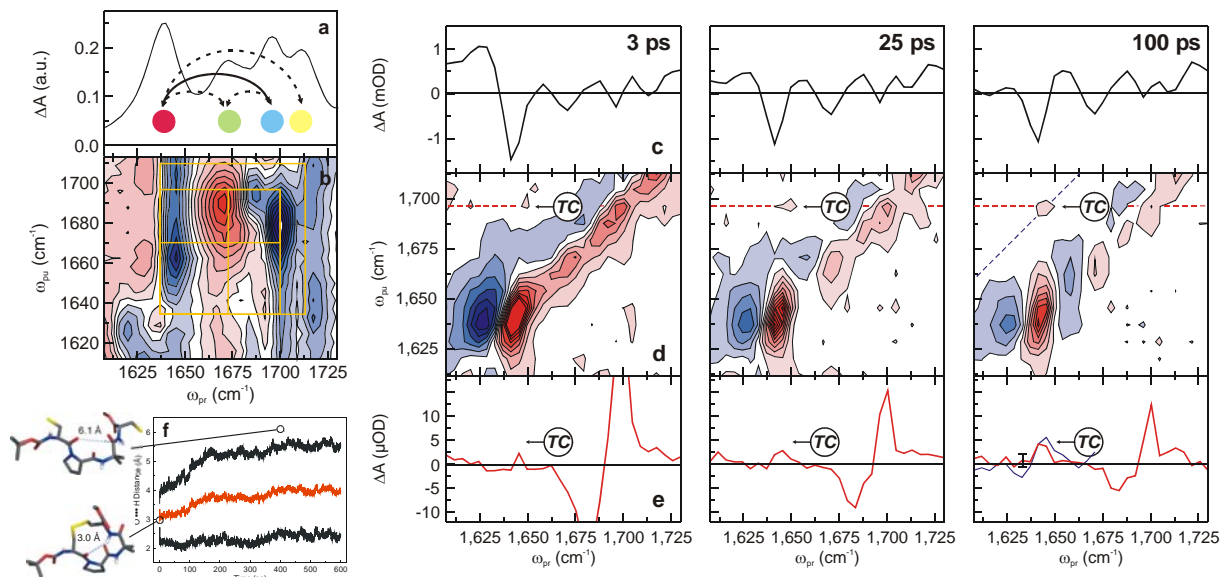
Figure 2: a: FTIR absorption spectrum of the amide I region of the peptide (Band assignment: see Scheme 1). **b:** Weighted difference between perpendicular and parallel polarization 2D-IR spectra. Blue signals: bleach; Red signals: excited state absorption. **c:** UV-pump-IR-probe spectra at three different delay times after photolysis of **1** with $\lambda_{exc.}$ = 266 nm. Bands appearing on irradiation are pointing upward; bands disappearing are pointing downward. **d:** T2D-IR spectra at UV-pump-2D-IR probe delay times of 3, 25 and 100 ps. In the T2D spectra, negative signals are depicted in blue and positive signals, in red. The labeled arrow highlights the transient crosspeak. **e:** Horizontal (red) and diagonal (blue) cuts through the T2D-IR spectra at the position shown by the red and blue dotted lines in d. The labeled arrow highlights the transient crosspeak. **f:** Mean O•••H distance averaged over 120 *non-equilibrium* trajectories (red curve) together with ± one standard deviation of the distribution of distances (black curves) *[adapted from Ref. [2]]*.

In conclusion, we were able to demonstrate that photo-cleavable disulfide bridges may serve as an intrinsic, naturally occuring photo-trigger to study protein dynamics opening a wide time-window from a few picoseconds to many hundreds of microseconds. T2D-IR spectroscopy is an ideal experimental tool combining structural resolution with high time-resolution.

[1] J. Bredenbeck, J. Helbing, R. Behrendt, C. Renner, L. Moroder, J. Wachtveitl, P. Hamm, J. Phys. Chem. B, **2003**, 107, 8654-8660

[2] C. Kolano, J. Helbing, M. Kozinski, W. Sander, P. Hamm, Nature, **2006**, 444, 469-472

[3] C. Kolano, K. Gomann, W. Sander, Eur. J. Org. Chem. **2004**, 20, 4167-4176

[4] M. Volk, Y. Kholodenko, H.S.M. Lu, E.A. Gooding, W.F. DeGrado, R.M. Hochstrasser, J. Phys. Chem. B, **1997**, 101, 8607-8616

[5] C. Kolano, J. Helbing, G. Bucher, W. Sander, P. Hamm, J. Phys. Chem. B. **2007**, *submitted*.

Understanding the Building Blocks of Life – Evidence of a High-Temperature Order-Disorder Transition in Peptide Model Compounds

Neil T. Hunt and Klaas Wynne

Department of Physics, SUPA, University of Strathclyde, Glasgow G4 0NG, Scotland, UK

The ultrafast rotational-diffusive dynamics of the peptide linkage model compounds N-methylacetamide (NMA), acetamide (Ac), and N,N-dimethylacetamide (DMA) have been studied [1] as a function of temperature using optically heterodyne-detected optical Kerr-effect (OHD-OKE) spectroscopy. [2] Both NMA and Ac exhibit a non-Arrhenius temperature-dependence of the rotational diffusive relaxation time. By contrast, the non-hydrogen-bonding DMA exhibits normal hydrodynamic behaviour. The unusual dynamics of NMA and Ac are attributed to the decoupling of single-molecule rotational diffusive relaxation from the shear viscosity via a transition between stick and slip boundary conditions, which arises from local heterogeneity in the liquid due to the formation of hydrogen-bonded chains or clusters. This provides new insight into the structure and dynamics of an important peptide model compound and the first instance of such a phenomenon in a room temperature liquid.

Inter- and intramolecular hydrogen bonding plays an important role in determining the structure and function of biological molecules. As such, a thorough understanding of the interactions between molecules in hydrogen-bonded liquids is crucial to our comprehension and exploitation of biological systems. Studying intermolecular interactions in complete biological systems is however problematical due to the size and complexity of the species involved. This has resulted in the use of simpler model systems to further our understanding.
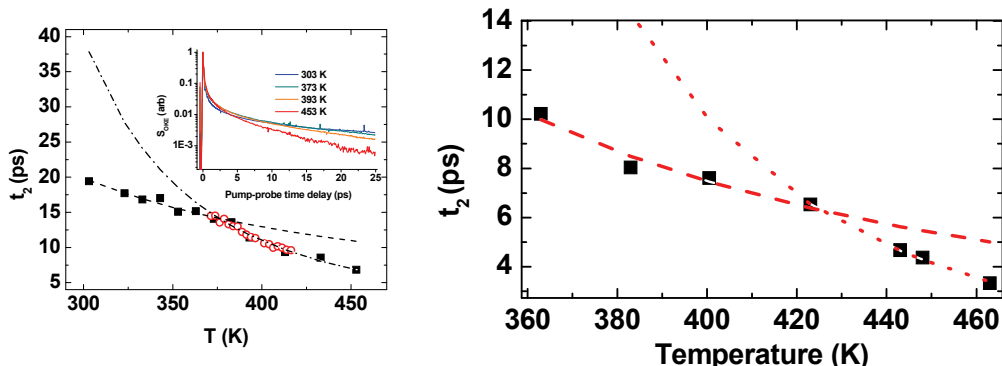
Figure 1. *(left) Temperature dependence of the OHD-OKE response of neat liquid NMA. The inset shows the OHD-OKE response of neat NMA in the time domain. The main picture shows the temperature dependence of the rotational-diffusive timescale of NMA. Black squares indicate previously published data [3] while red circles indicate new data points. Dash-dot and dashed lines are fits to Arrhenius-type behavior above and below 383 K respectively. (right) Temperature dependence of the rotational-diffusion time of neat acetamide. Red lines indicate fitting to Arrhenius profiles. The dotted line shows the results of fitting to the high temperature portion of the data while the dashed line corresponds to the low temperature results. [1]*

N-methylacetamide (NMA, $CH_3NHCOCH_3$), which closely resembles the peptide linkage is one such model system that has been extensively studied. The majority of this work has concentrated on determining the structure of NMA in the liquid phase and in solution. It has been suggested by theoretical simulations of liquid NMA that the molecules form hydrogen-bonded chain-like aggregates in the liquid phase similar to those found in the crystalline state. [4]

Here, we have studied the behaviour of neat liquid NMA [3] at higher temperature resolution to determine more accurately the nature of the temperature-induced transition point in the rotational diffusive dynamics. This new data has been combined with differential

scanning calorimetry (DSC) and measurements of the macroscopic liquid viscosity in order to shed further light on the origins of this unusual behaviour.
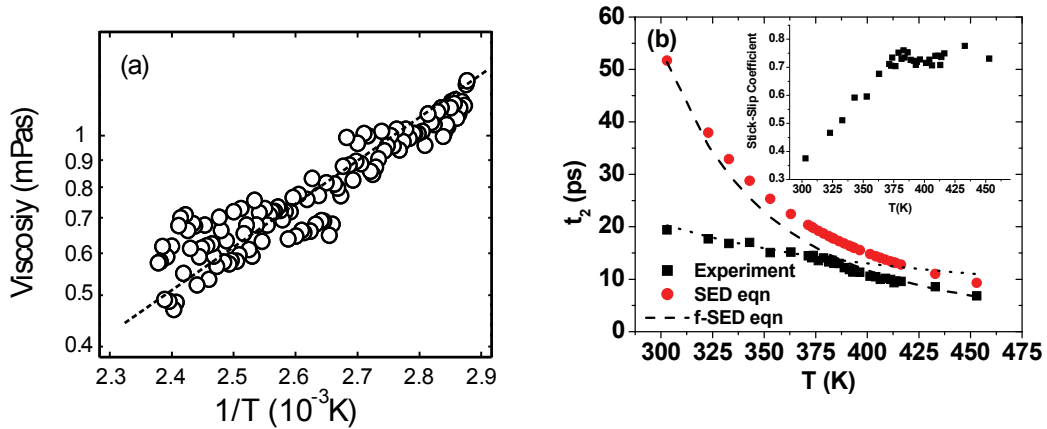
Figure 2. *(a) Temperature dependence of the shear viscosity of pure liquid NMA. The dashed line shows a fit to an Arrhenius expression. (b) Comparison of the t_2 values obtained via the OHD-OKE experiment and calculated using the SED equation. The inset shows the temperature variation of the stick-slip coefficient δ. Dashed and dotted lines show fits to fractional DSE equation. The dashed line has a ξ value of 1.04, the dotted line 0.3.* [1]

The changes in the rotational-diffusion time observed (see Figure 1) have several possible origins; These include a liquid-liquid phase transition between hydrogen-bonded and non-hydrogen-bonded states or an unusual temperature dependence of factors such as molecular volume, pairwise correlation effects, or in the coupling between macroscopic shear viscosity and microscopic molecular dynamics but to date the data are inconclusive. While liquid-liquid phase transitions (LLT) have been clearly observed for atomic liquids, [5] direct experimental evidence for such phenomena in molecular liquids has only been reported very recently and often close to the glass transition or freezing point of the liquids concerned. [6,7] It has been shown, however, that the possibility exists for an LLT in any molecular liquid that has a tendency to form long-lived locally favoured structures due to anisotropic interactions such as those arising from hydrogen bonds. [7,8]

Examples of non-Arrhenius temperature dependencies of rotational relaxation times have been observed previously. The origins of such phenomena are largely due to microscopic heterogeneities in the liquid structure, which enable the decoupling of molecular reorientation from the macroscopic liquid viscosity. [9,10] Most relevant to this work is the recent observation of fractional Stokes-Einstein behaviour in pure liquid HF. [9]

We have investigated other hydrogen-bonded systems; two further amides have been studied in an effort to determine whether the effects observed for NMA also occur in liquids with similar structural motifs. The systems chosen were the non-hydrogen-bonding N,N-dimethylacetamide (DMA) along with acetamide (Ac), which has the capacity to form two intramolecular hydrogen bonds via the amide nitrogen.
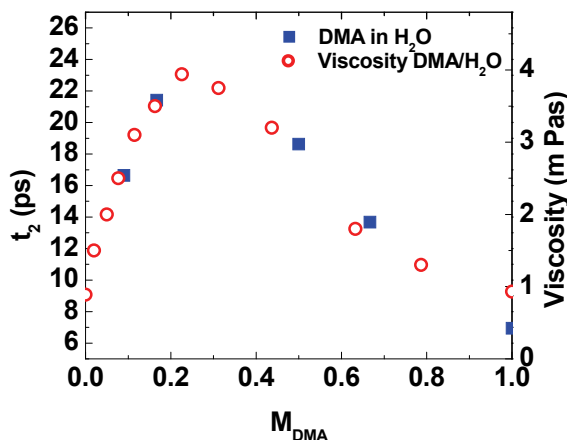
Figure 3. *Rotational-diffusion timescale (t₂) of DMA as a function of aqueous dilution (blue squares)* [1] *as compared to the viscosity of the solutions (red circles).* [11]

The high temperature behaviour of the rotational-diffusive dynamics of NMA has been studied as a function of temperature close to a previously observed transition point. It has been established through measurements of the shear viscosity and heat flow via DSC experiments that the behaviour is not due to a liquid-liquid phase transition but to a crossover transition to fractional Stokes-Einstein-Debye behaviour at low temperature caused by local heterogeneities in the liquid arising from the formation of hydrogen-bonded chains. This leads to the decoupling of the rotational relaxation time from the shear viscosity, an effect not previously observed in a pure room temperature liquid. Similar behaviour has been observed for Ac but not for the non-hydrogen bonding DMA.

References

1   Hunt, N.T., Turner, A.R., Tanaka, H. et al., *J. Phys. Chem. B* **in press** (2007).
2   Giraud, G., Karolin, J., and Wynne, K., *Biophys. J.* **85** (3), 1903 (2003).
3   Hunt, N.T. and Wynne, K., *Chem. Phys. Lett.* **431**, 155 (2006).
4   Whitfield, T.W., Martyna, G.J., Allison, S. et al., *Chem. Phys. Lett.* **414**, 210 (2005); Whitfield, T.W., Martyna, G.J., Allison, S. et al., *J. Phys. Chem. B* **110**, 3624 (2006).
5   Aasland, S. and McMillan, P.F., *Nature* **369**, 633 (1994); Angell, C.A., *Science* **267**, 1924 (1995); Poole, P.H., Grande, T., Angell, C.A. et al., *Science* **275**, 322 (1997); Mishima, O. and Stanley, H.E., *Nature* **396**, 329 (1998); Katayama, Y., Mizutani, T., Utsumi, W. et al., *Nature* **403**, 170 (2000).
6   Kurita, R. and Tanaka, H., *Science* **306**, 845 (2004).
7   Kurita, R. and Tanaka, H., *J Phys: Cond Matt* **17**, L293 (2005).
8   Tanaka, H., *Phys Rev E* **62**, 6968 (2000).
9   Fernandez-Alonso, F., Bermejo, F.J., McLain, S.E. et al., *Phys. Rev. Lett.* **98**, 077801 (2007).
10   Blanchard, G.J. and Wirth, M.J., *J. Phys. Chem.* **90**, 2521 (1986); Angell, C.A., Ngai, K.L., McKenna, G.B. et al., *Journal of Applied Physics* **88**, 3113 (2000).
11   Dutt, G.B. and Doraiswamy, S., *J. Chem. Phys.* **96**, 2475 (1992).

Real time investigation of turn opening and hydrogen bond breaking upon thiopeptide isomerization

H. Bregy[1], V. Cervetto[1], C. Kolano[1], J. Helbing[1]

[1] Physikalisch Chemisches Institut, Universität Zürich, 190, Winterthurerstrasse, 8057 Zürich, Switzerland.

hbregy@pci.uzh.ch, jhelbing@pci.uzh.ch

http://www.pci.uzh.ch

To investigate peptide dynamics on ultrafast time scale molecular photo switches can be incorporated to trigger conformational change. A very elegant way of creating a photoswitchable peptide is the substitution of the oxygen in one peptide bond with a sulphur atom. The resulting thionated peptide bond can now be excited and isomerized selectively from *trans* to *cis* because its electronic absorption is red-shifted compared to the one of a normal peptide bond (see figure 1)[1]. It has been shown that this minimal modification does not perturb the structure of a peptide significantly[2,3,4].
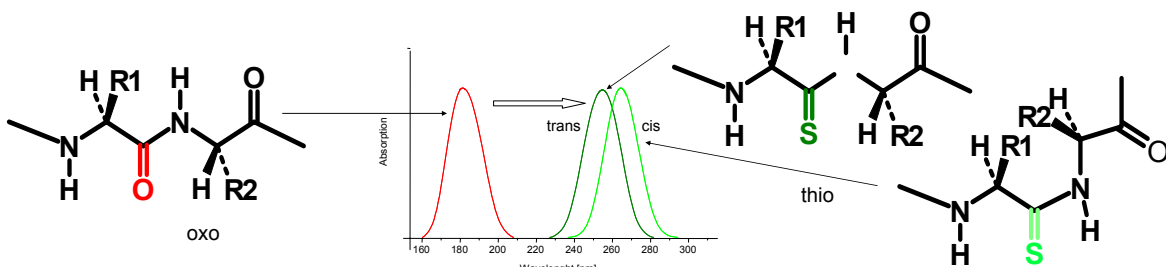
Figure 1: Schematic representation of a peptide bond and a modified peptide bond in its *trans* and *cis* conformation and their corresponding UV absorption spectra. The thermally more stable *trans* conformation can be isomerized by irradiation of ultraviolet light around 260 nm.

We have used time-resolved UV-pump IR-probe, 2D-IR and temperature-dependent ^{1}H-NMR measurements to investigate structural properties and molecular dynamics upon isomerizaton of the two thiopeptides Z-Ile(=S)-Aib-Gly-OMe[5] and Boc-Ala(^{13}C=O)-Pro(=S)-Aib-Ala-OMe[6] (see figure 2, top). Both molecules contain the non-proteinogenic amino acid 2-aminoisobutyric acid (Aib) which is known to stabilize β-turns[7], which are characterized by a 1→4 hydrogen bond. Proline at the N-terminal side of Aib additionally enhances the β-turn structure. X-ray crystallography has shown that an intramolecular hydrogen bond between the C=O of protecting group Z and the N-H of Gly is present in Z-Ile(=S)-Aib-Gly-OMe (see figure 2)[5]. The double peak of the C=O stretch vibration of the Z protecting group in the FT-IR spectrum in CD$_3$CN solution (figure 2, bottom left, marked red) therefore may originate from a non-H-bonded and a hydrogen-bonded conformation (red-shifted band)[4]. However, the temperature-dependent ^{1}H-NMR measurements do not unambiguously confirm this observation. Thus the double structure may also arise from *trans* and *cis* conformations of the NH-CO bond of the urethane moiety[8]. The situation for Boc-Ala(^{13}C=O)-Pro(=S)-Aib-Ala-OMe is much clearer. In this case, the temperature-dependent ^{1}H-NMR measurements clearly show the presence of a hydrogen bond between the two alanine residues (red and yellow in figure 2). For Ala(^{13}C=O) we see two bands in the IR spectrum (figure 2, bottom middle, marked red). The 1600 cm^{-1} is assigned to the hydrogen-bonded species, while the band at

1620 cm^{-1} belongs to the non-H-bonded species, which probably comprise the twelve percent of molecules with the proline amide bond in the *cis* conformation.

The 2D-IR (figure 2, top right) spectrum indicates that the coupling between the C=O vibrations of Ala(^{13}C=O) and Aib is stronger for the spectrally more distant band at 1600 cm^{-1} than for the band at 1620 cm^{-1}, indicating that the C=O groups of the hydrogen-bonded molecules are spatially closer. The cuts of the 2D-IR spectra (figure 2, bottom right) show that there is no population transfer between the two Ala(^{13}C=O) bands within 5 ps (red curves), while both bands do transfer population to the Aib band at 1680 cm^{-1}. This indicates two separated species in solution.

Furthermore, the temperature-dependent ^{1}H-NMR measurements indicate a second weaker intramolecular hydrogen bond for the NH proton of the Ala(^{13}C=O) (cyan) which most probably binds to the C=O group of Ala (dark blue).
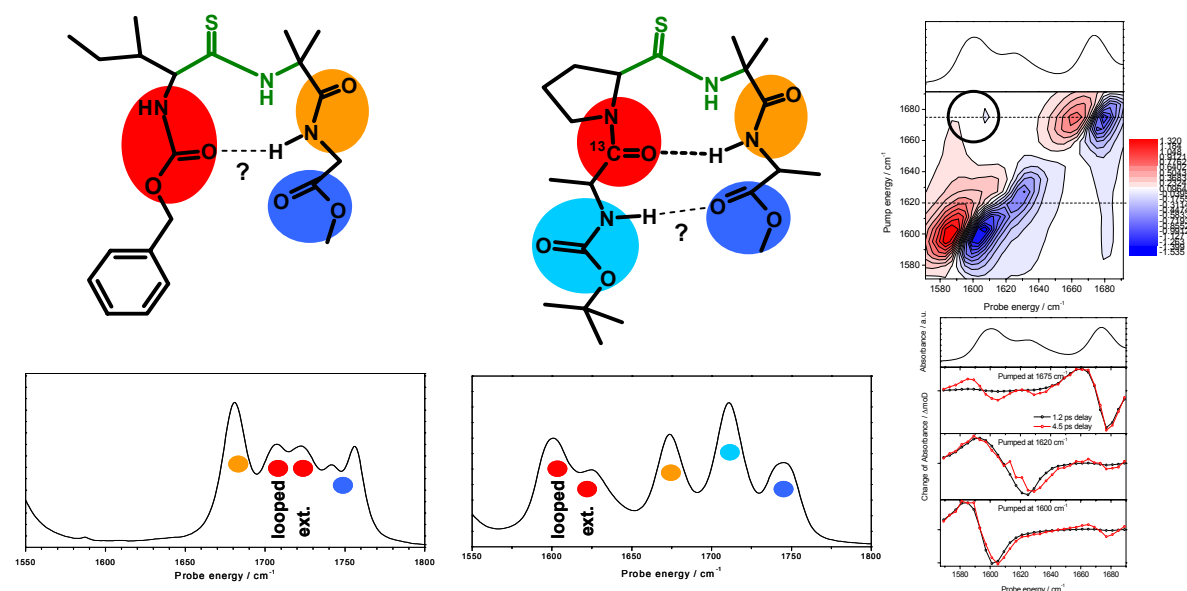
Figure 2: Top: Lewis structure and suggested intramolecular hydrogen bonds of Z-Ile(=S)-Aib-Gly-OMe (left) and Boc-Ala(^{13}C=O)-Pro(=S)-Aib-Ala-OMe (middle). Bottom: Corresponding amide I infrared spectra. Right: 2D-IR spectrum of Boc-Ala(^{13}C=O)-Pro(=S)-Aib-Ala-OMe (top) with 1.2 ps waiting time, and cuts for selected pump energies for waiting times 1.2 ps (black curves) and 4.5 ps (red curves).

The time-resolved UV-pump IR-probe data are shown in figure 3. The isomerization of the molecules is induced by a short (~1 ps) 260 nm pump pulse. The two molecules show very similar behaviour. At early times, a red shift for all bands is visible due to heating of the molecules by the excess energy as the molecules relax to the lowest-lying electronically excited state[9]. The heat dissipation to the solvent takes place on a 10 ps timescale. After 30 ps, remaining positive absorption is due to the fully relaxed molecules in the electronically excited state which decays on a 160 ps timescale. After 800 ns, no further changes appear. The spectra then show positive absorption at the position of the bands, which have been assigned to the non-H-bonded species (1730 cm^{-1} for Z-Ile(=S)-Aib-Gly-OMe and 1620 cm^{-1} for Boc-Ala(^{13}C=O)-Pro(=S)-Aib-Ala-OMe), while negative absorption is present at the positions, where the hydrogen-bonded species appear (1710 cm^{-1} for Z-Ile(=S)-Aib-Gly-OMe and 1600 cm^{-1} for Boc-Ala(^{13}C=O)-Pro(=S)-Aib-Ala-OMe). This can be assigned to molecules, which are isomerized at the CS-NH bond and due to sterical restrictions can no longer form a hydrogen bond. Additionally, the same shape can bee seen at 1740/ 1750 cm^{-1},

which is an indication that there is indeed a second hydrogen bond in Boc-Ala(^{13}C=O)-Pro(=S)-Aib-Ala-OMe) which also breaks upon isomerization. This signal may be much smaller because of stronger spectral overlap.
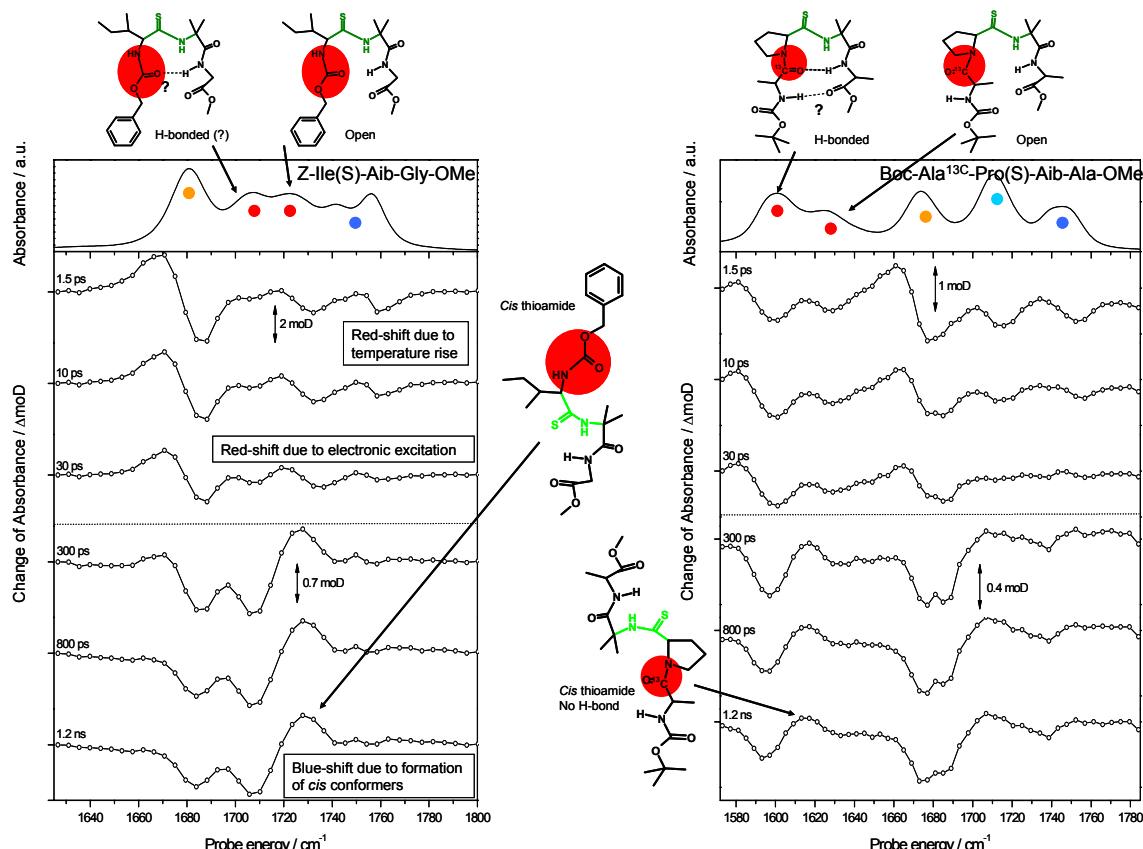
Figure 3: Top: FT-IR spectra of Z-Ile(=S)-Aib-Gly-OMe (left) and Boc-Ala(^{13}C=O)-Pro(=S)-Aib-Ala-OMe (right). Bottom: Corresponding transient infrared spectra (magic angle signal) with different time delays after irradiation with a 260 nm light pulse.

In the near future it is our aim to follow the isomerization of Boc-Ala(^{13}C=O)-Pro(=S)-Aib-Ala-OMe) by transient 2D-IR spectroscopy to get additional structural information during isomerization and intramolecular hydrogen bond breaking in essentially native peptides.

[1] H. Satzger, C. Root, P.Gilch, W. Zinth, D. Wildemann, G. Fischer, J. Phys. Chem. B, **2005**, 109. 4770-4775

[2] O. E. Jensen, S. O. Lawesson, R. Bardi, A. M. Piazzesi, C. Toniolo, Tetrahedron, **1985**, 41, 5595-5606

[3] J. H. Miwa, L. Pallivathucal, S. Gowda, K. E. Lee, Org. Lett, **2002**, 4, 4655-4657

[4] V. Cervetto, R. Pfister, C. Kolano, H. Bregy, H. Heimgartner, J. Helbing, Chem. Eur. J., **2007**, in press

[5] J. Lehmann, A. Linden, H. Heimgartner, Tetrahedron, **1999**, 55, 5359-5376.

[6] Boc-Ala(^{13}C=O)-Pro(=S)-Aib-Ala-OMe has been synthesized according the procedure described in ref. 5.

[7] R. Nagaraj, P, Balaram, Acc. Chem. Res., **1981**, 14, 356-362

[8] M. Branik, H. Kessler, Tetrahedron, **1973**, 30, 781-786

[9] J. Helbing, H. Bregy, J. Bredenbeck, R. Pfister, P. Hamm, R. Huber, J. Wachtveitl, L. DeVico M. Olivucci, JACS, **2004**, 126, 8823-8834

CHEMISTRY

Temporal vibrations of short-lived excited states observed by femtosecond time-domain spectroscopy

T. Tahara

Molecular Spectroscopy Laboratory, RIKEN, 2-1 Hirosawa, Wako, Saitama 351-0198, Japan. E-mail: tahei@riken.jp; URL: http://www.riken.jp/lab-www/spectroscopy/en/index.html.

Thanks to the advance of ultrafast lasers, we are now able to use extremely short optical pulses such as sub-10-fs pulses in a variety of femtosecond spectroscopy. This kind of short optical pulses have broad bandwidths in energy, so that they can excite bunch of vibrational eigen states simultaneously. The generated coherent state is not eigen state and hence it evolves in time. The evolution of the vibrational coherent state induces real-time nuclear motion of molecules, which is called nuclear wavepacket motion. Creation and observation of the nuclear wavepacket motion is an important aspect of femtosecond spectroscopy, and it has been attracting much interest. In the context of vibrational spectrosopy, the observation of the nuclear wavepacket motion in femtosecond spectroscopy is regarded as time-domain vibrational spectroscopy, in which vibrational coherence is measured directly in the time-domain. Information obtained from time-domain vibrational spectroscopy is equivalent to that from traditional frequency-domain vibrational spectroscopy, but the time-domain measurement is advantageous in the study of excited-state molecules that have very short lifetimes. Actually, femtosecond time-domain measurements can provide crucial information about the reacting excited states and the topology of the relevant potential energy surfaces (PESs)[1]. Here, we report our most recent results on two prototypical short-lived excited states that have lifetimes as short as 1 ps.

1. The S_1 state of *cis*-stilbene in ultrafast photoisomerization

Stilbene is a prototypical molecule showing photoisomerization. Especially, the isomerization from S_1 *cis* isomer proceeds within a few picoseconds in a nearly barrierless way. We carried out pump-probe measurements of *cis*-stilbene and observed a wavepacket motion ($\sim$240 cm^{-1}) of the S_1 state.[2] In this pump-probe experiment, we observed the nuclear wavepacket motion in the vicinity of the Franck-Condon region in the S_1 PES, because the wavepacket motion was induced by $S_1 \leftarrow S_0$ photoexcitation. To obtain more information about reactive PES of *cis*-stilbene, we carried out TR-ISRS measurements.[3] In TR-ISRS experiments, the uv pump pulse is used for generation of the excited-state population. Then, at an optional delay time (ΔT), the probe 1 pulse is introduced to induce wavepacket motion in the S_1 state by the impulsive Raman process. The time-evolution of the wavepacket motion is finally monitored by the probe 2 pulse through the intensity modulation of the $S_n \leftarrow S_1$ transient absorption[4].

Figure 1 depicts the change of the $S_n \leftarrow S_1$ absorption induced by irradiation of the probe 1 pulse. Because the probe 1 pulse excited the S_1 state to the S_n state, the transient signal was observed as a negative signal. The overall feature of the transient signal was well fitted with an instantaneous response and two exponential decays that have time constants of $\sim$70 fs and 1.6 ps. The instantaneous response is due to the coherent artifact, while the two exponential components are attributed to the $S_n \rightarrow S_1$ recovery and S_1 lifetime, respectively. In addition, the

[1] T. Tahara, S. Takeuchi, K. Ishii, J. Chin. Chem. Soc., **2006**, <u>53</u>, 181-189.
[2] K. Ishii, S. Takeuchi, T. Tahara, Chem. Phys. Lett., **2004**, <u>398</u>, 400-406.
[3] S. Takeuchi, S. Ruhman, K Ishii, T. Tahara, Ultrafast Phenomena XV, in press.
[4] S. Fujiyoshi, S. Takeuchi, T. Tahara, J. Phys. Chem. A, **2003**, <u>107</u>, 494-500.
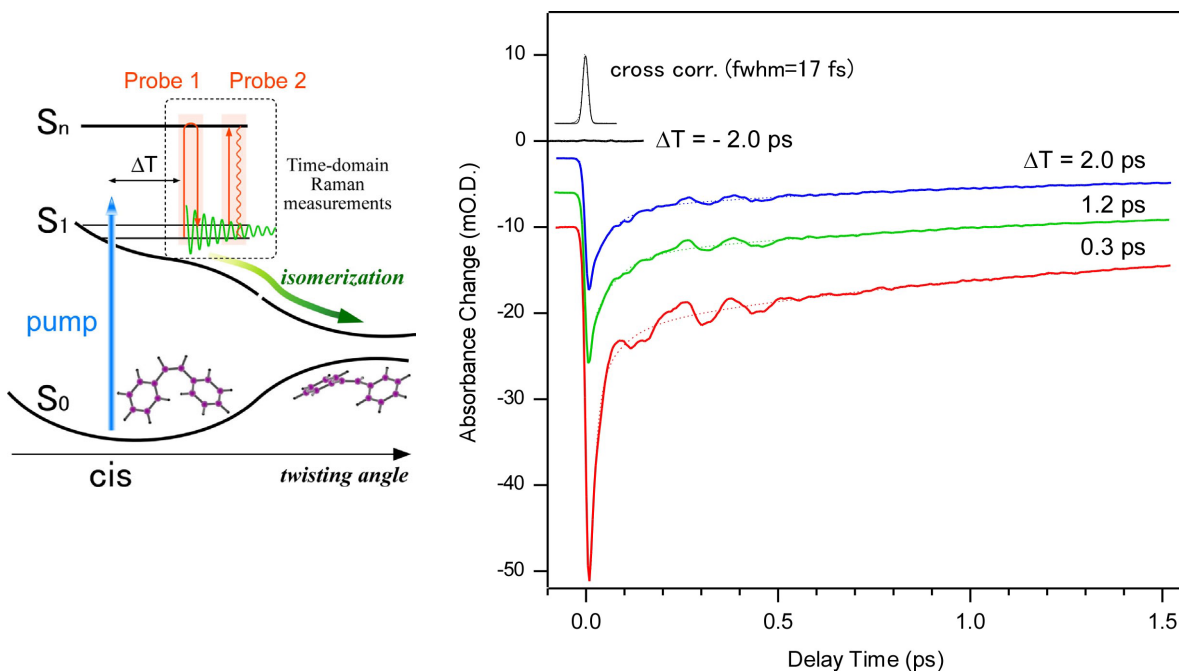
Fig.1 Scheme of TR-ISRS measurements (left) and the data of *cis*-stilbene (right) (pump 267 nm; probe 1&2 620 nm; in hexadecane).

oscillation due to the nuclear wavepacket motion induced by the impulsive Raman process was clearly observed. The dephasing time of the oscillation was about 200 fs, which is much shorter than the dephasing time of ordinary molecular vibrations (a few picoseconds). The short dephasing time reflects highly anharmonic nature of the S_1 potential of *cis*-stilbene. The Fourier analysis of the oscillation showed that a vibrational mode having a frequency of ~240 cm^{-1} predominantly contributes to the signal. This vibrational mode is the same as that observed in the pump-probe measurement.

We examined the change of the wavepacket motion by changing timing of its creation in the S_1 state (i.e., by changing the pump-probe 1 delay). The wavepacket motion was induced at three different times at ΔT=0.3 ps, 1.2 ps, and 2.0 ps. It was found that the frequency of the predominant vibrational motion significantly changes with the delay time: 239 cm^{-1} (ΔT=0.3 ps) $\rightarrow$ 224 cm^{-1} (1.2 ps) $\rightarrow$ 215 cm^{-1} (2.0 ps). Because the frequency of the wavepacket motion is determined by the curvature of the S_1 potential along the relevant coordinate, the temporal frequency change implies that the relevant curvature of the S_1 potential changes with time after photoexcitation. It indicates a structural change proceeding in a picosecond time scale in S_1 *cis*-stilbene. The solvent dependence of the rate of the frequency shift coincided well with the solvent dependence of the isomerization rate (lifetime) of S_1 *cis*-stilbene. Therefore, it was concluded that the structural change in a picosecond time scale is closely related to the isomerization coordinate[5]. These results demonstrated the highly anharmonic nature of the multidimensional reactive S_1 potential of *cis*-stilbene.

2. The S_1 state of [Cu(dmphen)$_2$]$^+$ in ultrafast photo-induced 'Jahn-Teller' distortion

Metal complexes usually show faster and more complicated excited-state dynamics than organic compounds, and hence elucidation of ultrafast dynamics is essential for understanding their photochemical properties. A copper (I) complex, [Cu(dmphen)$_2$]$^+$ (dmphen = 2,9-

---

[5] S. Takeuchi, S. Ruhman, T. Tsuneda, M. Chiba, T. Taketsugu, T. Tahara, in preparation.
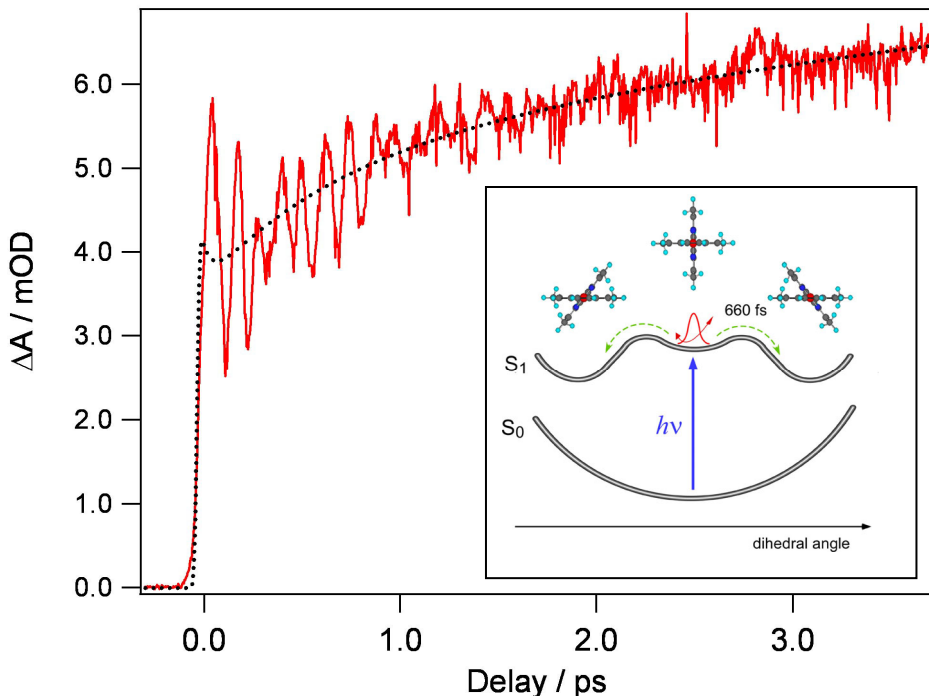
Fig.2 $S_n \leftarrow S_1$ transient absorption signal of $[Cu(dmphen)_2]^+$. (pump 550 nm; probe 650 nm; in dichloromethane). Inset: schematic potential curves of $[Cu(dmphen)_2]^+$.

dimethyl-1,10-phenanthroline), is a well-known metal complex that attracts much attention owing to its potential application as photocatalyst and photosensitizer in solar energy conversion. More importantly, this complex undergoes a photo-induced structural change, which is the change of the dihedral angle between the two ligand planes ('flattening' motion, Fig. 2 inset). In the ground state, Cu(I) complexes have tetrahedral-like structures whereas Cu(II) complexes have square planar-like structures. Because the ultrafast structural change of $[Cu(dmphen)_2]^+$ is induced by MLCT excitation that formally oxidizes the central copper from Cu(I) to Cu(II), the excited-state distortion of $[Cu(dmphen)_2]^+$ has been considered a model system where we can investigate the dynamics of the 'Jahn-Teller' distortion in real-time.

We studied ultrafast photochemical dynamics of $[Cu(dmphen)_2]^+$ by femtosecond and picosecond emission spectroscopy in solution at room temperature with optically-allowed $S_2 \leftarrow S_0$ photoexcitation[6]. The obtained results clearly showed that the initially populated S_2 state is relaxed to the S_1 state with a time constant of 45 fs, and the $D_{2d} \rightarrow D_2$ 'flattening' structural change occurs in the S_1 state with 660 fs. Importantly, the spectral evolution corresponding to the structural change in the S_1 state clearly showed an isoemissive point around 675 nm, indicating that a short-lived precursor state appears in the S_1 potential before the structural distortion. In other words, there exists a shallow potential minimum at the perpendicular geometry on the S_1 potential energy surface, which traps the S_1 state for a finite time (~ 660 fs) before the structural change.

To examine the existence of the "bound" S_1 state before the distortion, we carried out ultrafast pump-probe measurements using 15-fs pulses with direct $S_1 \leftarrow S_0$ photoexcitation[7].

---

[6] M. Iwamura, S. Takeuchi, T. Tahara, J. Am. Chem. Soc., **2007**, 129, 5248-5256.
[7] M. Iwamura, H. Watanabe, K. Ishii, S. Takeuchi, T. Tahara, in preparation.

As shown in Fig. 2, we clearly observed an oscillatory feature in the $S_n \leftarrow S_1$ transient absorption signal, which reflects the nuclear wavepacket motion of the S_1 state trapped in the shallow potential minimum immediately after photoexcitaiton. This observation of the temporal vibrations of the S_1 state at perpendicular configuration confirmed the existence of the "hollow" on S_1 potential minimum at the perpendicular geometry. This conclusion is essentially different from the ordinary picture of the 'Jahn-Teller' distortion, because the Jahn-Teller distortion is induced instantaneously by the instability of the molecule at the unperturbed perpendicular structure. Therefore, the femtosecond time-domain data request the revision of present understanding of the photo-induced structural change that occurs in the MLCT state of the metal complexes.

Ultrafast Dynamics of Model Molecular Photoswitches in Liquid and Solid Phase

Tung T. To[1] and Edwin J. Heilweil

[1]Guest Researcher, Optical Technology Division, Physics Laboratory, National Institute of Standards and Technology 100 Bureau Drive, Stop 8443, Gaithersburg, MD 20899, USA

There is great interest in developing high-speed reversible molecular photoswitches for photonic devices.[1] Fast rates, high quantum yields, and low fatigue are desirable features. The current challenge for the application of these novel molecules is that their desirable properties can be hindered by recombination and solvation cage processes. These processes are known to occur on the sub-picosecond timescale and so it is prudent to design the system to have ultrafast response, attain near unity quantum yield, and control the reaction mechanismthat is driven by transient molecular structures and thereaction environment. To reach these goals, we synthetically manipulate the molecular structures and use picosecond time-resolved infrared spectroscopy to directly measure their physicochemical response. We have synthesized and demonstrated model molecular photoswitches capable of chelation (ring formation of metal-multidentate ligand complexes) to the exclusion of ultrafast solvent coordination and cage recombination in solution.[2] In this poster, the ultrafast chelation dynamics of organomanganese complex, $Mn\{\eta^5\text{-}C_5H_4C(O)C(SCH_3)_3\}(CO)_3$, **1,** in solid Polyacrylonitrile (PAN) films is presented.[3]

The time-resolved infrared (TRIR) apparatus used in this work was described in previous publications.[2] For the present study, a typical 289 nm UV excitation pulse (ca. 120 fs pulse duration with 4 μJ to 6 μJ energy, 20 Hz repetition rate) was focused to approximately 100 μm diameter on the front surface of a 3 mm thick CaF_2 window spin-coated with PAN containing **1** (see below). To generate a single difference spectrum at a specific pump-probe time delay, an average of 500 laser shots was collected as the sample was mechanically raster-scanned through the excitation and probe beams to present fresh film for investigation between shots. Two to three of these combined TRIR difference spectra were averaged to obtain the final presented results. Time resolved spectra from different films coated onto various CaF_2 windows obtained over separate days were of similar quality. Analysis of averaged spectra (typically three) yielded an intensity uncertainty from the baseline of less than ± 0.003 optical density (OD) units (k = 1; type B analysis).

The molecular design and the synthesis of **1** were previously published.[2a] To prepare samples for time-resolved infrared experiments, compound **1** (30 mg) was dissolved in 2 mL of dimethylsulfoxide (DMSO, Aldrich) then polyacrylonitrile (PAN, powder, 300 mg, 150,000 Molecular Weight from Polysciences, Inc.) was added.[4] The resulting mixture was heated to ~333 K with stirring. One surface of a 50.8 mm diameter CaF_2 window was spin-coated with the transparent yellow amorphous viscous mixture to produce a uniform film of approximately 25 μm to 35 μm thickness. DMSO remaining in the film was removed by gently blowing warm air across the film before UV-pump/IR probe experiments. Obtaining the appropriate optical density of **1** in these cast PAN films (OD ~0.8) and subsequent removal of DMSO was checked by Fourier Transform infrared (FTIR) spectroscopy.

We found that UV irradiation of **1** in PAN efficiently dissociates a carbonyl ligand from the metal center, allowing for direct formation of a photoproduct within 160 ps assigned to be the Mn-S chelate. There is no evidence for competing solvation or polymer reaction pathways from these TRIR results. The overall reaction scheme of **1** in PAN is shown in Figure 1.
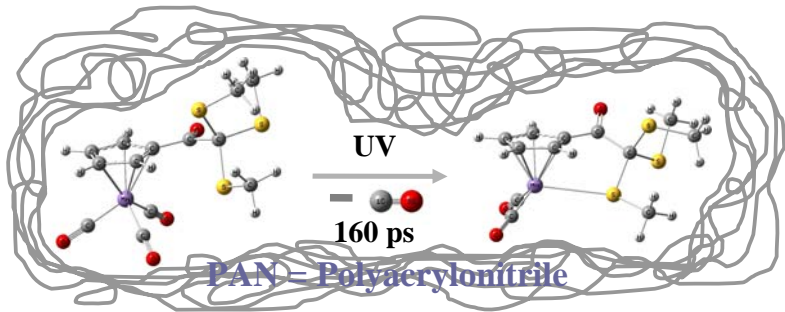
Figure 1: Solid-state reaction mechanism for $Mn\{\eta^5\text{-}C_5H_4C(O)(SCH_3)_3\}(CO)_3$, **1**, embedded in PAN polymer depicting the UV absorptive loss of a CO ligand and subsequent formation of the internally coordinated product species within 160 ps.

As shown in Figure 2, a bleach feature arising from the parent molecule's broadened CO-stretching band doublet is clearly observed near 1940 cm^{-1} immediately after UV irradiation of **1** at delay time t = 27 ps. The spectrum obtained at t = -13 ps demonstrates the baseline noise of the instrument is approximately +/-0.003 OD units for 2000 total laser shots. The second bleach feature of this molecule is found near 2024 cm^{-1} and was not examined in this study. A broad, slightly red-shifted absorption feature relative to the doublet bleach feature is observed at early time delays (<25 ps) which has been interpreted previously as arising from cooling of vibrationally hot species.[2] A new CO-stretching absorption band near 1874 cm^{-1} becomes resolved beginning at 93 ps time delay. Identical bleach and absorption features are also obtained during steady-state irradiation of these same films (Figure 2, bottom panel: FTIR difference spectrum taken before and after UV irradiation with a Hg-Ar pen lamp placed 10 cm away from the film for approximately 60 s). Except for being approximately 4 cm^{-1} red-shifted

Figure 2 : Transient TRIR difference spectral changes acquired after 289 nm irradiation of 1 in PAN. Spectra at different time delays are offset vertically by 0.017 OD units for clarity and dashed lines correspond to ΔOD=0 for each spectrum. The bottom panel shows the difference FTIR spectra of 1 in PAN before and after UV irradiation (OD amplitude divided by two for comparison).

compared to absorptions in liquid-phase acetonitrile (ACN), the positions and intensities of the bleach and newly formed absorption features of **1** in PAN are nearly identical to the previously obtained results for **1** in acetonitrile solvent in which it was determined that only the Mn-S chelate formed.[5] Therefore, we assign the new CO-stretching band near 1874 cm^{-1} to arise from the Mn-S chelate. The second CO-stretching band of the Mn-S chelate is obscured by the parent's spectrally broad, ca. 30 cm^{-1} FWHM (full-width at half-maximum), bleaching feature near 1940 cm^{-1}.

In acetonitrile, the two metal-CO stretching bands of the transient Mn-ACN solvate were previously assigned to be 20 cm^{-1} red-shifted relative to the CO-stretching bands of the Mn-S chelate.[5] The higher frequency band of these two bands was also at least 20 cm^{-1} red-shifted relative to the parent's doublet bleach feature. The absence of these red-shifted features during TRIR irradiation of **1** in PAN indicates that coordination of the unsaturated

Mn metal center with cyano groups in PAN ***does not occur***. We therefore conclude that UV irradiation of **1** in solid PAN effectively dissociates a CO group to yield the fully stable Mn-S chelate without an intermediary or slow (typically with lifetimes of many ns)[2] transient solvation or polymer binding step. This result is extremely important for developing future highly quantum efficient, ultrafast devices for optical switching applications.

In summary, for the first time to our knowledge, ultrafast solid phase dynamics of a tethered organometallic capable of chelation has been investigated on the picosecond timescale using UV-pump IR-probe transient absorption spectroscopy. The ultrafast photoinduced chelation of **1,** to the exclusion of other competing cage processes such as coordination with alkane solvent molecules,[2a] more reactive polar acetonitrile solvent,[5] or the cyano side-groups of PAN, demonstrates the robust and desirable features of this newly synthesized structure in a controlled solid-state reaction environment. This study also demonstrates that efficient chelation, with little or no apparent interference or degradation from cage CO-recombination, can be used as a mechanistic platform for the development of ultrafast solid state optical molecular devices. We are now investigating the possibility of measuring similar reaction behavior with photo-switchable species in polyethylene films.

---

[1] (a) For leading references on photochromic materials in photonic devices see Irie, M. Ed. *Chem. Rev.* **2000**, *100*, 1683. (b) For a recent review on the use of photochromic materials for optical switches see Raymo, F. A.; Tomasulo, M. *Chem. Eur. J.* **2006**, *12*, 3186.

[2] (a) Yeston J. S.; To T. T.; Burkey T. J.; Heilweil E. J. *J. Phys. Chem. B* **2004**, *108*, 4582. (b) Jiao,T.; Pang, Z.; Burkey, T. J.; Johnston, R. F.; Heimer, T. A.; Kleiman, V. D.; Heilweil, E. J. *J. Am. Chem. Soc.* **1999**, *121*, 4618.

[3] T. To and E. J. Heilweil, *Journal of Physical Chemistry A Letters, in press.*

[4] Certain commercial equipment, instruments, or materials are identified in this paper in order to adequately specify the experimental procedure. In no case does such identification imply recommendation or endorsement by NIST, nor does it imply that the materials or equipment identified are necessarily the best available for the purpose.

[5] To, T. T.; Burkey, T. J.; Heilweil, E. J. *J. Phys. Chem. A,* **2006**, 110, 10669.

Base-Induced Solvent Switches in Acid-Base Reactions

Omar F. Mohammed , Dina Pines[2], Ehud Pines[2], Erik T. J. Nibbering[1]

[1] Max Born Institut für Nichtlineare Optik und Kurzzeitspektroskopie, Max Born Strasse 2A, D-12489 Berlin, Germany. [2] Department of Chemistry, Ben Gurion University of the Negev, P.O. Box 653, Beer-Sheva 84125, Israel. E-mail: nibberin@mbi-berlin.de ; URL: http://www.mbi-berlin.de/en/research/projects/2-04/index.html and http://staff.mbi-berlin.de/nibberin/ .

Modern discussions of acid-base reactions have evolved from the seminal studies of Eigen and Weller[1,2]. The general kinetic approach for acid-base reactions in aqueous solutions consists of three reaction branches[2]: (a) direct proton exchange between acid and base, (b) acid dissociation to solvent followed by proton scavenging by the base, and (c) water hydrolysis by the base followed by the neutralization reaction of the acid by the hydroxyl anion. Judging by the magnitude of the reaction radius in typical (diffusion-controlled) acid-base reactions it has been estimated that up to 2-3 water molecules separate when acid and base exchange a proton through pathway (a)[1]. In reality, however, this value is likely to be an averaged value of several encounter complexes (with n rearrangements steps) leading to proton transfer.

Proton transfer reactions have to be treated in the context of chemical equilibria, i.e. forward and backward reaction steps. Photoacids can be used as a means to follow proton transfer dynamics to a neutralising base in real time by photoinitiation. The outcome of the observed dynamics, i.e. the reaction rates and yields depend on the relative strengths and concentrations of acid and base. We have investigated the aqueous neutralization reaction of the photoacid pyranine and carboxylate bases ($^-OOCCH_{3-x}Cl_x$) (x = 0-3) in deuterated water. Here we are able to dictate the outcome of the reaction dynamics by tuning the number of chlorine atoms x.

Femtosecond infrared spectroscopy enables to follow the reaction kinetics by inspection of species-specific vibrational marker modes[3]. Here the deuteron release can be monitored by following the rise of the 1435 cm^{-1} band of the conjugate photobase of pyranine in the S_1-state. The final deuteron transfer from the carboxylate bases can be determined by the rise of the C=O stretching band of the conjugate carboxylate acids located between 1720 and 1750 cm^{-1}. The transient behaviour of these marker modes result from the numerous reaction pathways that can occur upon photoexcitation, i.e. for pyranine and the carboxylate bases the protolysis pathway (b) and the direct deuteron transfer (a) between photoacid and carboxylate base separated by a different number n of water molecules. Under specific conditions where the photoacid and the carboxylate base form a complex with a single (n = 1) water molecule, a transient band at 1850 cm^{-1} can be observed, indicative of a hydrated deuteron, D_3O^+.

We have identified two innermost types of encounter complexes, indicated as tight (n = 0) and loose (n = 1) complexes, resulting in a sub-150 fs deuteron dissociation lifetime of the photoacid[4-6]. The deuteron transfer in both encounter complexes is found to be reversible. The step-wise, von-Grotthuss type[5-6], deuteron transfer in loose complexes involves a first step leading to a D_3O^+ like cation resembling the proton solvation core in the Eigen cation, $D_9O_4^+$, and a second and final transfer to the base on much slower picosecond time scales. The stability of the hydrated deuteron in the loose complex increases with decreasing reactivity (basicity) of the carboxylate base as measured in bulk water.
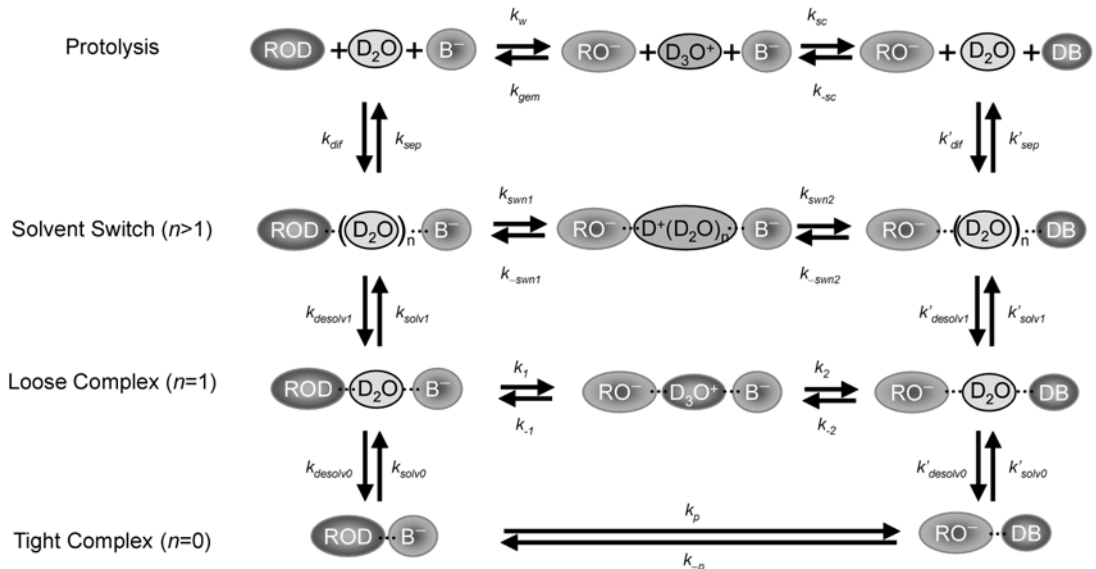
Kinetic model with reversible deuteron transfer reaction pathways coupled through solvation/desolvation steps .

We have applied a unified reaction dynamics model[6] in which we have approximated all possible configurations between acid and base by tight ($n = 0$), loose ($n = 1$) and solvent switch ($n > 1$) complexes, as well as acid and base fully separated by the solvent. Whereas the fully separated acid and base first have to diffuse, all other complexes are connected to each other through reversible deuteron transfer steps (see Figure).

The data fits have been carried out with each closed reaction loop obeying detailed balance while conforming to the pK_a values of the various acids as measured in water . All rate constants were assumed to be time independent and were initially varied one at a time to search for their best values. In the next round of fits the best values of the various rate constants were slightly modified to obey detailed balancing. A final round of fits was then carried out by simultaneously changing each time the values of two rate constants to ascertain detailed balancing while optimising for the best fit parameters. Whereas the fit values for the reversible steps in the protolysis pathway are consistent with previously obtained results[7,11-13], the fits to the deuteron transfer steps of the tight, loose and solvent switch pathways directly result from the extensive experimental data sets of the three vibrational marker modes of conjugate photobase, hydrated deuteron and carboxylate acid. The values obtained for the solvation/desolvation steps have a larger degree of uncertainty, lying in the tens to hundreds of picoseconds time range, but are within the dynamic range as expected from previous experimental and numerical studies on hydration time scales of simple ions.

From the fit results obtained with our kinetic model we conclude that step-wise proton shuttling through water provides a route for proton transfer which circumvents further desolvating the acidic and basic groups necessary for direct transfer. We find that for pyranine and trichloroacetate ($x = 3$), the weakest of investigated carboxylate bases, the bulk of the proton transfer reaction occurs through $n > 1$ solvent switches[6], in contrast to the stronger bases acetate ($x = 0$) and monochloroacetate ($x = 1$) where the observed kinetic data can be reproduced without the larger solvent switches, confirming our previous reports using less general kinetic models[4,5]. Whereas transfer in the tight complex with no water spacer ($n = 0$) occurs within time resolution of 150 fs, the transfer in the loose ($n = 1$) complex proceeds in a sequential fashion where the first transfer occurs within time resolution, irrespective of base strength, whereas the second transfer from the water to the base is activated and conforms to a correlation between free energy and reaction rate.

[1] A. Weller, Progr. React. Kinet., **1961**, 1, 187-213.

[2] M. Eigen, Angew. Chem., **1963**, 75, 489-508; Angew. Chem. Int. Ed., **1964**, 3, 1-19.

[3] E. T. J. Nibbering, H. Fidder and E. Pines, Annu. Rev. Phys. Chem. **2005**, 56, 337-367.

[4] M. Rini, B.-Z. Magnes, E. Pines, E. T. J. Nibbering, Science, **2003**, 301, 349-352.

[5] O. F. Mohammed, D. Pines, J. Dreyer, E. Pines, E. T. J. Nibbering, Science, **2005**, 310, 83-86.

[6] O. F. Mohammed, D. Pines, E. T. J. Nibbering, E. Pines, Angew Chem., **2007**, 119, 1480-1483; Angew Chem. Intl. Ed., **2007**, 46, 1458-1461.

[7] E. Pines, D. Huppert, N. Agmon, J. Chem. Phys. 88 (1988) 5620.

[8] E. Pines, B.Z. Magnes, M.J. Lang, G.R. Fleming, Chem. Phys. Lett. 281 (1997) 413

[9] R. Stewart, "The Proton: Applications to Organic Chemistry", Academic Press, New York, 1985.

[10] E. Pines, in: A. Kohen, H.-H. Limbach (Eds.), "Isotope Effects In Chemistry and Biology", CRC Press - Taylor and Francis, Boca Raton, 2005, p. 451.

N. Agmon, E. Pines, D. Huppert, J. Chem. Phys. 88 (1988) 5631.

[12] B. Cohen, D. Huppert, N. Agmon, J. Am. Chem. Soc. 122 (2000) 9838

[13] B. Cohen, D. Huppert, N. Agmon, J. Phys. Chem. A 105 (2001) 7165

Proton conduction in aqueous acid-base reactions

M.J. Cox[1], B..J. Siwick[1,2] and H.J. Bakker[1]

[1] FOM Institute AMOLF, Kruislaan 407, 1098 SJ Amsterdam, The Netherlands [2] Departments of Physics and Chemistry, McGill University, 3600 University St., Montreal, QC. H3A 2T8 Canada. bakker@amolf.nl www.amolf.nl

Many ultrafast studies on proton transfer (PT) have concentrated on the photo-acid pyranine: 8-hydroxy-1,3,6-pyrenetrisulfonic acid trisodiumsalt (HPTS). Excitation to the S_1 excited state with 400 nm light leads to an enhancement of the acidity of the molecule by a factor of 10^6. By measuring the transient fluorescence and absorption of the photo-acid (HPTS) and its conjugated photo-base (PTS⁻) it was found that the proton/deuteron is released with a time constant of approximately 90/220 ps in water/heavy water.

When a base is also added to the solution the reaction speeds up significantly. PT between HPTS and an acetate base has been described in terms of the Eigen-Weller picture[1] using the Smoluchowski-Collins-Kimball model for diffusion-controlled reactions[1]. In this model, the acid and base diffuse to a particular intermolecular separation (the reaction contact radius) at which the PT takes place at some intrinsic rate. Recently, the groups of Nibbering and Pines studied the intermolecular PT between HPTS and different carboxylate bases by probing the vibrations of the photo-acid and an accepting base with femtosecond mid-infrared laser pulses[2,3] and found that this model did not provide a good fit of their data. Two additional decay components were added, which were interpreted as "tight" and "loose" reaction complexes that exist prior to HPTS excitation.

Here we study the PT reaction between HPTS and a base by measuring the isotope effect of the PT and by directly probing the broad-band infrared response of the hydrated proton/deuteron with femtosecond mid-infrared laser pulses. HPTS is excited with 400 nm, 120 fs laser pulses containing an energy of 5 μJ per pulse. The mid-infrared probe pulses are tunable between 2.7 and 8 μm, have a typical pulse duration of ~150 fs, an energy of 0.1 μJ, and a frequency bandwidth of 200 cm⁻¹. The probe polarization is rotated to the magic angle so that only isotropic absorption changes are detected and the measurements are not affected by molecular reorientations.
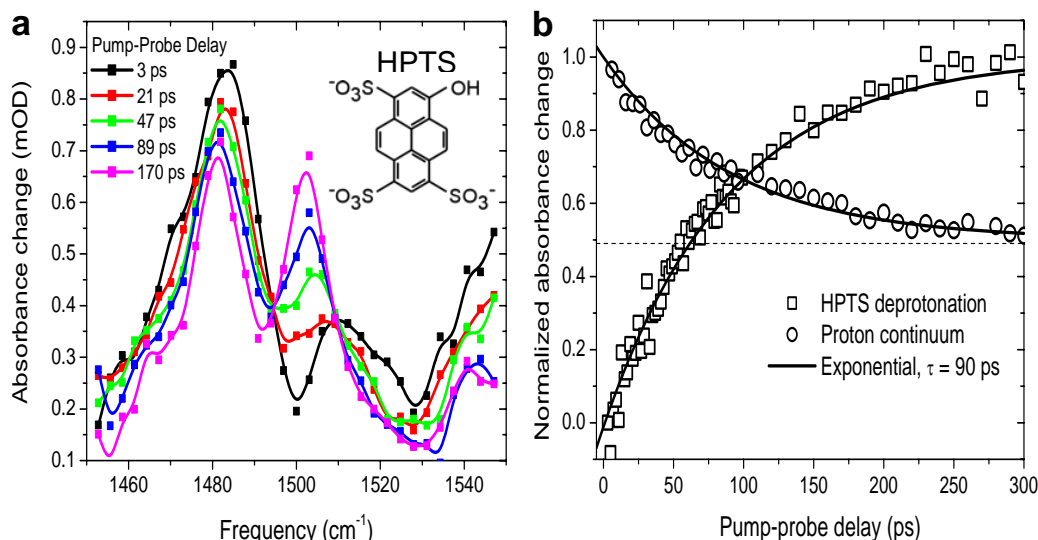
Figure 1: Transient spectra of the vibrational bands of HPTS* and its conjugated photo base PTS⁻ near 1500 cm⁻¹ at five different delays for a solution of 10 mM HPTS in H₂O (no added base).

In Fig. 1, transient infrared spectra are shown in the frequency region near 1500 cm^{-1} corresponding to the aromatic ring vibrational modes of HPTS and PTS$^-$. These spectra are measured without a base present. The spectrum measured 1 ps after the excitation shows the direct change in the aromatic ring system induced by the electronic excitation. With increasing delay, the amplitude of the bands at 1480 and 1540 cm^{-1} decreases and a new vibrational band centered at 1503 cm^{-1} arises. This latter band is assigned to the PTS$^-$ conjugate photo base, and its rise thus marks the transfer of a deuteron from HPTS to H$_2$O.

In addition to the spectral changes of HPTS and PTS$^-$, we observe a broadband infrared absorption directly after the excitation. The amplitude of this continuum absorption is linear in the pump intensity, which shows that this absorption is not the result of multi-photon excitation processes. The broadband infrared absorption shows very little structure, and extends up to frequencies >2800 cm^{-1} for a solution of HPTS in H$_2$O. Above 2800 cm^{-1} the broadband infrared response is obscured by the very strong absorption of the O-H stretch vibrations of the H$_2$O solvent. In the absence of base, the broadband infrared absorption shows a partial decay with exactly the same dynamics (90/220 ps) as the proton/deuteron transfer (Fig. 1b). Thus, we assign the broadband absorption observed directly after the excitation to the response of protons/deuterons that are loosely bound to HPTS*. The broadband absorption observed at large delay times is due to fully hydrated protons/deuterons.
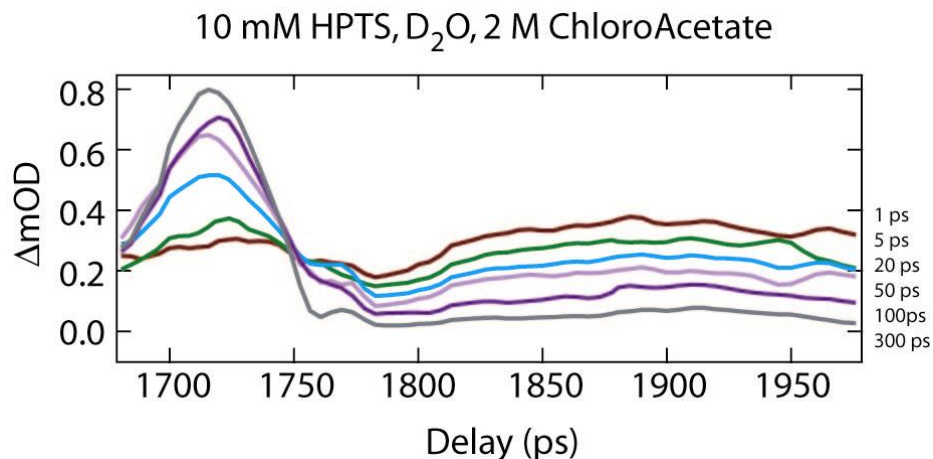
Figure 2: Transient spectra in the frequency region near the carbonyl stretch vibration (1720 cm^{-1}) of chloro-acetic acid at six different delays for a solution of 10 mM HPTS and 2 M chloro-acetate in D$_2$O.

In Fig. 2 the spectral response of the carbonyl stretch vibration and the continuum absorption is shown for a solution of 10 mM HPTS and 2 M chloro-acetate in D$_2$O. The observed spectrum strongly differs from the spectrum observed in a recent study by the groups of Nibbering and Pines. In this latter study, a narrow band centered at 1850 cm^{-1} was observed, and no signal was present at frequencies greater than 1900 cm^{-1}. This narrow band was interpreted as the result of a specific intermediate state in the PT reaction that consists of an H$_3$O$^+$ ion embedded between PTS$^-$ and chloro-acetate. Interestingly, in spite of this strong difference in spectral response, we observe the same delay-time dependence of the signal as in Ref. 3 (shown in Fig. 3).

Fig. 3 shows the dynamics of HPTS*, the conjugate photobase PTS$^-$, the broadband continuum and the carbonyl stretch vibration for a solution of 10 mM HPTS and 1 M chloro-acetate in D$_2$O. These transients represent the data at delays greater than 1 ps. At earlier delay times (~100 fs) the signals show a pulse-width limited component that results from the reaction between direct contact pairs of HPTS and acetate. This signal contribution was also

found in earlier work on the PT between HPTS and acetate[2]. In Fig. 3 it is seen that the carbonyl stretch vibration, which reflects proton uptake by the base, and the conjugated photo base PTS⁻ show exactly the same dynamics. This observation implies that there is not a long-lived intermediate in the PT from HPTS* to acetic acid, in contrast to what was reported in Ref. 3. The broadband signal shown in Fig. 2 is thus not due to an intermediate of the reaction but to the proton that is still loosely bound to HPTS*.
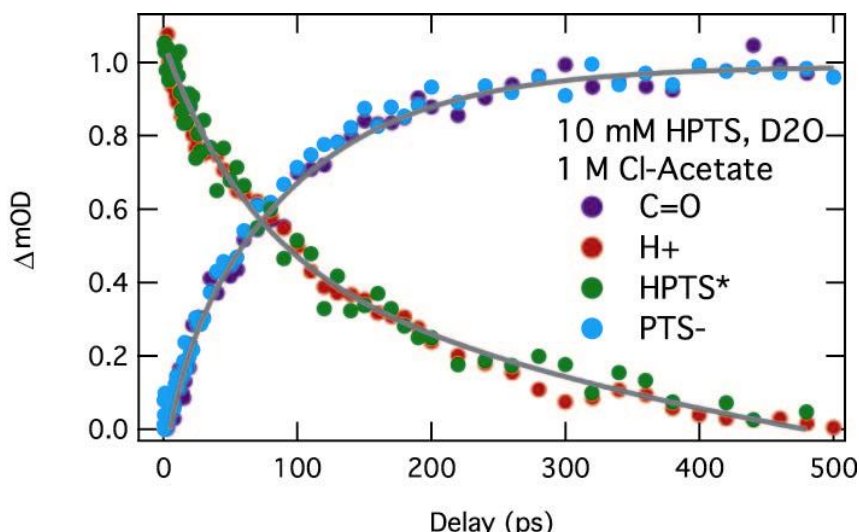
Figure 3 : Transients of HPTS* at 1430 cm⁻¹, the loosely bound proton at 1900 cm⁻¹, PTS⁻ at 1500 cm⁻¹, and chloro-acetic acid at 1720 cm⁻¹ for a solution of 10 mM HPTS and 1 M chloro-acetate in D₂O.

We observe an isotope effect of 1.5 for the PT/DT, which indicates that this rate is not determined by the diffusion of the reactants, but instead is determined by proton/deuteron conduction in water. Together with the absence of a long-lived intermediate, this leads to the following picture for PT by an excited photo-acid in water. Directly after the excitation of HPTS, the proton is loosely bound showing short-lived delocalizations along hydrogen bonds connected to the acidic proton. Solvent fluctuations are essential for the delocalization because these fluctuations lead to transient hydrogen-bond configurations of the nearby water molecules that favor the uptake of (part of) the protonic charge. During these delocalizations, the vibrational response of the aromatic ring modes of HPTS* is preserved. However, at some point the degree of delocalization can become so large that the proton escapes, which means that the proton no longer returns to the hydroxyl group of the HPTS molecule. From that time on the proton is only solvated by water molecules. When a nearby base is present, the picture changes slightly. The loosely bound proton again shows short-lived delocalizations, but the delocalization length required to escape from HPTS can be shorter depending on the distance to the base. The base will trap the proton as soon as the delocalized proton reaches the base with sufficient amplitude. We incorporated the above picture in a model in which the proton is conducted from the acid to the base via hydrogen-bonded water wires of different lengths. The distribution of wire lengths follows from the concentration of acetate, assuming a statistical distribution. With this model, we can describe the proton transfer at all delay times and all base concentrations with only two parameters, representing the conduction rate over a single hydrogen band and the decrease in rate with each additional hydrogen bond in the wire.

[1] L. T. Genosar, B. Cohen, D.J. Huppert, J. Phys. Chem. A **2000**, 104, 6689-6698.
[2] M. Rini, B.-Z. Magnes, E. Pines, E.T.J. Nibbering, Science **2003**, 301, 349-352.
[3] O.F. Mohammed, D. Pines, J. Dreyer, E. Pines, E.T.J. Nibbering Science **2005**, 310, 83-86.

Vibrational dynamics of benzoic acid in solutions studied by sub-picosecond time-resolved infrared spectroscopy

S. Yamaguchi[1], M. Banno[2], K. Ohta[1], K. Tominaga[1,2,3]

[1] Graduate School of Science and Technology, Kobe University, Nada, Kobe, Japan.

[2] Molecular Photoscience Research Center, Kobe University, Nada, Kobe, Japan. [3]CREST/JST

e-mail: K. Tominaga, tominaga@kobe-u.ac.jp

Biological macromolecules such as nucleic acid and proteins often express and control their functions by rearranging hydrogen bonds. To deepen our understanding on hydrogen bonds, it is necessary to obtain knowledge of intermolecular vibrations of hydrogen bonded complexes. Carboxylic acids in solutions are important model systems for studying hydrogen bonds. Benzoic acid (BA) is one of the carboxylic acids and forms dimer or complex with other molecules in various solutions (Figure 1).[1] Intermolecular hydrogen bonds of these complexes have much effect on dynamics of the vibrational modes associated with hydrogen bonds. The effects of hydrogen bond on dynamics in the vibrationally excited state of the hydroxyl stretching mode have been extensively studied by time-resolved vibrational spectroscopy.[2] Recently, Elsaesser and coworkers have studied the coupling between the hydroxyl stretch and low-frequency modes of acetic acid dimer by analyzing the quantum beat observed in the pump-probe signal.[3] More recently, they have extended their work to 7-azaindole dimer.[4] In this work we have studied vibrational energy relaxation of the OH stretching mode of the BA complex in various solvents by infrared (IR) pump-probe spectroscopy.

Figure 1. BA dimer

BA-d_5 and solvents (CCl$_4$, CDCl$_3$, benzene-d_6, THF-d_8, acetone-d_6, and acetonitrile-d_3) were used without further purification. Details of the sub-picosecond IR pump-probe spectroscopy will be described elsewhere.[5] We obtained IR pulses by difference frequency mixing with signal and idler pulses in the near-IR region generated by a home-built optical parametric amplifier. The pulse duration of the IR pulse is approximately 200 fs. We split the IR pulse into pump, probe, and reference pulses with frequencies at a peak of the OH stretching band in the solution. The probe and reference pulses were detected by an array detector after passing through a monochromator. The samples were contained in a cell with an optical path length of 0.1-0.5 mm depending on the solvents. The samples were prepared so that the optical density was around 0.6 at the excitation wavenumber.

Figure 2 shows solvent dependence of the IR spectra of the OH stretching mode of BA-d_5. In the solvents which do not form strong hydrogen bond with the hydroxyl group of BA (CCl$_4$, CDCl$_3$, and benzene-d_6), the peak wavenumber is located at around 3000 cm^{-1}, and the spectra show a broad band with complicated structures. These structures result from the intermolecular vibrations within the dimer, Fermi resonance, and Davydov coupling.[2] The spectra of the three solutions are identical to each other. From the dependence of the IR spectrum on the concentration of BA, the broad band at 3000 cm^{-1} is assigned to dimer of BA. On the other hand, for the other solvents forming strong hydrogen bond (THF-d_8, acetone-d_6, and acetonitrile-d_3) the peak is shifted to the higher frequency side depending on the solvent, indicating that the strength of HB of these complexes is weaker than that of the dimer in the former solvents. In addition,
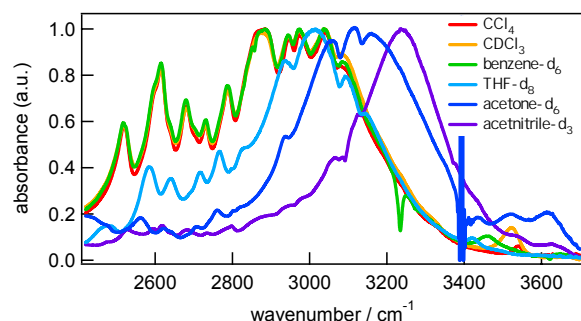
Figure 2. Absorption spectra of the OH stretching mode. The solvents are indicated in the inset.

the spectra are structure-less compared to those in the non-hydrogen bonding solvents. In these solvents, most of BA molecules exist as a complex with solvent molecules. In this article we discuss results of the pump-probe experiment on the non-hydrogen bonding solvents.

Figure 3 shows a frequency-resolved pump-probe signal of the OH stretching mode of BA-d_5 in CCl_4. The excitation and probe pulses have a central wavenumber at 3000 cm^{-1}. In the lower-frequency side the ground state bleach and the stimulated emission is observed, and in the higher-frequency side the transient absorption is observed. Figure 4 displays time profiles of the signal at 2840 cm^{-1}, 3000 cm^{-1} and 3124 cm^{-1}. All these signals show a double exponential decay with a

Figure 3. Frequency-resolved pump-probe signal of the OH stretching mode of 120 mM BA-d_5 in CCl_4.

pronounced oscillation. The obtained time constants of the decay are 730 fs and 12 ps at 3000 cm^{-1}. At 3124 cm^{-1} the signal turns to a transient absorption component instantaneously, which is followed by decay in a picosecond time scale. This transient absorption component in the higher-frequency side results from a blue shift of the spectrum in the vibrational ground state caused by local heating around the oscillator. Therefore, the vibrational population relaxation takes place within our time resolution (< 200 fs), and the pump-probe signals come from the vibrational ground state. For an acetic acid dimer, Elsaesser and coworkers observed decay of the vibrationally excited state of the OH stretching mode and obtained the vibrational population relaxation time of 230 fs. Interestingly, in the present case the fast sub-picosecond component depends on the excitation wavenumber, where the slow picosecond component nearly depends on it. For example, at 2800 cm^{-1} excitation, the two time constants are 1.5 ps and 14 ps at 2818 cm^{-1}. From these observations, we tentatively assign the fast and slow components to the vibrational relaxation of the low-frequency modes in the ground state of the OH stretching mode and cooling process in the environment locally heated, respectively.
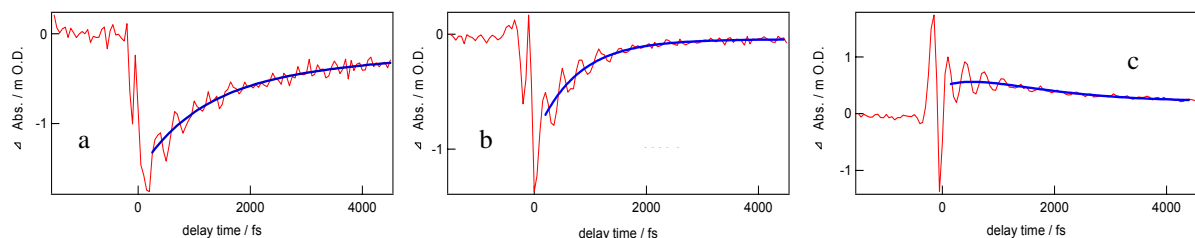
Figure 4. Pump-probe signals of 120 mM BA-d_5 in CCl_4 at 2840 cm^{-1} (a), 3000 cm^{-1} (b), and 3124 cm^{-1} (c). Blues curves are results of fitting by a double exponential function.

We analyzed the oscillation in the pump-probe signals of the non-hydrogen bonding solvents by Fourier transforming the oscillatory part. By subtracting the double exponential decay from the observed signal, we obtain a Fourier spectrum of the oscillation. Figure 5(a) shows the spectrum observed at a probe wavenumber of 3124 cm^{-1}, and Figure 5(b) displays a two-dimensional map of the Fourier spectra of the quantum beat. There is a single band located at around 100 cm^{-1}. This low-frequency mode couples to the OH stretching mode. In other words, this mode changes its equilibrium position when the OH stretch is excited from the $v=0$ to $v=1$ state. Elsaesser and coworkers also observed a low-frequency mode at 145 cm^{-1} which is coupled to the OH stretch of acetic acid dimer. They assigned this mode to in-plane dimer bending mode.[3]

In order to obtain the peak wavenumber of the low-frequency mode more accurately, we fitted the Fourier spectra with a Lorentzian function (Figure 5(a)). The results are shown in Figure 6. Although the points are rather scattered, it is observed that the peak wavenumber of the low-frequency mode depends on the frequency of the OH stretching mode; as the frequency of the OH stretching mode increases, the frequency of the low-frequency mode becomes smaller.

Let us briefly discuss the possible reasons for this dependence. First, the Fermi resonance may contribute to the oscillation. However, as discussed in detail by Elsaesser and coworkers,[3] oscillation due to the Fermi resonance should disappear within a dephasing time between the $v=0$ and $v=1$ states of the OH stretching mode. In this case the lifetime of the vibrationally excited state is shorter than the time resolution which is less than 200 fs, it is unlike that the Fermi resonance could contribute to the oscillation. Second, there may be another low-frequency mode which is coupled to the OH stretching mode. A band due to this mode may overlap with the band which couples with OH stretching mode strongly, and the coupling of this mode may depend on the wavenumber. Then, the band shape changes with the probe wavenumber, and, consequently, an effective peak position changes with the wavenumber. Actually, Elsaesser and coworkers observed another band due to in-plane dimer stretching mode at around 175 cm^{-1} depending on the probe wavenumber.[3] Thirdly, since we assign the fast sub-picosecond decay component to the vibrational relaxation of the low-frequency mode, if the higher-frequency side of the probe observes the higher excited state of the low-frequency mode by some reason, it could be expected to see such dependence. However, it is hard to come up with a physically accepted picture to explain this phenomenon. Finally, since the high-frequency side of the OH stretching mode corresponds to weaker hydrogen bonds, it may happen that the low-frequency intermolecular mode depends on the hydrogen bond strength. It is true only when the band is massively inhomogeneously broadened. The existence of the complicated structures in the IR spectrum suggests that the band may be homogeneously broadened. The key question is how large the inhomogeneity is for the OH stretching band, which can be clarified by an IR photon echo experiment.
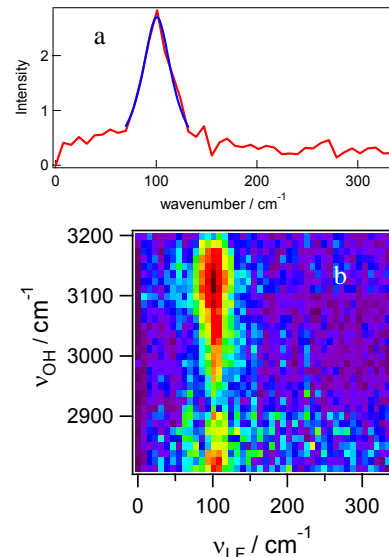
Figure 5. The Fourier spectrum of the quantum beat at 3124 cm^{-1} and fit by Lorentzian (blue line) (a), and 2D map of Fourier spectra in all the probe wavenumber region (b). ν_{LF} and ν_{OH} denote frequencies of the low-frequency mode and OH stretching mode, respectively.
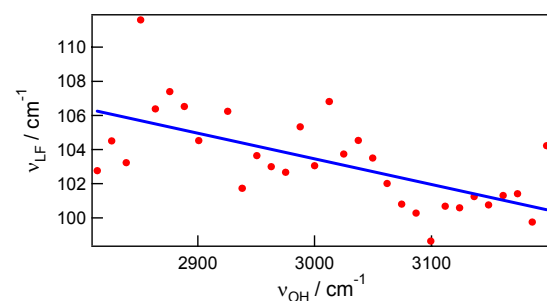
Figure 6. The dependence of the low-frequency mode (ν_{LF}) on the OH stretching mode (ν_{OH}). A blue is a least-squares fit for eye guidance.

[1] P. Novak et al., J. Mol. Struct., **1995**, 356, 131

[2] E. T. J. Nibbering and T. Elsaesser, Chem. Rev., **2004**, 104, 1887

[3] K. Heyne et al., J. Chem. Phys., **2004**, 121, 902

[4] J. R. Dwyer et al., Chem. Phys. Lett., **2006**, 432, 146

[5] M. Banno et al., to be submitted.

Photoinduced Bimolecular Electron Transfer Investigated by Femtosecond Time-Resolved Infrared Spectroscopy

O. F. Mohammed[1], N. Banerji[1], K. Adamczyk[2],

B. Lang[1], E. T. J. Nibbering[2], E. Vauthey[1]

[1] Department of Physical Chemistry, University of Geneva, 30, Quai Ernest Ansermet, CH-1211 Geneva 4, Switzerland. [2] Max Born Institut für Nichtlineare Optik und Kurzzeitspektroskopie, Max Born Strasse 2A, D-12489 Berlin, Germany. bernhard.lang@chiphy.unige.ch, http://www.unige.ch/sciences/chifi/Vauthey/

Since the pioneering work of Weller and coworkers[1], bimolecular photoinduced electron transfer (ET) reactions have been intensively investigated, a typical scheme in polar solvents being depicted in Figure 1. These processes are the simplest bimolecular reactions and have thus been object of many theoretical treatments. Furthermore, they play an important role in many areas of chemistry and biology and are involved in several practical applications such as solar energy conversion, and photopolymerisation. Despite the numerous studies carried out on bimolecular ET, important questions still remain unanswered[2], such as the nature of the primary ET quenching product and the various steps leading to the formation of free solvated ions in polar solvents.
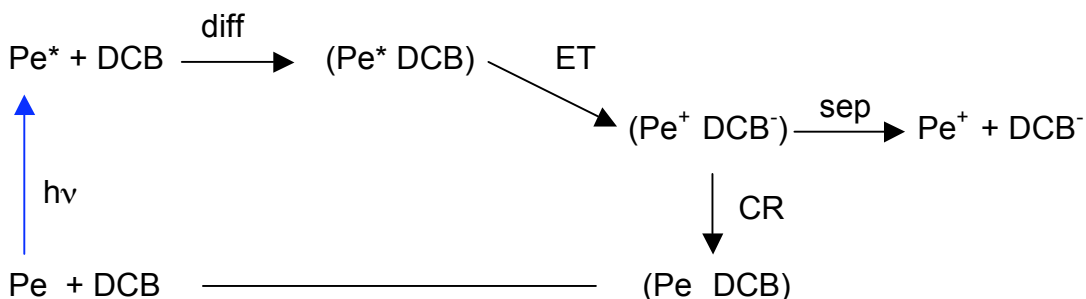
Figure 1: Scheme of the ET reaction between Pe and DCB.

A major experimental problem is that ion pairs and free ions cannot be easily differentiated from their electronic absorption spectra, and thus only indirect structural information could be inferred from their dynamics[3,4,5]. Time-resolved vibrational spectroscopy is apparently a more promising approach to obtain such information on these ion pairs. A nanosecond time-resolved resonance Raman study of photoinduced bimolecular ET reactions has been reported several years ago.[6,7] However, apart from one exception, the resonance Raman spectra of the ion pair and the free ions were identical. Moreover, the time-resolution of the experiment was not sufficient to perform this study in acetonitrile, where interconversion between ion pairs and dissociation into free ions takes place on a sub-nanosecond timescale.

Here, we report on an investigation of the photoinduced bimolecular ET reaction between the electron donor perylene (Pe) and the acceptor 1,4-dicyanobenzene (DCB) in acetonitrile (ACN) and dichloromethane (DCM) using femtosecond time-resolved IR

[1] H. Leonhard, A.Weller, Z. Phys. Chem, **1961**, 29, 277-280.
[2] E. Vauthey, Photochem. Photobiol A, **2006**, 179, 1-12.
[3] E. Vauthey, J. Phys. Chem. A, **2001**, 105, 340-348.
[4] E. Vauthey, J. Phys. Chem. A, **2000**, 104, 1804-1810.
[5] O. Nicolet, E. Vauthey, J. Phys. Chem. A, **2002**, 106, 5553-5562.
[6] E. Vauthey, D. Phillips, A. W. Parker, J. Phys. Chem., **1992**, 96, 7356-7360.
[7] E. Vauthey, A. W. Parker, D. Phillips, B. Nohova, J. Am. Chem. Soc. **1994**, 116, 9182-9186.

spectroscopy. Ultrafast vibrational spectroscopy has been used before to probe the rearrangement of hydrogen bonds and solvation shells[8]. Spectral shifts have been interpreted as hydrogen bond cleavage of complexes of a laser dye upon electronic excitation[9,10] and of solvation shell rearrangements due to coupling between the vibrational transition dipole moment of the spectator mode with the polar solvent[11]. By recording transient IR absorption spectra of the radical ions generated upon photoinduced ET and analysing height and width of the corresponding bands, we can directly follow the generation of both ions under identical conditions, which is often difficult to impossible in all-visible experiments.
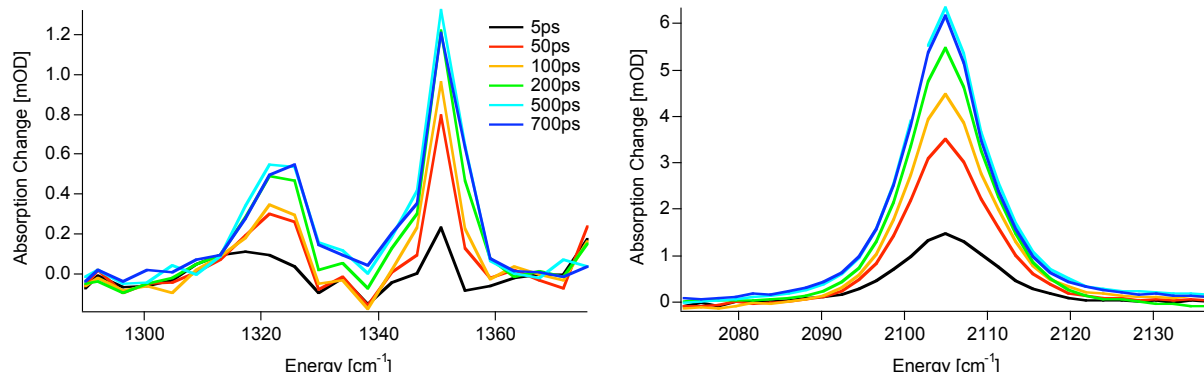
Figure 2, left panel: transient absorption spectra of the $Pe^{\bullet +}$ radical cation in the fingerprint region at different time delays; right panel: transient band associated with the antisymmetric stretch vibration of the $DCB^{\bullet -}$ radical anion (colour code as on the left panel).

Figure 2, left panel shows the temporal evolution of two transient bands in the fingerprint region measured after 400 nm excitation of Pe with 0.16 M DCB in ACN which are attributed to the $Pe^{\bullet +}$ radical cation. On the right panel, the band associated with the antisymmetric stretch vibration of the $DCB^{\bullet -}$ radical anion is depicted for the same time delays. Depending on the DCB concentration, these bands rise on a time scale of one to several hundreds of picoseconds and remain then constant within the observation window of the experiment up to 1 ns. From a peak height analysis as a function of time delay we obtain identical kinetics for both $Pe^{\bullet +}$ and $DCB^{\bullet -}$ bands, which indicates that the formation of the ionic product does not involve a third reactant such as a solvent molecule or an electronic excited state of one of the ions. This is not surprising for this donor-acceptor (DA) pair with its rather weak ET driving force. The time dependence of the $Pe^{\bullet +}$ cation population can also be measured by visible transient absorption spectroscopy on its D_0-D_5 transition at 530 nm[12], which yields the same result as obtained from the IR spectral domain. As shown in Figure 1, ET first requires the reactants to diffuse until they are sufficiently close for the reaction to become operative. This diffusive encounter limits the reaction rate and depends strongly on the DCB concentration. Upon ET, the radical ion pair may either undergo charge recombination (CR) to the neutral ground state or dissociate into free solvated ions.

Although the kinetics of the bands in the IR domain do not contain any new information with respect to what is already known for the DA pair investigated here, they serve as a cross check for the consistency of the data and demonstrate the potential of time-resolved mid-IR spectroscopy. Note that the kinetics of the $DCB^{\bullet -}$ radical anion cannot be

8   E. T. J. Nibbering, H. Fidder, E. Pines, Annu. Rev. Phys. Chem., **2005**, 56, 337-367.
9   C. Chudoba, E. T. J. Nibbering, T. Elsaesser, Phys. Rev. Lett., **1998**, 81, 3010-3013.
10   C. Chudoba, E. T. J. Nibbering, T. Elsaesser, J. Phys. Chem. A, **1999**, 103, 5625-5628.
11   E. T. J. Nibbering, C. Chudoba, T. Elsaesser, Isr. J. Chem., **1999**, 39, 333-347.
12   E. Vauthey, P. Suppan, E. Haselbach, R. S. Davidson, Helv. Chim. Acta, **1986**, 69, 430-437.

obtained from all visible experiments as this species does not exhibit absorption bands in the visible spectral domain. Even with DA pairs where both radical ions exhibit absorption bands in the visible, a detailed analysis of the bands is often difficult due to the large spectral broadening which leads to strongly overlapping bands.
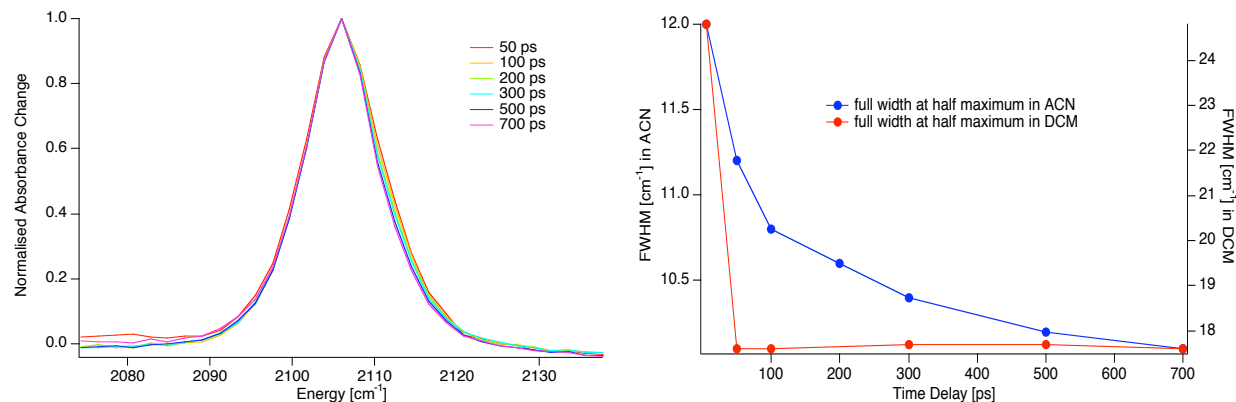
Figure 3, left panel: Normalised absorption band of the antisymmetric CN stretch vibration of DCB$^{\bullet-}$ in ACN at different time delays after photo triggering ET; right panel: full width at half maximum of the bands shown on the left panel as a function of time delay in ACN and in DCM.

New information on the reaction dynamics can be obtained from a band shape analysis of the antisymmetric CN stretch mode (fig. 3). It appears that the electron density on the cyano groups of DCB$^{\bullet-}$ is very sensitive to the local environment and thus the width and spectral position of the band corresponding to the antisymmetric CN stretch vibration can be used to probe the presence or absence of the nearby counter ion. In both solvents used here, ACN and DCM, this CN stretch band exhibits first a narrowing on a time scale of a few tens of picoseconds that is ascribed to vibrational cooling. This indicates that a substantial part of the excess energy is dumped into vibrational modes of the product, despite the fact that the reaction is weakly exergonic ($\Delta G = -0.26$ eV). An additional narrowing of the same band on a time scale of several hundreds of picoseconds is apparent in ACN only. We interpret this additional narrowing as a signature of the dissociation of the geminate ion pairs into free ions[13], as the observed time scale coincides with the time scale expected for the latter process. The fact that this narrowing only appears in ACN is also consistent with the free ion yields of 0.3 and ~0 measured in ACN and DCM, respectively. Indeed, in the weakly polar DCM, the loss of electrostatic stabilisation energy upon separating the ions is not compensated by solvation energy, and thus the ion pairs do not dissociate. The assignement of the spectral narrowing in ACN is further supported by the results of a pump-pump-probe experiment where the ground state recovery (GSR) of the Pe radical cation upon excitation of its D_0-D_5 transition has been recorded as a function of time delay between photo triggering ET and exciting the radical cation, i.e. as a function of the "age" of the ion pair[14].

In conclusion, we have demonstrated that time-resolved mid-IR spectroscopy allows for the first time to extract information about the primary reaction products of photoinduced bimolecular electron transfer, which cannot be obtained from conventional all-visible transient absorption experiments. With the DA pair Pe-DCB in acetonitrile, we observe a band narrowing on a 100 ps time scale which we interpret as a signature of the separation of the ion pair into free solvated ions.

[13]   O. F. Mohammed, N. Banerji, B. Lang, E. T. J. Nibbering, E. Vauthey, J. Phys. Chem. A, **2006**, <u>110</u>, 13676-13680.

[14]   S. Pagès, B. Lang, E. Vauthey, J. Phys. Chem. A, **2006**, <u>110</u>, 7547-7553.

Proton transfer at the alumina-air interface

Sophie Le Caër[1], D. Jason Palmer[2], Manuela Lima[2], Jean Philippe Renault[1], Georges Vigneron[1], Roberto Righini[2] and Stanislas Pommeret[1]

[1] CEA/Saclay, DSM/DRECAM/SCM, Laboratoire Claude Fréjacques, URA 331 CNRS, F-91191 Gif-sur-Yvette Cedex, France, [2] University of Florence, Polo Scientifico, Via Nello Carrara 1, I-50019 Sesto Fiorentino, Italy. e-mail address: sophie.le-caer@cea.fr and www-drecam.cea.fr/scm/radiolysis/

In a recent study[1], we have investigated the dynamical properties of water and OH groups layered on a γ-alumina surface by means of femtosecond IR-pump IR-probe transient absorption spectroscopy. We will hereafter focus on the proton transfer we have evidenced on the alumina surface. The framework of this study deals with the dynamical behavior of water at interfaces. Unfortunately, it is poorly understood compared to its behavior in neat liquid[2] although it is of crucial importance in many fields[3].

Due to its importance in catalysis, we chose to work with alumina. Alumina membranes[4] (Anodisc aluminum oxide membrane filters, Whatman International) used here are 47 mm in diameter with 200 nm pore diameters and 60 μm thick[5]. The alumina surface consists of pores which are cylinders parallel to one another in a honeycomb structure (Figure 1a). We performed nonlinear infrared experiments using an infrared-infrared pump probe experimental set-up[6]. The infrared output of the pump and of the probe is on the order of 1 μJ with a spectral width of ~ 200 cm^{-1} and a temporal width of approximately 100 fs. We used three pumping frequencies at 3460, 3200 and 3000 cm^{-1}(Figure 1b). More details are given in reference [1].

(a)   (b)
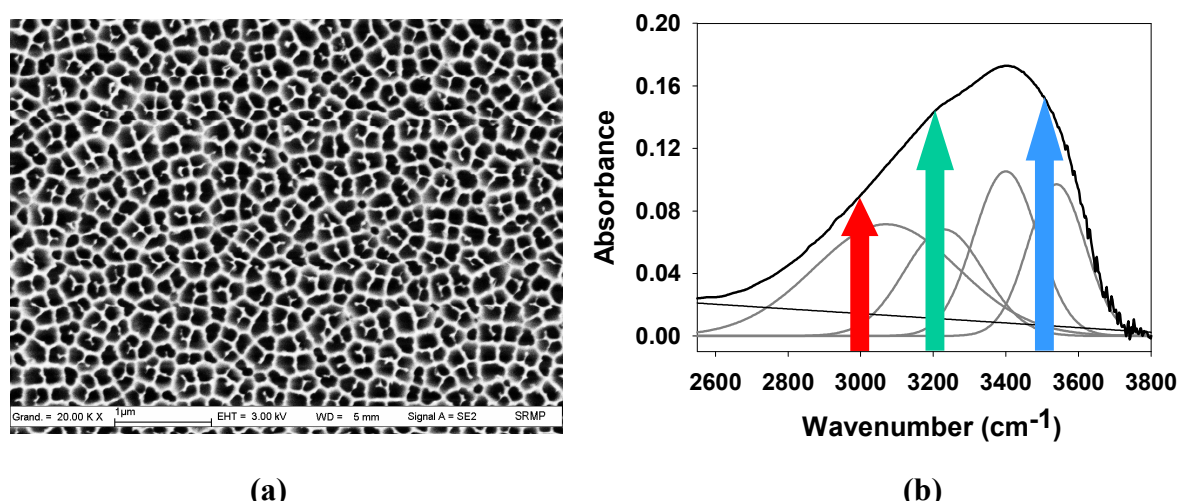
Figure 1: (a) SEM image of the alumina membranes: top view of the sample. The pore size is 200 nm. (b)FT-IR spectrum of the alumina membrane in the O-H stretching region together with the fit of the band. The band is deconvoluted into four bands (grey lines). The baseline is represented with the thin black line. The arrows represent the different pumping frequencies used at 3460, 3200 and 3000 cm^{-1}.

[1] S. Le Caër, D.J. Palmer, M. Lima, J.P. Renault, G. Vigneron, R. Righini, S. Pommeret, J. Am. Chem. Soc., in press

[2] E.T.J. Nibbering, T. Elsaesser, Chem. Rev., **2004**, 104, 1887-1914

[3] H.-S. Tan, I.R. Piletic, M.D. Fayer, J. Chem. Phys., **2005**, 122, 174501

[4] R.C. Furneaux, W.R. Rigby, A.P. Davidson, Nature, **1989**, 337, 147-149

[5] G.P. Crawford, L.M. Steele, R. Ondris-Crawford, G.S. Iannacchione, C.J. Yeager, J.W. Doane, D. Finotello, J. Chem. Phys., **1992**, 96, 7788-7796

[6] P. Hamm, M. Lim, R.M. Hochstrasser, J. Phys. Chem. B, **1998**, 102, 6123-6138

The O-H stretching band of the alumina membrane (Figure 1b) can be deconvoluted into the four following components:

(a) the 3530 cm^{-1} band is due to hydrogen-bonded alumina surface hydroxyls (AlO-H)[7,8];

(b) the 3410 cm^{-1} band is attributed to physisorbed water (i.e. the hydrogen bonding network of adsorbed water). Moreover, the O-H stretching vibration of aluminol groups can overlap with the molecularly adsorbed H_2O band [8];

(c) the 3220 cm^{-1} component corresponds to physisorbed water relatively strongly hydrogen bonded. As a matter of fact, the O-H stretching frequency decreases when the hydrogen bond energy increases. This contribution may thus be attributed to water in interaction with $AlOH_2^+$ sites on the surface (component d);

(d) the component at the lowest frequencies (3080 cm^{-1}) is due to chemisorbed species ($AlOH_2^+$ sites, see Figure 1b). The acidity of the site leads to strong hydrogen bonds with surrounding water molecules and thus to this very low characteristic frequencies. We will hereafter focus on this component.

The experimental transient absorption kinetics were fitted using a global model with four contributions (see Equation 1, with the time expressed in fs): a coherent contribution when the pump and the probe pulses significantly overlap (Dirac contribution, instantaneous); a dominating fast contribution (350 fs); a marginal slow contribution (2.5 ps), and a Heaviside contribution. The values of those time constants did not present any pump- and probe-frequency dependence. The non mono-exponential decay may be attributed to the wide variety of OH sites on the alumina surface. Nevertheless, the mean lifetime is well described by the fast decay time (350 fs).

$$
\left\{
\begin{aligned}
&Model(t) = a_1 \times \exp\left(-\frac{t}{350}\right) + a_2 \times \exp\left(-\frac{t}{2500}\right) + a_3 + a_0 \times \delta(t) \\
&Fit(t) = \int_{-\infty}^{t} Model(t-x) \times Gauss(x)\, dx \qquad \text{(Eq. 1)} \\
&Gauss(x) = \frac{2\sqrt{\ln(2)}}{FWHM \cdot \sqrt{\pi}} \times \exp\left(-\frac{4\ln(2)x^2}{FWHM^2}\right)
\end{aligned}
\right.
$$

In the preceding equations, $FWHM$ is the full width at half maximum of the temporal resolution of the setup, $\delta(t)$ is the Dirac function and the a_i are the amplitude parameters of the fit.

The results obtained in the case of a pump at 3000 cm^{-1} are displayed in Figure 2. Figure 2a exhibits an unusual behavior: as a matter of fact, we observe a bleaching for "low" frequencies and an induce absorption for "large" frequencies. Moreover, the bleaching is not located around the pump frequency but instead around 3175 cm^{-1}, corresponding to water interacting with $AlOH_2^+$ sites. The pre-exponential factor of the fast component is positive between 3450 and 3550 cm^{-1}, i.e. in the AlOH spectral region. This behavior might be understood if we consider a photoinduced proton transfer from $AlOH_2^+$ to its neighboring water molecule (Reaction 1, the backtransfer reaction was also detected, see [1]):

$$
AlOH_2^+ + H_2O \underset{\text{backtransfer}}{\overset{h\nu}{\rightleftharpoons}} AlOH + H_3O^+ \qquad \text{(Reaction 1)}
$$

[7] K.C. Hass, W.F. Schneider, A. Curioni, W. Andreoni, Science, **1998**, <u>282</u>, 265-268
[8] H. Knözinger, P. Ratnasamy, Catal. Rev.-Sci. Eng., **1978**, <u>17</u>, 31-69

Such a reaction would induce a bleaching around 3200 cm^{-1} (water molecule around the excited AlOH$_2^+$), a bleaching around the pump frequency, as well as an absorption above 3500 cm^{-1} (AlOH) and around 3000 cm^{-1} (H$_3$O$^+$)[9]. No clear signal can thus be detected in the 3000 cm^{-1} region, as the two signals (pump frequency and H$_3$O$^+$) compensate each other.
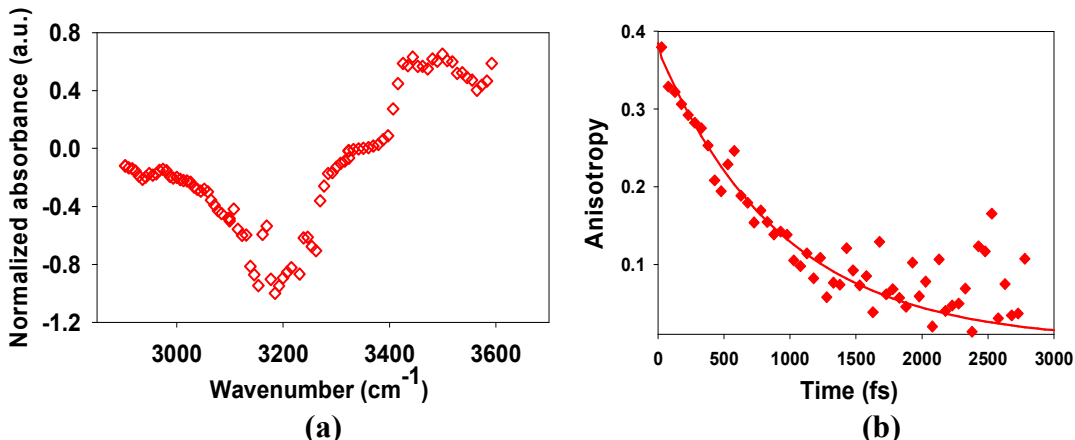
Figure 2: (a) Trends of the pre-exponential factor of the 350 fs contribution for a pump at 3000 cm^{-1}. The pump and the probe have parallel polarizations. (b) Evolution of the anisotropy after subtraction of the spectral component corresponding to the thermal and coherent contributions from the absorption changes measured with probe pulses that have parallel and perpendicular polarization with respect to the one of the pump. The pump and probe frequencies are 3000 cm^{-1}. The decay (line) has been fitted with a single exponential (a×exp(-t/τ)+b). The fitted values are: $\tau = 900 \pm 100$ fs, a = 0.38 and b = 0.0.

When pumping/probing at 3000 cm^{-1} (Figure 2b), the anisotropy decay is slow (900 fs) and complete. This time constant is not consistent with the value attributed to orientational dynamics of bulk water molecules ($\tau_{OR} = 2.6$ ps)[10]. In our case, the delocalized excited vibrational states of the OH stretching vibrator induce a proton transfer within the O-H….O system[11] (Reaction 1). Once the proton is transferred to one of the neighboring water molecules, the proton can either hop within the H-bond network or be back-transferred to the surface. The fact that the anisotropy decays to zero can be attributed either to a complete rotational dynamics or to a hopping process exploring all the possible configurations. Since water molecules are attached to the surface, their motions are restricted. Therefore, the anisotropy decay we observe is due to an other mechanism, which is possibly the coupled hopping process of a hydronium ion and a water molecule through Reaction 2. We may note that this implies a locally extended H-bond network.

$$H_3O^+ + H_2O \xrightarrow{H-bond\ network} H_2O + H_3O^+ \quad \text{(Reaction 2)}$$
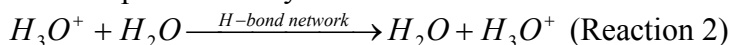
If the accessible H-bond network for the hydrated proton is large enough, the anisotropy will be totally lost after a few jumps. The measured decay time for the anisotropy at 3000 cm^{-1} (900 fs) might thus be attributed to the hopping time for the proton transfer. This time is consistent with recent studies on proton transfer in water[12] which support the idea of a proton jump within the picosecond time range.

[9] P.A. Giguère, S. Turrell, Can. J. Chem., **1976**, 54, 3477-3482

[10] Y.L.A. Rezus, H.J. Bakker, J. Chem. Phys., **2005**, 123, 114502

[11] H.J. Bakker, H.-K. Nienhuys, Science, **2002**, 297, 587-590

[12] W. Amir, G. Gallot, F. Hache, S. Bratos, J.-C. Leicknam, R. Vuilleumier, J. Chem. Phys., **2007**, 126, 034511

Femtosecond (Stimulated Raman) Spectroscopy of the

Photo-Tautomerisation of Nitrotoluene

S. Laimgruber[1], S. Berner[1], B. Heinz[1], T. Schmierer[1], P. Gilch[1]

[1]Department für Physik, Ludwig-Maximilians-Universität München, Oettingenstr. 67, D-80538 München, Germany, e-Mail: peter.gilch@physik.uni-muenchen.de, URL: http://www.imo.physik.uni-muenchen.de/~gilch/

Nitroarenes with a substituent located *ortho* to the nitro group are often photo-reactive. In the course of the photo-reaction the nitro group is reduced to a nitroso function and the substituent is oxidized. If the substituent carries a leaving group *L* this will be released (Figure 1). This photo-induced release opens the route for some applications of these compounds.
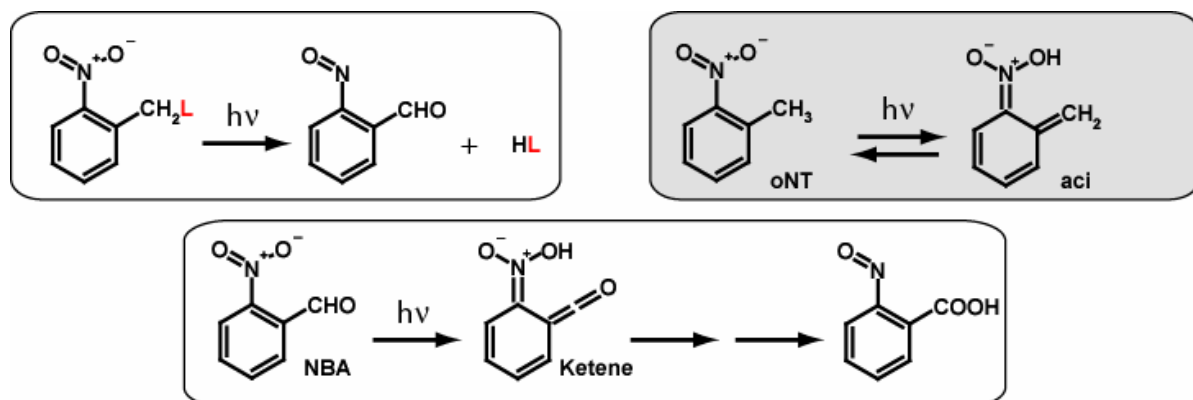
Figure 1 Molecular structures and photo-reactions relevant in the present study.

While bound to the nitroarene a functional moiety of the group *L* (for instance a hydroxy function) is protected and that moiety will only become reactive upon illumination. This behavior is refered to as photo-labile protection and is employed in caged compound experiments[1] and the in-situ synthesis of DNA chips[2]. We are currently seeking for a deeper understanding of these photo-reactions by means of femtosecond (vibrational) spectroscopy. Since reactive nitroarenes feature a hydrogen atom on the *ortho*-substituent it has been postulated that the primary photochemical process is a hydrogen transfer to the nitro group. For *ortho*-nitrobenzaldehyde (NBA) this transfer should result in a ketene intermediate (see Figure). By means of femtosecond IR spectroscopy we have observed the rise of this intermediate in ~ 400 fs and thereby have given evidence for the ultrafast nature of the hydrogen transfer[3].

   In this study we address the hydrogen transfer in a related compound, *ortho*-nitrotoluene (oNT). As first observed by Wettermark in the 1960s[4] photo-illuminated oNT forms a photo-tautomer (aci-nitro form, see Figure 1), which persists for milliseconds to seconds (depending on the solvent). Since oNT is structurally closely related to nitroarenes employed in photo-labile protection it is an ideal model compound to study their photo-reactivity. Previous experiments yielded seemingly contradictive results. Picosecond pump-probe experiments by Yip et al.[5] gave indications for the hydrogen transfer to occur on the 100 ps time scale via a triplet state. Experiments with a higher time resolution by Schwörer and Wirz[6] implied a transfer time of < 10 ps involving the singlet excited state. Further, with

[1] J.A. McCray, D.R. Trentham, Annu. Rev. Biophys. Biophys. Chem. **1989,** 18, 239
[2] X. Gao, E. Gulari, X. Zhou, Biopolymers **2004**, 73, 579
[3] S. Laimgruber et al., Angew. Chem. Int. Ed. **2005,** 44, 7901
[4] G. Wettermark, J. Phys. Chem. **1962,** 66, 2560
[5] R.W. Yip et al., J. Phys. Chem. **1984**, 88, 5770
[6] M. Schwörer, J. Wirz, Hel. Chim. Acta **2001**, 84, 1441

an elaborate H/D exchange experiment these authors determined the quantum yield of the transfer to be as small 0.1 – 1%. In contrast to that, the quantum yields of nitroarenes employed in photo-labile protection are of the order of 10%[7]. Here, we will present and discuss femtosecond transient absorption and stimulated Raman (FSRS) data that might resolve these discrepancies.

The aci-nitro form resulting from the hydrogen transfer is commonly identified via its absorption spectrum peaking around 400 nm[4]. When exciting a solution of oNT in THF with 260 nm femtosecond laser pulses this characteristic feature is seen in the transient absorption spectrum at a delay time of 2 ns. A comparison of the amplitude of this spectrum with that of the ketene intermediate in the NBA photoreaction allows to estimate the quantum yield of the aci nitro formation. The reasoning for this is as follows. The electronic structures of the ketene and the aci nitro intermediate are very similar and so we assume identical extinction coefficients. The ketene is known to transform quantitatively into the final photo-product[3] which is formed with a yield of ~ 50%[8]. Therefore, the quantum yield of the ketene has to be ~ 50%. Based on the relative amplitude (aci nitro versus ketene) of 1:2 we arrive at a quantum yield of ~ 25 % for the formation of the aci-nitro form – very much larger than the values reported before. An explanation could be that the spectroscopic species observed after 2 ns is not identical with species detected via the H/D exchange by Schwörer and Wirz[6]. To confirm that we recorded a transient absorption spectrum at a delay time of 1 ms (Figure 2).
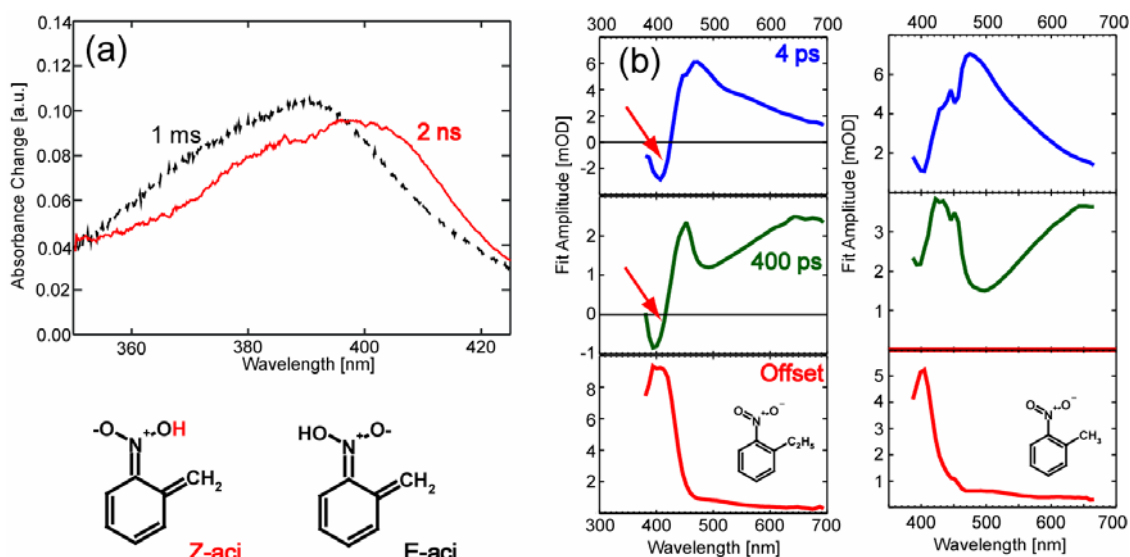
Figure 2 Transient absorption data of oNT and oENB in THF after 260 nm femtosecond excitation. (a) Transient spectra at delay times indicated. Possible assignments of the spectra are given. (b) Decay associated spectra for the kinetic components indicated. The arrows mark the formation of the aci nitro form.

Indeed, the 2 ns (λ_{max}= 400 nm) and 1 ms (λ_{max}= 390 nm) spectra are similar but clearly not identical. Based on TD-DFT calculations the 2 ns spectrum can be assigned to the *Z* isomer of the aci nitro form and the 2 ms spectrum to the *E* isomer. The H/D exchange experiments determine the yield of the *E* isomer which is apparently much lower than that of the *Z* isomer. Transient absorption data for delay times smaller than 2 ns deliver information on the formation of the *Z* aci nitro form. Global analysis of this data set delivers three constants of 0.2 ps, 4 ps, and 400 ps as well as an offset. The spectra associated with these constants (Figure 2b, right) deliver information on the processes underlying these kinetic components. The offset spectrum is simply that of the *Z* aci nitro from. The lifetime of the 400 ps component and the spectral characteristics associated with it match those of the triplet state of

[7] A.P. Pelliccioli, J. Wirz, Photochem. Photobiol. Sci. **2002**, 1, 441
[8] M.V. George, J.C. Scaiano, J. Phys. Chem. **1980,** 84, 492

nitrobenzenes[5]. Accordingly, the 0.2 ps and the 4 ps components are tentatively assigned to the decay of the excited singlet state and the population of the triplet state. The data for oNT do not show a direct indication for the aci-nitro formation. Yet, for the closely related compound *ortho*-ethylnitrobenzene (oENB) such an indication is observed. oENB has a higher aci-nitro yield[5] and therefore its formation shows up in the decay associated spectra (Figure 2b left). The time constants for oENB are nearly identical to those of oNT. Yet, in the 4 ps and 400 ps spectra a negative peak centered at 400 nm shows up. In this representation a negative peak stands for the rise of a spectroscopic species. This implies that for oENB the aci-nitro from is formed in a bi-phasic fashion involving singlet and triplet states. For oNT the negative peaks are reduced to dips at the same wavelength since the quantum yield is lower. Still, the spectra lend to the interpretation that also here singlet and triplet states contribute to the aci nitro formation. The postulated structure of the aci-nitro form finds strong support from first femtosecond stimulated Raman spectroscopy (FSRS) experiments[9] (Figure 3).
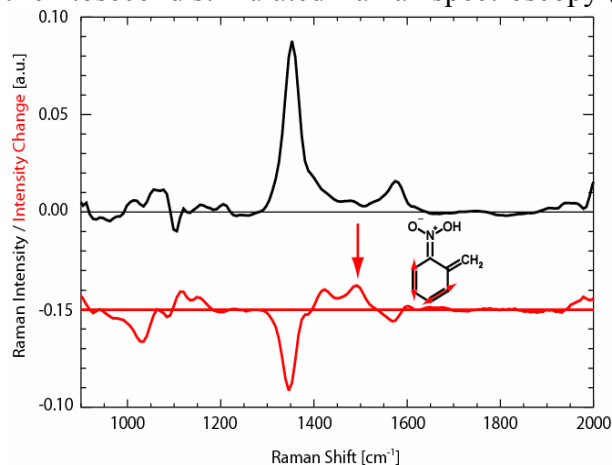
Figure 3 FSRS data of oNT in deuterated acetonitrile. The upper graph shows the stationary spectrum of oNT which is dominated by the symmetric ($\sim$ 1300 cm^{-1}) and anti-symmetric stretch ($\sim$ 1600 cm^{-1}) vibration of the nitro-group. The difference spectrum after 1 ns (lower graph) features bleaches at these frequencies and positive bands indicative for the photo-product. A strong resonance at 1500 cm^{-1} can clearly be assigned to the indicated vibration.

Based on these spectroscopic findings we suggest the model shown below for the photo-tautomerisation of oNT (Figure 4).
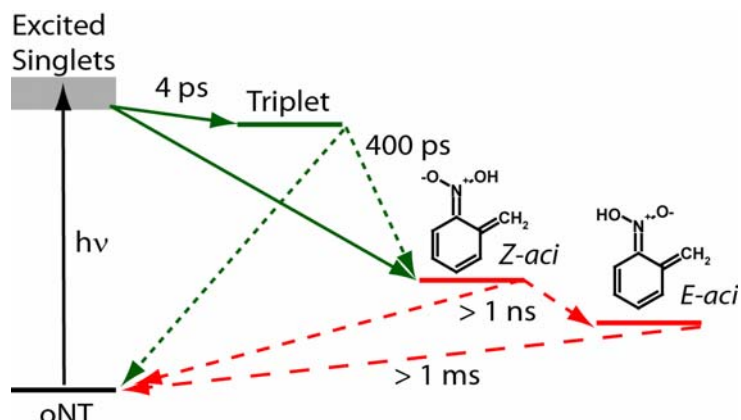
Figure 4 Kinetic scheme incorporating the spectroscopic findings of this study.

After UV excitation to an upper singlet state an ultrafast transitions to a lower excited singlet state occurs. The 4 ps decay of this state goes along with a branching. Either a triplet state is populated or directly the *Z*-aci form. During the 400 ps decay of the triplet state partially the oNT ground state is reformed and partially further *Z* aci molecules. Because of the proximity of the hydrogen atom on the nitro group to the CH$_2$ group, *Z* aci is prone to re-tautomerisation to oNT and the *E* isomer is formed in low yield on a time scale of > 1 ns.

[9] S. Laimgruber et al. Appl. Phys. B. **2006,** 85**,** 557-564

Picosecond Stokes- and anti-Stokes Raman spectroscopy of the excited state intramolecular proton transfer

V. Kozich[1], J. Dreyer[1], A. Vodchits[2] and W. Werncke[1]

[1]Max-Born-Institut, Max-Born-Strasse 2A, D-12489 Berlin, Germany. [2]B.I. Stepanov Institute of Physics, Minsk 220072, Belarus. E-mail: kozich@mbi-berlin.de

Vibrational populations after excited state intramolecular proton transfer (ESIPT) in 2-(2'-hydroxyphenyl)benzoxazole (HBO) have been investigated using transient Raman spectroscopy[1]. After electronic photoexcitation of the enol tautomer of HBO with a C–O-H↑N hydrogen bond, the keto tautomer with a C=O↑H-N hydrogen bond is formed in the first excited singlet state S_1.

Using resonance probe within the S_1-S_N absorption band, we measured time-resolved Stokes and anti-Stokes Raman spectra of this species for the first time. The Fig.1 shows the resonance Raman spectrum of the transient (upper panel) which was recorded by probing at 395 nm, 5 ps after excitation of a solution of HBO (5×10^{-3} mol/l in cyclohexane) with a pulse centered at 336 nm. The ultrashort rise time of the transient Stokes Raman line-intensities and a decay time of about 200 ps confirm their assignment to the S_1-keto tautomer. In the insert, an anti-Stokes spectrum of the transient recorded 2 ps after UV-excitation with a 402 nm probe pulse is shown. The lower panel displays a stationary Stokes Raman spectrum of the stable enol tautomer of HBO. The

Fig.1. Stokes resonance Raman spectra of keto and enol tautomers of HBO. *In the inset* − anti-Stokes Raman spectrum at 2 ps pump-probe delay.

observed vibrational modes were assigned with the help of normal mode calculations both for the S_0-enol and S_1-keto tautomers. Based on CIS/6-31 G(d,p) calculations the two most intense high-frequency Raman lines of the S_1-keto tautomer are assigned to delocalized vibrations with substantial CO-stretching or NH-bending components. Experimentally, these vibrations do not show any frequency shifts upon deuteration. In the frequency range between 1450 and 1700 cm^{-1} only two modes with very small isotopic frequency shifts (< 4 cm^{-1}) are calculated, whereas the isotopic shifts of the other modes in this range exceed ten wavenumbers. The latter should be easily detectable by our experiment.

We measured the kinetics of the Stokes resonance Raman line at 535, the doublets 832/871 cm^{-1} and 1564/1596 cm^{-1}. The intensities of all Raman bands show short rise times limited by our time resolution and a decay time of about 200 ps. We note that the observation of rise and decay times of the S_1-keto Raman bands in agreement with the corresponding times of the transient absorption bands implies that the influence of vibrational excitation on the Stokes resonance intensities due to the time-dependent resonance Raman line shape function can be neglected. This is probably because of the rather low (~2500 cm^{-1}) excess energy after ESIPT. This contrasts the significant influence which was observed for an about tenfold higher excess energy as discussed in Refs. 2 and 3.

In Fig. 2 we plot the anti-Stokes resonance Raman intensities of the Raman lines at 832/871, 610 and 535 cm^{-1} versus delay time. Because of the low signal to noise ratio we did not attempt to deconvolute the single line intensities from the doublet. The presented kinetics reveal excess populations of the observed modes at early times after excitation. In contrast, the high-frequency vibrations at 1596 and 1564 cm^{-1} representing the strongest peaks in the Stokes resonance Raman spectrum do not show excess population at any delay time. A fraction as low as about 0.02 of their Stokes Raman intensity corresponds to our detection limit on the anti-Stokes side of the spectrum. One should note that we carried out these experiments also for a probe wavelength of 420 nm to compensate for possible differences between Stokes and anti-Stokes Raman excitation profiles. The lack of anti-Stokes Raman signals from the high-frequency vibrations means that populations of their excited vibrational levels are always very low after ESIPT. Even, if we assume that these high-frequency vibrations loose their energy faster than our time resolution (e.g. with a population decay time of 500 fs) such scenario would still result in large anti-Stokes resonance Raman signals.

The measured excess populations have fast rise times close to our time-resolution and decay times of about 8 ps for the 535 cm^{-1} and 610 cm^{-1} vibrations and 5 ps for the 832/871 cm^{-1} doublet.

Fig.2. Time-dependent anti-Stokes resonance Raman intensities of the Raman bands at 832/871 cm^{-1}, 610 cm^{-1} and 535 cm^{-1} of the S$_1$-keto tautomer of HBO.

A comparison of the estimated maximum possible vibrational temperature T_{MAX} =425 K, which can be reached after distribution of the excess energy between all vibrational modes with the measured anti-Stokes to Stokes Raman intensity ratios shows that the S$_1$-keto tautomer is close to thermal equilibrium with a temperature about T_{MAX} already 2 ps after proton transfer. This means that the main processes of intramolecular vibrational redistribution proceed on even shorter times. Afterward it is cooled with a $(\approx 8 \text{ ps})^{-1}$ vibrational temperature decay rate.

In conclusion, we have observed time-dependent Stokes and anti-Stokes resonance Raman spectra after ultrafast ESIPT in HBO. Based on CIS/6-31 G(d,p) calculations the two most intense resonance Raman lines of the S$_1$-keto tautomer are assigned to delocalized vibrations with substantial ν(CO) and δ(NH) components. It is shown that these high-frequency modes are not directly vibrationally excited by the proton transfer reaction. About 2 ps after ESIPT the S$_1$-keto tautomers are already near to intramolecular thermal equilibrium and they cool down within about 8 ps.

[1] V. Kozich, J. Dreyer, A. Vodchits, W. Werncke, Chem. Phys. Lett., **2005**, 415, 121-125
[2] V. Kozich, J. Dreyer and W. Werncke, Chem. Phys. Lett., **2004,** 399, 484-489.
[3] V. Kozich and W. Werncke, J. Mol. Struct., **2005**, 735-736,145-151.

Methyl groups and vibrational energy relaxation of *para* - nitroaniline

M. Cather Simpson[1,2], J. Reddy Challa[2], Tissa C. Gunaratne[3]

[1] Departments of Chemistry & Physics, University of Auckland, Auckland New Zealand. [2] Center for Chemical Dynamics, Department of Chemistry, Case Western Reserve University, Cleveland, Ohio, 44106-7078, USA. [3] Department of Chemistry, Michigan State University, East Lansing, Michigan. c.simpson@auckland.ac.nz

Para-nitroaniline (PNA) belongs to the important push-pull class of molecules, characterized by an electron donating group connected via a conjugated linker to an electron withdrawing group. The large dipolar change that accompanies charge-transfer (CT) electronic excitation makes these promising nonlinear optical materials. The electronic and vibrational dynamics of PNA have been studied by several groups, most recently using UV–visible transient absorption[1-4], fs transient grating[5], and time-resolved anti-Stokes Raman[6-10] and IR[10]. These studies establish ultrafast nonradiative decay as the main relaxation pathway following CT excitation of PNA in polar solvents. In such cases, a large excess of vibrational energy is deposited in the ground state and must redistribute intra- and intermolecularly as the system returns to thermal equilibrium at room temperature. Previous single color, sub-ps anti-Stokes resonance Raman studies in our group at several pump wavelengths previously indicated that PNA S_1 dynamics are very fast relative to the intersystem crossing rate and found no evidence for inhomogeneous broadening of the CT absorption band[9]. In the current study, the impact of structural factors on vibrational dynamics has been explored by incorporating methyl groups at various positions on the pNA template. The vibrational excitation patterns and lifetimes of PNA, 2-methyl PNA (MPNA), 2, 6–dimethyl PNA (DMPNA) and N, N – dimethyl PNA (NNDMPNA) have been compared. Findings are interpreted in terms of access of the excited PNA system to dissipative pathways, in which consideration is given to the effectiveness of an individual substitutent, the number of substituents, and the pattern of substitution.

Methyl Groups and the Static Raman Spectra. Static Raman vibrational features are largely insensitive to N-methyl substitution; small shifts in the 600 – 1700 cm^{-1} region are seen in NNDMPNA. In contrast, direct methylation of the phenyl ring introduces more significant changes in the Raman spectrum. The ν_{19} vibration (860 cm^{-1} in PNA) is observed at 934 and 947 cm^{-1} in 2-MPNA and DMPNA, respectively. Two additional peaks appear at 771 and 815 cm^{-1} for MPNA and at 736 and 808 cm^{-1} for DMPNA. The symmetric NO_2 stretch (1310 cm^{-1} in PNA) has a low frequency shoulder in both MPNA and DMPNA.

Methyl Groups and Ground State Vibrational Dynamics. One-color time-resolved anti-Stokes resonance Raman spectra (TRARRS) were measured after UV/Vis excitation of the PNA derivative to the CT state. Since the lifetime of this state is sub-picosecond, these spectra reflect the vibrational dynamics of the excess vibrational energy deposited in the ground electronic state.

Figure 1 shows representative TRARRS spectra of the NNDMPNA in DMSO. The spectra reveal two strong vibrational bands at ~1300 and 850 cm^{-1}, and a weaker peak at ~1490 cm^{-1}. The integrated areas of these peaks grow and decay as Δt increases, and return to a flat
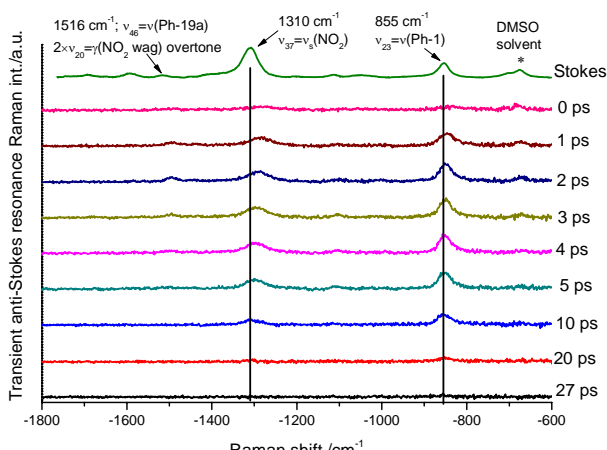
Figure 1. TRARRS of NNDMPNA in DMSO at 403.5 nm. Spectra are shown as the difference: {(pump + probe) – [(pump only) + (probe only)]} as described in the text.

transient by featureless transient by 30 ps. The transient vibrational peaks are initially quite broad and red-shifted relative to their room temperature, static values. As the intensities change, the bands spectrally narrow and blue-shift back to their static values as well. The transient peaks were fit with Lorentzian line shapes using non-linear least square fitting, where the S:N allowed. Kinetic traces were obtained by plotting the integrated intensity (Figure 2 (a)) or average peak intensity (Figure 2 (b)). The shift in the peak position as a function of Δt (Figure 2(c) & (d)) was evaluated as well. Analogous TRARRS studies of MPNA and DMPNA were also performed.

Analysis of the dynamics of NNDMPNA TRARRS data is presented in Figure 2. The phenyl breathing mode (ν_{23}) decays significantly slower than the symmetric NO_2 stretch (ν_{37}), though the modes exhibit a similar rise time of ~ 1.5 ps. The peak position and intensity evolve with indistinguishable kinetics for ν_{37} (~ 5.8 ps). In contrast, the intensity relaxes more slowly (10 ps) than the peak position (0.3 & 3 ps) for ν_{23}. The results for the full analysis of the NNDMPNA, and the other species, are summarized in Table 1 along with the lifetimes of PNA in DMSO from our previous work[9].

Figure 2 TRARRS kinetic analysis of NNDMPNA in DMSO. Symbols: Experimental data; Lines: Exponential fits at positive time delay. (A) integrated intensity, (B) average peak intensity, (C) and (D) peak positions.

The methyl groups exert minimal impact upon the electronic dynamics in this system. However, they clearly have a significant effect upon the vibrational dynamics of the central PNA unit. The data indicate that the NO_2 wagging overtone (~1495 cm^{-1}) acts as the coupling and primary accepting mode during internal conversion of all the four compounds. N-methyl substitution increases vibrational cooling lifetimes, possibly due to reduced H-bonding. The phenyl ring methyl groups have more dramatic impact upon pattern of vibrational energy deposition; two low frequency phenyl ring vibrational modes are observed in the TRARRS spectra of DMPNA and MPNA, but not observed in PNA or NNDMPNA. Finally, for a given mode, the decay of the TRARRS intensity can occur on a different time scale than the evolution of the vibrational frequency. We assign the intensity decay to population dynamics and the peak position dynamics to off-diagonal anharmonic coupling to populated low frequency phenyl ring vibrations. This latter coupling decays more rapidly than the population in the high frequency modes studied here.

Experimental Methods. Time resolved resonance Raman spectra were obtained in a single-color, pump-probe configuration as previously described in detail[9,11]. Briefly, the 800 nm output of a regeneratively amplified Ti:Sapphire laser system (Clark-MXR; NJA-5, CPA-1000) is frequency doubled in a long (15 mm or 30 mm) KDP crystal. The output is spectrally narrowed: ~400 nm, 1 kHz, 500-800 fs, 17-25 cm^{-1}. A beam splitter is used to create pump and probe beams. The time delay Δt is set with a motorized translation stage.

Pump-only, probe-only, and pump-probe spectra were collected, dispersed, and detected with a CCD. The time-resolve spectra are reported as {(pump + probe) − [(pump only) + (probe only)]}. Exponential analysis was performed with Origin[TM] software.

Table 1. Impact of Methyl Groups upon PNA Vibrational Dynamics.

Vibration	PNA[a]		NNDMPNA		MPNA		DMPNA	
	v/cm^{-1}	τ/ps	v/cm^{-1}	τ/ps	v/cm^{-1}	τ/ps	v/cm^{-1}	τ/ps
Peak Intensity								
Sym NO_2 stretch	1310	5.1±0.6	1310	6.1±0.3	1310	9.3±0.6	1307	5.7±0.5
Phenyl breathing Ph-1	860	8.1±0.6	855	10.2±0.4	934	8.8±1.6	947	9.2±0.7
NO_2 wagging overtone	1512	fast, weak	1516	4.2±0.2	1507	fast,weak	1492	2.9±0.3
Unassigned Phenyl ring vibration	-	-	-	-	815	8.9±0.9	808	8.2±1.4
Unassigned Phenyl ring vibration	-	-	-	-	768	9.5±2.6	743	weak
Peak Position								
Sym NO_2 stretch	1310	4.6±0.7	1310	5.6±0.4	1310	2.9±0.4	1307	0.3±0.1 3.6±0.5
Phenyl breathing Ph-1	860	3.2±0.5	855	0.3±0.1 3.2±0.6	934	-	947	-

[a]Lifetimes of PNA obtained from Gunaratne et al. *ChemPhysChem* **2005**, 6, 1157-63.

[1]C.L. Thomsen, J. Thogersen, S.R. Keiding, J. Phys. Chem. A, **1998,** 102, 1062-7.

[2]S.A. Kovalenko, R.Schanz, V.M. Farztdinov, H.Hennig, N.P. Ernsting, Chem.Phys.Lett., **2000** 323, 312-22.

[3]S.A. Kovalenko, R. Schanz, H. Hennig, N.P. Ernsting, J. Chem. Phys., **2001**, 115, 3256-73.

[4]V.M. Farztdinov, R. Schanz, S.A. Kovalenko, N.P Ernsting, J. Phys. Chem. A, **2000**, 104, 11486-96.

[5]Y. Kimura, M. Fukuda, O. Kajimoto, M. Terazima, J. Chem. Phys., **2006**, 125, 194516/1-12.

[6]V. Kozich, W. Werncke, J. Dreyer, K.W. Brzezinka, M. Rini, A. Kummrow, T.Elaesser, J. Chem. Phys., **2002**, 117, 719-26.

[7]V. Kozich, W. Werncke, A.I. Vodchits, J. Dreyer, J. Chem. Phys., **2003**, 118, 1808-14.

[8]Q. An, P. Gilch, Chem. Phys. Lett., **2002**, 363, 397-403.

[9]T. Gunaratne, J.R. Challa, M.C. Simpson, ChemPhysChem, **2005**, 6, 1157-63.

[10]T. Schrader, A.Sieg, F. Koller, W. Schreier, Q. An, W. Zinth, P. Gilch, Chem. Phys. Lett., **2004**, 392, 358-64.

[11]J.R. Challa, T. Gunaratne, M.C. Simpson, J. Phys. Chem. B. **2006**, 100, 19956-19965.

The photo-induced decomposition of aryl peroxycarbonates studied by time-resolved infrared spectroscopy

Christian Reichardt[1], Jörg Schroeder[1,2], and Dirk Schwarzer[1,]*

Abteilung Spektroskopie und Photochemische Kinetik, Max-Planck-Institut für Biophysikalische Chemie, Am Fassberg 11, D-37077 Göttingen. [2]Institut für Physikalische Chemie, Universität Göttingen, Tammannstraße 6, 37077 Göttingen. *dschwar@gwdg.de, http://www.mpibpc.gwdg.de/english/research/ags/schwarzer/index.html.

The decomposition mechanism of organic peroxyesters has attracted considerable interest because of their importance as initiators in free radical polymerization. For the photo-induced fragmentation two modes of bond scission are discussed in the literature[1], namely a sequential process (see Fig. 1) where the peroxide bond O–O breaks almost instantaneously (<100 fs) followed by decarboxylation of the carbonyloxy intermediate to yield CO_2 plus radicals R1• and •O-R2, and simultaneous breakage of O–O and R1–C bonds. To elucidate the dissociation mechanism we studied *tert*-butyl-2-naphthylperoxycarbonate (TBNC) and *tert*-butyl-phenylperoxycarbonate (TBPC) using UV excitation at 266 nm and mid-IR laser pulses to monitor the temporal evolution of vibrational marker bands with 100 fs time resolution.

In Fig. 2 the linear IR spectrum (a) of TBNC is compared with its transient absorption spectrum (b) measured 1.3 ns after UV excitation. Four prominent negative peaks (●) indicate photobleaching of TBNC. Additional positive bands appearing in the spectrum are due to the ν_3 asymmetric stretch vibration of newly formed CO_2 at 2336 cm^{-1} (○) and the 2-naphthyloxy
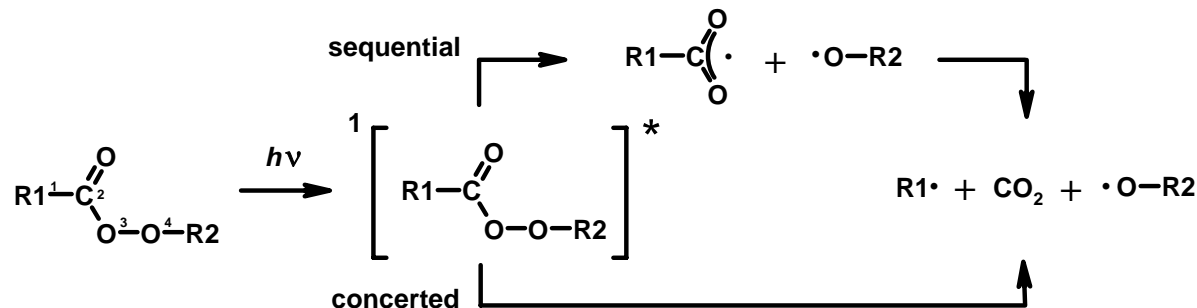
Figure 1. Sequential and concerted fragmentation path of peroxyesters (R2 = *tert*-butyl; R1 = 2-naphthyloxy (TBNC), phenyloxy (TBPC)).
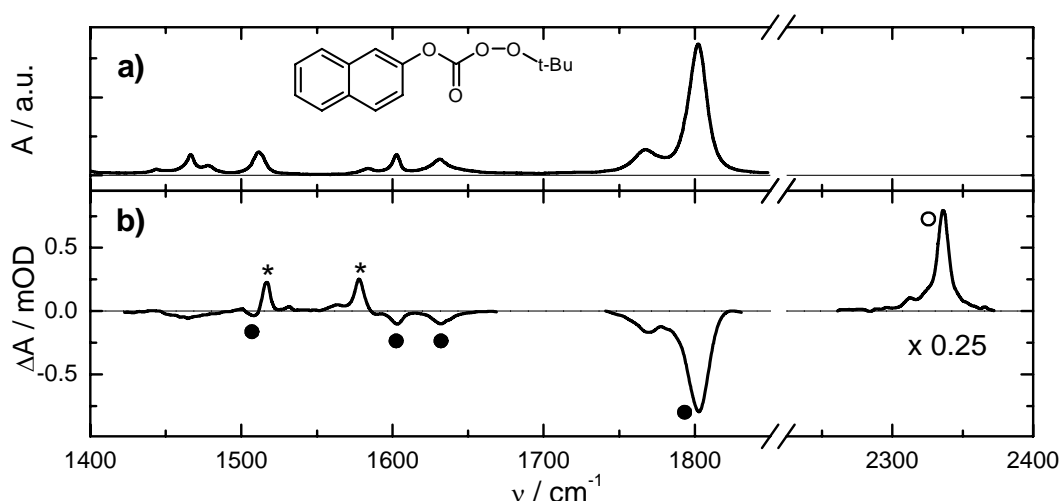
Figure 2. (a) linear absorption spectrum of TBNC in CD$_3$CN; (b) transient spectrum 1.3 ns after 267 nm excitation in CD$_3$CN (the 2220-2370 cm^{-1} range was recorded in CCl$_4$).

[1] M. Buback, M. Kling, S. Schmatz, and J. Schroeder, *Phys.Chem.Chem.Phys* **2004**, 6, 5441-5455.

radical (R1• in Fig. 1) at 1518 and 1577 cm^{-1}(*). According to DFT UB3LYP calculations we attribute the radical bands to CO stretch (calculated 1532 cm^{-1}) and CC ring stretch (calculated 1624 cm^{-1}) vibrations, respectively.

In Figs. 3-5 the spectral and temporal evolution of selected transient bands of Fig. 2 are presented. Immediately upon UV excitation the CO stretching band of TBNC in the electronic ground state and the lowest excited singlet state S_1 appear as bleach and absorption, respectively. With increasing pump-probe delay the excited state decays and, as photoproducts are formed, only ground state bleach finally remains. From the decay of the integrated band intensity the S_1 life time of (25 ± 2) ps is obtained by exponential fitting. Up to 1.5 ns no repopulation of the ground state can be observed. In addition, in the frequency window accessed there is no transient absorption that could be assigned to the CO band in other excited electronic states. Therefore, one may conclude that the quantum yield of photofragmentation has to be close to unity.
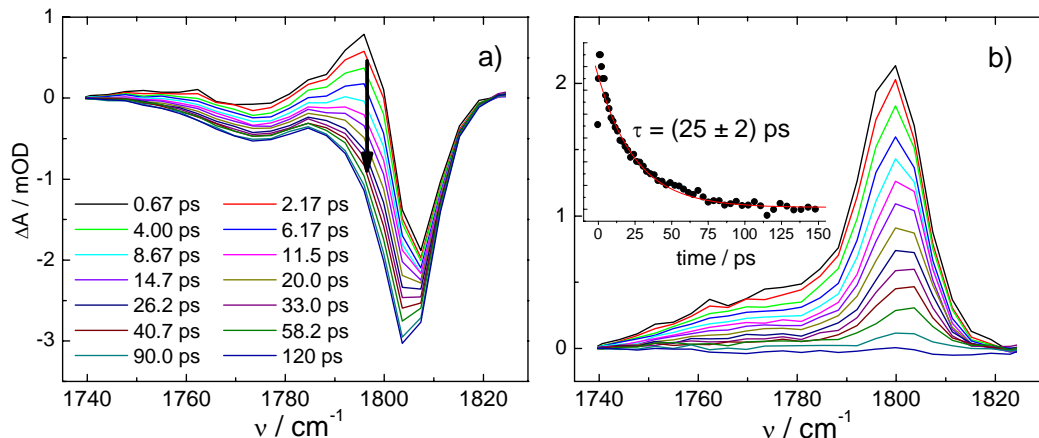
Figure 3. (a) Transient spectra of the CO stretch absorption band of TBNC in CCl$_4$ recorded at selected pump-probe delays; (b) evolution of the excited state CO stretching band derived from the difference between the transients of a) and the spectrum at 150 ps pump-probe delay; the insert shows the integrated band intensity.
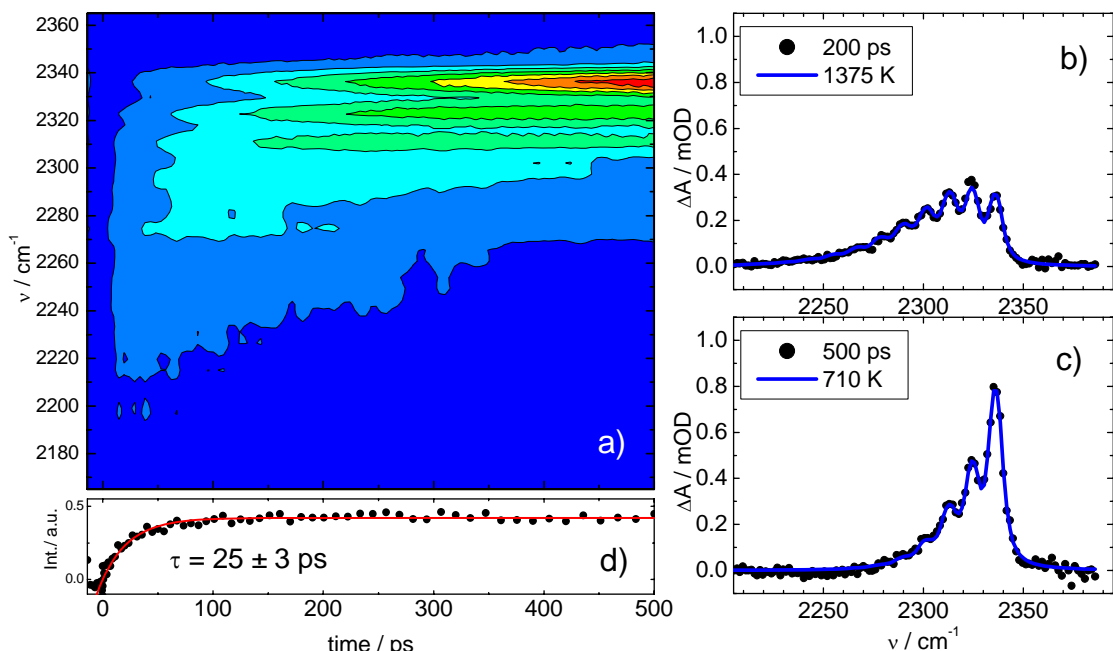
Figure 4. (a) Spectral evolution of the ν_3 absorption band of CO$_2$ produced in the photodissociation of TBNC in CCl$_4$; (b)-(c) individual spectra measured at selected pump-probe delays (blue lines are simulated thermal spectra); (d) integrated band intensity.

Fig. 4 shows the formation of CO monitored at the asymmetric stretch absorption band after photoexcitation of TBNC in CCl_4. The contour diagram demonstrates that the early spectrum is broad and red-shifted with respect to the band origin at 2336 cm^{-1}. With time the spectrum narrows and simultaneously more intensity is accumulated at 2336 cm^{-1}. This behaviour can be attributed to the formation of vibrationally hot CO_2 cooling down by energy transfer to the surrounding medium[2]. The excess energy originates from the energy release associated with the structural relaxation of the bent OCO moiety in TBNC to form the linear CO_2 molecule. The progression seen in the individual spectra at selected pump-probe delays (Fig. 4b and c) arises mainly from anharmonic coupling of the asymmetric stretching to the bending vibration and represents a direct image of the bend population in the individual quantum states. Assuming Boltzmann distributed populations within the normal modes of CO_2 the spectra are characterized by a single parameter namely the temperature. The analysis shows[3] that the fragmentation of both TBNC and TBPC leads to CO_2 with an excess energy of about 5000 cm^{-1}. The energy transfer times are 200 ps in CCl_4 and 110 ps in n-heptane. The temporal evolution of the CO_2 concentration is derived by evaluating the integral absorbance of the band as shown in Fig. 4d. Exponential fitting gives a characteristic time of CO_2 formation of (25 ± 3) ps.

Fig. 5 shows the formation of the naphthyloxy radical after UV excitation of TBNC in CD_2Cl_2. At early times a weak bleaching arises from the superposition of ground state bleach and excited state absorption of TBNC. Subsequently, an absorption peak at 1519 cm^{-1} with a satellite at 1526 cm^{-1} emerges on a timescale of (26 ± 3) ps.

Our experiments clearly demonstrate that for the TBNC photodissociation the time constants of S_1 decay and of CO_2 and 2-naphthyloxy radical formation are identical, which leads to the conclusion that the fragmentation rate is limited by the S_1 lifetime of the peroxyester. For TBPC the situation is the same, the only difference being that the S_1 lifetime is (6 ± 1) ps in CD_2Cl_2 and CD_3CN. From the point of view of photochemical kinetics our results favour the concerted mechanism as a carbonyloxy intermediate R1-C(O)O would be extremely short lived. However, we cannot rule out an ultrafast sequence of bond scissions, in which the O–O bond is broken first, followed by R1–C bond cleavage at an order of magnitude faster rate.
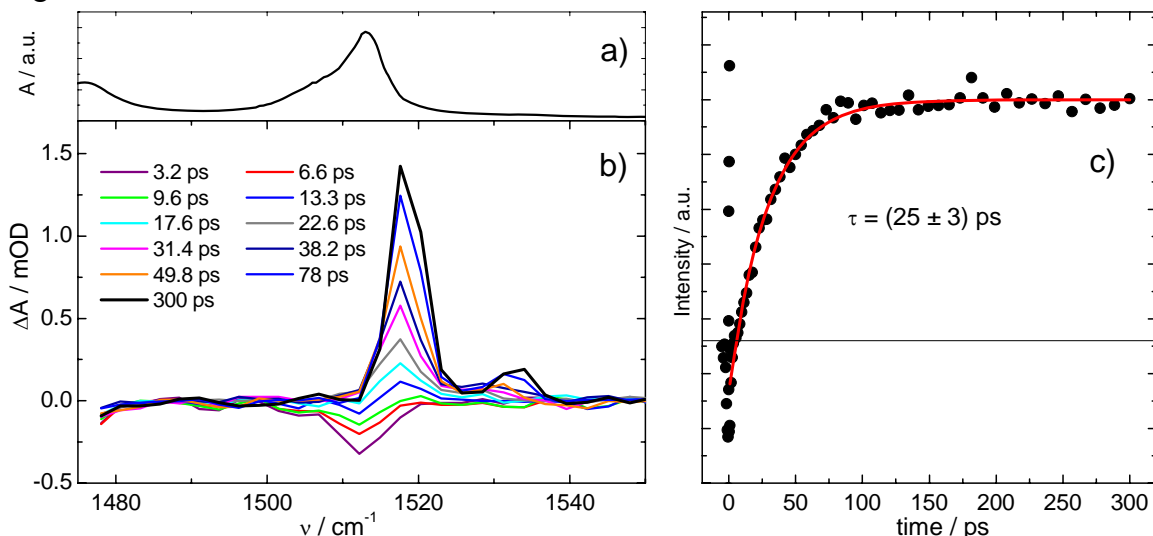
Figure 5. Formation of the 2-naphthyloxy radical after photodissociation of TBNC in CD_2Cl_2; (a) linear absorption spectrum of TBNC in CD_2Cl_2; (b) the emerging strong absorption band is attributed to the CO stretch vibration of the radical; (c) integrated band intensity vs. time.

[2] M. Buback, M. Kling, M. T. Seidel, F. D. Schott, J. Schroeder, U. Steegmüller, *Z.Phys.Chem.* **2001**, *215*, 717.
[3] C. Reichardt, J. Schroeder, and D. Schwarzer, *J. Phys. Chem. A*, submitted.

Ion-Molecule reactions in XB-NH3 clusters: Determining reactant geometries using Franck-Condon simulations

Igor Pugliesi*, Nicola M. Tonge and Martin C. R. Cockett

York Centre for Laser Spectroscopy, Department of Chemistry, The University of York, Heslington, York, YO10 5DD, UK
* New affiliation: Institut für BioMolekulare Optik, Ludwig Maximilians Universität, Oettingenstrasse 67, 80538, München, Germany

1. Introduction

Clusters between aromatic systems and key reagents such as ammonia are ideal systems to study ion-molecule reactions as the cold conditions of a molecular beam provide a solvent free environment and allow for state selective preparation of the reagents though interaction with laser radiation[1]. Crucial in this endeavour is the determination of the possible equilibrium structures of the cluster as this corresponds to the arrangement of the reagents prior to reaction.

1.1 Spectroscopic Techniques

Resonance Enhanced Multi Photon Ionisation has been used to characterise the vibrational energy levels of the first singlet excited state of the fluoro- and bromo-benzene-ammonia clusters.

1.2 Ab initio Calculations

Geometry optimisations and numerical vibrational frequency calculations were performed on the neutral ground (S_0) and first electronically excited state (S_1) using the second order resolution of identity approximate coupled cluster with singles and doubles RI-CC2 method implemented in TURBOMOLE 5.8. Basis sets included the doubly polarised triple and quadruple-zeta TZVPP and QZVPP basis sets of Ahlrichs. A coupled cluster wavefunction was chosen as it is very well suited for the description of hydrogen and Van der Waals bonds, and thus an appropriate method in the structural determination of clusters. Furthermore the resolution of the identity approximation greatly increases computational efficiency whilst still delivering 90 % of the electron correlation recovered by the full CC2 wavefunction. It uses a combination of local correlation methods to reduce the size of the configuration expansion, and an approximate representation of products of orbital basis functions as a linear combination of atom-centred auxiliary basis functions.

1.3 Franck-Condon Simulations

REMPI spectra were simulated by performing multidimensional Franck-Condon (FC) calculations, carried out using the recursion relations developed by Doktorov *et al.*[2]. It expresses a given vibronic integral as a linear combination of lower vibrational quantum number integrals requiring only the <0¦0> integral to be calculated explicitly and is exact in the harmonic approximation. Any differences in the standard orientation of the S_0 and S_1 states, are accounted for by the inclusion of a Hougen-Watson axis switching matrix[3] into the standard linear Duschinsky normal coordinate transformation procedure[4].

2. Results

2.1 FB-NH₃
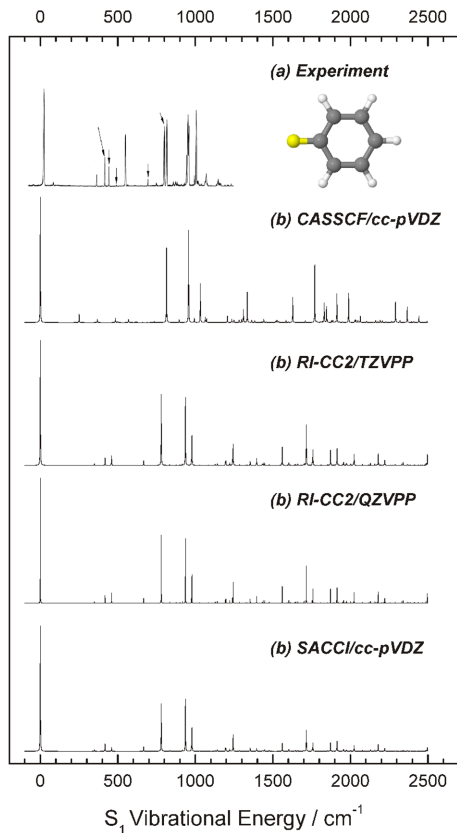
Figure 2.1: *REMPI spectrum and FC Simulations of the S_0-S_1 vibronic transitions for the fluoro-benzene.*
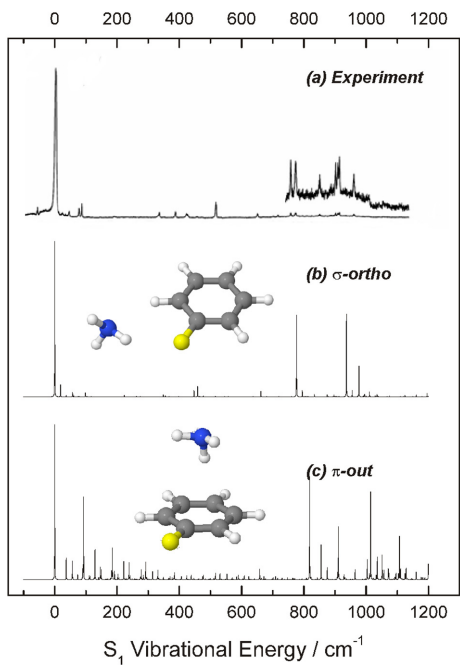
Figure 2.2: *REMPI spectrum and FC Simulations of the S_0-S_1 vibronic transitions for the FB-NH₃.*

Recently, Pugliesi et al. have shown for phenol and phenol-N_2 [5,6] that among the coupled cluster wavefunction family, the SACCI (Symmetry Adapted Cluster Configuration Interaction) method yields S_0-S_1 geometry changes that allow for REMPI spectra simulations very faithful to experiment. A similar situation arises for fluorobenzene (see figure 2.1). However, also the less computer intensive RI-CC2 wavefunction generates geometries and frequencies that yield FC simulations that are very close to the experimental REMPI spectrum. Figure 2.1 also shows that a considerable improvement in the normal mode frequencies is obtained when going from the TZVPP to the QZVPP basis set. This validates the use of FC simulations obtained from RI-CC2/TZVPP or QZVPP geometries in the structural assignment of fluorobenzene-ammonia (FB-NH₃) [7].

MP2 calculations on FB-NH₃ found three stable isomers; σ-ortho, π-out and π-bridge, two of which are shown as insets in figure 2.2. The RI-CC2 calculations matched MP2 in the ground state; for the S_1 state only the σ-ortho and π-bridge structures are stable, while π-out has a negative frequency of 70cm⁻¹ in NH₃ intermolecular torsion mode. While the overall S_0-S_1 geometry change is small for σ-ortho complex, it is considerably larger for the two π isomers. This is a direct consequence of the fact that the S_0-S_1 excitation is a π - π* transition and thus the largest changes in the electron density occur above and below the ring. Therefore, the FC simulations yield spectra with little FC activity in the intermolecular region for the σ-ortho isomer, which allows an unambiguous assignment of the experimental spectrum to this isomer, while for the π-out complex a large progression in the rocking mode is present (see figure 2.2 b). For the π-bridge isomer the S_0-S_1 change was so large as to yield simulations with null spectra.

135

σ-halo

σ-ortho

π-bridge
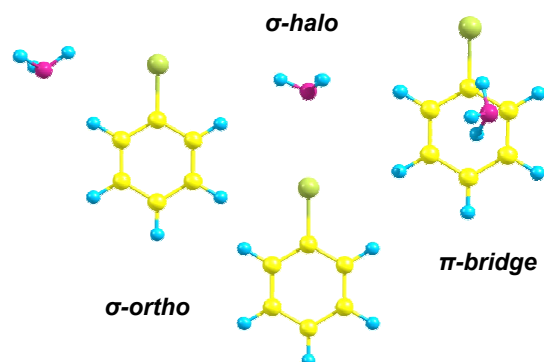
Figure 2.3: *BrB-NH₃ structures predicted by the MP2/aug-cc-pVDZ level of theory*

(a) Aniline

(b) BrB-NH₃

One Photon Energy / cm⁻¹
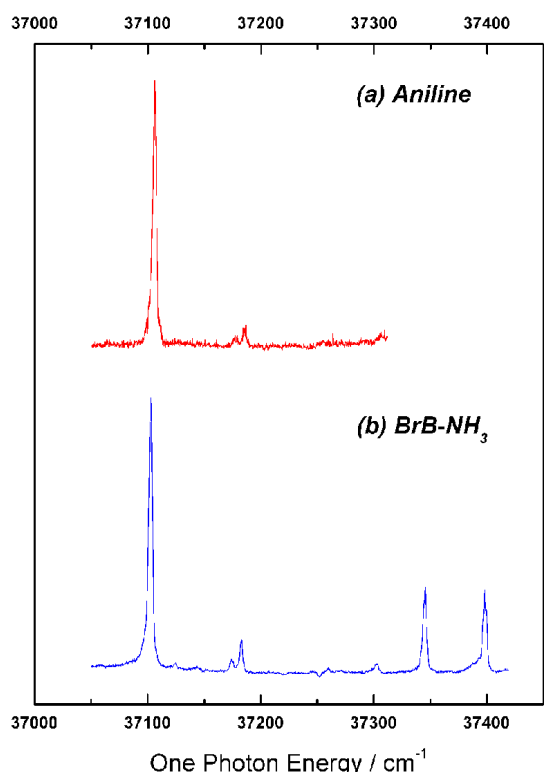
Figure 2.4: *REMPI spectrum of BrB-NH₃ obtained from the BrB-NH₃ and aniline mass channels.*

As with FB-NH₃, MP2 calculations predict the existence of three conformers, of similar structure to those of FB-NH₃ (figure 2.3). The REMPI spectrum of BrB-NH₃ is also very similar to that of FB-NH₃ (see figure 2.4 b) and it can thus be readily assigned to the σ-ortho isomer. Unlike FB-NH₃, BrB-NH₃ however undergoes an ion-molecule reaction producing aniline⁺ upon ionisation. The REMPI spectrum obtained when this channel is gated is analogous to that of BrB-NH₃ (figure 2.4 a). These facts suggest that the

reactants BrB and NH₃ are in a σ-ortho arrangement at the start of the reaction. Furthermore the apparent dependence of the conversion probability of BrB-NH₃ to aniline on the FC factors of the S₀-S₁ vibronic transitions might be an indication of a barrier less reaction mechanism in the cationic state as depicted in figure 2.5.

The industrial process of producing aniline from BrB requires high temperature and pressure. Through isotope labelling and trapping experiments it is known that the reaction proceeds via the highly reactive benzyne intermediate. In the molecular beam, however, the reaction mechanism seems to be of a concerted nature as otherwise the FC factors would be scrambled (broad spectrum) or at least substantially different.

It should be stressed that the results presented in this section are still somewhat preliminary ad thus subject to revision once the full data evaluation has been completed.

D_0

S_1

S_0

Reaction Coordinate ?

H
C
N
Br
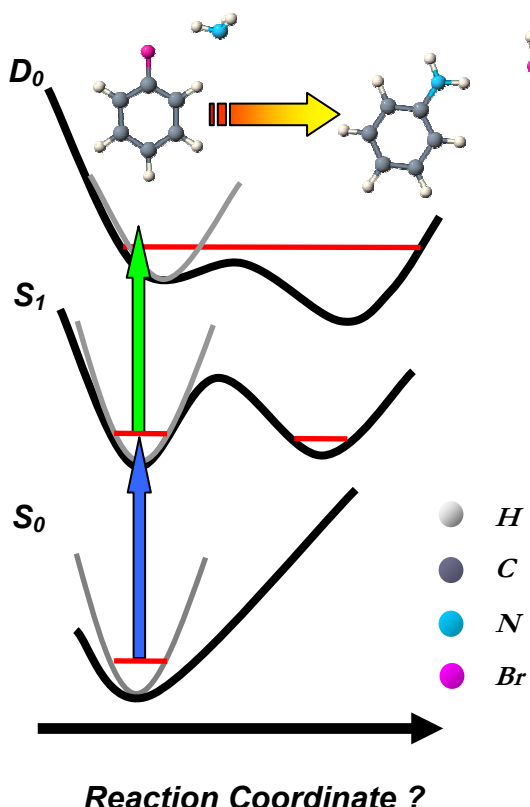
Figure 2.5: *Potential Energy Surfaces involved in the BrB-NH3 to Aniline reaction.*

3. Conclusion

The combination of REMPI spectroscopy, ab initio calculations and FC simulations allowed for the determination of the arrangement of the reactants ammonia and BrB prior to the ionisation induced reaction and even give some information about aspects of the reaction itself. However, the unravelling of the exact reaction mechanism / reaction coordinate of this ion-molecule reaction can only be achieved through time-resolved photoelectron spectroscopy and a complementary ab initio analysis of the relevant portions of the potential energy surface joining the reactants with the products.

References

1. Brutschy B., *Chem. Rev.*, **1992**, *92*, 1567
2. Doktorov, E.V.; Malkin, I. A.; Man'ke, V. I.; *J. Mol. Spectrosc.*, **1977**, *64*, 302.
3. Hougen, J.T; Watson, J.K.G. *Can. J. Phys.* **1965**, *43*, 298.
4. Duschinsky, F. *Acta Physicochim. URSS*, **1937**, *7*, 551-566.
5. Pugliesi I. and Müller-Dethlefs K. *J.Phys. Chem. A*, **2006**, *110*, 4657
6. Pugliesi I. and Müller-Dethlefs K. *J.Phys. Chem. A*, **2006**, *110*, 4668
7. Pugliesi I, Tonge N. M. and Cockett M. C. R., in preparation
8. Tonge N. M., MacMahon E. C., Pugliesi I. and Cockett M. C. R., *J. Chem. Phys.*, **2007**, *126*, 154319

Johari–Goldstein β relaxation in NMA and water: Glass-like behaviour at normal temperatures or a general model of liquids?

David A. Turton and Klaas Wynne

Department of Physics, SUPA, University of Strathclyde, Glasgow G4 0NG, Scotland, UK
david.turton@phys.strath.ac.uk

Johari and Goldstein[1] established that glass-forming liquids are characterised by the presence of a β relaxation mode that accompanies the slower fundamental structural relaxation due to rotational and translational diffusion, termed α relaxation. Glass-forming liquids generally possess two properties: strong electrostatic interactions and strong steric factors. More common liquids that share these properties include certain hydrogen bonding liquids. N-methylacetamide (NMA) and water are of great importance in bio-molecular physics and are well studied, both experimentally and theoretically. NMA is essentially a single peptide linkage terminated by a pair of methyl groups. The dipole moment of the HN–CO motif enables hydrogen bonding and the formation of chains, and it has been suggested that the structure of the pure liquid has an unusual temperature dependence[2,3].

Optical Kerr effect (OKE) spectroscopy[4,5] allows relaxation to be measured in a range from sub-picosecond to nanoseconds or more in a single scan. NMA is a normal liquid from ~300 K to 470 K. The OKE decay was measured at eight temperatures in this range and representative signals are shown in Fig. 1.
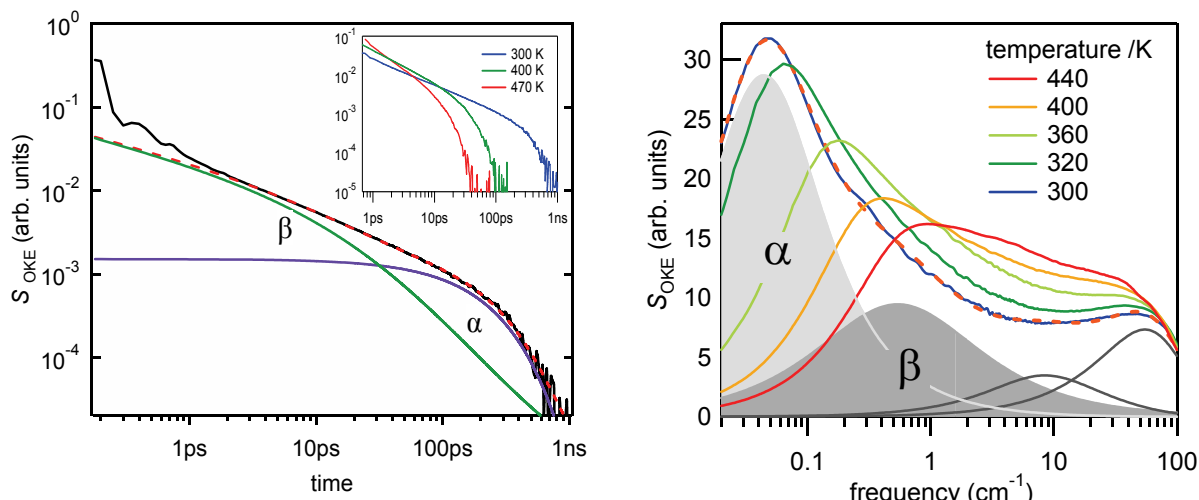
Fig. 1. OKE signals for NMA. (Left) Time-domain at 300 K showing the librational modes up to 1 ps followed by the relaxation fitted (dashed line) by Eq 1 and shown decomposed into α and β relaxation. Inset are shown signals for 300, 400, and 470 K. (Right) Equivalent signals transformed to the frequency domain. The fit at 300 K is also shown (dashed line).

At low temperature, several cycles of the strongly damped librational modes can be seen up to 1 ps. After this, the decay is monotonic through the intermediate region where on the log-log scale it appears linear. Then at the longest times, α relaxation becomes apparent. This power-law behaviour at intermediate times is characteristic of β relaxation in glassy liquids[6,7]. In the time domain, Kohlrausch-Williams-Watts (stretched-exponential) and power

1   G. P. Johari and M. Goldstein, J. Chem. Phys. **1970** <u>53</u> 2372-
2   T. W. Whitfield et al, Chem. Phys. Lett. **2005** <u>414</u> 210-.
3   N. T. Hunt and K. Wynne, Chem. Phys. Lett. **2006** <u>431</u> 155-.
4   N. A. Smith and S. R. Meech, Int. Rev. Phys. Chem. **2002** <u>21</u> 75-.
5   G. Giraud, J. Karolin, and K. Wynne, Biophys. J. **2003** <u>**85**</u> 1903-
6   H. Cang, J. Li, H. C. Andersen et al., J. Chem. Phys. **2005** <u>123</u> 064508-.
7   P. Lunkenheimer and A. Loidl, Chem. Phys. **2002** <u>284</u>, 205-

law functions have been applied to such decays and in the frequency-domain, where line shapes have been analysed in detail, Cole-Cole, Cole-Davidson, and Havriliak-Negami functions have been used. The simplest model that accurately fits these data was found to be the sum of a Debye function and a Cole-Cole function:

$$S(\omega) = \frac{A_D}{1 - i\omega\tau_D} + \frac{A_{CC}}{1 - (i\omega\tau_{CC})^\gamma} . \tag{1}$$

The first term represents α relaxation as a simple Debye function whereas the second, β relaxation, term is a Cole-Cole function, which with respect to the Debye is broadened by the exponent γ. The origin of β relaxation has been widely discussed, but is generally assigned to short-range correlations due to the formation of a transient "cage" of neighbouring particles. The broadening can then be interpreted simply as heterogeneity in the liquid structure.

The parameters obtained from fitting the whole temperature range by Eq (1) are shown in Fig. 2 (left). The two lifetimes, τ_D and τ_{CC}, are fitted according to the Stokes-Einstein-Debye relation $\tau \propto \eta$ with $\eta \propto \exp(E_a / k_B T)$ describing the Arrhenius dependence of the viscosity η with activation energy, E_a. Over this temperature range, both lifetimes are in good agreement with the Arrhenius expression giving very similar activation energies of 2400 K (0.2 eV). The Cole-Cole exponent increases with temperature to become approximately unity near the boiling point showing that the β relaxation band reduces to a Debye function whereupon the decay becomes a double exponential as widely used to describe relaxation in simple liquids. This shows that the heterogeneity is temperature dependent, which we expect due to the break-up of the hydrogen bonding structure at higher temperature.
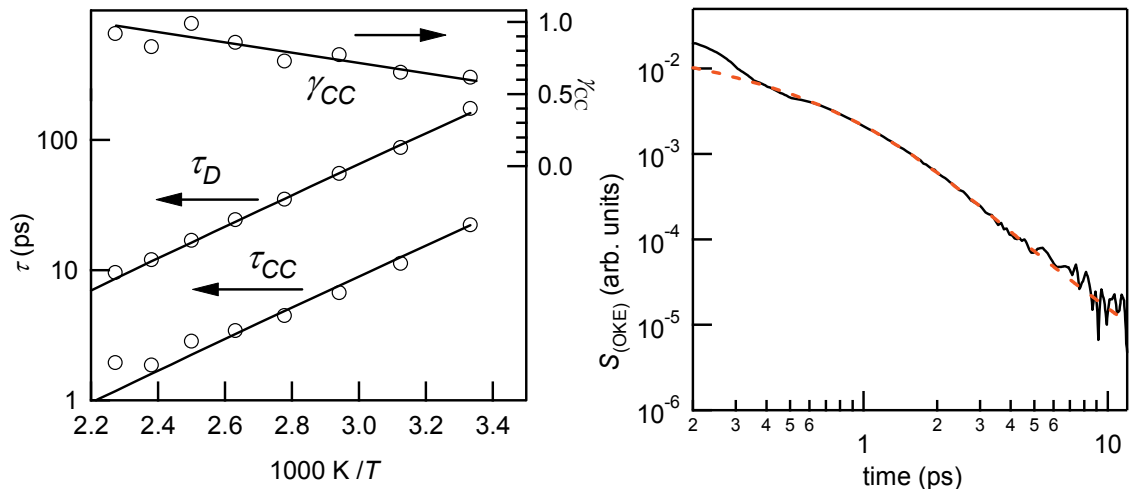
Fig. 2. (Left) The parameters returned from fitting Eq. (1) to the OKE time-domain decay of NMA. The Debye lifetime τ_D, Cole-Cole lifetime τ_{CC}, and Cole-Cole exponent γ. The two lifetimes are fitted by Arrhenius dependencies. The line through the data for γ_{CC} is a guide to the eye. (Right) Relaxation of water measured by OKE at 295 K and fit by the Cole-Cole function (dashed).

Hydrogen bonding in water results in structure, which is to a first order tetrahedral although the extended structure is still debated. The decay measured by OKE at room temperature is shown in Fig. 2 (right). Here we find that the Cole-Cole function gives the most accurate fit. The returned parameters are $\tau_{CC} = 0.57$ and $\gamma = 0.86$.

In water, the polarisability tensor is almost isotropic, so the signal arises predominantly from interaction-induced effects. Fundamental relaxation, then, of a rotational nature is expected to be extremely weak in the OKE signal. In comparison, dielectric and infrared spectroscopies interact through the permanent dipole moment and observe relaxation

with Debye time constants of ~10 ps and ~0.7 ps. In Ref. 8, the dielectric relaxation spectrum up to approximately 400 GHz is fitted by a Debye function with τ_D = 8.4 ps at 298 K with a weak secondary mode at 1 ps which is barely resolved. The 0.57 ps Cole-Cole relaxation lifetime from OKE is consistent with the faster of these two bands. The relaxation measured in water is then seen to be β relaxation rather than rotational α relaxation again consistent with the model described by Eq (1). The Cole-Cole exponent again indicates the degree of heterogeneity in the liquid.

The addition of a high-charge-density ion like Mg^{2+} to water increases the viscosity through the formation of clusters. This is reflected in the OKE data (Fig. 3) as an increase in relaxation time. On fitting by the Cole-Cole function, the returned parameters have a form that suggests a theoretical glass transition at a concentration above the saturation limit.
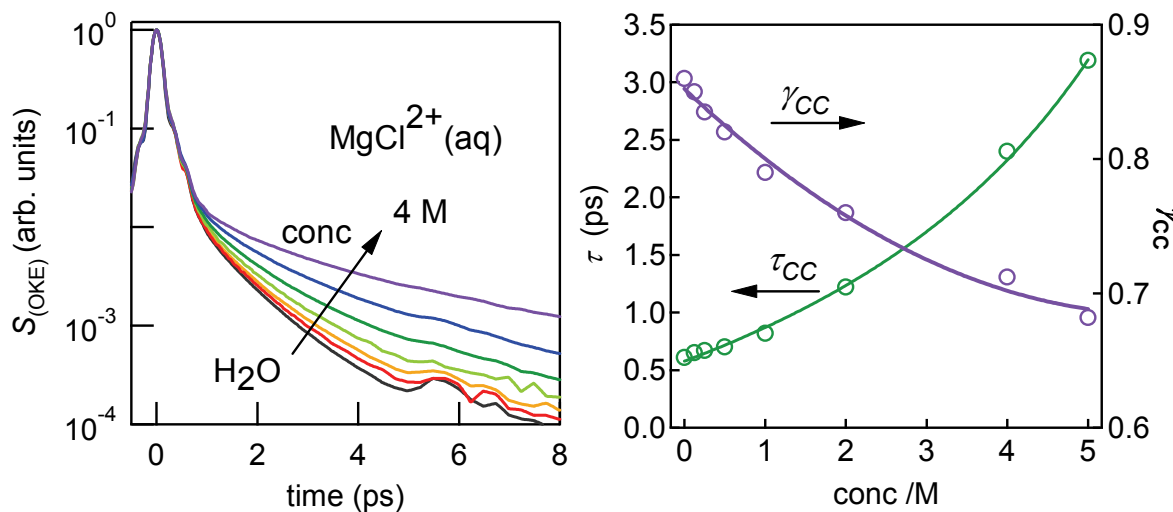
Fig. 3. (Left) OKE signals for aqueous MgCl$_2$. (Right) The parameters returned from fitting these data by a Cole-Cole function. With increasing concentration, the exponent γ_{CC} falls as the time-constant increases. The concentration dependence of the time constant is fitted by $\tau - \tau_0 \propto 1/(c - c_g) - 1/c_g$ which shows that it is consistent with glass forming behaviour.

Conclusions

By studying relaxation in N-methylacetamide (NMA) and water by optical Kerr effect spectroscopy (OKE) we show that there is a well defined β relaxation band as seen in the relaxation of glass-forming liquids. These observations support the view that the well-developed model of Johari-Goldstein behaviour is a good basis for a universal model of relaxation in liquids.

---

8   R. Buchner, J. Barthel, and J. Stauber, Chem. Phys. Lett. **1999** <u>57</u> 306-

Time-Resolved Transient Infrared Investigations of a Bistable Photochromic Organometallic Switch Based on Linkage Isomerization

Kristy M. DeWitt[1], Tung T. To[2], and Edwin J. Heilweil[3]

[1]NIST/NRC Postdoctoral Associate and [2]NIST Guest Researcher in the [3]Optical Technology Division, Physics Laboratory, National Institute of Standards and Technology, Gaithersburg, MD, 20899-8443

Photochromic materials are of increasing commercial importance because of their potential applications as reversible molecular photoswitches in nanotechnology, biomedicine, high-density optical memories, and optical computing technologies.[1] Desirable properties for such systems include high quantum yields, ultrafast response times, and low fatigue. The formation of shared intermediate species is problematic, since this leads to slow response times and unwanted side reactions, as illustrated in Figure 1a.

Previous work has shown that the cyclopentadienylmanganese complex $(\eta^5$-$C_5H_4CH_3)Mn(CO)_2$(3-cyanomethylpyridine) can act as a bistable photochromic organometallic switch via linkage isomerization.[2] Steady-state room temperature experiments in solution showed that the red-orange pyridine nitrogen bound complex, Mn-Py, isomerizes to the yellow cyano bound isomer, Mn-CN, upon visible irradiation. Further irradiation with UV light reverses ligand coordination back to the pyridine ring, restoring the red-orange solution color (Figure 1b). This switching behavior is also readily observed in the mid-infrared (IR) spectral region (Figure 1c). In isooctane solution at 293 K, the symmetric and asymmetric CO-stretching vibrations of Mn-Py appear at 1932 cm^{-1} and 1868 cm^{-1}, respectively, while the CN-stretch of the cyano-Mn bound species absorbs at 2025 cm^{-1}. As visible irradiation converts Mn-Py to Mn-CN, the CO-stretching absorptions blue-shift to 1943 cm^{-1} and 1880 cm^{-1} while the CN-stretch red-shifts to 2025 cm^{-1}. In this work, a time resolved transient infrared (TRIR) study was performed to investigate the mechanism and timescale of this linkage isomerization.
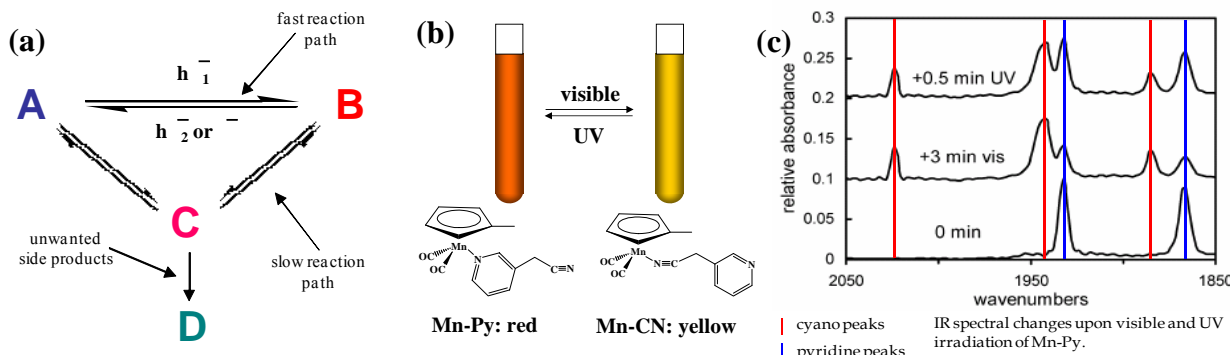
Figure 1: (a) Problems associated with switching mechanism proceeding at least partly by a slow reaction step through a shared intermediate. (b) $(\eta^5$-$C_5H_4CH_3)Mn(CO)_2$(3-cyanomethylpyridine) photochromic linkage isomerization. (c) Infrared absorption spectral changes associated with the reversible linkage isomerization process.

Experiments were performed with the home-built KHz repetition-rate Ti:Sapphire based UV/visible pump dual-beam IR probe femtosecond TRIR spectrometer schematically depicted in Figure 2. To minimized sample decomposition and complications from N_2 coordination, all samples were handled under argon atmosphere.

In Figure 3 the red traces show TRIR data for Mn-Py under visible (400 nm) irradiation with pump/probe delays ranging from the ps to the μs timescale. Bleaches at 1932 cm^{-1} and 1868 cm^{-1} correspond to loss of the parent compound. A single transient absorption peak at 1985
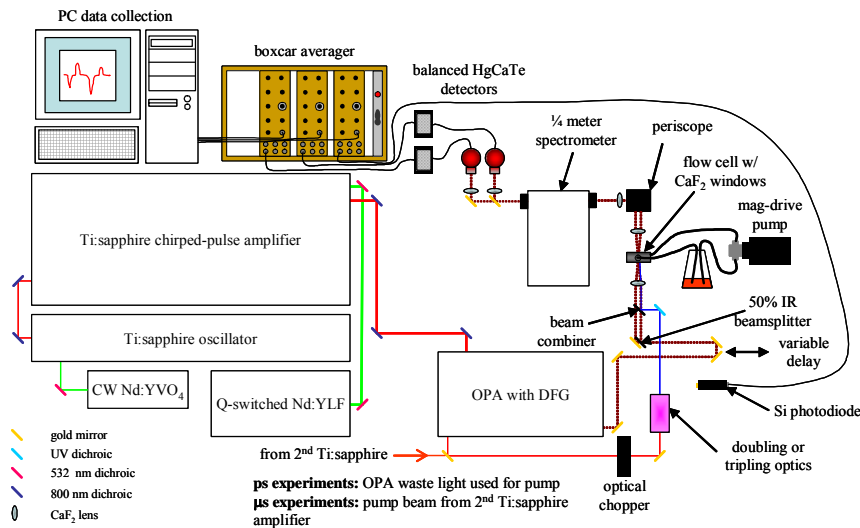
Figure 2: Schematic diagram of optical set-up.

cm^{-1} appears at early delay time, decaying with a time constant of approximately 100 ps. This band is tentatively suggested to be one of the CO bands of a ring-slip η^3 dicarbonyl species.[3] On the same timescale as the transient band disappears, two strong absorption features grow in at 1957 cm^{-1} and 1888 cm^{-1}. We assign these features as Mn-dicarbonyl absorptions with solvent transiently coordinated to the unsaturated metal center. On the microsecond timescale, no changes are observed in the TRIR spectrum except for a slow decrease in overall signal intensity, probably due to excited molecules flowing out of the beam volume before the probe interrogates the sample. The green traces in Figure 3b shows µs TRIR data for Mn-Py under visible irradiation with two procedural modifications: the isooctane solution was dried over molecular sieves to minimize water content, and free 3-cyanomethylpyridine ligand was added to the solution at 10X the Mn-Py concentration. Under these conditions, at 50 ns pump/probe delay the TRIR difference spectrum appears identical to the previous µs data, but by 5 µs delay blue-shifted absorption shoulders are beginning to appear on the sides of the 1957 cm^{-1} and 1888 cm^{-1} peaks. At 100 µs pump/probe delay, the only absorbance features remaining are at 1943 cm^{-1} and 1880 cm^{-1}, the positions expected for Mn-CN absorption.

Control experiments were performed using MMT (methylcyclopentadienyl manganese tricarbonyl) dissolved in isooctane solvent or with added ligands (e.g., acetonitrile = ACN). In pure isooctane the only reaction pathway possible for MMT after UV irradiation is loss of a single CO to form a solvated complex. Similarly, if a small amount of ACN is added to the solution, the MMT solvate can further react via a bimolecular diffusion mechanism to form Mn-ACN, which is expected to have very similar IR frequencies to Mn-CN. In Figure 3 the blue traces shows ps and µs data for 266 nm irradiation of MMT. The single bleach feature at 2025 cm^{-1} and the unresolved doublet centered at 1943 cm^{-1} correspond to loss of the parent tricarbonyl species. On the ps timescale, a single absorption peak at 1985 cm^{-1} appears at early time, decaying with a time constant of approximately 100 ps. This is identical to the behavior seen with Mn-Py. Also, with the same time constant, two strong absorption bands grow in at 1957 cm^{-1} and 1888 cm^{-1}. These can now be conclusively identified as isooctane solvate bands because there are no other ligands available to coordinate to the newly generated Mn center. On the µs timescale, no change is observed except an overall decay in signal due both to recombination by bimolecular diffusion of CO restoring the parent compound, and electronically excited molecules flowing out of the excitation volume before the probe pulse interrogates the sample. However, when ACN is added to the MMT/isooctane solution at approximately 2X the molar concentration of MMT, the solvate bands completely disappear and are replaced by Mn-ACN peaks at 2025, 1943, and 1880 cm^{-1} (purple traces in Figure 3b) at 100 µs time delay.

Unfortunately, only the 1880 cm^{-1} band can be directly observed in the TRIR spectra since the Mn-ACN product bands at 2025 cm^{-1} and 1943 cm^{-1} directly overlap the parent MMT bleaches and therefore can only be observed as a decrease in the relative bleach intensities.

Figure 3: (a) ps TRIR spectra for My-Py with 400 nm pump and MMT with 266 nm pump. (b) µs TRIR data.

TRIR difference spectra for Mn-CN in isooctane were also obtained using 266 nm pump irradiation, with pump/probe delays on the µs timescale. Bleaches at 1943 cm^{-1} and 1880 cm^{-1} corresponding to loss of the parent compound were observed, as well as new transient absorbances at 1957 cm^{-1} and 1888 cm^{-1} indicating formation of the same solvent-coordinated intermediate observed after visible irradiation of Mn-Py. The only evidence of Mn-Py formation were very small bleach features at 1932 cm^{-1} and 1868 cm^{-1}, probably resulting from a buildup of Mn-Py in solution during the course of the step-scan and subsequent UV re-bleaching. A similar experiment employing ten times ligand concentration added to the Mn-CN in isooctane sample was attempted, but was unsuccessful. The excess ligand concentration absorbed most of the UV pump light making it impossible to achieve enough Mn-CN excitation to observe any TRIR transients.

In summary, the photochromic activity of $(\eta^5\text{-}C_5H_4CH_3)Mn(CO)_2(3\text{-}$ cyanomethylpyridine) in room temperature isooctane solvent was investigated. For both reversible pathways, the reactions were found to be controlled by bimolecular diffusion and proceed through a common Mn-isooctane solvate intermediate. Future work will involve designing and testing homologous photochromic molecules that undergo switchable ligand interchange without a solvated intermediate. Two possible approaches include tethering the ligand to the Cp ring so that it cannot diffuse away or imbedding the molecular switch in a polymer film so the ligand cannot escape the metal reaction site.

[1] (a) Balzani, V.; Venturi, M.; Credi, A. *Molecular Devices and Machines-A Journey into the Nanoworld*; Wiley-VCH: Weinheim, Germany, **2003**. (b) Feringa, B. L. *Molecular Switches*; Wiley-VHC: Weinheim, Germany, **2001**. (c) Irie, M., Ed. *Thematic issue on Photochromism: Memories and Switches. Chem. Rev.* **2000**, 100, issue 5.
[2] To, T. T.; Barnes, C. E.; Burkey, T. J. *Organometallics* **2004**, *23*, 2708.
[3] Yang, H. Kotz, K. T.; Asplund, M. C.; Harris, C. B. *J. Am. Chem. Soc.* 1997, 118, 9564.

Time-Resolved UV/Vis-Pump IR-Probe Spectroscopy on Photochromic Indolylfulgides

F.O. Koller [1], *W. J. Schreier* [1], *T. E. Schrader* [1], *S. Malkmus* [1], *S. Draxler* [1], *T. Brust* [1], *W. J. Lees* [2], *M. Braun* [1]

[1] Lehrstuhl für BioMolekulare Optik, Ludwig-Maximilians Universität München, Oettingenstr. 67, D-80538 München. [2] Department of Chemistry and Biochemistry, Florida International University, 11200 SW 8th St., Miami, FL, 33199 (USA).
E-mail: Florian.Koller@physik.uni-muenchen.de, URL: http://www.bmo.physik.uni-muenchen.de/

Organic photochromism can be simply defined as "light-induced reversible change of colour". Photochromic molecules are interesting for applications and can be used e. g. in molecular electronics, quantum control or as molecular data storage[1,2,3]. Prototype examples of photochromic molecules are fulgides and their derivatives.

The trifluoromethyl-substituted indolylfulgide (Fluor-fulgide) investigated in this work exists in three different conformers (Fig. 1a): the ring-opened E- and Z-forms and the closed C-form. The conformers can be switched into each other by light at appropriate wavelengths as indicated in Fig. 1a. The ground state conformers are thermally stable. As the reaction probability Z→E is very low, the experiments are performed so that the presence of E conformer can be neglected. The ground state absorption spectra of the conformers C and Z are shown in Fig. 1b. By application of light pulses at 400 nm or 570 nm it is possible to selectively induce the ring closure Z→C or the ring-opening C→Z, respectively. In the few femtosecond time-resolved studies on fulgides typically only one of the two photo-reactions has been addressed [4,5]. In this work we present femtosecond UV/Vis-pump broad-band infrared-probe experiments examining both, ring-opening and -closure.
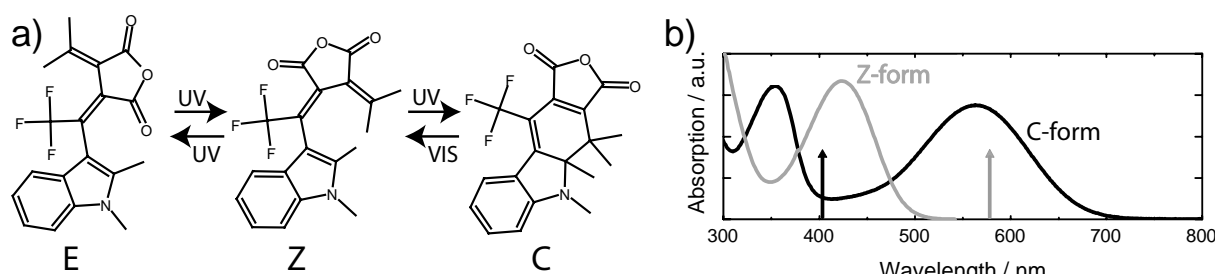
Fig. 1: (a) Structure and conformers of the investigated Fluor-fulgide. (b) UV/Vis absorbance spectra of the relevant Z and C-forms. The arrows indicate the colours of the laser pulses used to selectively trigger the photoreactions Z→C (black) and C→Z (gray).

Synthesis of the Fluor-fulgide is reported elsewhere[6]. The molecules were dissolved in tetrachloroethylene at a concentration of 8 mM. The educt forms of the photo-reactions can be accumulated to at least 95% by appropriate steady-state illumination. For a description of the experimental set-up based on a 1 kHz Ti:sapphire regenerative amplifier laser system see Schrader et al.[7] In brief: the IR probe pulses were generated by multi-stage optic parametric

[1] Y. Yokoyama, Chem. Rev., **2000**, 100, 1717
[2] D. Geppert et al., Appl. Phys. B, **2004**, 79, 987
[3] M. Seibold et al., Chem. Phys. Lett., **1996**, 283, 75
[4] M. Handschuh et al., J. Phys. Chem. A, **1997**, 101, 502
[5] S. Malkmus et al., Chem. Phys. Lett., **2005**, 417, 266
[6] C. J. Thomas et al., J. Org. Chem., **2001**, 66, 1914
[7] T. Schrader et al., Chem. Phys. Lett., **2004**, 392, 358

amplification. The UV/Vis pump pulses to induce the photo-reactions were produced by second harmonic generation (400 nm) and a NOPA[8] stage (570 nm). The achieved temporal resolution was about 300 fs.

Not only in the UV/Vis spectral range but also in the IR the two relevant conformers of the investigated Fluor-fulgide can be identified due to their different absorption patterns (Fig. 2a, b). The IR spectra are dominated by the CO stretch vibrational modes around 1780 cm^{-1}. For the closed C-form there are additional major absorption bands around 1550 cm^{-1} whereas the open conformer does not show significant bands in this spectral range. Beyond 1300 cm^{-1} there are strong absorption bands for both forms of the Fluor-fulgide.
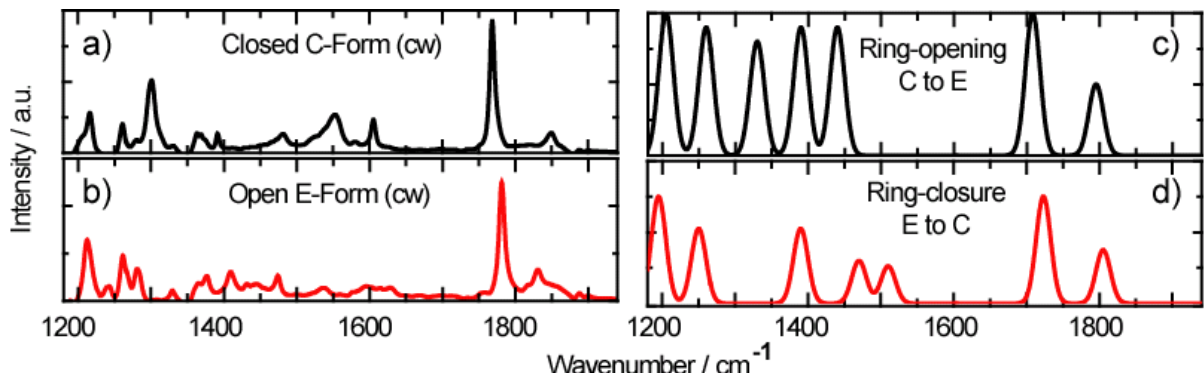
Fig. 2: Steady-state IR absorption spectra of the closed (a) and opened (b) conformers of the Fluor-fulgide. In (c) and (d) the vibrational spectra of the electronic excited states as occurring during the different photo-reactions are plotted.

An overview of the time-resolved IR data is given by Fig. 3, both for ring-opening C→Z and ring-closure Z→C reactions. As common features in both measurements one finds at the positions of the ground-state absorption bands large bleach-signals which rise within the temporal resolution of the experiment. The bleach-recovery essentially occurs on two time-scales, first with a time-constant of some ps and second with a time-constant in the order of 15 ps.

The induced absorption can be classified into three groups. (i) At the low-frequency wings of the bleached ground-state bands induced absorption signals occur. These bands predominantly decay with a time-constant of ~15 ps. This behaviour is typical for ground-state bands of hot molecules. Thus the time-constant for the vibrational cooling of the excited molecules to the solvent surrounding is about 15 ps. (ii) At many positions induced absorption instantaneously forms with the excitation. These signals decay with time-constants of a few ps (see e. g. at 1715 cm^{-1}). These bands can be attributed to vibrational modes of the electronically excited state (ES). (iii) The built-up of product bands proceeds in parallel with the decay of the ES (e. g. at 1550 cm^{-1}). It should be noted that the absorption due to the product bands is relatively weak because of the small reaction quantum yields (ca. 9% for C→Z, and 20% for Z→C).

The time-resolved IR data give the following information on the reaction kinetics: After roughly 50 ps the transient spectra resemble the steady-state difference spectra (not shown here) and all dynamics are completed. The cooling of the hot molecules to the solvent takes place on a 15 ps time-scale. The products of the photo-reactions are formed with the decay of the ES. For the ring-opening C→Z the ES life-time is found to be ~3 ps.

[8]   E. Riedle et al., Appl. Phys. B, **2000**, _71_, 457

For the ring-closure the dominant time-constant is ~10 ps. No long-living intermediate states during the photo-reactions could be identified in the IR.
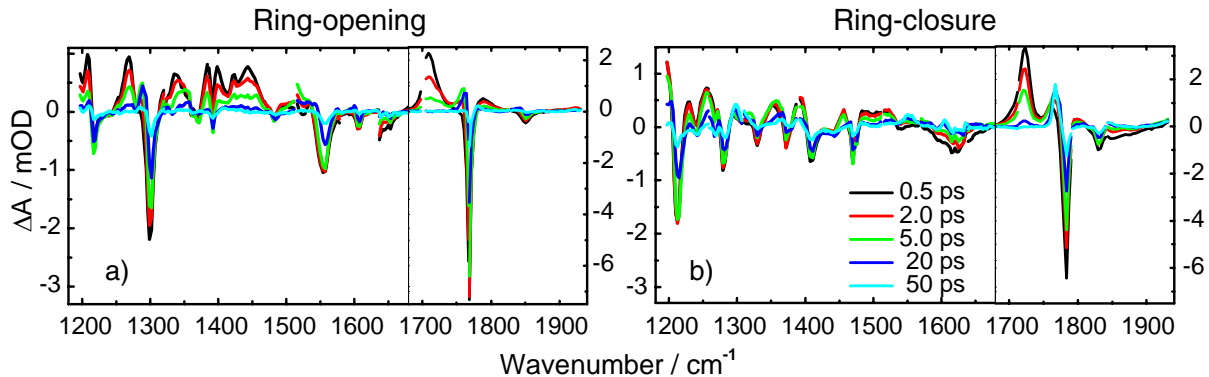
Fig. 3: Transient spectra for ring-opening (a) and ring-closure reactions (b) of the Fluor-fulgide at different delay times. The transient spectra recorded at 50 ps resemble the steady-state difference spectra (not shown). Note the different scaling within the plots.

In the present investigation a wide spectral range from 1200 to 1900 cm^{-1} was covered by the IR probing. This broad spectral range makes it possible to derive reliable vibrational spectra of the ES (Fig. 2c, d). The ES spectra as observed for the reactions C→Z and Z→C, respectively, clearly differ from each other.

The ES spectra yield important experimental information for the comparison with future calculations on the excited state properties of these molecules. An assignment of the monitored bands of the ES to normal modes would lead to a deeper understanding of the ES.

In conclusion: The ring-opening and -closure reactions of a special Fluor-containing indolylfulgide have been investigated with femtosecond UV/Vis-pump IR-probe spectroscopy. Both reactions occur on ultrafast time-scales and are finished after ~50 ps. Product formation happens with the decay of the electronically excited state (life-time of a few ps) without the appearance of intermediate states. The very broad probe range also permitted to derive IR spectra of the electronically excited state.

Ultrafast Chelation Dynamics of Model Photoswitches: Arene Chromium Tricarbonyl Derivatives with Pendant Sulfides

Tung T. To,[1] Charles B. Duke III,[2] Theodore J. Burkey,[2] and Edwin J. Heilweil[1]

[1]Guest Researcher, Optical Technology Division, Physics Laboratory, National Institute of Standards and Technology 100 Bureau Drive, Stop 8443, Gaithersburg, MD 20899, USA and . [2] Department of Chemistry, Campus Box 526060, University of Memphis, Memphis, Tennessee 38152-6060

Reversible molecular photoswitches have potential applications as recordable media and reversible optical switches,[1] and high quantum yields, rapid response rates, and low fatigue are desirable properties of these systems. Our studies indicate that ultrafast chelation can be a mechanistic platform for developing future molecular photoswitches.[2] In our earlier work we investigated several model organometallic compounds capable of chelation following CO photodissociation. The structure of the chelatable functional groups and solvent can greatly influence the quantum yield, reaction rate, and chelation pathways of organometallic complexes.[2]

UV pump/IR probe transient ps to μs infrared experiments of manganese compounds **4**, **5**, and **6** (Chart 1) in *n*-heptane show that chelation can occur via two pathways: a direct subpicosecond chelation pathway and a slower (> ns) solvent coordination pathway (Scheme 1). It appears that the fast chelation pathway depends on the close proximity of a sulfide group to the metal center to intercept the metal before solvent coordination occurs.

Chart 1

To understand how the metal center and the structure of the chelating ligand may affect chelation rates and pathways, we prepared three new derivatives of the Cr species, **1**, **2**, and **3**, bearing identical sulfide side chains as the analogous Mn species, **4**, **5**, and **6**, respectively (Chart 1). In this poster, we describe the photoinduced dynamics of **1**, **2**, and **3** in three solvents, *n*-heptane, tetrahydrofuran (THF), and acetonitrile and compare them to our earlier studies of **4**, **5**, and **6**.[3]

Scheme 1

A detailed description of the time-resolved UV-pump infrared probe (TRIR) apparatus used for this study was previously reported.[2] In a typical experiment with picosecond time resolution, a 289 nm UV pulse (ca. 120 fs pulse duration with 4 μJ to 6 μJ energy) was focused to approximately 100 μm diameter in a 2 mm pathlength flow cell with CaF_2 windows. For nanosecond to millisecond resolution, 355 nm harmonic pulses from a Q-switched Nd:YAG laser (4 ns pulse duration, 30 μJ to 40 μJ energy), were electronically synchronized and timed to the femtosecond IR probe pulses. We averaged 2000 laser shots to obtain a single difference spectrum. Two to four of these spectra were averaged for each time delay presented. Analysis of averaged spectra (typically four) yielded an intensity uncertainty from the baseline of less than ± 0.005 optical density (OD) units (k = 1; type B analysis).

To prepare samples for the TRIR experiments, the Cr complexes (30 mg to 50 mg) were dissolved in 50 mL to 80 mL of solvent to produce millimolar concentrations (e.g. 1.2×10^{-3}
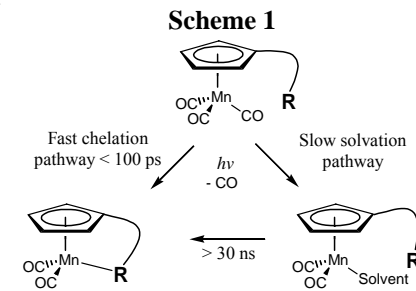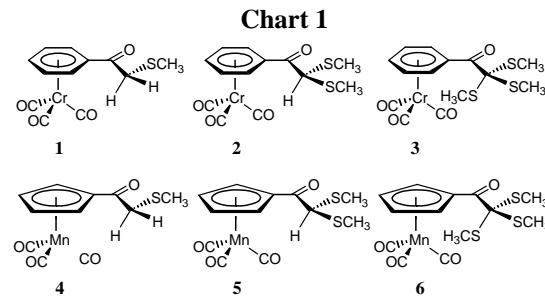
mol/L from 30 mg of **1** in 80 mL of *n*-heptane) with optical density (OD) ~1 measured at the higher frequency (e.g. near 1990 cm^{-1} in heptane) of the two parent CO-stretching bands. All samples were studied at room temperature (ca. 293 K).[4,5]

TRIR experiments performed in this work show that irradiation of **1**, **2**, or **3** in *n*-heptane solution at either 289 nm or 355 nm results in CO dissociation to initially form two photoproducts: the transient Cr-heptane solvate and stable Cr-S bound chelate. The Cr-heptane solvate eventually converts to the Cr-S chelate on the nanosecond timescale. Upon examining the difference TRIR spectral changes of **1** in Figure 1, strong bleaching signals from the starting compound's CO-stretching band doublet near 1926 cm^{-1} and 1932 cm^{-1} are clearly observed at 8 ps time delay, indicating efficient photoexcitation and CO loss. A third bleach signal for the parent compound's highest frequency CO-stretch occurs at 1990 cm^{-1} but is not examined in this study. A broad red-shifted absorption feature (relative to the doublet bleach feature) is observed around 1915 cm^{-1} that has been interpreted previously as arising from cooling of vibrationally hot species.[2b] At the intermediate time delay 102 ps, two absorption bands are observed near 1888 cm^{-1} and 1940 cm^{-1}. As the two features near 1888 cm^{-1} and 1940 cm^{-1} decay in intensity on the nanosecond timescale, we note that the absorption intensity near 1880 cm^{-1} increases to generate a newly observed feature. Coincident with the growth of absorption intensity at 1880 cm^{-1}, another new absorption feature centered near 1934 cm^{-1} also emerges on top of the parent bleach feature. We assign the blue shifted pair of CO-stretching bands near 1888 cm^{-1} and 1940 cm^{-1} to the Cr-solvate, and the red shifted pair of CO-stretching bands near 1880 cm^{-1} and 1934 cm^{-1} (identical to that observed in the difference FTIR at the bottom of Figure 1) to the Cr-S chelate. The overall chelation reaction mechanism is summarized in Scheme 2.

These assignments are also consistent with previously obtained results from transient and steady-state IR studies of **4**, **5**, and **6** in *n*-heptane in which the metal-heptane solvate intermediate has CO-stretching bands blue-shifted relative to the CO–stretching bands of the metal-S chelate.[2b] Additional support for these spectral assignments are derived from previously reported observations that (arene)Cr(CO)$_2$-alkane complexes are spectroscopically observed and are stable for many microseconds.[6]

The difference TRIR spectral changes observed for **2** and **3** in heptane (Figure 1) are similar to that of **1**. However, having additional sulfide groups on the pendant side chain appears to diminish the competing solvent coordination. Apparently solvent coordination is not completely excluded for **3** as was previously observed for the Mn analog (**6**).[2b] Examining the two overlapping absorption bands of **1** near 1880 cm^{-1} and 1888 cm^{-1} at 102 ps time delay, we
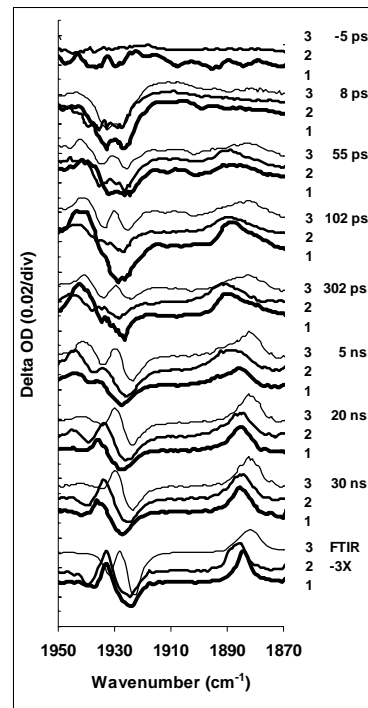

Figure 1: Transient TRIR difference spectra acquired after UV irradiation of **1**, **2**, and **3** in *n*-heptane at 298 K. At each time delay, the spectra are offset vertically by 0.01 OD units for clarity. At the bottom are the difference FTIR spectra of **1**, **2**, and **3** (amplitude divided by a factor of 3) in *n*-heptane acquired before and after

Scheme 2
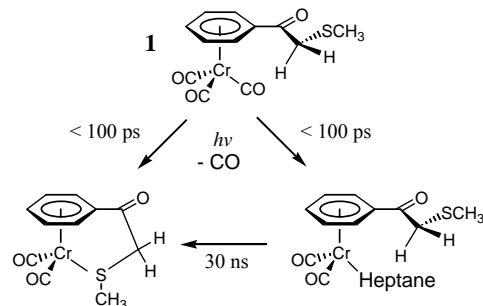
note that the absorption intensity at 1880 cm^{-1} of the Cr-S chelate is approximately half the absorption intensity at 1888 cm^{-1} arising from the Cr-heptane solvate. Assuming the Cr-S chelate and the Cr-heptane solvate have similar IR absorption cross-sections, this result suggests that the initial Cr-S chelate/Cr-heptane solvate ratio is approximately 1:2. Applying the same analysis to the other Cr-S species, the initial Cr-S chelate/Cr-heptane solvate distribution is slightly larger than 1:2 upon irradiation of **2** and ~ 2:1 upon irradiation of **3**.

Figure 2 shows transient difference spectra of **2** and **3** in THF solution recorded at pump-probe delay times ranging from picoseconds to milliseconds and FTIR difference spectra of **1**, **2**, **3**, and **7** (Scheme 3) before and after 30 seconds of UV irradiation with a xenon arc lamp. Since **7** has no chelatable side chain, we conclude that irradiation of **7** in THF yields the Cr-THF adduct, **8**, having characteristic IR bands at 1842 cm^{-1} and 1906 cm^{-1}. These same absorption bands, also observed in the difference TRIR experiments, are therefore assigned to the Cr-THF solvate. Apparently, the chelation dynamics of **1**, **2**, and **3** in THF are similar to that observed in *n*-heptane with the exception that the dominant chelation pathway in THF is via the Cr-THF solvate. Broad absorptions (*ca.* 30 cm^{-1} full-width at half-maximum (FWHM)) near 1842 cm^{-1} from **1** and **2** and 1858 cm^{-1} from **3** are observed, particularly in the nanosecond regime which remained unchanged up to microsecond time delays (not shown). Two additional bands near 1906 cm^{-1} and 1918 cm^{-1} are largely obscured by the parent species bleach band at 1906 cm^{-1}. The combined results from the TRIR and steady-state FTIR experiments indicate that the solvate Cr-THF species eventually converts to the Cr-S chelate on the > 5 ms timescale. These findings indicate that (1) the ultrafast coordination of solvent is more favorable for the stronger coordinating solvent and therefore chelation in THF occurs mainly via the Cr-solvate and (2) the stronger the Cr-solvent bond, the longer time it takes for the Cr-solvate to convert to the Cr-S chelate.

Figure 3 shows transient difference spectra for **1**, **2**, and **3** in acetonitrile recorded at pump-probe delay times ranging from -4 ps to 80 ps. Unlike the results obtained from irradiation of **1**, **2**, and **3** in *n*-heptane and THF, the spectral changes observed for all three complexes in acetonitrile are nearly identical. A bleach band from the starting compound is clearly observed at 1905 cm^{-1} (a second higher frequency bleach band occurs at 1977 cm^{-1} and was not examined). For delay times greater than 23 ps, a broad absorption band (ca. 20 cm^{-1} full-width at half-maximum (FWHM)) appears at 1846 cm^{-1}. The transient difference spectra after 27 ps are nearly identical to those obtained from the steady-state experiments (bottom of Figure 3). The acetophenone chromium tricarbonyl complex **7** has similar ground state CO-stretch absorption bands (appearing as bleaches in the difference FTIR spectra) as those of **1**, **2**, and **3**, and the FTIR difference spectrum obtained by steady-state irradiation of **7** producing **9** (Scheme 3) in
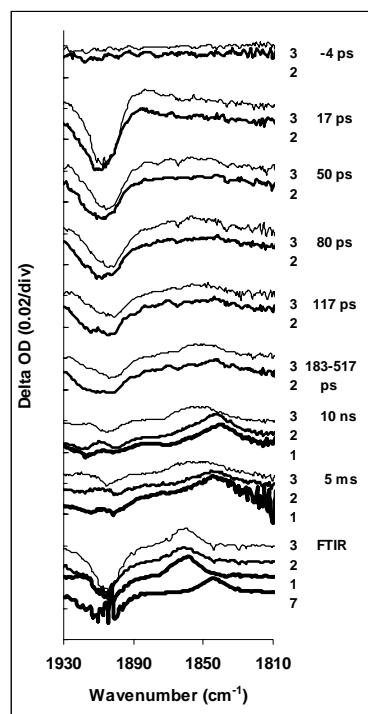
**Figure 2 :** Transient TRIR difference spectra acquired after UV irradiation of **1**, **2,** and **3** in THF at 298 K. At each time delay, the spectra are offset vertically by 0.01 OD units for clarity. At the bottom are difference FTIR spectra of **1**, **2**, **3**, and **7** in THF acquired before and after irradiation with a xenon arc lamp.

Scheme 3

8 Sol. = THF
9 Sol. = NCCH$_3$
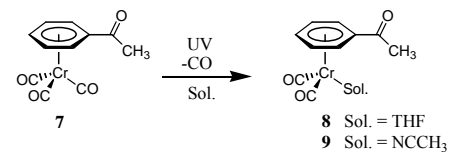
acetonitrile results in nearly identical TRIR difference spectra of **1**, **2**, and **3** in acetonitrile.
Despite many attempts to prepare Cr-S chelates in acetonitrile, they could not be isolated or observed, whereas stable isolated chromium acetonitrile complexes are known.[7] These results suggest that the bond energies of the Cr-S chelate and the Cr-solvate are most likely in the order Cr-heptane < Cr-THF < Cr-S (chelate) ≤ Cr-acetonitrile. If the initial product distribution upon irradiation of **1**, **2**, and **3** is determined not only by the accessibility of the sulfide group but also by the coordination power (as was observed from the TRIR experiments in *n*-heptane and THF), then the transient TRIR experimental results suggest that irradiation of **1**, **2**, and **3** in acetonitrile yields the Cr-NCCH$_3$ solvate, with no evidence for sulfur chelation.

In summary, the results from this investigation indicate that the reaction rates and chelation pathways of the chromium series (**1-3**) complexes depend on the conformational accessibility of the chelatable side group. These substitution reactions are influenced by the structure of the side chain, the metal center, and coordination power of the solvent. We found that there is competition between immediate chelation and solvent coordination following CO dissociation of **1**, **2**, or **3** in *n*-heptane and THF solutions to form two initial products: Cr-S chelate and Cr-Sol solvate (Sol = *n*-heptane or THF) which is a similar pattern observed for the analogous

Figure 3: TRIR difference spectra acquired after UV irradiation of **1**, **2**, and **3** in acetonitrile at 298 K. The spectra are offset vertically by 0.01 OD units for clarity.

manganese compounds (**4-6**). The picosecond dynamics is governed by side chain availability versus solvent strength and these factors determine the product distribution of solvate versus chelate. The interconversion of solvate to chelate occurs on the nanosecond to much longer timescales depending on the Cr-solvent bond strength. This study highlights how subtle structural changes may be used to tailor picosecond processes for the design of ultrafast molecular switches. More extensive studies are underway where the multiplicity of the electronic state will be considered.

[1]   (a) For leading references on photochromic materials in photonic devices see Irie, M. Ed. *Chem. Rev.* **2000**, *100*, 1683. (b) For a recent review on the use of photochromic materials for optical switches see Raymo, F. A.; Tomasulo, M. *Chem. Eur. J.* **2006**, *12*, 3186.

[2]   (a) To, T. T.; Burkey, T. J.; Heilweil, E. J. *J. Phys. Chem. A* **2006**, *110*, 10669. (b) Yeston, J. S.; To, T. T.; Burkey, T. J.; Heilweil, E. J. *J. Phys. Chem. B* **2004**, *108*, 4582.

[3]   Tung T. To, Charles B. Duke III, Theodore J. Burkey, and Edwin J. Heilweil, J. Phys. Chem. A, in press.

[4]   Detailed synthetic procedures of 1, 2, and 3, are to be published in the *Journal of Physical Chemistry A*.

[5]   Certain commercial equipment, instruments, or materials are identified in this paper in order to adequately specify the experimental procedure. In no case does such identification imply recommendation or endorsement by NIST, nor does it imply that the materials or equipment identified are necessarily the best available for the purpose.

[6]   (a) Creavens, B. S.; George, M. W.; Ginsburg, A. G.; Hughes, C.; Kelly, J. M.; Long, C.; McGrath, K. M.; Pryce, M. T. *Organometallics* **1993**, *12*, 3127. (b) Walsh, E. F.; George, M. W.; Goff, S.; Nikiforov, S. M.; Popov, V. K.; Sun, X.-Z.; Poliakoff, M. *J. Phys. Chem.* **1996**, *100*, 19425-19429.

[7]   Ross, B. L.; Grasselli, J. G.; Ritchey, W. M.; Kaesz, H. D. *Inorg. Chem.* **1963**, *5*, 1023.

Femtosecond Infrared-Spectroscopy
of the Photorearrangement of a Heterocyclic N-Oxide

T. Cordes[1], N. Regner[1], F. Michalik[2], and P. Gilch[1]*

[1]Lehrstuhl für BioMolekulare Optik, Department für Physik, Ludwig-Maximilians-Universität München, Oettingenstraße 67, 80538 München, Germany. [2]Institut für Chemie, Technische Universität Berlin, Straße des 17. Juni 135, 10623 Berlin, Germany.

The photo-rearrangement of organic N-oxides is a useful transformation in synthetic organic chemistry. It allows synthesizing chemicals which are difficult to access by other methods. It has been shown for a large variety of N-oxides that these compounds show photo-reactivity[1]. In contrast to this wealth of empirical data, experimental studies and information on the kinetics and mechanisms of these reactions are scarce. In particular, no spectroscopic experiments with a suitable time resolution have yet been published. We here report on a femtosecond-IR study of the rearrangement of a heterocyclic N-oxide (2-benzoyl-3-phenylquinoxaline-1,4-dioxide). This molecule shows drastic structural changes finally yielding an imidazolone as indicated in Fig. 1. A mechanism for this reaction has been proposed[2] (see Fig. 1), though it lacks experimental verification. The aim of the present study is a spectroscopic identification of reaction intermediates in order to derive a reaction model based on experimental evidence.
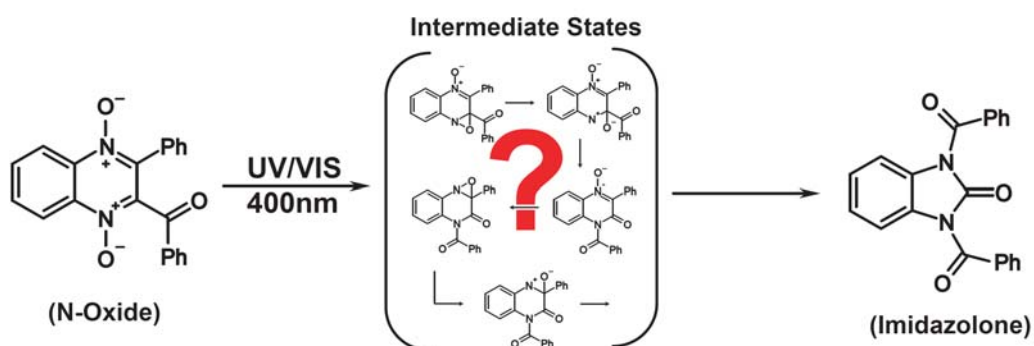
Figure 1. Schematic of the photoinduced rearrangement of the N-Oxide resulting in the formation of the Imidazolone. Proposed structures of intermediates are depicted in the center[2].

The N-Oxid structure shown in Fig. 1 exhibits a strong absorption band in the blue part of the visible spectrum ($\lambda_{max} \sim 390$ nm). Photolysis of the compound with cw-light at 400/430 nm bleaches this absorption band. We found that the photoproduct is formed with a quantum yield of 0.1 ± 0.02 (solvent ethanol) which is in good agreement with values in the literature.[3] To investigate the photochemical pathway N-Oxide molecules are excited with ultrashort light pulses (~150 fs) centred at 402 nm. The pump induced absorption changes in the infrared spectrum are detected with delayed infrared pulses. Experimental details can be found in ref. [4].

The stationary infrared spectrum of the N-Oxide is shown in the upper panel of Fig. 2. Several IR bands highly characteristic for reagent and the photoproduct are marked and assigned in Fig. 2. The reactant is characterized by a very pronounced band at 1350 cm^{-1}

[1] A. Albini, M. Alpigiani, Chem. Rev. **1984**, 84, 43-71

[2] M. J. Haddadin, C. H. Issidorides, Tet. Lett. **1967**, 8, 753-756

[3] N. A Masoud, J. Olmsted, III J. Phys. Chem. **1975**, 21, 2214-2220

[4] T. E. Schrader, A. Sieg, F. O. Koller, W. J. Schreier, Q. An, W. Zinth, P. Gilch, Chem. Phys. Lett. **2004**, 392, 358 –364.
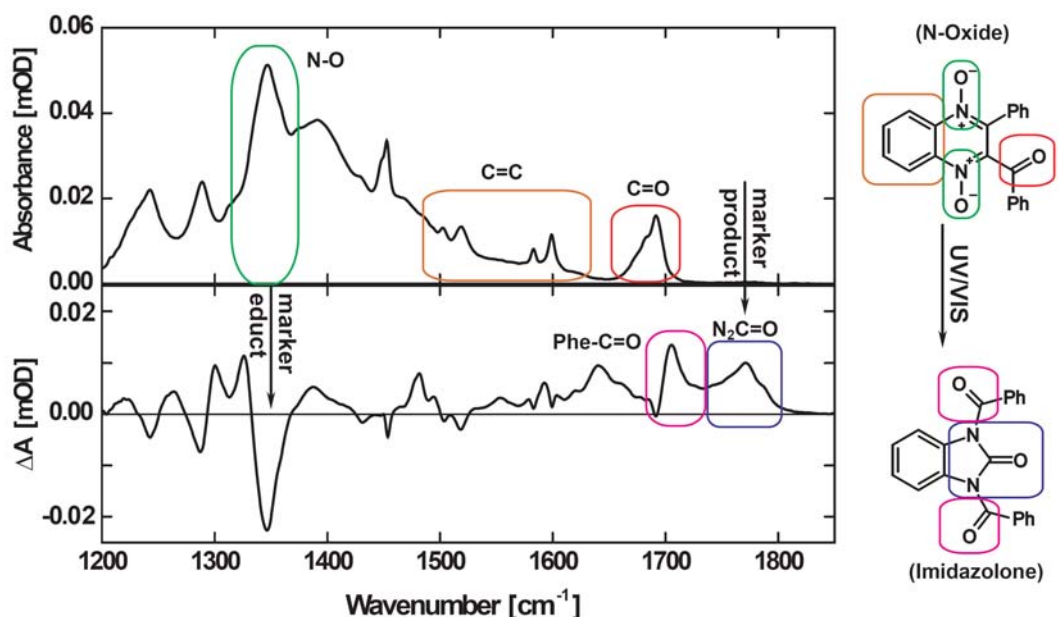
Figure 2. The stationary infrared absorption spectrum of the N-Oxide is shown in the upper panel. The absorbance changes resulting from the photoreaction illustrated next to the figure are shown in the lower part. A band assignment for the functional groups is indicated in the figure.

which is a typical region for N-O vibrations (green rectangle). Aromatic C=C double bond stretches are located between 1500 cm^{-1} and 1600 cm^{-1} (orange rectangle). The C=O oscillator is found at ~1690 cm^{-1} (red rectangle) which is a characteristic region for aromatic keto-groups. Illumination of the sample (λ_{Exc} = 402 nm) transforms the molecule into a symmetric Imidazolone. The structure in Fig. 1 and Fig. 2 shows that the N-Oxide function is lost and new carbonyl-groups (blue, magenta rectangle) are formed in the rearrangement process. The lower part of Fig. 2 shows a difference spectrum of the sample after several seconds of light exposure. As expected the N-O band shows a strong bleaching signal while new bands in the carbonyl-region appear. These vibrational frequencies are now taken as marker bands for the time-resolved experiments: The region around 1350 cm^{-1} will monitor the behavior of the reactant while product formation is observed > 1700 cm^{-1}.
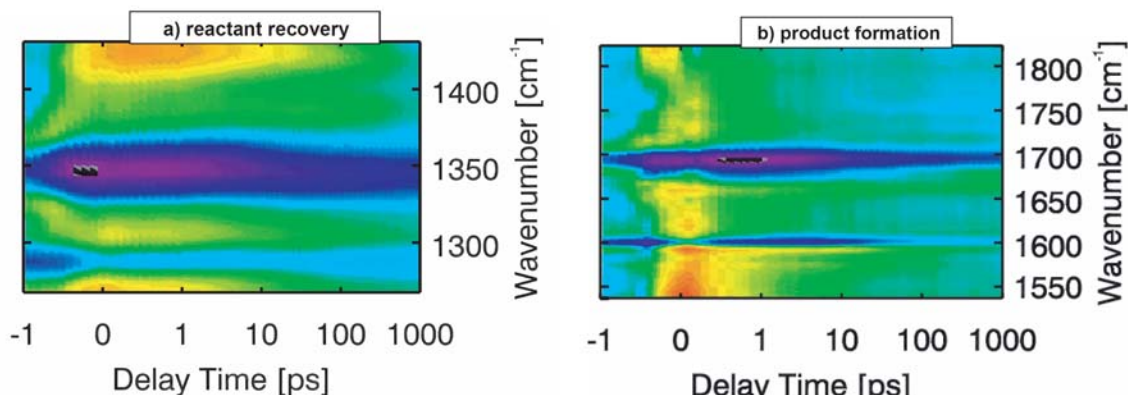
Figure 3. Time-resolved infrared measurements monitoring different probe regions: The left panel a) shows the reactant recovery from 1280 cm^{-1} – 1430 cm^{-1}. The right panel b) monitors reactant states from 1540 cm^{-1} – 1700 cm^{-1} and product states from 1700 cm^{-1} – 1820 cm^{-1}. Please note the linear timescale from -1 ps to 1 ps and the logarithmic thereafter. Blue signals indicate a negative absorbance change while red signal stand for positive signals.

The pump-probe data shown in Fig. 3a reveals an instantaneous bleaching (GSB) of the N-O band at 1350 cm^{-1} after excitation. The GSB-signal shows pronounced transients on the 1-10 ps timescale and seems to recover on the timescale of 100 ps and 1000 ps to a constant offset. Within a global fit these observations can be described by three time constants of 0.7 ps, 10 ps, and 200 ps. The 0.7 ps component describes kinetic processes involving exclusively excited electronic states. The population of the ground-state is recovered (~80 %) to a large amount with the two time constants 10 ps and 200 ps. In the carbonyl range of the IR spectrum a bleach recovery of the reactant band is observed which matches the temporal behaviour of the NO-recovery. Quite surprisingly no high frequency carbonyl vibration, indicative of the photoproduct, rises. Obviously, product formation takes longer than a couple of nanoseconds.
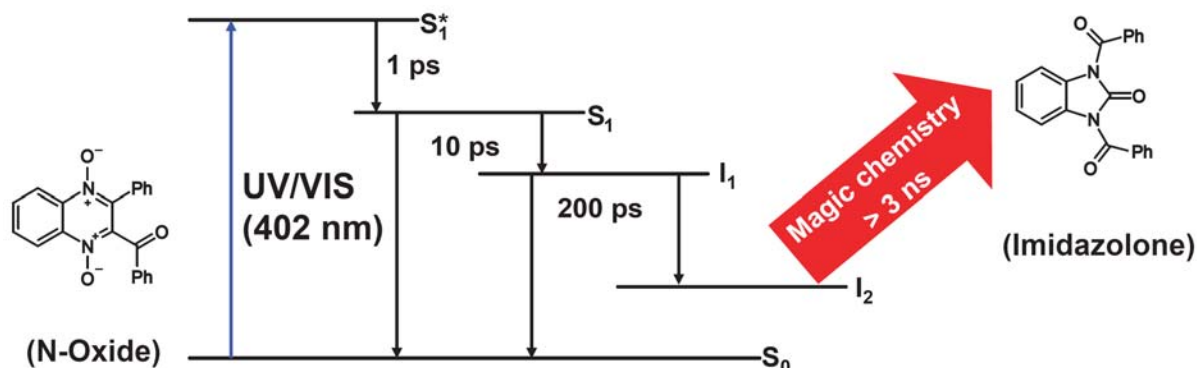
Figure 4. State model describing the fastest photochemical processes of the N-Oxide after 400 nm excitation.

We summarize our experimental in Fig. 4. Photoexcitation populates a Franck-Condon state (S^*_1) which relaxes within ~1 ps (S_1). This process is not accompanied by ground state recovery. The S_1 state then decays within 10 ps partially repopulating the ground state and partially populating an intermediate I_1. This intermediate is then depopulated in 200 ps which is again accompanied by a branching. Now 20 % of the initially excited molecules remain in the intermediate state I_2 which forms the final product on timescales longer than 3 ns.

The presented results are a first step on the way to a complete understanding of the complex photochemical rearrangement process of the N-Oxide. Infrared measurements have to be complemented by time-resolved visible and fluorescence measurements for a clear structural and electronic assignment of the intermediate states I_1, I_2. Solvent dependent experiments may reveal their electronic character. The timescale of product formation, which extends the time range accessible with ultrafast spectroscopic techniques (~3 ns), has to be determined using time-resolved techniques on longer timescales.

Vibrational dynamics in hydrogen-bonding and non-hydrogen bonding liquids and complexes

Kaoru Ohta [1], Keisuke Tominaga [1, 2, 3]

[1] Graduate School of Science and Technology, Kobe University, Nada-ku, Kobe 657-8501, JAPAN
[2] Molecular Photoscience Research Center, Kobe University, Nada-ku, Kobe 657-8501, JAPAN
[3] CREST, JST
E-mail address tominaga@kobe-u.ac.jp

Solute-solvent interaction plays an important role in chemical reaction dynamics and in many relaxation processes in the condensed phase. Ultrafast nonlinear infrared (IR) spectroscopy was shown to be a powerful tool to investigate solute-solvent interactions and vibrational dynamics in solution. Among these studies, vibrational population relaxation, orientational dynamics and spectral diffusion process of small ions, such as azide (N_3^-), cyanate (OCN^-), and thiocyanate (SCN^-), have been investigated extensively over the last decade.[1-3] In parallel to the experimental studies, a number of theoretical works provide detailed information on the vibrational population relaxation and spectral diffusion process of small ions, especially for azide in water.[4,5] Recently, we investigated the vibrational dynamics of the anti-symmetric stretching mode of OCN^- and SCN^- in methanol and the CN stretching mode of $Fe(CN)_6^{4-}$ in water (H_2O and D_2O) by transient grating and three-pulse IR photon echo methods.[6]

Most of the time-resolved studies for small ions so far have been focused on the vibrational dynamics in protic solvents such as water and alcohols. In order to understand the nature of the dynamical interactions in protic solvents, it is important to compare the dynamical properties of the vibrational transitions in aprotic solvents with those in protic solvents. In this contribution, we extended our studies to investigate the vibrational population relaxation of the anti-symmetric stretching mode of SCN^- in polar solvents by using IR pump-probe method.[7] The details of the experimental procedure for IR pump-probe measurements have been published in the previous publication.[7] Briefly, IR pulse used for the measurements has a pulse width of about 150 fs and a pulse energy of 2 μJ. This IR pulse was split into two, one of which was used for a pump pulse and the other was used for a probe pulse. After the sample, the probe pulse was dispersed in a monochromator and was detected with a liquid N_2-cooled InSb detector. The concentration of the samples was around 180-190 mM and the optical path length was 25 μm.

Figure 1 displays the FT-IR spectra of the anti-symmetric stretching mode of SCN^- in various protic and aprotic solvents. The peak of the absorption spectrum is located at around 2056 cm^{-1}, which is not sensitive to the solvent used. On the other hand, as clearly seen in the
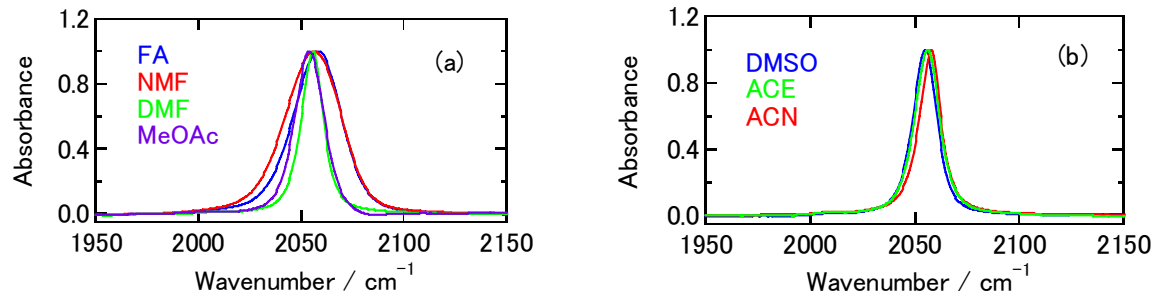
Figure 1. (a) FT-IR spectra of the anti-symmetric stretching mode of SCN$^-$ in formamide (FA), and *N*-methylformamide (NMF), *N,N*-dimethylformamide (DMF), and methyl acetate (MeOAc). (b) FT-IR spectrum of the anti-symmetric stretching of SCN$^-$ in dimethylsulfoxide (DMSO), acetonitrile (ACN), and acetone (ACE).

absorption spectra, the linewidth of the absorption spectrum in protic solvents is much broader than in aprotic solvents. Based on the results of *ab initio* calculations, the anti-symmetric stretching mode of SCN^- is localized as a CN stretching motion and a shift in the vibrational frequency depends on the number and location of the hydrogen bonds between SCN^- and the solvent moelcules. We measured the pump-probe signals originating from both $v=0-1$ and $v=1-2$ transitions at the magic angle condition. The temporal profiles of the pump-probe signals from the $v=1-2$ transition are the same as those from the $v=0-1$ transition within experimental uncertainity. From our experimental results, the vibrational population relaxation in aprotic solvents takes place about 2-2.5 times slower than in protic solvents. Similar trends were observed in the anti-symmetric stretching mode of N_3^- and the other systems, though the limited number of the solvents was investigated.[2]

Figure 2 displays the plot of the vibraitonal population relaxation rates with respect to the width of the absorption spectra to observe the relationship between them. Relaxation rates may be classified into two groups, one consisting of protic solvents and the other of aprotic solvents. There are a large variation in relaxation rates among protic solvents, while the solvent dependence of the relaxation rates is rather small in aprotic solvents. For polyatomic solute molecules in solution, vibrational population relaxation takes place via intramolecular vibrational energy redistribution (IVR) to the other solute modes and/or intermolecular vibrational energy relaxation (VER) to the solvent vibrational modes. So far VER in solution has been often discussed in terms of short-range interactions between the solute and solvent molecules. Recently, it was observed experimentally that the vibrational population relaxation is strikingly rapid in polar solvents, and that Coulombic forces are somehow responsible for the acceleration of the relaxation process. In our systems, we do not observe any correlation between the relaxation rates and the electrostatic properties of the solvent. As shown in Fig. 2, both the vibrational relaxation rate and the linewidth of the absorption spectrum are strongly affected by the hydrogen bonding interactions. Hydrogen bonding interaction between SCN^- and the solvent molecule induces additional friction and thus accelerates the vibrational relaxation. Further experimental and theoreitcal studies are necessary to obtain detailed information on the role of electrostatic interaction in the relaxation process.

Another possibility to explain the acceleration of the relaxation in protic solvents may be due to the enhancement of IVR process by the hydrogen bonding interaction. For the IVR process of SCN^-, vibrational energy transferred into the symmetric stretching and bending modes. Theoretical studies of N_3^- in water by Morita and Kato showed that the direct relaxation to the ground state and the IVR to the symmetric stretching mode equally contribute to the overall vibrational population relaxation, and charge fluctuation effect of the ion greatly enhances the relaxation rate of both the processes.[4] The symmetric stretching and bending modes for SCN^- have lower vibrational frequencies than those of N_3^-. IVR for SCN^- may be less efficient due to the large energy gap between the anti-
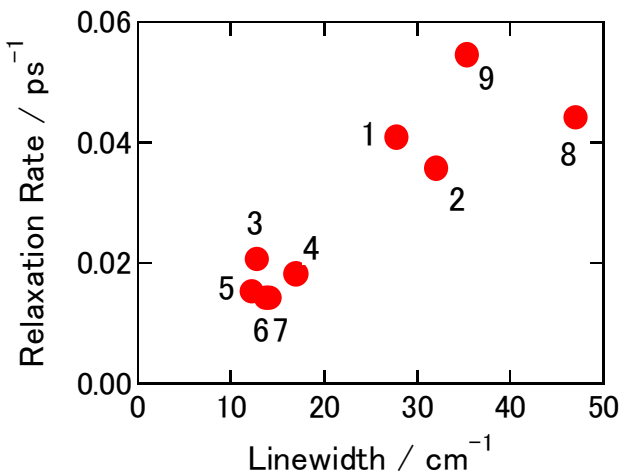
Figure 2. Plot of vibrational relaxation rates vs. linewidth of the absorption spectra. The relaxation rates are inverses of the relaxation times for the $v = 0 - 1$ transition. 1: FA, 2: NMF, 3: DMF, 4: MeOAc, 5: ACN, 6: DMSO, 7: ACE, 8: Methanol[2], 9: D_2O[1].

symmetric stretching mode and the symmetric stretching and bending modes. In order to resolve this issue, two-color IR pump-probe methods are very helpful to monitor the population dynamics of the low-frequency vibrational mode. Furthermore, studies by molecular dynamics simulation for SCN$^-$ will provide detailed information on the role of IVR in the vibrational relaxation.

As discussed both experimentally and theoretically, a hydrogen bonding interaction is not static, but intrinsically time-dependent. Three-pulse IR photon echo method has been shown to be very powerful to study the dynamics of solute-solvent interaction in condensed phases. Recently we have investigated the vibrational frequency fluctuations of several ions in protic solvents by three-pulse IR photon echo measurements.[6] The correlation functions of the vibrational frequency fluctuations show a bimodal feature. The fast decaying components of the correlation functions have time constants of about 100 fs, while the slower ones have the time constants of about 4 ps in methanol and 1.5 ps in water, respectively. Combined with the results of N_3^- in D_2O, we found that the time scales of the solvation dynamics in methanol and D_2O do not depend on the nature of the vibrational mode of the solute.[3,6] In our preliminary measurements, Figure 3a shows the results of the IR photon echo signals of SCN$^-$ in dimethylsulfoxide. Details of the experimental procedures and definition of the time delays were given elsewhere.[6] As shown in the previous studies, the peak position of the photon echo signals is a sensitive measure for the degree of the "transient" inhomogeneity in the distribution of the vibrational frequencies. In order to characterize the degree of asymmetry of the photon echo signals with respect to τ=0 fs, the first moments of the echo signals are calculated as a function of T as shown in Figure 3b. The first moment of the photon echo signals for SCN$^-$ in dimethylsulfoxide decays with a time constant of 5.4 ps. Currently, we are analyzing the data to obtain information on the magnitude and decay time scales of the correlation function of the vibrational frequency fluctuations.
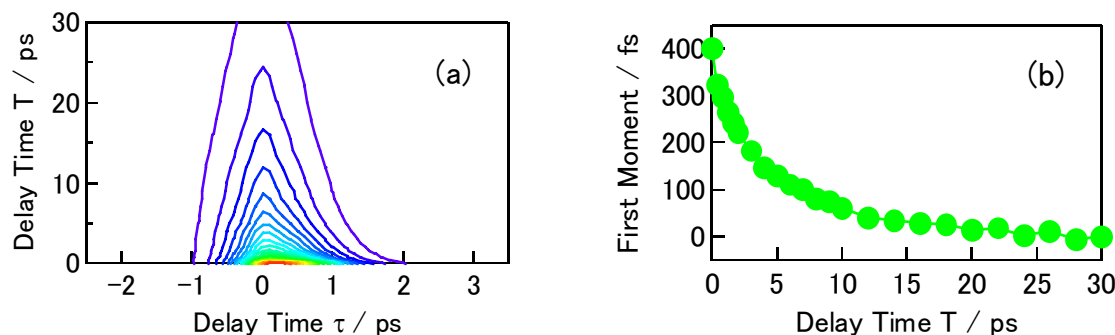
Figure 3. (a) Three pulse photon echo signals plotted against the delay times τ and T for SCN$^-$ in dimethylformamide. (b) The first moment of the photon echo signals calculated from the experimental data.

1   M. Li, J. Owrutsky, M. Sarisky, J. P. Culver, A. Yodh and R. M. Hochstrasser, J. Chem. Phys., **1992**, 98, 5499-5507

2   K. Dahl, G. M. Sando and J. C. Owrutsky, J. Chem. Phys., **2005**, 123, 084504/1-084504/11

3   P. Hamm, M. Lim and R. M. Hochstrasser, Phys. Rev. Lett., **1998**, 81, 5326-5329

4   A. Morita and S. Kato, J. Chem. Phys., **1998**, 109, 5511-5523

5   S. Li, J. R. Schmidt, A. Piryatinski, C. P. Lawrence and J. L. Skinner, J. Phys. Chem. B, **2006**, 110, 18933-18938

6   K. Ohta and K. Tominaga, Bull. Chem. Soc. Japan, **2005**, 78, 1581-1594

7   K. Ohta and K. Tominaga, Chem. Phys. Lett., **2006**, 429, 136-140

Vibrational Dynamics of the CO Stretching of Fluorenone in Various Alcohols

S. Hirai[1], M. Banno[2], K. Ohta[1], D. K. Palit[4], and K. Tominaga[1,2,3]

[1] Graduate School of Science and Technology and [2] Molecular Photoscience Research Center, Kobe University

[3] CREST/JST, 1-1, Rokkodai-cho, Nada-ku, Kobe 657-8501, Japan

[4] Radiation & Photochemistry Division, Bhabha Atomic Research Center, Mumbai 400 094, India

e-mail, Tominaga; tominaga@kobe-u.ac.jp

Hydrogen bonds play an important role in determining stability of three-dimensional structures of many chemical complexes and biological macromolecules.[1] In these hydrogen-bonded complexes various dynamical features such as reactivity and energy relaxation are strongly influenced by intramolecular hydrogen bonds as well as intermolecular ones. Among them, effect of hydrogen bond on vibrational energy relaxation has been recently investigated by time-resolved infrared (IR) spectroscopy.[2] For example, the OH stretching mode of alcohols or water shows a significant red shift of about 300 cm^{-1} when they form hydrogen bond with other molecules, and the vibrational energy relaxation of the OH stretching mode is accelerated by more than one order of magnitude.[3] In this work we focus on the hydrogen bond effect on the vibrational relaxation of the CO stretching mode.

The carbonyl molecule chosen for the present study is 9-fluorenone (FL), which is a planar molecule with a rigid framework. The photophysical properties of FL are well studied,[4] and in alcohol solutions the excited state dynamics is strongly affected by hydrogen bonding interaction with the solvent molecules. We have studied the vibrational energy relaxation of the CO stretching mode of FL in non-hydrogen bonding solvent and in alcohol by sub-picosecond IR pump-probe spectroscopy to investigate the hydrogen-bonding effect on the vibrational energy relaxation.

Details of the IR pump-probe apparatus will be described elsewhere.[5] Briefly, a home-built optical parametric amplifier and difference frequency generator, which are pumped by a Ti:sapphire regenerative amplifier, delivers a short pulse in the IR region with a pulse width of about 150 fs. The output pulse was divided into three, pump, probe, and reference pulses. The probe and reference pulses were detected by a 32 channel array detector after passing through the monochromator. The sample was contained in a cell with an optical path length of 0.1 mm and CaF$_2$ windows. 9-fluorenone was purchased from Sigma-Aldrich and used after recrystalized from ethanol. The solvents, cyclohexane (Wako) and 1-octanol (Wako) were used without further purification. The measurements were done at room temperature (20   ) if it is not specified.

Figure 1 shows IR absorption spectrum of 9-fluorenone (FL) in cyclohexane, a non-hydrogen bonding solvent. The CO stretching mode of FL shows a sharp band in cyclohexane with a peak wavenumber of 1725 cm^{-1} and fwhm of 4.5 cm^{-1}. The IR absorption spectrum of FL in 1-octanol is superimposed in Figure 1. The spectrum shows pronounced structures with two peaks at around 1713 cm^{-1} and 1721 cm^{-1}, and a shoulder at around 1700 cm^{-1}. In other alcohol solvents such as 1-propanol or 1-butanol (not shown in the figure), similar spectral shapes
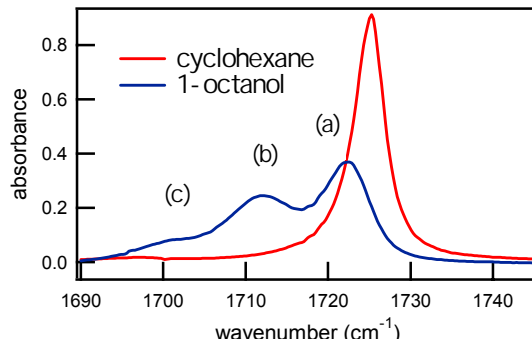
Figure 1. Absorption spectra of 9-fluorenone in cyclohexane (red) and in 1-octanol (blue). The concentrations are 25 mM.

with three bands were observed though the relative intensities of the three bands depend on the alcohol.

We have obtained optimized geometries and normal mode coordinates and their frequencies of the free FL and complexes in gas phase by performing DFT calculation with a basis set of 6-31++G(d) using B3LYP functional. We chose methanol as an alcohol. The oxygen atom has two lone pairs which act as hydrogen bonding sites, and there are two possible hydrogen-bonding complexes with one and two methanol molecules. The wavenumber of the CO stretching vibration of free FL is 1784 cm^{-1}, and those of FL:MeOH and FL:(MeOH)$_2$ are 1761 cm^{-1} and is 1736 cm^{-1}, respectively. The results show that the peak shifts to the lower frequency side by forming complexes. Therefore, we assign the observed bands in the IR spectrum to different complexes of FL and solvent molecules, that is, the (a), (b) , and (c) bands correspond to free FL, FL and one alcohol complex, and FL and two alcohol complexes, respectively.

Figure 2 displays the temperature dependence of the spectrum of FL in 1-octanol from 296 K to 332 K. The relative intensities of the three bands at 1713 cm^{-1} 1721 cm^{-1}, and 1700 cm^{-1} depend on the temperature. With increase of the temperature, the intensities of the bands at 1713 cm^{-1} and 1700 cm^{-1} decreases, while that at 1723 cm^{-1} increases. Consequently, the spectral intensity at 1718 cm^{-1} is nearly isosbestic. This indicates that the three bands result from three different species in equilibrium and not from intramolecular effect such as Fermi resonance, supporting the assignment of the spectral component.

Figure 2. Tenperature dependence of the absorption spectrum of 9-fluorenone in 1-octanol.

Figure 3 displays the IR pump-probe signal of FL in cyclohexane at 1727 cm^{-1}, which is close to the peak wavenumber. The signal corresponds to the recovery of the ground state bleach and the decay of the stimulated emission. The signal shows a sharp spike at around $t = 0$ ps, which we assign to a coherent artifact. For all the pump-probe signals investigated in this work, we fit the time profile of the signal from the delay time of 0.30 ps. After $t = 0.30$ ps, the signal decays exponentially with a time constant of 4.07±0.07 ps. As for the measurement of

Figure 3. IR pump-probe signal of 9-fluorenone in 1-octanol. A blue line is a fit by a single exponential.

vibrational energy relaxation of the CO stretching mode in non-hydrogen bonding solvents, Lim and Hochstrasser studied the CO stretch of methylacetate in carbon tetrachloride.[6] The signal decay was fitted well by a biexponential function with time constants of 0.23 ps and 8.2 ps.

Figure 4(a) shows a pump-probe signal at 1723 cm^{-1} that is close to the peak of the CO stretching vibration of the free FL. The signal decays exponentially with a time constant of 5.00±0.14 ps. The time constant is similar to that in cyclohexane. On the other hand, the left figure is the pump-probe signal at 1712 cm^{-1}, closed to the peak of the CO stretching vibration of the FL:(1-octanol) complex. The signal decays exponentially with a time constant of 2.45±0.09 ps. The fact that both the signals at 1723 cm^{-1} and 1712 cm^{-1} can be reproduced

well with a single exponential suggests that at these wavenumbers a single species is selectively probed by the IR pulse. In other words, the pump-probe signals do not reflect dynamics of a mixutre of different chemical species in equilibrium. This is true only when the interconversion between these species is not fast, which will be discussed later.

The mechanism that speeds up the vibrational relaxation by hydrogen bond formation has been often discussed in terms of Fermi Golden Rule. Namely, the transition rate is determined by density of states, coupling strength, and energy gap. The formation of hydrogen bond could influence all the three factors. For example, the OH stretching of water shows a red shift of about 300 cm^{-1} by hydrogen bond formation, that facilitates coupling with overtone of the bending mode. In the present case, the energy shift due to the bond formation is about 10 cm^{-1}, and it is not likely that the energy gap change is a major effect of the change of the vibrational relaxation time. Rather than that, the increase of the density of states may be a cause for this acceleration of the relaxation. The DFT calculation shows that there are intermolecular vibrational modes with frequencies of 15 cm^{-1}, 37 cm^{-1} and 49 cm^{-1} for the FL:methanol complex, which may be accepting modes in the relaxation process.

Finally, we make a brief comment on the hydrogen bond making and breaking dynamics of the complexes. The hydrogen-bonded complexes may interconvert rapidly in

Figure 4. IR pump-probe signals of 9-fluorenone in 1-octanol at 1723 cm^{-1} (a) and 1712 cm^{-1} (b). Blue lines are fits by a single exponential.

both the vibrationally excited and ground states. The fact that the time constant of the 1:1 and 1:2 complexes have different values indicates that the interconversion between the two conformers is not faster than vibrational relaxation of the two complexes. If it is faster, the average lifetime would be observed. It should be also noted that the interconversion rate should be smaller that the inverse of the frequency difference between the two peaks of about 10 cm^{-1}, consequently, the motional narrowing is not occurred. Woutersen *et al*. investigated equilibrium dynamics of hydrogen bond of *N*-methyl-acetamide (NMA) dissolved in methanol-*d*$_4$ by two-dimensional vibrational spectroscopy.[7] For this particular solute-solvent system, roughly equal populations are found for two conformers of the solute-solvent complex, one of which forms a hydrogen bond from the CO of NMA to the surrounding solvent, and the other does not. They concluded that the formation and breaking of the hydrogen bond occurs on a time scale of 10-15 ps.[7]

1   C. L. Perrin, J.B. Nielson, Annu. Rev. Phys. Chem., **1997,** 48, 511.
2   E.T.J. Nibbering, T. Elsaesser, Chem. Rev., **2004**, 104 1887.
3   K. Ohta, K. Tominaga, submitted.
4   V. Samant, A. K. Singh, G. Ramakrishna, H.N. Ghosh, T.K. Ghanty, D.K. Palit, J. Phys. Chem. A, **2005**, 109, 8693.
5   M. Banno, K. Ohta, K. Tominaga, to be submitted.
6   M. Lim, R. M. Hochstrasser, J. Chem. Phys., **2001**, 115, 7629
7   S. Woutersen, Y. Mu, G. Stock, P. Hamm, Chem. Phys., **2001**, 266, 137.

Vibrational population relaxation of hydrogen-bonded phenol in solution studied by ultrafast infrared pump-probe spectroscopy

Kaoru Ohta [1], Keisuke Tominaga [1, 2]

[1] Graduate School of Science and Technology, Kobe University, Nada-ku, Kobe 657-8501, JAPAN
[2] Molecular Photoscience Research Center, Kobe University, CREST/JST, Nada-ku, Kobe 657-8501, JAPAN
E-mail address kohta@kobe-u.ac.jp

A great deal of effort has been devoted to study the structural and dynamical properties of hydrogen-bonded molecular complexes both in the gas and condensed phase because hydrogen bonds play an important role in many chemical and biological systems. Infrared (IR) spectroscopy is one of the most powerful methods to study both structure and dynamics of such a complex. In particular, it is well known that the frequency of the OH stretching mode is very sensitive to the strength and type of hydrogen bond. Extensive studies using ultrafast IR spectroscopy have been performed to study the vibrational population relaxation and spectral diffusion process for hydrogen bonded systems by probing OH or NH stretching modes.[1] However, most of such studies so far have focused mainly on the vbirational dynamics of rather simple systems such as water and methanols. It is very interesting to extend the studies of the vibrational dynamics of larger systems with complex structures. We expect to obtain insight into the role of the hydrogen bonding dynamics in the vibrational population relaxation in such systems.

In this contribution, we investigated the vibrational population relaxation of the OH stretching mode of hydrogen-bonded phenol complexes with a couple of bases (benzonitrile, acetone, diethylether, and tetrahydrofuran) in carbon tetrachloride (CCl_4) by ultrafast IR pump-probe spectroscopy. By using different bases which act as a hydrogen-bond acceptor, we can change the strength of the hydrogen bond in the complex and thus investigate the influence on the vibrational dynamics in detail. We also studied the vibrational population relaxation of hydrogen-bonded phenol oligomers in CCl_4. In this study we focus on the probe freqeuncy dependence of the decay rates of the IR pump-probe signals for these hydrogen-bonded complexes. Femtosecond IR pump-probe measurements were performed with a broadband infrared light source (center freqenecy : 3300-3450 cm^{-1}) and frequency resolved detection.

Figure 1 displays the FT-IR spectra of phenol-benzonitrile in CCl_4. For phenol in CCl_4, we observed a sharp peak at 3610 cm^{-1}, which is attributed to the OH stretching mode of the phenol monomer. For phenol-benzonitrile solution, a new band appears at 3450 cm^{-1} and the

Figure 1. FT-IR spectrum of phenol (0.15 M)-benzonitrile (1.0 M) in CCl_4.

intensity of the monomer band decreases. This new band is attributed to the hydrogen-bonded phenol complex with benzonitrile. We performed IR pump-probe measurements on phenol-benzonitrile complex in CCl_4 by exciting the OH stretching mode of the complex (Figure 2). The pump-probe spectrum originates from the v=0-1 transition of the OH stretching mode and recovery of the bleach corresponds to the vibrational population relaxation from the v=1 state. From the decay of the pump-probe signals, we found that the vibrational population relaxation takes place on 5 ps time scale. The time

Figure 2. Transient absorption spectra of phenol-benzonitrile in CCl_4 at the time delay of 0.3, 1.0, 3.0, and 5 ps.

scale of the decay of the transient spectrum does not depend on the probe frequency.

We also measured the pump-probe signals for the other hydrogen-bonded complexes. The decay time constants of the pump-probe signals for phenol-acetone, phenol-diethylether and phenol-tetrahydrofuran complexes are about 1.4 ps, 1.3 ps and 1.0 ps, respectively. We found that the time scales of the vibrational population relaxation for these complexes are correlated with the strength of the hydrogen bond, i.e., a stronger hydrogen bond leads to a faster vibrational population relaxation. There are a couple of possible origins to explain the shortening of the lifetime of the OH stretching vibrations in hydrogen-bonded systems. First, the energy gap between the OH stretching mode and the combination tone of the accepting modes decreases as the hydrogen bond becomes stronger. The spectral overlap between these becomes larger in hydrogen-bonded phenol complexes compared with that observed for phenol monomer. Furthermore, hydrogen bond stretching vibrations and the lower frequency intramolecular vibrational modes, such as the OH bending mode, may contribute to the acceleration of vibrational population relaxation from the OH stretching mode.

We also studied the vibrational dynamics of hydrogen-bonded phenol oligomers in CCl_4. As increasing the concentration of phenol in CCl_4, broader bands peaked at around 3480 cm^{-1} and 3350 cm^{-1} are clearly observed, which indicates the formation of phenol oligomers. We can consider three types of OH groups for the assignment of observed bands in addition to the free OH group. Similarly to the assigment of methanol oligomers, an OH group which donates and accepts a hydrogen bond (δ type) has lower frequency than one donates, but does not accept hydrogen bond (γ type) [2,3]. We consider that a band at 3350 cm^{-1} is attributed to the δ type of OH group, while a band at 3480 cm^{-1} is γ type. The frequency of an OH group which accepts, but does not donate (β type) may be similar to that of free OH group. We measured the pump-probe signals for phenol oligomers in CCl_4 at different probe frequencies. For these measurements, we used two different IR pulses with different center frequencies. Above 3401 cm^{-1}, we used a pulse with a peak at around 3470 cm^{-1}, while below 3356 cm^{-1}, we used a pulse peaked at around 3380 cm^{-1}. At 3521 cm^{-1}, the transient signal decays with a time constant of 2.1 ps. As decreasing probe frequency, the decay of the transient signals becomes faster. At 3320 cm^{-1}, the decay time constant of the pump-probe signal is around 0.7 ps. In contrast to phenol-base complexes, the decay of the pump-probe signals of the OH stretching modes for phenol oligomers depends strongly on probe frequency. Furthermore, the remaining components was clearly observed on a picosecond time scale at a probe frequency of 3303 cm^{-1}.

Figure 3 displays the probe frequency dependence of the decay time constants of pump-probe signals for the OH stretching vibrations of hydrogen-bonded phenol complexes in CCl_4. For hydrogen-bonded phenol complexes with bases, we found that decay time does not depend significantly on probe frequency. We consider that the lack of the probe frequency dependence in the vibrational population relaxation times of phenol-base complexes results from rapid evolution among different conformations with different hydrogen-bond strengths. This rapid evolution causes fast fluctuation of the OH stretching frequency. The vibrational population relaxation times are averaged out over all conformations. We consider that in our

system, at least, a portion of spectral diffusion takes place faster than vibrational population relaxation. Therefore, some of the inhomogeneity due to possible conformations of hydrogen-bonded phenol complexes is destroyed by the fast fluctuation of the vibrational frequency of the OH stretching modes.

Figure 3. Plot of the vibrational relaxation rates vs. the probe frequency.

For hydrogen-bonded phenol oligomers in CCl_4, we found that the decay of the pump-probe signal depends strongly on the probe frequency, becoming faster as the probe frequency decreases. One possibility to explain this observation is that the vibrational population relaxation of the OH stretching mode of the δ-type phenol may take place faster than that of the γ type. The OH stretching frequency of δ-type molecule is lower than that of the γ type, and thus the energy gap between the OH stretching mode and the accepting mode is smaller, which leads to the faster vibrational population relaxation, similarly to phenol-base complexes. As clearly seen in the bleach components of the pump-probe signals at 3303 cm^{-1}, excitation of the OH stretching mode of the δ-type phenol molecule leads to dissociation of the hydrogen bonds. For phenol oligomers, it is likely that dissociation of hydrogen bonds competes with vibrational population relaxation of the OH stretching mode, because a bleach component at 3303 cm^{-1} appears in the early stage of the pump-probe signal. This may also be the reason in the probe frequency dependence of the vibrational population relaxation times. However, in our experimental results, it is difficult to separate the two contributions in the pump-probe signals, i.e., the decay of the initially excited OH stretching vibrations and the formation of photoproducts by dissociation of the hydrogen bonds. Further experiments are necessary to obtain detailed information on the vibrational dynamics of phenol oligomers.

In summary, we investigated the vibrational population relaxation of hydrogen-bonded phenol in solution using ultrafast IR pump-probe spectroscopy, and discussed the probe frequency dependence of the signals. For phenol-base complexes, rapid evolution among different conformations with different hydrogen-bond strength causes fast fluctuation of the OH stretching frequency, which averages out the vibrational population relaxation times among different conformations. In contrast, for hydrogen-bonded phenol oligomers, our results suggest that the vibrational population relaxation rate of the OH stretching mode in δ-type phenol molecules may be faster than that of the γ type. For hydrogen-bonded phenol oligomers, dissociation of hydrogen bonds competes with the vibrational population relaxation of the OH stretching mode. This may also be the cause of the frequency dependence of the pump-probe signal decay rates for phenol oligomers in solution.

1   E. T. J. Nibbering and T. Elsaesser, Chem. Rev., **2004**, 104, 1887-1914
2   J. R. Dixon, W. O. George, M. F. Hossain, R. Lewis and J. M. Price, J. Chem. Soc. Faraday Transactions, **1997**, 93, 3611-3618
3   K. J. Gaffney, P. H. Davis, I. R. Piletic, N. E. Levinger and M. D. Fayer, J. Phys. Chem. A, **2002**, 106, 12012-12023

Vibrational relaxation of OH and OD stretching of methanol
in isotopically diluted solutions

K. Ikeshima[1], M. Banno[2], K. Ohta[1], K. Tominaga[1, 2, 3]

[1] Graduate School of Science and Technology, Kobe University, Nada, Kobe 657-8501, Japan.

[2] Molecular Photoscience Research Center, Kobe University, Nada, Kobe 657-8501, Japan.

[3] CREST/JST, Nada, Kobe 657-8501, Japan.

e-mail: K. Tominaga, tominaga@kobe-u.ac.jp

The interactions and dynamics of hydrogen bonding liquids such as water and alcohol play an important role in chemical reactions and biological activities. Hydrogen bond forms a characteristic network structure of a finite size in such liquids. Hydrogen bonding liquids also form complexes with solute molecules, which perturbs the vibrational and electronic states of the solute. From a dynamical point of view, microscopic structures formed by hydrogen bonds fluctuate by collective motions. Furthermore, hydrogen bonds in liquids continuously repeat formation and breakage of the bonds. The hydroxyl stretching vibrations of alcohols are very sensitive to microscopic environment around the hydrogen bond, and the vibrational spectra of the mode are a good probe to investigate hydrogen bond dynamics.

Methanol is the simplest alcohol and is a model system to investigate static and dynamics effects of the hydrogen bond on the hydroxyl stretch.[1] Recently, the vibrational relaxation of the hydroxyl stretch of methanol has been measured by time-resolved vibrational spectroscopy.[2, 3, 4] For example, in carbon tetrachloride (CCl_4), methanol forms clusters, and infrared (IR) pump-probe experiments were conducted on the OH[2] and OD[3, 4] stretch of this system. Dlott and coworkers studied vibrational energy relaxation in pure methanol (CH_3OH) by IR pump-Raman probe technique.[5] It is found that lifetime of the hydroxyl stretch depends on the strength of the hydrogen bond; for isolated methanol, the vibrational relaxation times (T_1) is in a picosecond order,[6, 7] and it becomes shorter than 1 ps when it forms hydrogen bond.? In this work we have measured vibrational relaxation times of the OH and OD stretching in isotopically diluted methanols. Furthermore, we have studied isotope effects of the methyl group on the vibrational relaxations of the OH and OD stretching modes.

Details of the sub-picosecond IR pump-probe spectroscopy will be described elsewhere.[8] We obtained IR pulses by difference frequency mixing with signal and idler pulses in the near-IR region generated by a home-built optical parametric amplifier. The pulse duration of the IR pulse is approximately 200 fs. We split the IR pulse into pump, probe, and reference pulses with frequencies at a peak of the OH or OD stretching band. The probe and reference pulses were detected by an array detector after passing through a monochromator. Methanols (CH_3OH, CH_3OD, CD_3OH, and CD_3OD) were purchased from Sigma-Aldrich and used without further purification. We prepared the following four different isotopically diluted solutions; CH_3OH/CH_3OD, CD_3OH/CD_3OD, CH_3OD/CH_3OH, and CD_3OD/CD_3OH. The volume ratio of the solute and solvent is 1:19, and the samples were contained in a cell with an optical path length of 50 μm. The optical density was around 0.6 at the excitation wavenumber.

Figure 1 shows IR absorption spectra of the OH and OD stretching region of methanols in isotopically diluted solutions. The absorption spectra of the OH stretching mode have a peak at 3340 cm^{-1} with FWHM of 210 cm^{-1}, and the two spectra of the CH_3OH/CH_3OD and CD_3OH/CD_3OD systems are identical with each other. The spectrum of the OD stretch, on the other hand, has a narrower spectral width of about 140-150 cm^{-1}. The CH_3OD/CH_3OH system shows a shoulder at around 2450 cm^{-1}, which was attributed to Fermi resonance with an overtone of the methyl rocking mode.[9]
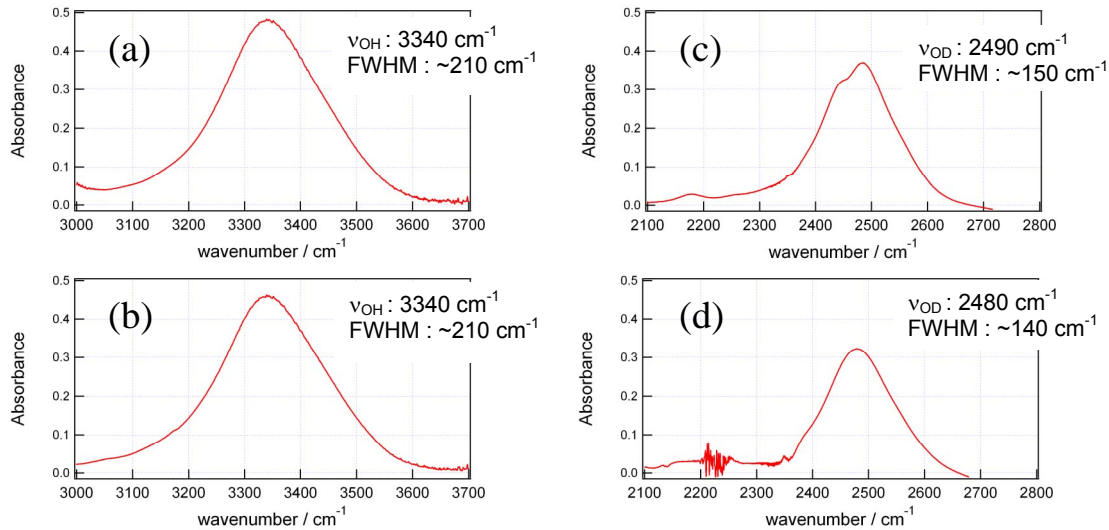
Figure 1. Absorption spectra of (a) CH_3OH/CH_3OD, (b) CD_3OH/CD_3OD, (c) CH_3OD/CH_3OH, and (d) CD_3OD/CD_3OH. Peak frequencies and FWHM are shown in the figure.
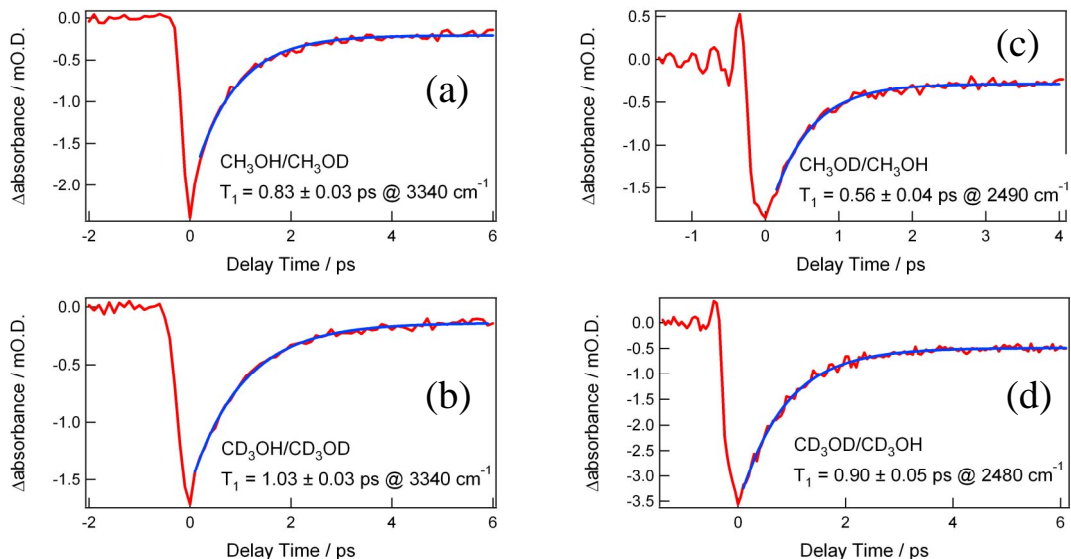
Figure 2. Pump-probe signals of (a) CH_3OH/CH_3OD, (b) CD_3OH/CD_3OD, (c) CH_3OD/CH_3OH, and (d) CD_3OD/CD_3OH. Vibrational relaxation times (T_1) and excitation wavenumbers are shown in the figure. Blue curves are results of fitting by a single exponential function.

Figure 2 shows the pump-probe signals of the four systems. The time profiles of the signals were fitted well by a single exponential function ($A_1\exp(-t/T_1)+A_0$). To avoid complication due to coherent artifact at around $t = 0$ ps, we fitted the time profiles of the signal from $t = 0.20$ ps. A small offset A_0 at long delay times has been often observed in other systems such as ethanol[10], which was attributed to be a cooling process of the locally heated environment.

The CH_3OD/CH_3OH system shows the fastest decay of the pump-probe signal. This is because strong Fermi resonance with other modes enhances the relaxation process. Consequently, it is suggested that the pathway of the vibrational energy relaxation after the excitation of the OD stretch of CH_3OD is different from the hydroxyl stretches of the other isotopically substituted methanols. In CCl_4, Fayer and coworkers observed a decay of the OD stretching mode of CH_3OD with a similar time constant.[3]

The vibrational relaxation of the OH stretching mode of CH_3OH takes place about 20% faster than that of the OH stretch of CD_3OH. This fact suggests mechanism of the energy

relaxation of the OH stretching mode. Dlott and coworkers performed IR-pump and Raman-probe experiment on methanol to study energy relaxation pathways.[6] They excited the hydroxyl stretch by an intense IR pulse and probed time dependence of other vibrational modes by Raman scattering. They observed an instantaneous rise of the other vibrational modes such as $\nu(CH_3)$, $\delta(CH_3)$, $\delta(COH)$, $\gamma(CH_3)$, and $\nu(CO)$ modes within the time resolution of their setup of 1 ps, leading to a conclusion that intramolecular process is important for the vibrational energy relaxation. Our observation is consistent with their conclusion. For example, a combination band of $\delta(CH_3)$ and $\delta(COH)$ can be one of the accepting modes for the energy relaxation of the OH stretch. The frequency of this combination band is about 2900 cm^{-1} for CH_3OH and 2400 cm^{-1} for CD_3OH, resulting in a larger energy gap from the OH stretching mode by deuteration of the methyl group. The intramolecular isotope effect on the vibrational relaxation in methanol can be rationalized in terms of Fermi golden rule in a qualitative level.

Figure 3 displays pump-probe signals measured at different probe wavenumbers. The time constants of the decay monotonically increase as the probe frequency shifts to a higher side. A variation in the decay with wavelength has been discussed in terms of a wavelength-dependent population relaxation rate, where the population decay becomes faster as the wavelength is moved to the red.[2,11] Asbury *et al*. observed frequency-resolved pump-probe spectra of 10% CD_3OD in CCl_4.[4] They mentioned that the excited state lifetimes of the oligomers are wavelength independent. They pointed out that the time profiles of the signal are influenced by hydrogen bond breaking dynamics as well as the excited state lifetime, so that the initial decay seems to be wavelength dependent in their data. Their frequency-time contour plots of spectrally resolved pump-probe data are similar to our plots for CD_3OD/CD_3OH in a qualitative level (our contour plots are not shown here). By the kinetic model they proposed to include all these effects in the pump-probe data, they reproduced

Figure 3. Pump-probe signals of CD_3OD/CD_3OH probed at (a) 2470 cm^{-1}, (b) 2510 cm^{-1}, and (c) 2550 cm^{-1}. Vibrational relaxation times (T_1) are show in the figure. Blue lines are results of fitting by a single exponential function.

the contour plot very well. Therefore, similar dynamics such as hydrogen bond breaking may influence the pump-probe data in the system of CD_3OD/CD_3OH.

[1] T. Uemura, S. Saito, Y. Mizutani, K. Tominaga, *Mol. Phys.,* **2005,** 103, 37.

[2] R. Leanen G. M. Gale, N. Lascoux, *J. Phys. Chem. A*, **1999,** 103, 10708.

[3] K. J. Gaffney, P. H. Davis, I. R. Piletic, N. E. Levinger, and M. D. Fayer, *J. Phys. Chem. A*, **2002**, 106 12012.

[4] J. B. Asbury, T. Steinel, C. Stromberg, K. J. Gaffney, I. R. Piletic, and M. D. Fayer, *J. Chem. Phys.*, **2003**, 119, 12981.

[5] L. K. Iwaki, Dana D. Dlott, *J. Phys. Chem. A*, **2000,** 104, 9101.

[6] R. Leanen and K. Simeonidis, *Chem. Phys. Lett*., **1999,** 299, 589.

[7] N. E. Levinger, P. H. Davis, and M. D. Fayer, *J. Chem. Phys.*, **2001**, 115, 9352.

[8] M. Banno, K. Ohta, K. Tominaga, to be submitted.

[9] J. E. Bertie, S. L. Zhang, *J. Mol. Struct*., **1997** 413-414 333

[10] S. Woutersen U. Emmerichs, H.J. Bakker, *J. Chem. Phys*., **1997** 107 1483

WATER

Ultrafast Structural Dynamics of Liquid H_2O Probed by Vibrational Excitations

T. Elsaesser, S. Ashihara, N. Huse, A. Espagne, E.T.J. Nibbering

Max-Born-Institut für Nichtlineare Optik und Kurzzeitspektroskopie, Max-Born-Str. 2 A, 12489 Berlin, Germany, elsasser@mbi-berlin.de, http://www.mbi-berlin.de

In the liquid phase, water molecules form a disordered network of intermolecular hydrogen bonds. This equilibrium structure fluctuates on femto- to picosecond time scales, involving multiple molecular rearrangements, the breaking and the reformation of hydrogen bonds. Most experimental probes of water structure such as neutron scattering[1], x-ray diffraction[2] and x-ray absorption[3,4] average over these fluctuations in space and time, thus giving limited insight into the elementary microscopic dynamics. In contrast, femtosecond vibrational spectroscopy provides direct information on transient local structure and allows to separate molecular interactions underlying structural fluctuations and changes[5].

So far, femtosecond vibrational spectroscopy of neat H_2O has mainly concentrated on intramolecular water vibrations, i.e., the OH stretching[6,7] and – to much lesser extent – the OH bending mode[8,9]. The OH stretching band (Fig. 1) of liquid H_2O is red-shifted and substantially broadened compared to the OH stretching absorption of water monomers. Such changes originate from the attractive hydrogen bonding interactions, resulting in a lowering of the vibrational (v=0 to 1) transition frequency via an enhancement of the diagonal anharmonicity of the OH stretching oscillator and a broadening due the distribution of hydrogen bond strengths and vibrational dephasing. Structural fluctuations in the network of hydrogen bonded molecules and the resulting fluctuating forces lead to a fast sweep of OH stretching transition frequencies, i.e., spectral diffusion. The time scale of and the mechanisms behind spectral diffusion have been uncovered recently by measuring two-dimensional (2D) OH stretching spectra of neat water[10,11]. Under ambient conditions, the initial inhomogeneous broadening of the vibrational spectra is washed out on a 50 to 100 fs time scale, due to local structural fluctuations originating from librational excitations. In addition, the resonant transfer of OH stretching quanta between water molecules on a 100 fs time scale contributes to the loss of the initial spectral correlations. Such processes occur well within the v=1 lifetime of the OH stretching oscillator of 200 fs. The OH bending mode displays a v=1 lifetime of 170 fs[8]. Its v=2 state is in Fermi resonance with the v=1 state of the OH stretching mode[9].

The population decay of the intramolecular modes is connected with a transfer of excess energy into the hydrogen bond network and a subsequent redistribution over many molecules. Here, we present evidence for a two-stage structural response of the network to energy disposal by monitoring the transient librational and OH bending absorption in a wide

[1] A. K. Soper, Chem. Phys. **2000,** 258, 121.

[2] T. Head-Gordon, G. Hura, Chem. Rev. **2002**, 102, 2651.

[3] P. Wernet *et al.*, Science **2004**, 304, 995.

[4] J. D. Smith, C. D. Cappa, K. R. Wilson, B. M. Messer, R. C. Cohen, R. J. Saykally, Science **2004**, 306, 851.

[5] E.T.J. Nibbering, T. Elsaesser, Chem. Rev., **2004**, 104, 1887.

[6] A. Pakoulev, Z. Wang, D.D. Dlott, Chem. Phys. Lett. **2003**, 371, 594.

[7] A.J. Lock, H.J. Bakker, J. Chem. Phys. **2002**, 117, 1708.

[8] N. Huse, S. Ashihara, E.T.J. Nibbering, T. Elsaesser, Chem. Phys. Lett. **2005**, 404, 389.

[9] S. Ashihara, N. Huse, E.T.J. Nibbering, T. Elsaesser, Chem. Phys. Lett. **2006**, 424, 66.

[10] M. L. Cowan, B. D. Bruner, N. Huse, J. R. Dwyer, B. Chugh, E. T. J. Nibbering, T. Elsaesser, R. J. D. Miller, Nature, **2005,** 434, 199.

[11] D. Kraemer *et al.*, Proc. TRVS XIII
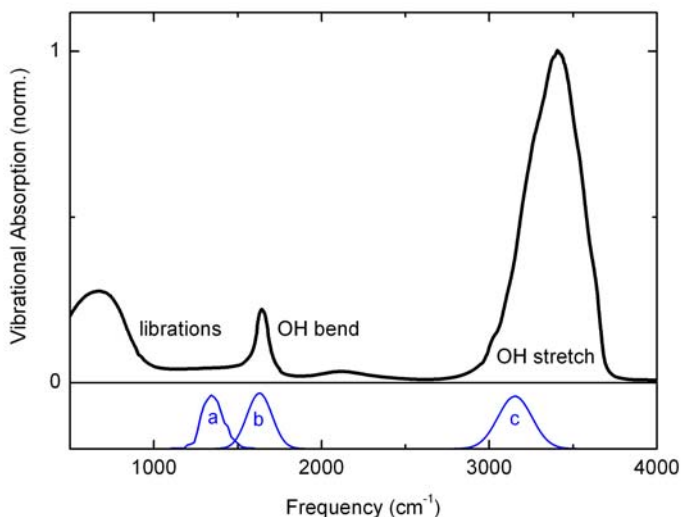
Figure 1. Infrared absorption spectrum of liquid H_2O (black solid line, sample temperature 300 K). In addition to the (intramolecular) OH stretching and OH bending absorption, the spectrum displays the librational L2 band with a maximum at 670 cm^{-1}, an extended librational absorption between 800 and 1700 cm^{-1} and the combination band of the OH bending mode and low-frequency librations with a maximum at 2100 cm^{-1}. The lower panel shows spectra of femtosecond pump pulses used in the different measurements.

spectral range from 550 to 1700 cm^{-1}. Vibrational energy is transferred from excited water molecules to intermolecular modes, resulting in a sub-100 fs nuclear rearrangement that leaves the local hydrogen bonds weakened but unbroken. Subsequent energy delocalization over many molecules occurs on a ~1 ps time scale and is connected with the breaking of hydrogen bonds, resulting in a macroscopically heated liquid.

In our experiments with a 100 fs time resolution, we measure transient infrared spectra of intermolecular librational modes and the intramolecular OH bending vibration in a very broad frequency range from 550 to 1700 cm^{-1} after excitation of three different modes, namely (a) high-frequency librations, (b) the OH bending mode, and (c) the OH stretching mode (cf. lower panel in Fig. 1)[12]

$_3N_4$ windows of a nanofluidic water cell[10,11] or prepared as a water film flowing between two stainless steel wires of a lateral separation of 1 cm.

In Fig. 2, we present data measured with excitation at E_{ex}=1350 cm^{-1} [spectrum (a) in Fig. 1] and E_{ex}=3150 cm^{-1} [spectrum (c) in Fig. 1]. Upon excitation of high-frequency librations (E_{ex}=1350 cm^{-1}), the L2 band with maximum absorption at 670 cm^{-1} displays a pronounced shift to lower frequency (Fig. 2b) which builds up on a sub-100 fs time scale. This fast rise is followed by a slower ~1 ps component (Fig. 2d). In contrast, the concomitant red-shift of OH bending absorption exclusively displays the ~1 ps component (Fig. 2e). The transient spectra measured with OH stretching excitation (Fig. 2c) exhibit a similar behavior. However, the red-shift of the L2 absorption shows a delayed initial rise followed by the 1 ps component (Fig. 2f).

The L2 librations are a sensitive probe of water structure. Their force constants are determined by the geometries and the strengths of intermolecular hydrogen bonds. The red-shift of the L2 band in the transient spectra thus reflects a softening of the intermolecular

---

[12] S. Ashihara, N. Huse, A. Espagne, E.T.J. Nibbering, T. Elsaesser, J. Phys. Chem. A **2007**, <u>111</u>, 743.
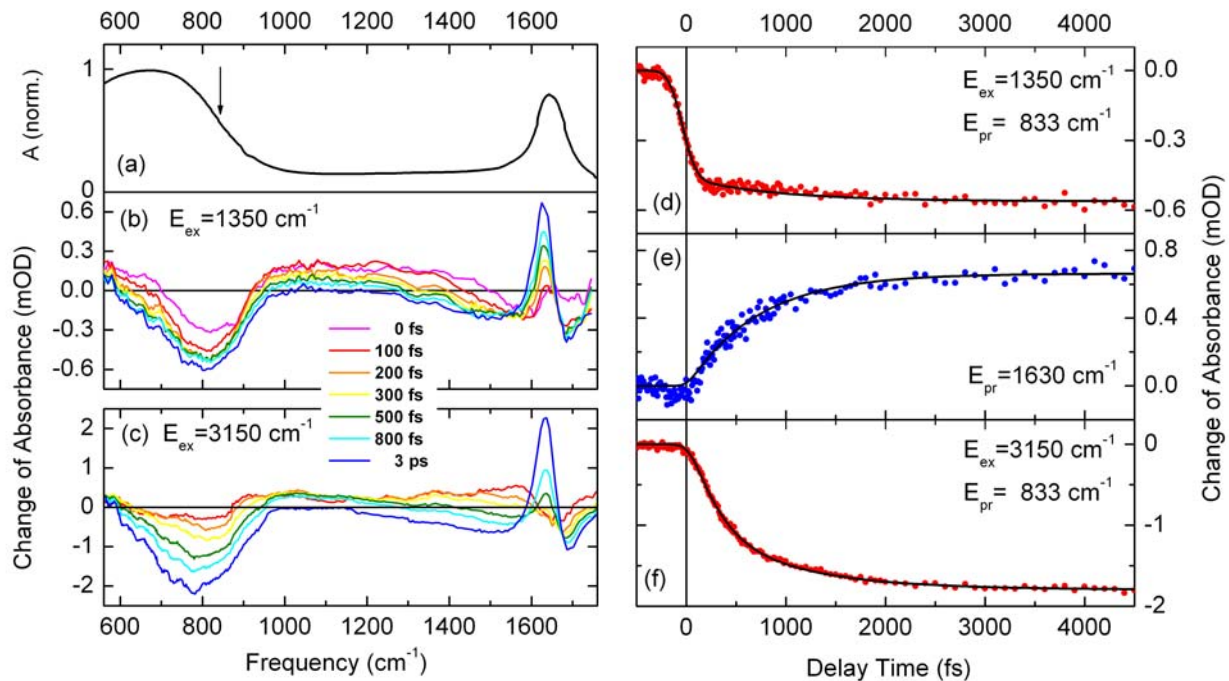
Figure 2. (a) Infrared absorption of neat water consisting of the librational L2 band with maximum at 670 cm^{-1} and the OH bending absorption with maximum at 1650 cm^{-1}. (b) Transient vibrational spectra after excitation of high-frequency librations at E_{ex}=1350 cm^{-1}. The change of absorbance ΔA=-log(T/T$_0$) is plotted versus probe frequency for different time delays after excitation (T, T$_0$: sample transmission with and without excitation). (c) Transient vibrational spectra after excitation of the OH stretching mode at E_{ex}=3150 cm^{-1}. (d,e) Time evolution of the absorbance changes at E_{pr}=833 cm^{-1} in the L2 band (cf. arrow in Fig. (a)) and E_{pr}=1630 cm^{-1} after excitation at E_{ex}=1350 cm^{-1} (symbols: data, solid lines: numerical fits). (f) Time dependent absorbance change at E_{pr}=833 cm^{-1} after excitation at E_{ex}=3150 cm^{-1}. Note the pronounced delay of the initial rise compared to Fig. (d).

vibrational potential due to a weakening of intermolecular hydrogen bonds. Such weakening originates from the transfer of excess energy from the initial vibrational excitation into the hydrogen bond network. The initial excitation at E_{ex}=1350 cm^{-1} decays within 100 fs[8] and the L2 red-shift builds up on the same time scale (Fig. 2d). It is important to note that the red-shift and the underlying change of hydrogen bond structure occur on a time scale set by librational periods, well below the average lifetime of a hydrogen bond of ~1 ps[13]. Thus, the initial energy transfer weakens the local hydrogen bonds, e.g., via an increase of bond length and angle, but leaves them unbroken.

The OH stretching excitation at E_{ex}=3150 cm^{-1} decays stepwise via the OH bending mode: in a first step, the v=1 state of the excited OH stretching oscillator decays to the v=1 bending state with the energy difference being transferred to the surrounding. The energy transfer occurs with the v=1 lifetime of 200 fs. In a second step, the v=1 decay of the OH bending oscillator with a 170 fs lifetime transfers a second OH bending quantum of energy to the hydrogen bond network. The rise of the librational red-shift in Fig. 2f is determined by this sequential 2-step energy transfer with an overall rise time given by the sum of OH stretching and bending lifetimes. This analysis is confirmed by kinetics calculated from a rate equation model using the lifetimes of the v=1 states and a slower ~1 ps component (solid line in Fig. 2f).

---

[13] D. Laage, J.T. Hynes, Science **2006**, _311_, 832.

The spectral position of the OH bending absorption is quite insensitive to a change in hydrogen bond strength[14]. This band, however, undergoes a red-shift whenever hydrogen bonds are broken, i.e., defects are formed in the hydrogen bond network[15]. The transient spectra in Figs. 2b,c display such a red-shift at longer delays, demonstrating that eventually the number of broken hydrogen bonds increases. The related kinetics is most evident from the data in Fig. 2e measured with librational excitation at an energy $E_{ex}=1350$ cm^{-1}, below the OH bending absorption. Under such conditions, the OH bending oscillators remain unexcited and the absorbance change reflects the red-shift of the v=0 to 1 transition. This red-shift builds up with a ~1 ps time constant, close to the hydrogen bond lifetime, and remains constant after several picoseconds when the liquid is heated macroscopically. The transients in Figs. 2d,f display similar kinetics at longer delay times. We conclude that the delocalization of energy over many molecules is connected with the breaking of hydrogen bonds somewhere in the hydrogen bond network, in this way establishing an enhanced 'defect density' in the network that is characteristic for its elevated temperature[15].

In conclusion, our results give the first direct insight into the structural aspects of energy dissipation and delocalization in liquid water. They underline the key role of librational degrees of freedom for both the loss of local structural correlations and ultrafast energy dissipation.

---

[14] J.E. Bertie, M.K. Ahmed, H.H. Eysel, J. Phys. Chem. **1989**, 93, 2210.
[15] G.E. Walrafen, M.S. Hokmabadi, W.H. Yang, J. Phys. Chem. **1988**, 92, 2433.

Femtosecond mid-infrared spectroscopy on liquid-to-supercritical water: Vibrational energy relaxation versus spectral diffusion

D. Schwarzer[1], J. Lindner[2], P. Vöhringer[2]

[1] Max-Planck-Institute for biophysical Chemistry, Am Fassberg 11, 37077 Göttingen, Germany, and [2] Institute for Physical and Theoretical Chemistry, University of Bonn, Wegelerstraße 12, 53115 Bonn, Germany.

Liquid water exhibits an intriguing hydrogen bond (H-bonds) network, which is structurally and dynamically highly random in nature. Breakage and formation of H-bonds continuously interconvert local H-bonded structures on a variety of time scales and result in spectral diffusion within the intramolecular vibrational resonances of the liquid. To disentangle the two fundamental vibrational dynamics, i.e. vibrational energy relaxation (VER) on one hand and vibrational spectral diffusion (VSD) on the other, we performed fs-mid-IR pump-probe spectroscopy on the OH-stretching mode of HOD in D_2O over wide ranges of pressure and temperature corresponding to the liquid and the supercritical phase of the solution.[1,2]
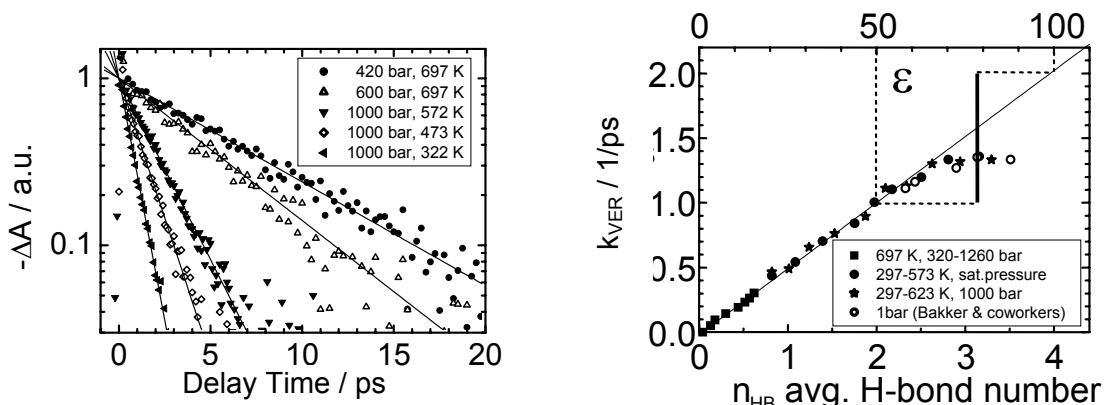
Fig. 1. Left panel: Normalized transient absorption signals of HOD in D_2O. Right panel: OH-stretch relaxation rate constant of HOD versus the dielectric constant of D_2O (top axis) and the average number of hydrogen bonds per HOD molecule as derived from MD simulations [3].

Several pump-probe transients for representative pairs of temperature T and density ρ are displayed in Fig. 1 (left panel), where the negative pump-induced optical density is plotted semi-logarithmically versus the pump-probe time delay. The displayed data were taken with a probe frequency located in the transient bleach region, an excitation bandwidth of 120 cm^{-1} and the relative pump-probe polarization set to the magic angle. Within our time resolution (200 fs), the ground-state bleach was found to recover strictly mono-exponentially at temperatures above 400 K. Under these conditions the anharmonically red-shifted excited state transient absorption behaves as a mirror image of the ground-state bleach and yields within the experimental accuracy identical time constants. Transient differential transmission spectra display a characteristic isosbestic point which separates excited-state absorption from ground state bleach. The observation of an isosbestic wavelength above 400 K suggests that under such conditions the spectral diffusion dynamics must be much faster than those of vibrational energy relaxation. Furthermore, spectral diffusion obviously proceeds on considerably shorter time scales as compared to room temperature. The vibrational relaxation rate constants, $k_{VER} = 1/\tau_r$, are determined by fitting single exponential decays to the data. Our

---

[1] D. Schwarzer, J. Lindner, P. Vöhringer, J. Chem. Phys. **2005**, 123, 161105.
[2] D. Schwarzer, J. Lindner, P. Vöhringer, J. Phys. Chem. A **2006**, 110, 2858.

surprising experimental results complement previous fs-mid-IR pump-probe[3] and 2D-IR studies[4], which were preformed on the same system under atmospheric pressure only.

We correlate our experimentally determined VER rate constants with the pressure and temperature dependent dielectric constant, $\varepsilon(T,p)$, of fluid D_2O. Recent molecular dynamics simulations suggest that $\varepsilon(T,p)$ can be taken as a measure of the average H-bond connectivity within the random D_2O network[5]. As Figure 2 demonstrates impressively, a strict linear correlation exists between these two independently determined experimental quantities, i.e. k_{VER} on the one hand and $\varepsilon(T,p)$ on the other. Only for $\varepsilon > 70$, the data seem to level off at a constant value for kr of 1.4 ps-1. Also shown in this figure are temperature dependent rate constants obtained by Bakker et al.[67] for the liquid at 1 bar (open symbols), which are in good agreement with our results. The thick bar assigns the range of relaxation rates reported in the literature from experiments carried out under ambient conditions.

Based on such a correlation, it is possible to demonstrate that the nature of the apparent pump-probe decays changes as the temperature of the liquid is lowered. We simplify the competition between spectral diffusion and vibrational energy relaxation in a kinetic scheme that decomposes OH oscillators in the D_2O bath into two subensembles denoted W_2 and W_4. The former represents those hydroxyls that undergo slow vibrational relaxation with rate constant k_2 and may be associated with doubly-coordinated HOD particles. The latter corresponds to OHs that rapidly relax with rate constant k_2 and could be viewed as 4-fold coordinated HOD molecules. Interconversion between the two sub-ensembles occurs with a rate constant k_D which equals the sum of the rate constants, k_{24} and k_{42}, for the forward and backward reactions. These dynamics are responsible for spectral diffusion and are brought about by breakage and formation of hydrogen bonds. Assuming identical forward and backward rates and hence, an equilibrium constant of unity for the $W_2 - W_4$ interconversion, we can ascertain that the number of hydrogen bonds per molecule on average is $n_{HB} = 3$. Such a kinetic model can be solved analytically and generally leads to non-exponential decays of the individual vibrationally excited sub-ensembles. Whereas the short time dynamics of the OH-stretch population decay strongly depends on which sub-ensemble is excited by the pump and monitored by the probe pulse, the long time decay rate constant is then given by the expression

$$k_{VER} = \frac{k_2 + k_4}{2} + \frac{k_d + \sqrt{(k_2 - k_4)^2 + k_D^2}}{2}$$

In the high-temperature limit, when spectral diffusion is so fast that our pump pulses are unable to photo-select any local H-bonded structures, $k_D \gg k_2, k_4$, the long-time decay is governed by the first term of this expression, which is the average of the vibrational relaxation rate constants of the two individual sub-ensembles. Generalizing the kinetic model to allow for arbitrary cluster sizes, the average rate constant becomes $k_{VER} = \sum x_i k_i$, where x_i is the mole fraction of the sub-ensemble W_i relaxing with its proper cluster-specific vibrational relaxation rate coefficient k_i.

In the low-temperature limit (e.g. 298 K), spectral diffusion and vibrational energy relaxation occur on similar time scales and the second term of the above equation cannot be neglected anymore. Indeed, using a rate constant of $1/(1.4\ ps)$ for spectral diffusion in accordance with the long-time decay of the OH-frequency correlation function obtained with

[3] see e.g. H.J. Bakker, H.K. Nienhus, G. Gallot, N. Lascoux, et.al, J. Chem. Phys. **2002**, 116, 2592.
[4] J.J. Loparo, S.T. Roberts, A. Tokmakoff, J. Chem. Phys. **2006**, 125, 194522.
[5] N. Yoshii, S. Miura, S. Okazaki, Chem. Phys. Lett. **2001**, 345, 195-200
[6] S. Woutersen, U. Emmerichs, H.-K. Nienhuys, H. J. Bakker, Phys. Rev. Lett. **1998, 81**, 1106.
[7] H.-K. Nienhuys, S. Woutersen, R. A. van Santen, H. J. Bakker, J. Chem. Phys. **1999** 111, 1494.

mid-IR echo-peak shift measurements[8] and adopting the individual cluster-specific rate constants for the trimer (2 H-bonds) and the pentamer (4 H-Bonds) from the empirical correlation shown in Figure 1, we obtain an apparent rate constant for vibrational energy relaxation of 1.24 ps^{-1}. This value is indeed in excellent agreement with the experimental observation.

In summary, temperature and density dependent pump-probe experiments in the mid-infrared spectral region has been carried out to elucidate the competition between vibrational energy transfer and vibrational spectral diffusion. A perfect empirical correlation was found between the rate constant for vibrational relaxation and the temperature and the hydrogen-bond connectivity in the bulk liquid as quantified by the experimentally determined density- and temperature dependent dielectric constant of the liquid. Based on such a correlation, we unequivocally demonstrate that the nature of the apparent pump-probe decays changes as the temperature of the liquid is lowered. For high temperatures, spectral diffusion is much faster than energy relaxation and the observed decay rates can be understood as "ensemble-averaged" quantities. In contrast, for sufficiently low temperatures, energy relaxation and spectral diffusion due to hydrogen bond breakage and formation occur on similar time scales, yet the apparent decays are biased to slower relaxing OH-oscillators that are only weakly connected to the random D_2O network. Consequently, a fall-off behavior is observed in our $k_{VER}(\varepsilon)$-correlation when the dielectric constant approaches a value characteristic for the bulk liquid under ambient conditions.

[8] Fecko, C. J.; Loparo, J. J.; Roberts, S. T.; Tokmakoff, A. J. Chem. Phys. **2005**, 122, 054506.

Temperature Dependence of the 2D IR Spectrum of Liquid H_2O

D. Kraemer[1], M. L. Cowan[1], A. Paarmann[1], N. Huse[2], E. T. J. Nibbering[2], and

T. Elsaesser[2] and R. J. Dwayne Miller[1]

[1] *Departments of Chemistry and Physics, Institute for Optical Sciences, University of Toronto,*
80 St George Street, Toronto, Ontario, Canada, M5S 3H6 , [2] *Max-Born-Institut für Nichtlineare Optik und*
Kurzzeitspektroskopie, Max-Born-Strasse 2A, D-12489 Berlin, Germany

The dynamics and coupling within the fully resonant hydrogen bond network of liquid H_2O is directly linked to the special properties of water. The OH stretching vibration is a direct probe of these dynamics, and has been studied extensively with infrared pump-probe [1], and photon echo spectroscopy [2, 3]. Two-dimensional (2D) infrared spectroscopy has recently proven extremely useful in revealing the femtosecond timescales of the hydrogen bond network dynamics [4].

We have extended our previous studies of the 2D IR spectrum of liquid H_2O to include temperature dependen   -dimensional spectroscopy, described elsewhere [4], utilized the diffractive optic approach [5] with 70-fs pulses centered at 3,400 cm^{-1} in the OH stretching band. Novel nanofluidic technology based on silicon nitride membranes created from wet etching of silicon was demonstrated as an enabling technology to achieve such optical densities with very low non-resonant signals of the thin (800nm) Si_3N_4 windows. For these experiments the design was improved allowing us to flow liquid through the cell. The 400 nm thick water layer was sandwiched between two Si_3N_4 windows, each having a 1 mm x 1 mm clear aperture and being 800 nm thick. A syringe pump controlled by optical transmission feedback was used to flow the liquid and actively stabilize the water layer thickness. Stabilities of the optical density (OD) in the OH stretch spectral region of ~ 5 % could be achieved over several hours for an average OD of ~ 0.2.

2D spectra of H_2O, Fig. 1, show the loss of frequency correlations which occur due to fluctuations in the nuclear configurations of the bath. Such fluctuations generate a long-range fluctuating electric field modulating the transition energy of the OH stretching oscillator. At high frequencies, the fluctuations are dominated by librational excitations, i.e. hindered rotations of water molecules, whereas hydrogen bond modes and translational motions contribute at lower frequencies. At 304 K, the initial loss of frequency correlation occurs on a sub-50 fs time scale, roughly corresponding to the period of librational excitations between 650 and 1000 cm^{-1}. [6,7,8,9]
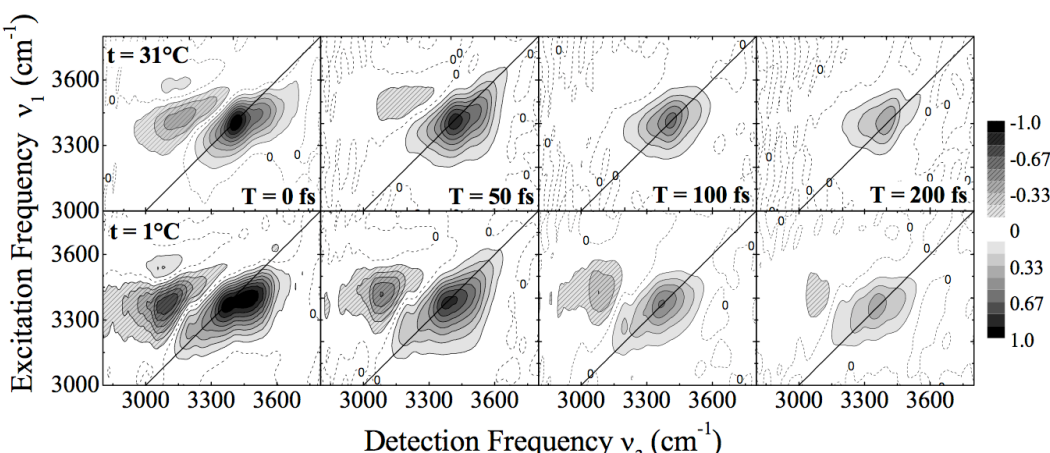

Figure: Representative data for the absorptive component of vibrational 2D spectra at population time T = 0, 50, 100, 200 fs (left to right). Structural correlations are lost within ~50 fs for ambient water temperature of 31°C (top), they persist significantly longer (~200 fs) for 1°C .

The most surprising feature to the 2D spectra shown in Figure 1 is the dramatic increase in the persistence of the frequency correlations with a decrease in temperature. The dominant effect in decreasing the temperature is to increase the degree of hydrogen bonding between waters and the spatial correlation length of the water structure corresponding to a given frequency. Furthermore, the thermal population of excited librational states in this range is reduced by a factor of ~1.5 when going from 31 ^{o}C to 1 ^{o}C and shifts to somewhat higher frequencies with decreasing temperature, leading to a substantial decrease of spectral density between 200 and 700 cm^{-1}. [9] This behavior points to an enhanced spatial correlation of water molecules by reducing the fraction of molecules with less than 4 hydrogen bonds and a moderate increase of the hydrogen bond strength. The combination of such changes results in a slower spectral diffusion at lower temperatures.

The other important distinction in the present work is the spectral dependence of the dephasing processes. Inspection of Figure 1 at the different temperatures shows the dramatic retardation of the red part of the 2D spectrum with decreased temperature. At room temperature, dephasing occurs within 50 fs on the red side of the 2D spectrum, with slightly longer correlations persisting on the blue side of the spectrum. As the temperature is lowered, the spectral dependence of the frequency correlations becomes much less pronounced. All spectral components show longer lived frequency correlations in the inhomogeneously broadened contributions. However, it is the red part of the spectrum that changes the most. The degree of hydrogen bonding clearly dominates the degree of conserved frequency correlations.

This spectral dependence was confirmed by geometric analysis. Considering the points in (ω_3, ω_1) space where the gradient of the response function for a given population time T is zero,

$$\nabla S(\omega_1, T, \omega_3) = 0$$

occur at the maxima, (ω_3, ω_1^o) and (ω_3^o, ω_1) , of each slice of the spectra parallel to the ω_1 and ω_3 axes.
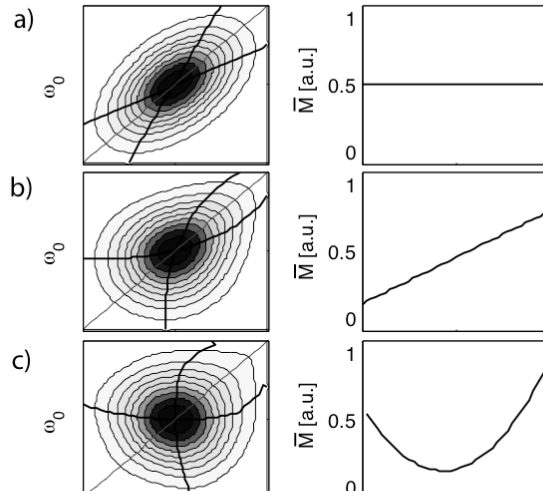
Fig 2. Simulated elliptical response functions for values of the average eccentricity, $\overline{M}$. a) For a constant eccentricity across the spectrum, the slope of the peaklines, which are shown in black, are straight and are equivalent. b) Examples of response functions that are simulated using an eccentricity with a linear wavelength dependence. c) with second order wavelength dependence.

These maxima are connected by two paths on the surface of the response function, the 'peak' lines. The slope of these peak lines gives the eccentricity function,

$$\frac{\partial \omega_1^o}{\partial \omega_3} = \frac{\partial \omega_3^o}{\partial \omega_1} = \frac{1}{M}$$

For a perfect ellipsoidal spectrum, the peak lines are a measure of the instantaneous value of the eccentricity $M=(a^2-b^2)/(a^2+b^2)$ where a and b are the diagonal and anti-diagonal widths of the ellipsoid.

Population and re-orientation dynamics were investigated with pump probe measurements. Fast decay in the polarization anisotropy, ~80 fs, without significant residual anisotropy plus the lack of a significant temperature dependence, imply that the decay in polarization anisotropy is due to resonant intermolecular energy transfer.

In conclusion, these results suggest that ultrafast librational fluctuations within the hydrogen bonded network contribute to dephasing of the OH-oscillator frequency at most temperatures, while increased spatial correlations in the hydrogen bond network preserves the excited frequency correlations at temperatures near freezing. At low temperature the frequency correlations persist longer than the excitation hopping time suggesting a certain degree of delocalization of the vibrational excitation at low temperatures and a correlation length scale that extends beyond the first solvation shell. A better understanding of the dynamics of pure water and the microscopic mechanisms that lead to energy redistribution and spectral diffusion within the hydrogen bonded network requires new theoretical models that include the dynamics of the fluctuating network of hydrogen bonds, energy transfer mechanisms, and anharmonic couplings sensitive to details in the intermolecular potential.

[1] S. Woutersen, and H. J. Bakker, Nature 402: p. 507, 1999.

[2] J. B. Asbury, et al., J. Phys. Chem. A 108(7): p. 1107, 2004.

[3] J. Stenger, et al., Phys. Rev. Lett. 87: p. 027401, 2001.

[4] M. L. Cowan, et al., Nature 434 (7030), 199-202 (2005)

[5] M.L. Cowan, J.P. Ogilvie, R.J.D. Miller, Chem. Phys. Lett. 386(1-3), 184-189. 2004

[6] Walrafen, G. E., in: Franks, F., Ed. *Water: a comprehensive treatise*, vol. 1, Plenum, New York **1973**.

[7] Hale, G. M.; Querry, M. R., *Appl. Opt.* **1973**, *12*, 555.

[8] Ashihara, S; Huse, N.; Espagne, A.; Nibbering, E. T. J., Elsaesser, T. *J. Phys. Chem. A* **2007**, *111*, 743.

[9] Zelsmann, H. R. *J. Mol. Struct.* **1995**, *350*, 95.

Mode-selective O-H stretching relaxation and energy redistribution in a hydro-gen bond studied by ultrafast vibrational spectroscopy

W. Werncke, V. Kozich, J. Dreyer, S. Ashihara and T. Elsaesser

Max-Born-Institut, Max-Born-Strasse 2A, D-12489 Berlin, Germany

Vibrational excitations play a central role for the ultrafast nonequilibrium dynamics of intra- and intermolecular hydrogen bonds [1]. The stretching vibration of hydrogen-bonded O-H groups undergoes pronounced changes of frequency and vibrational lineshape upon hydrogen bonding and frequently displays subpicosecond population lifetimes. In the theoretical literature, both relaxation via the v=2 overtone of the O-H bending vibration and a decay into low-frequency hydrogen bond modes have been invoked to explain such short lifetimes [2]. Experimental evidence for each of the relaxation pathways has remained very limited and – in most cases – the overall relaxation scenario is not understood. Here, we study the O-H stretching relaxation and subsequent vibrational redistribution in the strong intramolecular O-H...N hydrogen bond of the prototype system (2'-hydroxy-5'-methyl-phenyl)benzotriazole (TINUVIN P, TIN, inset Fig. 1 (a)) [3] by combining ultrafast infrared and Raman spectroscopy [4]. In particular, infrared pump- anti-Stokes resonance Raman probe experiments provide detailed insight into mode-specific kinetics and identify population trans-fer to fingerprint modes with a pronounced O-H bending component as major relaxation channels. Theoretical calculations of vibrational energy transfer rates based on a Fermi golden rule (FGR) approach account for the experimental findings.

TIN was studied in the nonpolar solvent C_2Cl_4 (concentrations $c=10^{-2}-10^{-1}$ M). The intramolecular hydrogen bond results in a ~ 200 cm^{-1} broad O-H stretching band with a maximum at 3200 cm^{-1}. The v=1 lifetime of the O-H stretching mode was measured in infrared pump-probe experiments with a resonant pump centered at 3200 cm^{-1} and spectrally dispersed detection of the probe pulses. The transient in Fig. 1 (a) was recorded at a probe frequency of 2850 cm^{-1} and displays the decay of the red-shifted excited state absorption of the O-H stretching vibration. The fast exponential decrease of the signal with a decay time of 200 fs (solid line: exponential decay) reflects the depopulation of the v=1 state.
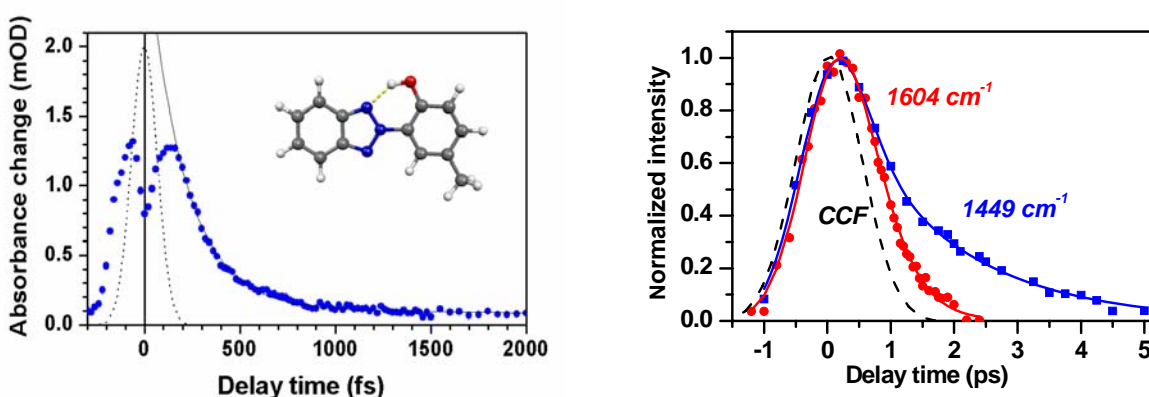
Fig. 1. (a) Decay of the excited state absorption of the O-H stretching vibration at 2850 cm^{-1} after excitation with a pump pulse centered at 3200 cm^{-1} (symbols). The decay reflects the O-H stretching lifetime T_1= 200 fs (solid line). Dashed line: cross-correlation (CCF) of pump and probe pulses. Inset: Tinuvin P (b) Time evolution of anti-Stokes intensities at 1604 (circles) and 1449 cm^{-1} (squares) after resonant infrared excitation of the vibra-tions. The transients are fitted (solid lines) by an instantaneous response (due to hyper-Rayleigh scattering) and a Raman contribution resulting in T_1 = 600±200 fs and 1.7±0.3 ps for the modes at 1604 and 1449 cm^{-1}, respectively.

In the infrared-pump/Raman-probe experiments of 1 ps time resolution, pump pulses tunable between 2.6 and 10 μm were used for vibrational excitation and ultraviolet pulses at 400 nm were applied for anti-Stokes resonance Raman probing, both delivered by a picosecond 1 kHz laser system. Transient Raman spectra were recorded in the 300-1650 cm^{-1} range for pump-probe delays up to 30 ps.

In Fig. 1 (b), we show the temporal evolution of anti-Stokes intensities after resonant infrared excitation of the modes at 1604 and 1449 cm^{-1}. After deconvolution with the CCF and subtraction of additional contributions due to hyper-Rayleigh scattering, a lifetime of T_1=600±200 fs and 1.7±0.3 ps was determined for the modes at 1604 and 1449 cm^{-1}, respectively.
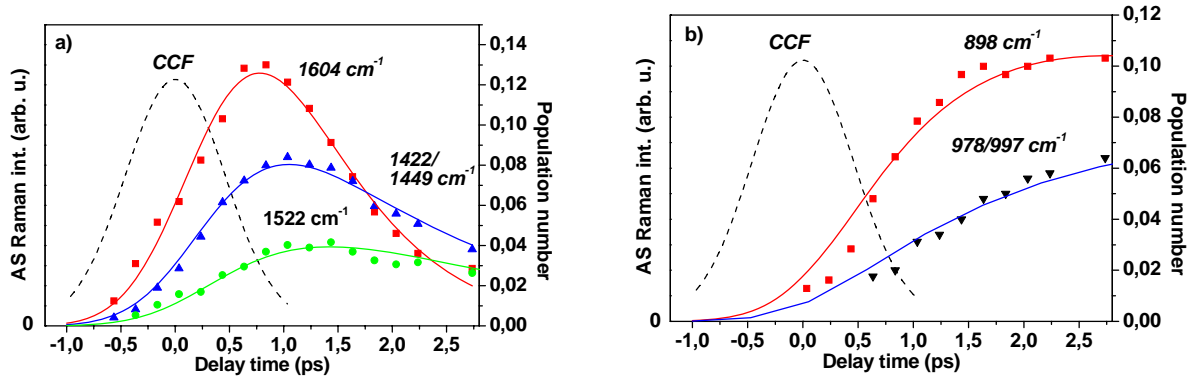
Fig. 2: Time evolution of vibrational population numbers for some of the fingerprint modes after O−H stretching excitation. Solid lines: Fits with rise (τ_1) and decay times (τ_2) of the excited vibrational levels using a three-level model. Population numbers are derived for an excitation density of the O−H stretching vibration of 10%. CCF: cross correlation function (dashed line).

In a second series of measurements, anti-Stokes intensities of the fingerprint modes were measured after infrared excitation of the O-H stretching mode. Population kinetics are summarized in Figure 2, displaying a distinctly different behavior of the individual modes. The data were analyzed by a three-level model with rise (τ_1) and decay times (τ_2) of the excited vibrational levels. For vibrations above 1000 cm^{-1} τ_2 is determined by the vibrational lifetime T_1 measured with resonant excitation (Table 1, cf. Fig. 1). The doublets at 1449/1422 and 997/978 cm^{-1} are not spectrally resolved.

Time-resolved anti-Stokes Raman measurements after O−H stretching excitation reveal selective energy transfer into distinct vibrational modes in the fingerprint spectral region. We identify primary accepting modes with fast rise times of 400±200 fs (1604, 1449/1422 cm^{-1}), close to the population decay time of the O−H stretching vibration. In contrast, the modes at 898 and 997/978 cm^{-1} are populated substantially slower.

Taking the τ_2 times of the 1604 and 1422/1449 cm^{-1} modes into account, we estimate from the population numbers shown in Fig. 2 that about 40 % of the initial O-H stretching population decays through the 1604 cm^{-1} mode, whereas only about half of this fraction is transferred through both the 1449 and 1422 cm^{-1} modes. Thus, such modes accept a total of about 70-80 % of the initial O-H stretching population. Other modes are considerably less populated within the first picosecond. It should be noted that non-equilibrium populations of the different modes exist up to delay times of 10 ps pointing to the nonthermal character of the intramolecular population distribution [6].

Table 1. Rise (τ_1) and decay times (τ_2) of the modes after OH-stretching excitation.

Wavenumber [cm^{-1}]	τ_1 [ps]	τ_2 [ps]	Assignment *	δ(OH) contribution [%]
1604	0.4±0.2	0.6±0.2	δ(OH) + ν(ph$_{OH}$-8b)	26
1522	0.8±0.3	1.8±0.3	ν(ph$_{OH}$-19a) + δ(CH$_{OH}$-18a)	< 1
1422 / 1449	0.4±0.2	1.7±0.3	ν(ph$_{OH}$-19a) + δ(CH$_{OH}$-18a) / δ(CH$_3$)$_{scissor}$ + δ(OH)	9/18
997 / 978	2.4±0.4	15±3	γ(CH$_3$)$_{rock}$ / γ(CH$_3$)$_{rock}$ + δ(CH-18b)	< 1
898	1.1±0.3	8±3	ν(ph$_{OH}$-6b) + δ(ph-6a)	< 1

* nomenclature according to Varsanyi [5]; index OH denotes phenolic TIN moiety.

Relaxation rates of the excited O–H stretching mode into overtones and combination bands of modes at lower frequencies were modeled by a FGR approach [8]. The rates are proportional to the square of vibrational Hamiltonian matrix elements between the respective states as well as to a function which accounts for the energy mismatch between the initial and final states. Vibrational Hamiltonian matrix elements are calculated based on density functional theory cubic and quartic anharmonic couplings between the O–H stretching and 16 selected normal modes from the fingerprint as well as the low-frequency spectral region [8]. The usual delta function in the FGR expression, which assures energy conservation, is replaced by a normalized Lorentzian function to account for a homogeneous line width (fwhm ≈ 200 cm^{-1}) of the O–H stretching mode absorption band. In good agreement with experimental results, the calculations predict a predominant relaxation channel into the 1604 cm^{-1} overtone band. The next efficient energy transfer channels consist in combination tones of the 1604+1449 and 1604+1487 cm^{-1} modes followed by the 1604+1374 and 1604+1422 cm^{-1} combination bands. All participating normal modes have large contributions of in-plane O–H bending motions in common (cf. Table 1). This is most pronounced for the 1604 and 1487 cm^{-1} normal modes, the latter being Raman inactive and thus not observed experimentally.

Assuming that the overtone and combination tones exclusively relax into their fundamental modes, FGR calculations predict about 50 % of the initial population going into the 1604 cm^{-1} mode, ≈19 % into the 1449 cm^{-1} mode, ≈13 % into the IR active 1487 cm^{-1} mode, ≈9 % into the 1422 cm^{-1} mode and ≈7 % into the mode at 1374 cm^{-1}, which qualitatively accounts for the experimental findings. The remaining deviation from experiments indicates that the assumptions made are not entirely valid. In particular it is likely that the combination and overtones partly decay into combinations of other modes rather than their fundamentals.

In conclusion, our combined ultrafast infrared/Raman study demonstrates that the hydrogen-bonded O–H stretching mode in TIN relaxes through in a few major channels that all involve combination and overtone bands of modes with considerable in-plane O–H bending character. In particular, the mode at 1604 cm^{-1}, which contains the largest O–H bending contribution, plays a prominent role for primary IVR processes. This highlights the important role of energy transfer from stretching to bending motions in hydrogen bonds.

[1]   E.T.J. Nibbering, and T. Elsaesser, Chem. Rev. **104**, 1887-1914 (2004).
[2]   R. Rey, K.B. Møller, and J.T. Hynes, Chem. Rev. **104**, 1915-1928 (2004).
[3]   T. Elsaesser, in "Ultrafast hydrogen bonding dynamics and proton transfer processes in the condensed phase", eds. T. Elsaesser and H. J. Bakker, Kluwer Academic Publishers, 2002, p. 119-153.
[4]   V. Kozich, J. Dreyer, S. Ashihara, W. Werncke, and T. Elsaesser, J. Chem. Phys. **125**, 074504 (2006).
[5]   G. Varsanyi, "Vibrational spectra of benzene derivatives (Academic, New York 1969)"
[6]   K. Lenz, M. Pfeiffer, A. Lau, and T. Elsaesser, Chem. Phys. Lett. **229**, 340-346 (1994).
[7]   V. M. Kenkre, A. Tokmakoff and M. D. Fayer, J. Chem. Phys. **101**, 10618-10629 (1994).
[8]   J. Dreyer, J. Chem. Phys. **122**, 184306/1-10 (2005).

Solvent dependence of OH stretch and bend vibrational relaxation of monomeric water molecules in liquid solution

G. Seifert, A. Abdolvand, H. Graener

Physics Department, Martin-Luther-Universität Halle-Wittenberg, Hoher Weg 8, D-06120 Halle (Saale), Germany

E-mail: gerhard.seifert@physik.uni-halle.de; URL: http://www.physik.uni-halle.de/Fachgruppen/optik

The vibrational dynamics of isolated water molecules dissolved in several nonpolar organic liquids have been studied using an IR pump-probe experiment with ≈ 2 ps time resolution. Analyzing transient, time- and spectrally resolved data in both the OH bending and the OH stretching region, the relaxation pathways of single water molecules were disentangled comprehensively[1], proving that the vibrational energy of H_2O molecules is relaxing following the scheme OH-stretch $\rightarrow$ OH bend overtone $\rightarrow$ OH bend $\rightarrow$ ground state, as indicated in Fig. 1.
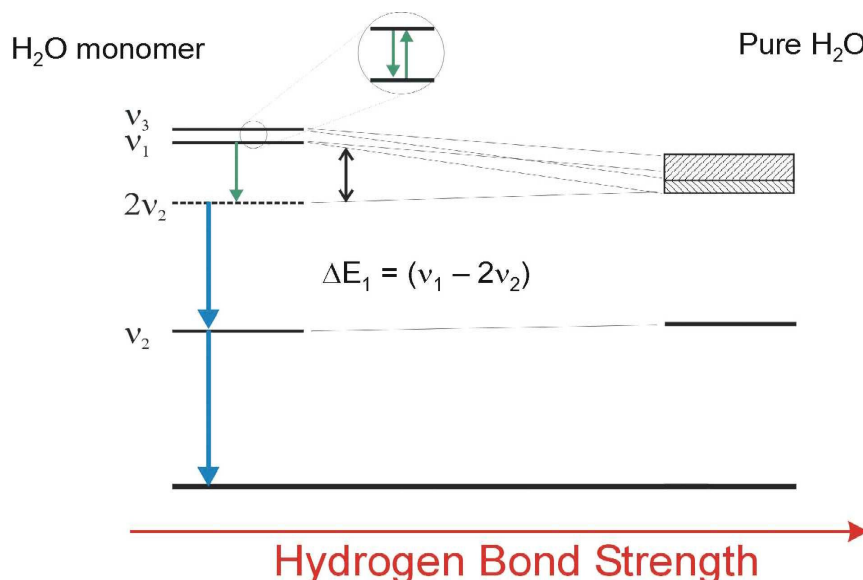

Figure 1: Schematic view of H_2O relaxation pathways. The anharmonic shift of the energy levels with increasing hydrogen bond strength increases the OH stretch relaxation rate, whereas the OH bend lifetime does not follow this correlation.

In a previous work we have shown that the OH stretch relaxation is accelerated monotonically upon increase of the solute-solvent interaction[2]. In contrast, OH bending relaxation shows an individual behavior for various solvent-solute combinations indicating that this last, intermolecular relaxation step[3] thermalizing the excess vibrational energy is depending on the individual resonance structure (accepting modes) of the solvent molecule.

To get a more complete, systematic picture of this solvent dependence of the OH bending relaxation of monomeric water, we have studied saturated solutions of H_2O in the methane derivates $CHCl_3$, $CDCl_3$, $CHBr_3$, $CDBr_3$ and CH_2Br_2, and in the ethane derivates 1,2-dichlorethane ($C_2H_4Cl_2$), 1,1,2,2-tetrachloroethane ($C_2H_2Cl_4$), and pentachloroethane (C_2HCl_5). The saturation concentrations are in the range of 0.03 mol/ℓ to 0.1 mol/ℓ; all experiments were done at ambient temperature. The sample length was 500 µm in all cases, which corresponds nearly perfectly to the overlap volume (Rayleigh length) of pump and probe beam in our setup. Time-resolved monitoring of the transient transmission changes at

the frequency position of the OH bend fundamental (~1600 cm^{-1}) and at the first overtone transition (~1565 cm^{-1}) yielded vibrational lifetimes from 4.8 ps to 40.5 ps.

In the already mentioned previous work[2] a monotonous increase of OH stretch relaxation rate was found for increasing solute-solvent interaction. A simple measure for the strength of this interaction is the energy distance between the symmetric OH stretch fundamental ν_1 and the bending overtone $2\nu_2$ (see Figure 1). Since ν_1 is red-shifted, whereas $2\nu_2$ is blue-shifted upon increasing interaction, this energy distance decreases when solvent-solute interaction is getting stronger. Trying to explain the strong solvent variation of the OH bending mode by the same general interaction strength fails, as is easily seen in Fig. 2: when the measured OH bend relaxation rates for all solvents are plotted against the energy distance [ν_1 - $2\nu_2$] for all mixtures studied, there is clearly no correlation.
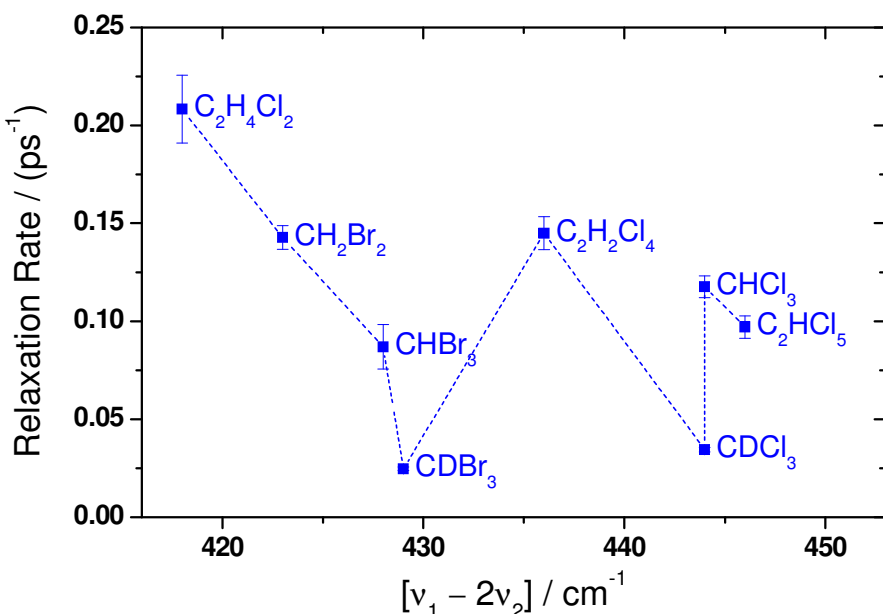

Figure 2: OH bending relaxation rates obtained for all solvents studied, plotted versus overall solvent solute interaction, as measured by the energy distance [ν_1 - $2\nu_2$]; smaller energy distance means stronger interaction.

Another straightforward idea is more successful: as the OH bending relaxation is necessarily an intermolecular relaxation process[3], the available acceptor modes of each solvent should play an important role. If this is true, the most probable vibrational mode to be populated on the solvent molecules is the fundamental mode with the lowest relative energy gap to the OH bend. Such a relaxation step requires the smallest change of vibrational quantum numbers; and the energy mismatch to be transferred to the thermal bath has often been found to be a crucial parameter for energy relaxation.

To check this idea, we have plotted the OH bending relaxation rates again in Fig. 3, but now versus the energy gap from either OH bending mode to the nearest fundamental CH or CD bending mode of the solvent. It is easily seen that now there is a very reasonable trend of decreasing relaxation rate, when the energy gap increases. There are, however, still some individual deviations which most probably are caused by different interaction potentials and geometries of the solvent molecules. This explanation becomes obvious when only the very similar haloform molecules (open circles in Fig. 3) are being compared: their relaxation rates

follow, more or less perfectly, an exponential dependence of the energy gap ν_{if}. Although this empirical relation is not obtained directly from a theoretical model of vibrational relaxation, it can be taken as strong hint that the intermolecular relaxation of the water OH bending vibration is really exciting close-lying vibrational modes (here CH or CD bending modes) of the solvent.
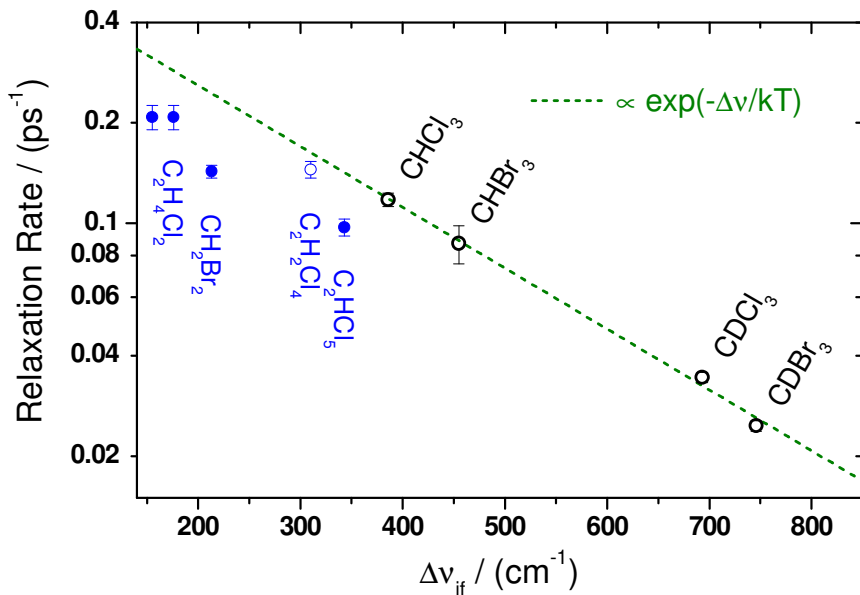
Figure 3: OH bending relaxation rates obtained for all solvents studied, plotted versus energy distance from water OH bend to nearest solvent CH (CD) bend fundamental.

A more detailed analysis of the data presented here will be given in an upcoming publication. Also, we are now performing experiments aiming to the proof of the population being transferred to the respective solvent modes.

[1] G. Seifert, T. Patzlaff, H. Graener, *J. Chem. Phys.* **125**, 154506 (2006)
[2] H. Graener, G. Seifert and A. Laubereau, *Chem. Phys.* **175**, 193 (1993)
[3] G. Seifert, T. Patzlaff and H. Graener, *J. Chem. Phys.* **120**, 8866 (2004)

Superheating of bulk ice. Transient temperature and pressure measurements.

Marcus Schmeisser, Hristo Iglev and Alfred Laubereau

Physik-Department E11, Technische Universität München, D−85748 Garching, Germany

E-mail: mschmeis@ph.tum.de

Abstract. A sensitive picosecond thermometer and manometer for hydrogen-bonded systems is demonstrated. The technique is applied for temperature jumps in ice by the help of subpicosecond pulses in the mid-infrared. The hydroxilic stretching vibrations (OH or OD) are applied for energy deposition and for the fast and sensitive spectral probing of local temperature and structure. The method is verified for isotopically mixed ice I_h at 200 K and ambient pressure, where the local thermodynamic quasi-equilibrium builds up within 25 ps. The technique is also suitable for measurements close to the melting point, where superheating of ice can be investigated.

Introduction

Almost every physical and chemical process in condensed matter strongly depends on temperature. An increasing interest for studying processes on shorter and shorter timescales makes it also necessary to have a fast and sensitive probe of the transient local temperature.

Here we present a picosecond thermometer and manometer for hydrogen-bonded systems, demonstrated in the particular case of ice[1,2]. The OH- or OD-stretching vibrations of an isotopically mixed ice I_h sample with subpicosecond lifetimes allow a rapid energy deposition and heating of the ice lattice and are sensitive probes for H-bonding [3], which makes them suitable spectral tools to distinguish local molecular structures with a time resolution of a few picoseconds.[3] The pronounced temperature dependence of these modes is illustrated by FT-IR spectra in Fig. 1a. The spectra of the crystalline mixture HDO:D_2O (15*M*) and the drastically different spectrum of the molten sample are shown for comparison (melting point T_m = 274.8 K). Significant changes of amplitude and position of the OD- and OH-band around 2400 and 3300 cm^{-1}, respectively, are readily seen.

Data Analysis and Results

The transient differential spectra measured 40 ps after ultrafast heating of the HDO ice at T_i = 200 K are presented in Figs. 1b and c in comparison to two different models. In Fig. 1b the data are compared to thermal differential spectra derived from steady-state absorption spectra at constant pressure (215 200 K: dashed line, 220-200 K: solid line, 225-200 K: dotted line). The similarity of these spectra with the time-resolved data verifies the expected heating of the ice sample.

[1] H. Iglev, M. Schmeisser, K. Simeonidis, A. Thaller, A. Laubereau, Nature, **2006**, 439, 183

[2] M. Schmeisser, A. Thaller, H. Iglev, A. Laubereau, New J. Phys., **2006**, 8, 104+

[3] R. Laenen, C. Rauscher, and A. Laubereau, Phys. Rev. Lett. **80**, 2622–2625, 1998
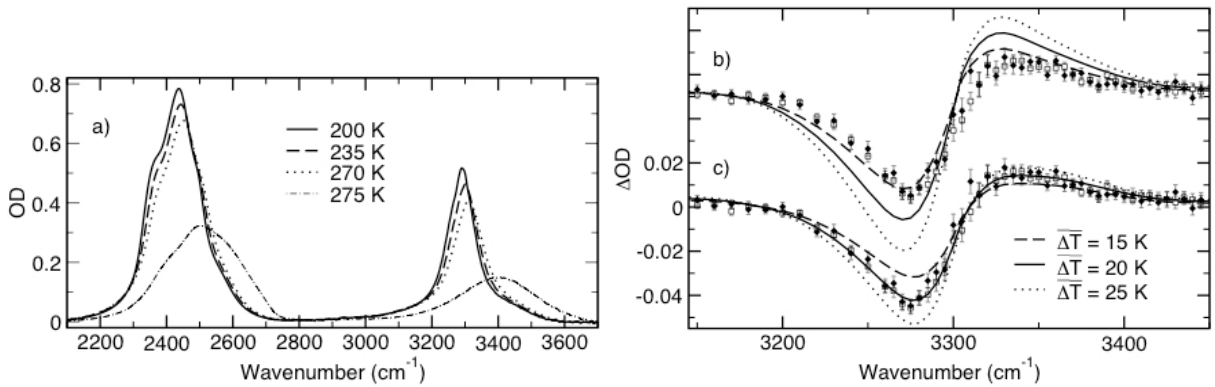
Fig. 1. (a) FT-IR absorption spectra of HDO:D$_2$O (15M) ice at 200 K (solid line), 235 K (dashed) and 270 K (dotted). Water spectrum at 275 K (dash-dotted). (b) Transient differential spectra measured with tunable subpicosecond pulses 40 ps after OH- (hollow squares) or OD-pumping (filled diamonds) of the HDO:D$_2$O ice at 200 K. The curves represent steady-state thermal differential spectra for ΔT = 15, 20 and 25 K and constant ambient pressure. (c) Same picosecond data (experimental points) as in (b) but compared to steady-state differential spectra for isochoric temperature jumps (calculated curves).

Both, IR excitation at 3290 cm^{-1} (OH-pumping) and at 2435 cm^{-1} (OD-pumping), respectively, is applied. The pulse energies are adjusted to deposit approximately equal amounts of energy in both cases. The two excitation schemes induce almost the same spectral changes, which indicates that the OH- and OD-oscillators are already in a local equilibrium at t_D = 40 ps.

Assuming a constant volume during the ultrafast temperature rise because of the slow volume expansion, a simultaneous pressure increase occurs. From the coefficient of thermal volume expansion of ice and the isothermal compressibility we obtain the isochoric pressure increase of approximately 1.3 MPa/K. Using the pressure shifts of the hydroxilic Raman bands of HDO ice[4] we estimate an additional frequency shift of -0.10±.01 cm^{-1}/K for the OH-mode and -0.07±.01 cm^{-1}/K for the OD-mode, respectively. Fig. 1c shows the same data as in 1b in comparison the computed spectra for isochoric temperature jumps of 15, 20 and 25 K are shown. The good agreement of the solid line with the transient data (experimental points) is noteworthy, illustrating the sensitivity of the OH-stretching vibrations for local pressure and temperature. An average temperature rise of $\overline{\Delta T}$

pressure increase of $\overline{\Delta P}$ = 26±4 MPa is estimated. The considerably improved agreement between transient and stationary results in Fig. c relative to b gives experimental support to the isochoric character of the picosecond temperature jump of the sample.

Analyzing the transient differential spectra in terms of thermal (stationary) differential spectra, we are able to extract the slow changes of average temperature and pressure in the sample. The temporal evolutions of average temperature and pressure in the sample are presented in Fig. 2 for T_i = 200 K (a) and 270 K (b). Our analysis shows that the H-bonding network in the ice sample reaches a local quasi-equilibrium at t_D = 15 ps, which allows to define a temperature value. Assuming an exponential decay the time constant for the heat dissipation is 2.5±1.0 ns (solid line in Fig. 2a and b), consistent with estimations of the heat conduction to the cell windows. The pressure drops somewhat faster with ~1 ns.

---

[4] B. Minceva-Sukarova, W.F. Sherman, and G.R. Wilkinson, J. Phys. C: SolidStatePhys. **17**, 5833–5850, 1984
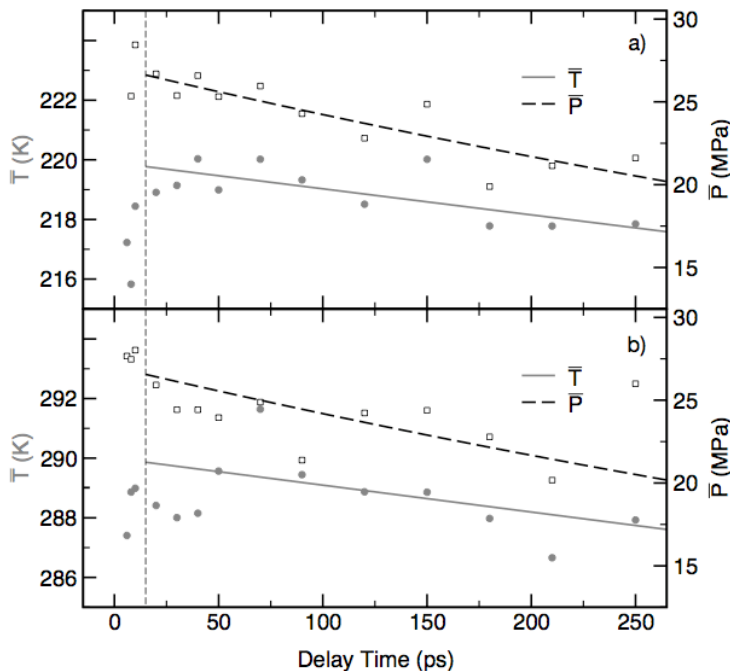
Fig. 2. (a) Average temperature and pressure of the probed sample volume after ultrafast heating of HDO:D$_2$O (15M) at 200 K. The initial temperature jump (filled circles, solid line, left ordinate scale) to a local quasi-equilibrium after ~ 15 ps (vertical line) is consistent with an isochoric pressure , dashed line, right ordinate scale). Temperature and pressure develop differently later on. (b) Same as a) but for an initial temperature of 270 K. A similar temporal behavior is observed.

The number is in good agreement with a volume expansion by the speed of sound in ice (3.9/km/s) through the thin ice specimen (2.5 µm), which is estimated to be 1.3 ns. These findings demonstrate the sensitivity of this method to transient temperature and pressure changes in the sample.

The measurements performed for the same pumping conditions but with initial temperature of 270 K show a remarkable similarity to the transient data at 200 K. Therefore, we assume that the optical excitation induces almost the same process, i.e. an average temperature increase of approximately 20 K without evidence for breaking the ice structure.[1] With respect to the variation of the induced temperature rise along the propagation direction in the sample because of the strong absorbing samples, we estimate a superheating up to 301 K close to the front face of the ice specimen. Recent measurements provide no indication for melting the ice lattice within a time interval of 1.33 ns even for initial superheating up to 330 K.[5]

Conclusions

We have presented a method for measuring transient temperature and pressure in H-bonded systems on a picosecond timescale. The technique was demonstrated for a HDO:D$_2$O (15M) ice sample at 200 K and is also suitable for measurements close to the melting point observing substantial superheating up to 330 K.

---

[5] M. Schmeisser, H. Iglev, A. Laubereau, Chem. Phys. Lett 2007, in press.

Melting of bulk ice on the picosecond timescale

Hristo Iglev and Marcus Schmeisser

Physik-Department E11, Technische Universität München, D−85748 Garching, Germany

E-mail: higlev@ph.tum.de

Abstract. The ice-water phase transition after an ultrafast temperature jump is studied in HDO:D_2O (15 M) ice using 2-color IR spectroscopy. Shock heating of bulk ice leads to substantial superheating of the solid phase. For energy depositions beyond the limit of superheating (330 ± 10 K) partial melting in two steps is observed and assigned to: (i) catastrophic melting within the thermalization time of the excited ice lattice of 5 ± 2 ps; and (ii) secondary melting with a time constant of 33 ± 5 ps.

Introduction

Melting usually starts at the surface at temperatures above the melting point. On the other hand, we recently demonstrated[1,2] that shock laser heating of bulk ice can avoid the common surface melting, leading to substantial superheating of the ice lattice. Maximum superheating of bulk ice to 330 ± 10 K was observed.[3] The superheated ice state is found to be amazing stable and persists for more than 1.3 ns.

Here we present an experimental study on melting of bulk HDO ice the using recently developed ultrafast temperature jump technique. The OH stretching vibration is applied for rapid heating by intensive IR pulses. The same mode is known as a fast and sensitive probe of local temperature, pressure and structure.[4,5] The amplitude and spectral shape of steady-state differential spectra for a fixed temperature rise ΔT vary slightly with initial sample temperature and pressure, whereas the spectral position shows a distinct, nearly linear dependence. The features allow the extrapolation of the steady-state spectra to temperatures above the melting point. It is important to recall the isochoric character of the ultrafast temperature jump because of the slower volume expansion of the sample; in other words, a pressure increase is involved that can also be measured with our technique.

Results and Discussions

Time-resolved data measured after excitation at 3290 cm^{-1} of HDO ice at 255 K are presented in Fig.1. The solid green lines represent the calculated differential spectra obtained by a superposition of the absorption of superheated ice (red curves) and liquid water (blue). The ice contribution represents the bandshape of superheated ice at the fitted average temperature and average pressure of the probed sample volume (for more details see Ref. 2 and Figs. 1b and c). For the water contribution, the temperature and the pressure dependence of the steady-state spectrum is neglected. The good agreement of the curves with the experimental data gives spectroscopic evidence that water already appears during the initial thermalization process of the ice lattice (measured time constant of 5.4±0.5 ps).[1]

The spectral properties of the molten species in the sample are presented in Fig. 2. The bandshape of the molten component as derived from the measured transient differential spectrum by substraction of the bandshape of the superheated ice component is depicted for

[1] H. Iglev, M. Schmeisser, K. Simeonidis, A. Thaller, A. Laubereau, Nature, **2006**, 439, 183
[2] M. Schmeisser, A. Thaller, H. Iglev, A. Laubereau, New J. Phys., **2006**, 8, 104+
[3] M. Schmeisser, H. Iglev, A. Laubereau, Chem. Phys. Lett., **2007**, in press
[4] R. Laenen, C. Rauscher, A. Laubereau, Phys. Rev. Lett., **1998**, 80, 2622
[5] S. Woutersen, U. Emmerichs, H.J. Bakker, Science, **1997**, 278, 658
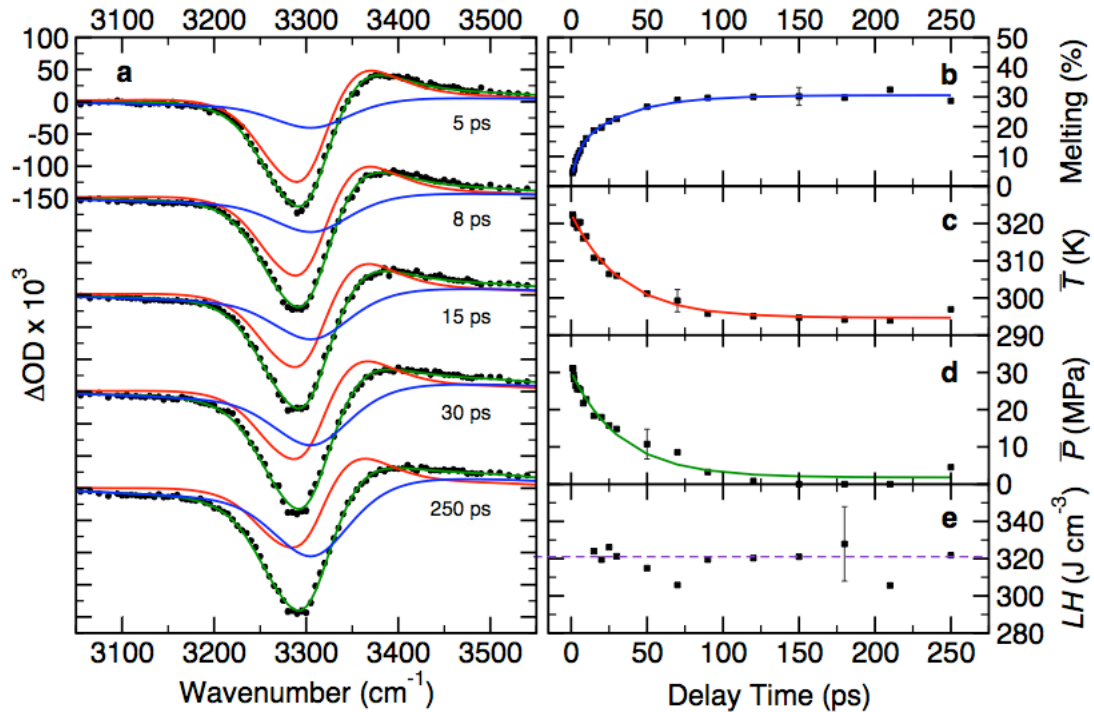
Fig. 1. Kinetics of partial melting of HDO ice after energy deposition of 165±5 J/cm³ at T_i= 255 K. **a**, Transient absorption changes at various delay times; experimental points, calculated solid lines. The green curve is a superposition of the absorption of superheated ice (red line) and molten liquid (blue). **b**, Temporal evolution of the amount of molten liquid. **c**, **d**: Time-evolution of the residual ice, average temperature (c) and average pressure (d) in the probing volume. **e**, Transient latent heat LH consumed by the melting process.

delay times of 15 and 250 ps. For comparison the well-known bandshape of liquid HDO at 275 K is also shown. The agreement is noteworthy. It is concluded that liquid water is formed without evidence for a pre-molten species after 15 ps or later.

The temporal evolution of the molten fraction is illustrated by Fig. 1b as derived from the decomposition of the measured transient bandshapes. The observed time dependence can be fitted with a simple relaxation model (blue calculated curve) with two assumed exponential time constants. The first kinetic step (i) involves melting of ≈12 % of the ice molecules in the probing volume with a time constant of 5±2 ps that is consistent with the thermalization time of the H-bonded network of the ice specimen.[1] This process is proposed to represent ultrafast thermal melting via homogeneous nucleation. Here it is important to note, that the observed initial melting cannot be explained with a progressive movement of a melting front starting from the sample surface with the speed of sound. It is concluded that homogeneous melting leads to the formation of small water droplets in the ice crystal.

The initial melting is followed by a second, slower process (ii) that increases the molten component by another 19 % with an effective time constant of τ_2 = 33±5 ps. A similar number of 37±5 ps was reported for surface melting of ice after ultrafast heating.[6] The accordance suggests that the time constant is τ_2 connected to secondary interfacial melting at the phase boundaries obviously generated during the initial (homogeneous) melting.

The secondary melting (ii) is accompanied by a decrease of the average ice temperature in the probing volume with the same time constant of 33±5 ps (Fig. 1c). The initial melting step (i)

---

[6] Ch-Y. Ruan, V.A. Lobastov, F. Vigliotti, S. Chen, and A. Zewail, Science **304**, 80-84, 2004
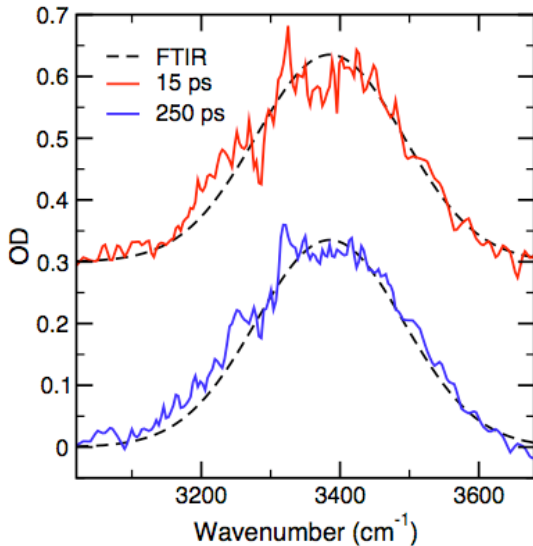
Fig. 2. Spectral properties of the molten species. Transient absorption spectra of the molten HDO:D_2O component measured at various delay times (colored lines, see inset). The steady-state spectrum of liquid HDO:D_2O at 275 K is shown for comparison (dashed curves).

is obviously continued by a secondary process (ii) that consumes thermal energy of the superheated ice component and seems to be governed by heat conduction.

Of special interest are the data on the average pressure of the residual ice component in the probing volume presented in Fig. 1d. In fact, the measured probing spectra suggest a rapid decrease of the average ice pressure in the probing volume after the initial isochoric pressure increase produced by the pumping process. This feature is much faster than the pressure decay for the superheating case without melting[2] and presents striking thermodynamic evidence for structural changes in the sample. We recall the 9% ice-to-water volume decrease so that rapid melting on a sub-100-ps time scale should be accompanied by a pressure decay. Quantitatively speaking, the large experimental uncertainty of the measured time constant of 35±10 ps should be noticed, since the separation of a simultaneous temperature and pressure change (producing both band shifts) relies on minor bandshape changes.

Knowing the deposited energy of the excitation pulse from simple transmission data, the separation of the transient differential spectra into an ice and a melt contribution allows to deduce the latent heat for partial melting of the HDO crystal (Fig. 1e). The experimental points start for a delay time of 15 ps when a local quasi-equilibrium of the ice phase should be reached.[2] It is interesting to see that the consumed energy of the melting process is constant and agrees with the steady-state latent heat of HDO ice within the measuring accuracy (note dashed line on Fig. 1e). The finding supports the spectroscopic result that liquid water is formed, without evidence for a pre-molten species.

Conclusions

We report on ultrafast bulk melting of ice after laser induced temperature jumps. We found that homogeneous melting of ice on a picosecond timescale can only occur for an energy deposition above the superheating limit of 330 K. The present result underlines the stability of the linear H-bonds of a water molecule to its neighbors in the ice lattice.

Vibrational energy dynamics in glycine/water solution studied with ultrafast IR–Raman spectroscopy

Shinsuke Shigeto, Yoonsoo Pang, Dana D. Dlott

School of Chemical Sciences, University of Illinois at Urbana-Champaign, 600 S. Mathews Ave. Urbana, IL 61801, USA. E-mail: sshigeto@uiuc.edu.

1. Introduction

In this work, we use ultrafast IR–Raman spectroscopy[1,2] to study vibrational relaxation (VR) of glycine in aqueous solution. In the IR–Raman method, a mid-IR pulse excites a higher-energy vibrational fundamental. The subsequent redistribution of vibrational energy from the parent to lower-energy daughter vibrations and eventually into the bath, a process termed vibrational cooling (VC), is monitored via spontaneous Raman scattering. There have been a number of VR studies of small peptides and proteins, especially on the amide I vibrations (C=O stretch modes).[3,4,5] However those studies are based on the IR pump–probe techniques that were limited to watching energy leave the initial vibrational state. Compared to the IR pump–probe methods, the present study is unique because we can now for the first time trace vibrational energy flow throughout the entire molecule.

Glycine has the chemical formula $H_2N–CH_2–COOH$. In aqueous solution near the isoelectric point, glycine is mainly zwitterionic $^+H_3N–CH_2–COO^-$. An intriguing feature of our glycine VR study stems from the fact that the partial charges on the glycine zwitterion can contribute to the fluctuating forces which govern VR rates in solution,[6] in addition to hard-wall repulsive interactions and attractive dispersive interactions. Since partially-charged macromolecules are ubiquitous in biological systems, the present study serves as an important glimpse into the detailed mechanisms of vibrational energy flow in biological systems.

2. Experimental

The sample was a 2.0 M glycine/H_2O solution. Regent-grade glycine (98%, Sigma-Aldrich) was recrystallized once and dissolved in doubly-distilled H_2O. This solution is slightly acidic, close to the isoelectric point of glycine (pH = 6.0), so most glycine exists as zwitterion.

The laser apparatus of the IR–Raman measurement has been described elsewhere.[7] A kilohertz Ti:Sapphire laser system with two optical parametric amplifiers generated mid-IR pulses (~0.7 ps duration, 25 cm^{-1} bandwidth, 370 μm diameter, 20 μJ energy) at 2980 cm^{-1} (λ_{IR} = 3.36 μm) and time-delayed 532 nm probe pulses (~0.7 ps duration, 25 cm^{-1} bandwidth, 400 μm diameter, 40 μJ energy). The sample was a flowing liquid jet with a thickness of ~60 μm. Scattered light was detected with a multichannel spectrograph that covered the –3800 to +3800 cm^{-1} range. At each delay time only a 3 min integration time was required to obtain the spectrum. The Stokes Raman intensity of the glycine transitions evidenced little change during data acquisition, making sure that variation in the glycine concentration due to solvent evaporation or molecular decomposition was negligible.

[1] A. Laubereau, W. Kaiser, Rev. Mod. Phys. **1978**, 50, 607.
[2] D. D. Dlott, Chem. Phys. **2001**, 266, 149.
[3] M. F. DeCamp, L. DeFlores, J. M. McCracken, A. Tokmakoff, K. Kwac, M. Cho, J. Phys. Chem. B **2005**, 109, 11016.
[4] L. P. DeFlores, Z. Ganim, S. F. Ackley, H. S. Chung, A. Tokmakoff, J. Phys. Chem. B **2006**, 110, 18973.
[5] P. Hamm, M. Lim, R. M. Hochstrasser, J. Phys. Chem. B **1998**, 102, 6123.
[6] D. W. Oxtoby, Annu. Rev. Phys. Chem. **1981**, 32, 77.
[7] Z. Wang, Y. Pang, D. D. Dlott, J. Phys. Chem. A **2007**, 111, 3196.

3. Results and discussion

Figure 1 displays a time series of transient anti-Stokes spectra of the glycine/H_2O solution with ~2980 cm^{-1} pumping, together with steady-state IR and Raman spectra. The vibrational assignments[8,9] are also shown in this figure. In the transient spectra, the ambient-temperature spectrum obtained at negative delay time ($t = -5$ ps) was subtracted off as a background. The mid-IR pulse deposits energy into the CH$_2$ symmetric stretch ν_s(CH$_2$) of glycine and the red edge of the OH stretch ν(OH) of H_2O. The sharper transient feature at the pump wavenumber at early delay times results from a coherent artifact due to nonlinear light scattering (NLS).[10]

From the lower traces in Fig. 1, the rise and subsequent decay of glycine daughter vibrations can be clearly seen. The anti-Stokes transients of six glycine daughter vibrations are plotted in Fig. 2. The anti-Stokes transient intensities were obtained by a least-squares fitting of the spectra with six Voigt lineshape functions plus a slowly-varying polynomial to account for the background rising toward zero Raman shift.

All glycine transients in Fig. 2 rise with a slight lag relative to the apparatus response and then decay to a plateau associated with the equilibrium temperature jump ΔT. In the present study, ΔT was estimated to be $\approx$10 K. To determine the VR lifetime T_1 of each transition, we carried out least-squares fitting to a phenomenological model function with exponential rise and decay into thermal equilibrium, convolved with a 1.1 ps FWHM apparatus response. The lifetimes T_1 thus obtained were all in the 1.1 to 1.8 ps range and there was no systematic dependence on vibrational frequency. The three lower-energy daughter vibrations in the 887–1107 cm^{-1} region (the "lower-energy" vibrations) have clearly slower rise times than the three higher-energy daughters in the 1313–1586 cm^{-1} region (the "mid-range" vibrations). This delay is too short to originate from a parent → mid-range → lower-
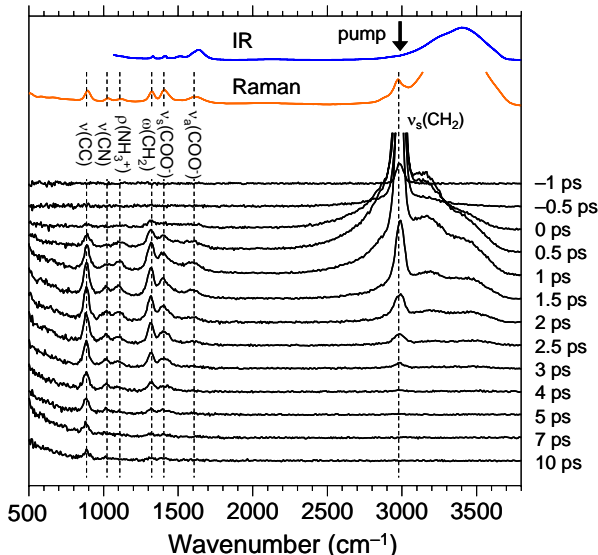

Figure 1. Upper two traces: IR and spontaneous Raman spectra of glycine/H_2O solution (2.0 M). The arrow indicates the location of the mid-IR pump pulse (~2980 cm^{-1}). Lower traces: Transient anti-Stokes spectra of the glycine/H_2O solution.
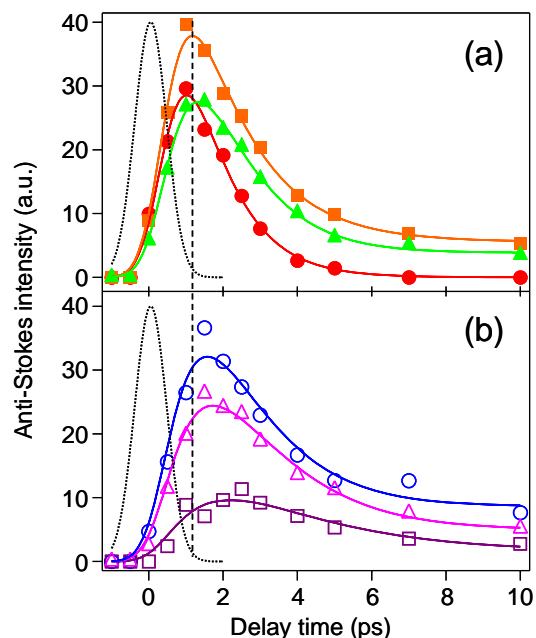
Figure 2. Time dependences of transient anti-Stokes intensities of (a) ν_a(COO$^-$) (●), ν_s(COO$^-$) (■), ω(CH$_2$) (▲) and (b) ρ(NH$_3^+$) (○), ν(CN) (□), ν(CC) (△). The dotted curves represent the 1.1 ps FWHM apparatus response.

[8] K. Furić, V. Mohaček, M. Bonifačić, I. Ŝtefanić, J. Mol. Struct. **1992**, 267, 39.
[9] S. Suzuki, T. Shimanouchi, Spectrochim. Acta **1963**, 19, 1195.
[10] J. C. Deàk, L. K. Iwaki, S. T. Rhea, D. D. Dlott, J. Raman Spectrosc. **2000**, 31, 263.

energy vibration cascade. The overall VC process is best explained by the three-step mechanism as follows: First, the parent decay populates, to some extent, all the daughter vibrations. The next stage is relaxation of the mid-range vibrations to excite the lower-energy vibrations or directly to the ground state. Finally, the lower-energy vibrations relax to the ground state. This scheme is similar to what has been observed previously in methanol[11] and nitromethane.[12]

Figure 3 shows the transient Stokes spectra with 2980 cm^{-1} pumping of pure H_2O and the glycine/H_2O solution, in the OH and CH stretch regions. An NLS artifact is observed, along with a well-known bimodal difference spectrum[7,13,14] arising from heated thermalized water. At early delay times, the spectrum is complicated by the coexistence of heated water and ν(OH) and ν_s(CH$_2$) excitations plus the NLS artifact. The important feature in Fig. 3 is that the water heating process is clearly slower in the glycine solution. To best see this, compare the spectra at t = 1.5 and 3 ps.

To distinguish the spectra of heated thermalized water from nonequilibrium vibrational excitations, we analyzed the data using singular value decomposition (SVD).[13,15] SVD of the transient Stokes data set in the OH and CH stretch regions at 13 values of delay time (represented by a 13×411 matrix) yields two principal singular values for both pure H_2O and the glycine/H_2O solution. The largest component will be denoted 1 and the second-largest 2. Since SVD is a purely mathematical procedure with no physical constraint, SVD spectra do not necessarily have physical meaning as they are. In order to find the linear combinations of the SVD spectra that could be related to molecular processes, we made the assumption that the time dependences of the SVD spectra could be represented by an exponential rise $[1 - \exp(-t/\tau_{th})]$ for component 1 and exponential decay for component 2.

Figure 4 shows the reconstructed time dependences and spectra for pure H_2O and the glycine/H_2O solution. The spectra in Figs. 4(b) and 4(d) have the major component 1
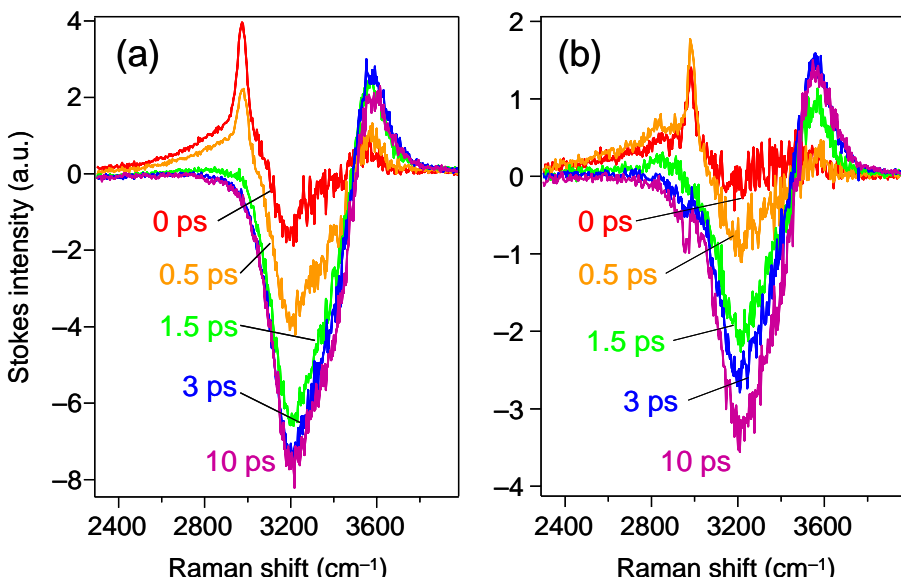
Figure 3. Transient Stokes spectra in the OH and CH stretch regions with 2980 cm^{-1} pumping of (a) pure H_2O and (b) the glycine/H_2O solution.

[11] L. K. Iwaki, D. D. Dlott, J. Phys. Chem. A **2000**, <u>104</u>, 9101.
[12] S. Shigeto, Y. Pang, Y. Fang, D. D. Dlott, J. Phys. Chem. A, submitted.
[13] T. Steinel, J. B. Asbury, J. R. Zheng, M. D. Fayer, J. Phys. Chem. A **2004**, <u>108</u>, 10957.
[14] H. J. Bakker, A. J. Lock, D. Madsen, Chem. Phys. Lett. **2004**, <u>384</u>, 236.
[15] M. Hashimoto, T. Yuzawa, C. Kato, K. Iwata, H. Hamaguchi, in "Handbook of Vibrational Spectroscopy," edited by J. M. Chalmers and P. R. Griffiths, John Wiley and Sons, Chichester, U. K. **2002**.

dominated by heated thermalized water. The minor component 2, which will not be discussed in detail, includes the NLS artifact and water $v(OH)$ excitation seen via $v = 1 \rightarrow 2$ transition. The time dependence of component 1 is our molecular thermometer.

When the pump pulses excite pure water only, the molecular thermometer indicates the build-up of heated thermalized water occurs within ~2.5 ps. The exponential time constant $\tau_{th} = 1.0 \ (\pm 0.2)$ ps. This is in agreement with previous studies from our laboratory,[7] and the 1.0 ps time constant represent a complicated process that includes water OH-stretch, OH-bend, and libron decay plus time needed for stabilization of the local hydrogen-bonding network.[7,16] In the glycine solution the molecular thermometer indicates that about 5 ps is needed for the solution to thermalize. The exponential build-up time constant $\tau_{th} = 1.8 \ (\pm 0.1)$ ps.

The 1.8 ps time constant represents a simplified single-step description of the three-step VC process of the solute glycine as discussed above. This 1.8 ps glycine thermalization process is remarkable for being so fast. It is quite a bit faster than the 10–100 ps that would be expected on the basis of studies of small molecules and ions in solution,[17] molecular liquids such as acetonitrile or methanol,[2] and only a factor of two slower than water, which thermalizes faster than any other known liquid system.[7,15,18] The ~1–2 ps time scale associated with VR is the same time scale associated with hydrogen-bond making and breaking in water. The glycine zwitterion is capable of forming on average 5.7 hydrogen bonds with surrounding water molecules.[19] So it is plausible that the fluctuating forces which induce VR of glycine might be associated with hydrogen-bond making and breaking.

4. Acknowledgements
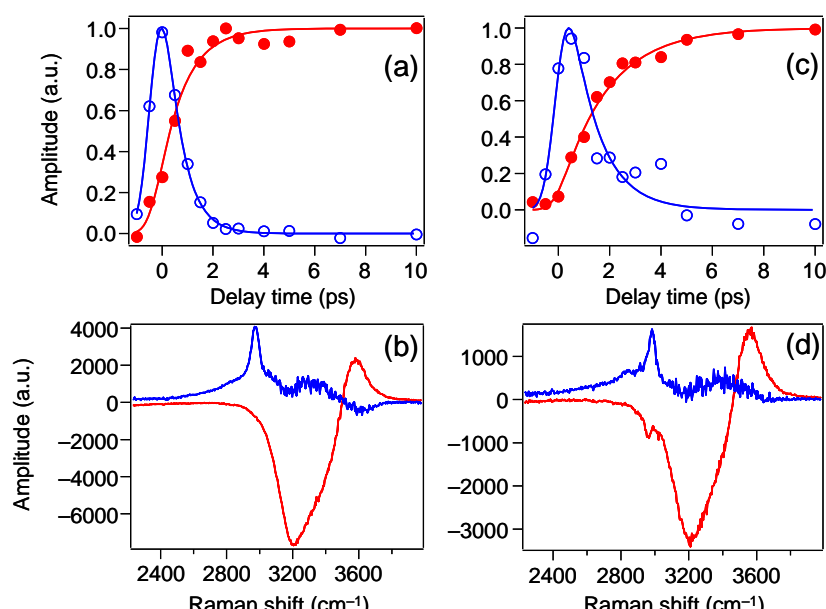
Figure 4. SVD results from transient Stokes data of (a), (b) pure H_2O and (c), (d) glycine/H_2O solution. (a), (c) Time dependences of components 1 (filled circles) and 2 (open circles). Solid curves are the results of a global fit. (b), (d) Intrinsic spectra of components 1 (red curve) and 2 (blue curve).

[16] J. Lindner, P. Vöhringer, M. S. Pshenichnikov, D. Cringus, D. A. Wiersma, M. Mostovoy, Chem. Phys. Lett. **2006**, 421, 329.
[17] J. C. Owrutsky, D. Raftery, R. M. Hochstrasser, Annu. Rev. Phys. Chem. **1994**, 45, 519.
[18] A. J. Lock, H. J. Bakker, J. Chem. Phys. **2002**, 117, 1708.
[19] M. G. Campo, J. Chem. Phys. **2006**, 125, 114511.

Carbonyl stretch vibrational dynamics of acetic acid
in water and alcohol studied by time-resolved IR spectroscopy

Motohiro Banno[1], Kaoru Ohta[2], Keisuke Tominaga[1,2,3]

[1] Molecular Photoscience Research Center and [2] Graduate School of Science and Technology, Kobe University,
[3] CREST/JST, Rokkodai-cho 1-1, Nada, Kobe 657-8501, Japan.

E-mail: mban@garnet.kobe-u.ac.jp

In nature, many important chemical reactions occur in aqueous solution. The mechanisms and dynamics of the chemical reactions are determined by the solute-solvent intermolecular interactions. Especially in protic solvents as water and alcohol, the solute-solvent intermolecular interactions are mainly dominated by hydrogen bonds. The elucidation of the intermolecular hydrogen bond dynamics is essential to understand the reaction mechanisms and dynamics in the protic solvents.

In this study, we observed the vibrational population dynamics of the carbonyl (C=O) stretch mode of acetic acid in D_2O and methanol by time-resolved IR pump-probe spectroscopy. The carboxylic acid group should play important roles in biological fields. The oxygen atom of the C=O group of acetic acid forms hydrogen bonds with solvent water molecules when the concentration is less than 1 mol dm^{-3}.[1] The vibrational dynamics of the C=O group should include the information on the solute-solvent intermolecular hydrogen bonds.

We measured the time-resolved IR difference spectra of CH_3COOD in D_2O after the vibrational excitation of the C=O stretching mode, as shown in Fig. 1. The bleaching of the ground state absorption and the transient absorption corresponding to the v=2←1 transition are observed at 1710 and 1660 cm^{-1}, respectively. The time dependences of the absorbance change at all the wavenumbers from 1630 to 1770 cm^{-1} are well reconstructed by a bi-exponential function,

$$A(v,t) = a(v)\exp\left(-\frac{t}{\tau_1}\right) + b(v)\exp\left(-\frac{t}{\tau_2}\right), \quad (1)$$

where A is the recorded absorbance change at wavenumber v and delay time t, τ_1 and τ_2 are the decaying time constants common to all the wavenumbers, and a and b are the spectral components decaying with the time constants τ_1 and τ_2. The determined time constants τ_1 and τ_2 are 0.45 ps and 0.98 fs, respectively. The spectral components a and b are also separated from the recorded time-resolved difference spectra, as shown in Fig. 2. As shown in Fig. 2, the spectrum a, decaying with the smaller time constant τ_1, 0.45 fs, locates at the wavenumbers lower than the spectrum b, decaying with the larger time constant τ_2, 0.98 fs.
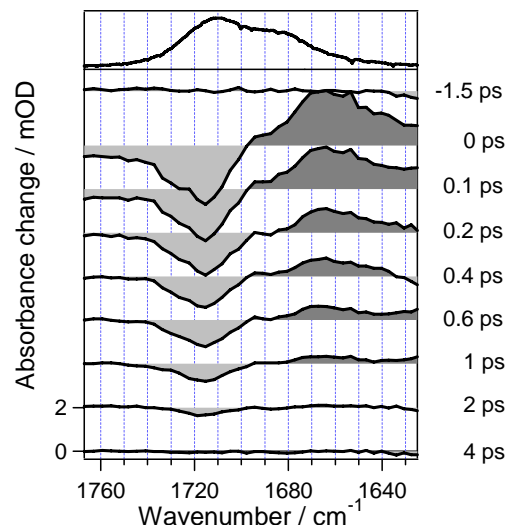

Fig.1. Time-resolved difference spectra after excitation of the C=O stretch vibration of CH_3COOD in D_2O. The top solid line is the ground state absorption spectrum.

---

[1] F. Genin, F. Quiles, A. Burneau, *Phys. Chem. Chem. Phys.*, **2001**, 3, 932-942.

We also observed the time-resolved IR difference spectra of CD_3COOD in D_2O, and of CH_3COOD and CD_3COOD in three kinds of methanol, CH_3OH, CH_3OD, and CD_3OD. For all the solutions we used, the recorded time-resolved difference spectra are well reconstructed by the bi-exponential function (1), as in the CH_3COOD/D_2O solution mentioned above. The determined time constants τ_1 and τ_2 are summarized in Table 1. The spectral components a and b are also separated. In all the solutions, the spectral component a, decaying with the time constant τ_1, locates at the wavenumbers lower than the spectral component b, decaying with the time constant τ_2.

In order to discuss origins of the two components a and b, it should be necessary to consider the solvation structure of acetic acid in D_2O and methanol. Because the oxygen atom of the C=O group has two electron lone pairs, the C=O group can forms hydrogen bonds with one solvent D_2O or methanol molecule (1:1 complex) or two solvent molecules (1:2 complex). The optimized structures of the complexes by DFT calculation (B3LYP method) with the 6-31G(d) basis set are shown in Fig. 3. By the two hydrogen bonds, the frequency of the C=O stretch vibration of the 1:2 complex will shift to the direction of lower wavenumber than that of the 1:1 complex. In addition, the number of low frequency vibrational modes of the 1:2 complex is larger than that of the 1:1 complex. By the large number of the low frequency vibrational modes, the vibrational density of states (DOS) of the 1:2 complex should be larger, resulting in faster vibrational energy relaxation of the C=O stretch mode. In the time-resolved experimental results, the spectral component a locating in the lower wavenumbers decays with the smaller time constant τ_1, while the component b locating in the higher wavenumbers decays with the larger time constant τ_2. From these results, it may be natural to attribute the components a and b to the 1:2 and the 1:1 complexes, respectively.


Fig. 2. Spectral components a (dotted line) and b (solid line) in the time-resolved spectra of CH_3COOD in D_2O. The top solid line is the ground-state absorption spectrum.
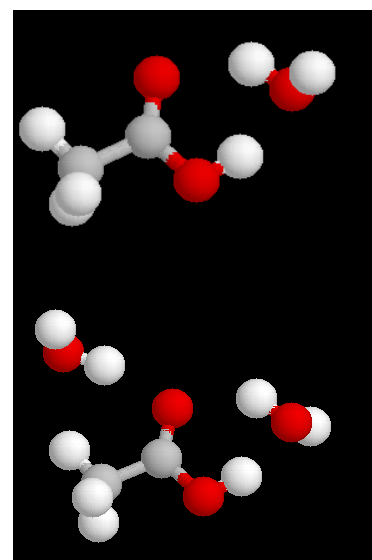
Fig. 3. Complex structures of acetic acid and one water molecules (1:1 complex, top) and of acetic acid and two water molecules (1:2 complex, bottom). White, gray, and red spheres are hydrogen, carbon, and oxygen atoms, respectively.

Table 1. Vibrational energy relaxation time τ_1 (upper) and τ_2 (lower) of acetic acids in D_2O and methanols. Unit: picoseconds.

	D_2O	CH_3OH	CH_3OD	CD_3OD
$CH_3COOH(D)$	0.45±0.20	0.52±0.11	0.98±0.16	0.85±0.08
	0.98±0.04	1.55±0.12	3.02±0.55	2.36±0.45
$CD_3COOH(D)$	0.39±0.19	0.62±0.23	0.90±0.26	0.90±0.24
	0.93±0.04	1.39±0.15	1.40±0.19	1.37±0.19

The time constants τ_1 and τ_2 show unexpected solute and solvent dependences. As shown in Table 1, when the solute or solvent is changed, the time constants τ_1 and τ_2 change their values in the ranges from 0.39 to 0.98 ps and from 0.93 to 3.0 ps, respectively. The vibrational energy relaxation rate is controlled by the DOS around the vibrational frequency of the excited mode and the coupling factors between the excited vibrational mode and the vibrational-energy-accepting modes. The time constants τ_1 and τ_2 should be determined by the vibrational DOS around 1700 cm^{-1}, corresponding to the vibrational frequency of the C=O stretch mode, and the coupling factors. In addition, the Fermi resonance may contribute to the vibrational energy relaxation rate. It has been reported that the C=O stretch vibration is possibly resonant with the second overtone of the stretch vibration of C-C single bond.[1] Actually, in the decomposed spectral components *a* and *b* of CD_3COOD in CH_3OD, split band features are observed, as shown in Fig. 4. This splitting should result from the Fermi resonance. Because the vibrational energy relaxation times should be controlled by these factors in a complicated way, at the present stage, it is impossible to discuss the solute and solvent dependences of the time constants τ_1 and τ_2 in detail.

Fig. 4. Spectral components *a* (dotted line) and *b* (solid line) in the time-resolved spectra of CD_3COOD in CH_3OD. The top solid line is the ground-state absorption spectrum.

In summary, we observed the vibrational dynamics of the C=O stretch mode of acetic acid in water and methanol. The vibrational energy relaxation process included two components, which were faster-decaying lower-wavenumber and slower-decaying higher-wavenumber ones. From the decaying rates and the band positions, the two components are possibly attributed to different solvation species of acetic acid, 1:1 and 1:2 complexes. By the observation of the vibrational energy relaxation, the two solvation species of acetic acid in protic solvents are separated.

Water as a molecular hinge in amide-like structures[1]

R. L. A. Timmer and H. J. Bakker**

* FOM-institute for Atomic and Molecular Physics, Kruislaan 407, 1098 SJ Amsterdam, The Netherlands.

Water plays an important role in a wide variety of chemical interactions. In protein folding, single embedded water molecules can form connections between oxygen atoms of different amide groups through double hydrogen bond formation[2]. In this way water holds together bio-molecular chains and assists in the formation of tertiary structures. Here we study the molecular motions and energy dynamics that single water molecules exhibit in interaction with such amide groups.

As a model system, we used a dilute solution of water dissolved in N,N-Dimethylacetamide (DMA). DMA possesses the same characteristic O=C–N group that is also present in amides while the N–H groups are substituted by amino-methyl groups (N–CH$_3$) to avoid spectral interference with the O–H groups of water in our measurements. From the linear spectra, we derived that each water molecule was embedded between DMA molecules through double hydrogen bond formation. Using polarization-resolved pump-probe spectroscopy, we examined the depolarization of three different directions of transition dipole moments of the OH stretch vibration of the water molecules (OH-stretching mode in HDO and symmetric and asymmetric stretching modes in H$_2$O). By combining these measurements we extract detailed information about the specific reorientation of this water around different axes.

We found that the system exhibits bimodal rotational dynamics with two distinct timescales: a slow (7±1 ps) reorientation of the entire DMA-water-DMA complex and a fast (0.5±0.2 ps) 'hinging' motion of the water molecule around the axis parallel to the connecting hydrogen bonds (i.e. parallel to the asymmetric mode of H$_2$O). We found that this hinging motion is not cylindrically symmetric but instead limited to a range of about a quarter circle (52±8°) around the equilibrium position. Additionally, we observed an exchange of energy between the two normal modes of H$_2$O at a timescale of 0.8±0.1 ps and found that the vibrational excitation decays almost exclusively through the symmetric stretch normal mode with a time constant of 0.8±0.2 ps.
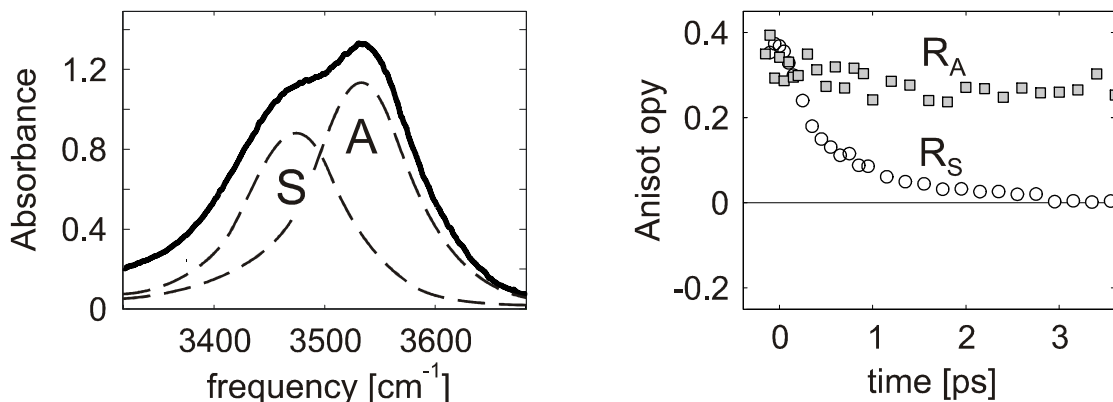
Figure 1: Left: linear absorption spectrum of H$_2$O in DMA showing the symmetric (S) and asymmetric (A) normal modes. Right: Anisotropy of water pumped and probed in the symmetric normal mode (R$_S$) shows a faster initial decay than water pumped and probed in the asymmetric normal mode (R$_A$)

[1] R.L.A. Timmer and H. J. Bakker, J. Chem. Phys. **126**, 154507 (2007)
[2] S.K. Pal, J. Peon, B. Baghi, and A.H. Zewail, J. Phys. Chem. B **106**, 12376 (2002)

Ultrafast dynamics of water in ionic micelles

A.M. Dokter, Sander Woutersen, H.J. Bakker

FOM-Institute for Atomic and Molecular Physics, Kruislaan 407, 1098 SJ, Amsterdam, The Netherlands. Email: a.dokter@amolf.nl

Water plays a crucial role as a solvent in many systems found throughout biology and chemistry. Often such systems do not contain water as a bulk liquid, but as a limited number of water molecules in a confined environment. In bulk water, H_2O molecules arrange in a dynamical hydrogen bond network, in which most molecules are tetrahedrally coordinated to four other water molecules. Nanoconfinement can have a strong effect on the strength, the structure, and the mobility of the network

Reverse micelles have proven to be excellent model systems for studying the properties of water in strong confinement. Such micelles consist of small aqueous droplets that are coated by a layer of surfactant molecules and are dispersed in an apolar solvent. The hydrophilic head groups of the surfactant molecules point toward the micelle interior, while their hydrophobic tails point outward to the exterior solvent (See Fig. 1). For a large variety of surfactants and solvents, the size of the micelles increases monotonically with the water content (conventionally denoted by the parameter w_0, defined as the molar ratio [water]/[surfactant]). This property makes it very easy to vary the degree of confinement of water inside the micelles.
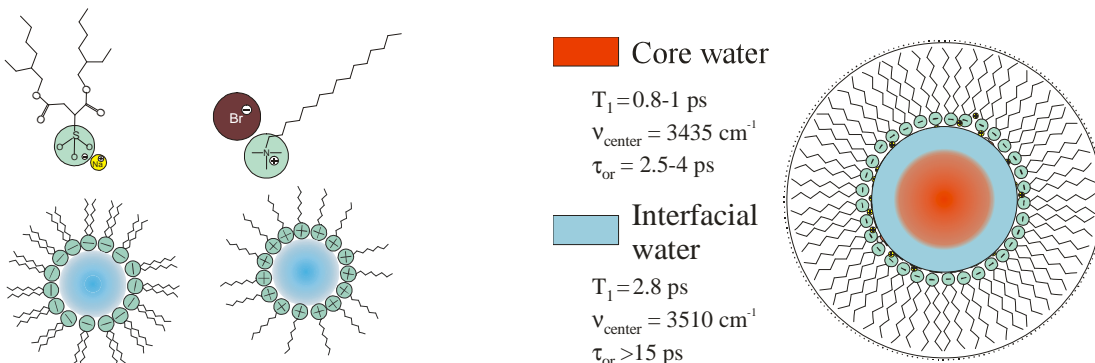

Fig. 1 *Left*: Schematic of water-in-oil AOT and CTAB reverse micelles The water pool is coated with a mono-layer surfactant molecules. **Fig. 1** *Right*: For anionic AOT micelles core and interfacial water could be distinguished by difference in vibrational relaxation rate T_1, absorption frequency ν_{center} and molecular reorientation rate τ_{or}.

We performed mid-infrared ultrafast pump-probe spectroscopy on the OH-stretch vibration of isotopically diluted HDO in D_2O in cationic (cetyltrimethylammonium bromide / CTAB) and anionic (sodium bis(2-ethylhexyl) sulfosuccinate / AOT) reverse micelles of various sizes. For anionic AOT micelles we found recently[1], that water molecules in the outer shell of the micelles are strongly immobilized by the confining interface, while molecules in the micelle core behave much like bulk water (See Fig. 1 *Right*). Because specific interface-water interactions are expected to be very important in explaining the different behaviour of interfacial water compared to bulk water, we studied how cationic instead of anionic surfactants affect water dynamics within reverse micelles[2].

Figure 2 shows the rotation-free signal recorded for four sizes of micelles at a single absorption frequency in the OH-stretch band. The vibrational relaxation contains a short- and a long-lived component, the short-lived component becoming more pronounced with increasing micelle size. We find that the slow decay can be assigned to water solvating the surfactant counter ions, while the fast decay is due to molecules outside these bromide solvation shells.
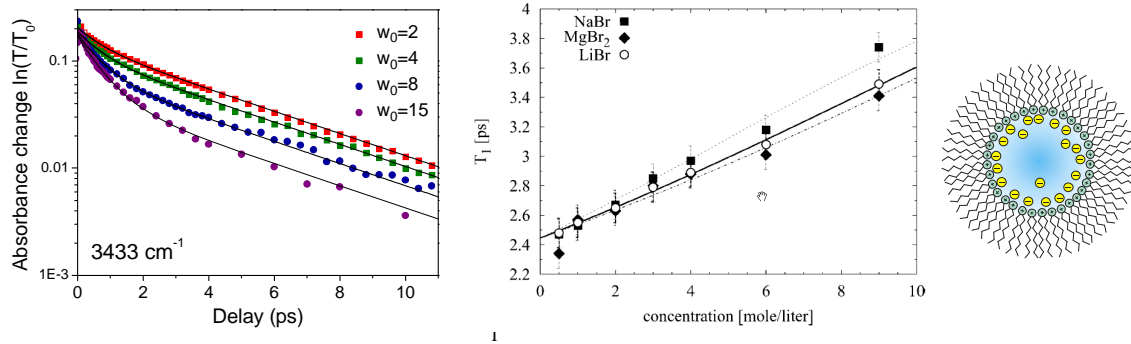

Fig. 2 *Left*: Pump induced absorbance change plotted as a function of probe delay at 3443 cm^{-1} at various micelle sizes. **Fig. 2 *Middle*:** Vibrational relaxation rates of Br$^-$ bound water for different bromide salts at different concentration. **Fig. 3 *Right*:** The Br$^-$ counter ions are found to be inhomogeneously distributed throughout the CTAB micelles, concentrating at the interfacial Stern layer.

For bulk ionic solutions it was found that the relaxation rate of anion-bound water increases with anion concentration[3]. Using these previous results as a reference, we can use the measured vibrational relaxation rates in the reverse micelles to determine the local concentration of bromide ions. The relaxation of anion-bound water in the micelles is remarkably slow (4.1 ps), which implies that a very high local concentration of Br$^-$ must be present. To compare, a nearly saturated solution of 10M NaBr in water gives rise to a vibrational relaxation rate of anion-bound water of only 3.6 ps. In reverse micelles even denser regions of bromide ions must occur, at molarities that cannot be reached in bulk solutions.

Interestingly, the vibrational relaxation of anion-bound water is anomalously slow for all studied sizes of micelles, as shown in Fig. 2 *Left*. For all micelles the T_1 times are >3.6 ps, showing that the local bromide concentration must be higher than 10M in each case. This is quite remarkable, as the average bromide concentration per micelle decreases from 18M to 3.5M when increasing the micelle size from w_0=2 to w_0 =15. The data thus show that the bromide ions are strongly inhomogeneously distributed over the micelles. The large value of T_1 found for all micelles indicates that a very high density of ions must be present in a restricted region at the micellar interface. We thereby show that most anions are located inside or directly adjacent to the interfacial (Stern) layer.

Figure 3 shows anisotropy decay curves for three sizes of cationic micelles. From 0 to 2 ps an initial fast decay is observed in the anisotropy curves. Within this time window, the short-lived signal of bulklike water molecules contributes to the anisotropy. The fast decay is on the order of 2.5 ps, similar to the orientational relaxation found for bulk water. The fast component in the anisotropy decay becomes more pronounced for larger micelles, where the bulklike water fraction is also larger. This suggests that bulklike water is at least partially responsible for the fast anisotropy decay. After ~2 ps only bromide solvation shell water contributes to the signal because of its much longer vibrational lifetime than bulklike water. We observe a monoexponential decay which is much faster for micelles with a high water

content than for micelles with a low water content. This shows that the mobility of the anion-bound water gets considerably lowered when the confinement is increased.
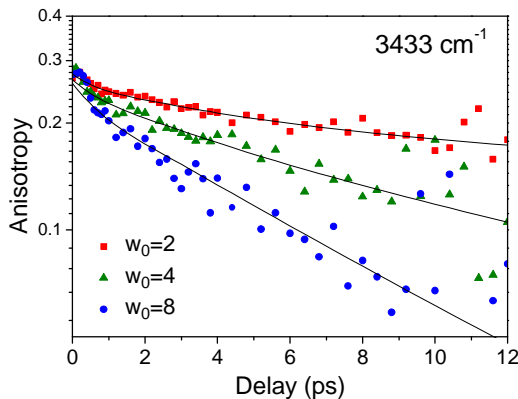

Fig. 3: Anisotropy decay of the OH-stretch vibration at 3433 cm−1 for three sizes of water in CTAB reverse micelles (w0=2, 4, and 8). The mobility of anionbound water increases when the micelle water content is increased.

In addition to the slow reorientation, we also observe a fast orientational component for the bromide bound water molecules, with a time constant that is similar to that of the reorientation of bulklike water[2,4]. Such fast reorientation of anion-bound water was not observed in AOT reverse micelles[1]. For CTAB and AOT, the hydrogen bonding of water to anionic groups is strikingly different, as illustrated in Fig. 4. The bromide ion is much larger than the oxygens of AOT sulfonate that accept hydrogen bonds from water. Because of the large polarizable electron cloud of the bromide ion, its hydrogen bonding will be much less directional than in the case of sulfonate. A less directional hydrogen bond will allow for a higher orientational mobility of water molecules in the bromide solvation shell, resulting in fast reorientational motion of these molecules over a limited solid angle.
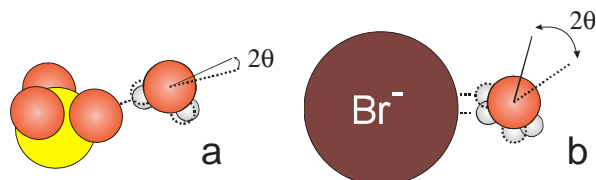
Fig. 4: Directionality of the hydrogen-bond between water and sulfonate (a, the anionic headgroup of AOT) and between water and bromide (b, the anionic counter ion of CTAB). Besides slow reorientation that involves breaking the hydrogen bond, a faster reorientational motion can occur at the reorientation rate of bulk like water. This reorientational motion occurs however over a larger angle θ for bromide bound water compared to sulfonate bound water.

1 A.M. Dokter, S. Woutersen, H.J. Bakker, Proc Natl Acad Sci USA, **2006**, 103, 15355
2 A.M. Dokter, S. Woutersen, H.J. Bakker, J. Chem. Phys., **2007**, 126, 124507
3 M. F. Kropman. H. J. Bakker, J. Am. Chem. Soc., **2004**, 126, 9135
4 I. R. Piletic, D. E. Moilanen, D. B. Spry, N. E. Levinger, M. Fayer, J. Phys. Chem. A , **2006**, 110, 4985

Immobilized water molecules in hydrophobic solvation

Y.L.A. Rezus[1] and H.J. Bakker[1]

[1] FOM-institute for Atomic and Molecular Physics, Kruislaan 407, 1098 SJ Amsterdam, The Netherlands.

Hydrophobic interactions play an important role in many biochemical processes. The folding of globular proteins, the self-assembly of lipid membranes and the binding of drugs to proteins are examples of processes driven by these interactions. In essence one can describe the hydrophobic effect as the tendency of apolar groups to associate in aqueous solution, thereby minimizing the total hydrophobic surface that is exposed to water.

The origin of hydrophobic interactions can be found in the way hydrophobic groups are solvated by water. In the 1940s it has been suggested by Frank and Evans[1] that a rigid, ice-like shell of water molecules is formed around hydrophobic groups, which, being entropically unfavorable, leads to the association of these groups in water. Experimental evidence for the existence of an ice-like solvation shell, however, is indirect (e.g. heat capacity measurements) because of the inherent difficulty in separating the response of bulk and solvation shell water molecules.

In this contribution we use mid-infrared pump-probe spectroscopy to directly probe the orientational dynamics of water molecules in the solvation shells of hydrophobic groups. In particular, we use HDO as a probe molecule, the orientational dynamics of which we determine by measuring the anisotropy of the pump-probe response of its OD-stretch vibration. To investigate the effect of hydrophobic groups on the orientational motion of water molecules, we add amphiphilic solutes to a dilute solution of HDO in H_2O. We have studied solutions of a number of amphiphilic molecules in water, each containing different numbers of hydrophobic groups. Figure 1 displays the structures of the molecules used in this study.

Figure 2a shows the anisotropy decays for solutions containing different concentrations of TMAO. At low TMAO concentrations we observe an anisotropy decay with a time-constant of 2.5 ps, which is typical for the reorientation of water molecules in the pure liquid. As the TMAO concentration is increased the anisotropy decay becomes biexponential, with a fast component and a slow component. The fast component is associated with the bulk water molecules in the solution. The slow component has a time-constant >10 ps. In order to investigate the origin of the slow component, we plot its amplitude as a function of the TMAO concentration (figure 2b). We observe that the amplitude of the slow component scales linearly with the TMAO concentration, which demonstrates that the slow component is associated with the water molecules in the solvation shells of the TMAO molecules. Since these water molecules reorient much slower than the bulk water molecules, we refer to them as immobilized water molecules. From the slope of the linear part of figure 2b we calculate that every TMAO molecule immobilizes approximately 12 water OH groups.
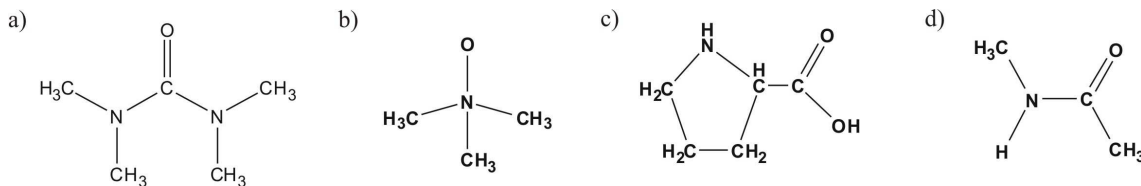

Figure 1: Molecular structure of the amphiphiles used in this study. a) tetramethylurea (TMU), b) trimethylamine N-oxide (TMAO), c) proline, d) N-methylacetamide (NMA)

[1] H. S. Frank and M. W. Evans, J. Chem. Phys. 13, 507 (1945)
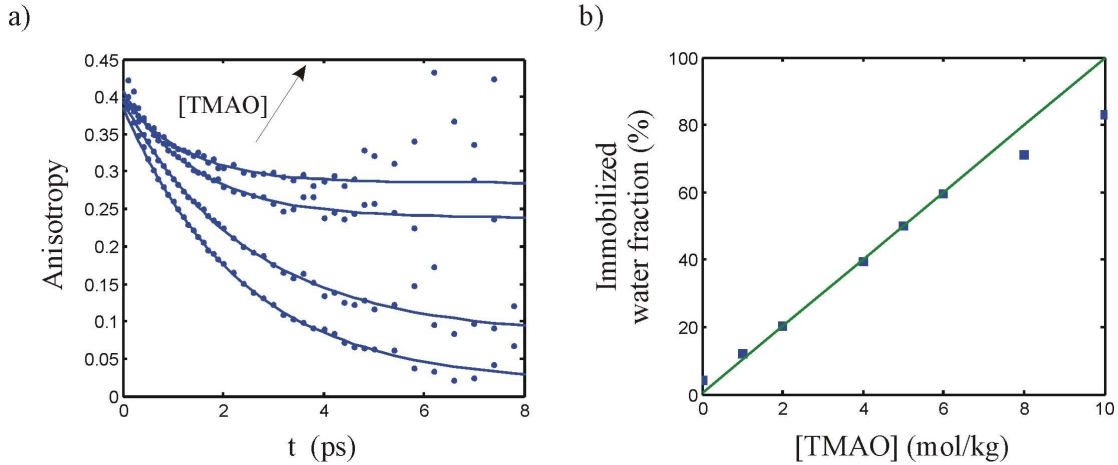
Figure 2: a) Anistropy decay of HDO molecules in aqueous trimethylamine-N-oxide (TMAO) solutions of varying concentrations. b) Fraction of immobilized water molecules as a function of the TMAO concentration.

As the TMAO molecule is amphiphilic we are faced with the question as to which part of the molecule is the cause of the immobilized water molecules: the hydrophilic NO group or the hydrophobic methyl groups? To investigate this issue we have varied the nature of the solute. We have determined the number of immobilized OH groups for each of the solutes in figure 1. Figure 3 shows this quantity as a function of the number of CH_3 groups in the solute molecule. The observed linear relation unambiguously proves that the immobilized water molecules are part of the hydration shell around the *hydrophobic* methyl groups of the solutes. Apparently the *hydrophilic* groups of the solutes do not lead to the immobilization of water molecules. The slope of the graph in figure 3 has a value of 3.9, indicating that every methyl group is responsible for the immobilization of approximately 4 water OH groups.
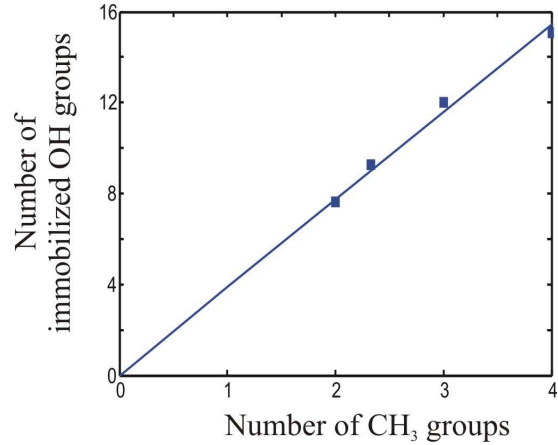

Figure 3 : Number of immobilized OH groups as a function of the number of methyl groups in the solute molecule.

We now consider the physical mechanism that underlies the immobilization of water molecules in the vicinity of hydrophobic groups. A number of molecular dynamics studies on liquid water have appeared in the past years. Sciortino et al. have shown that the relatively high orientational mobility of pure water is related to the presence of defects (i.e. five-coordinated water molecules) in the tetrahedral hydrogen-bond network of liquid water.[2] They have suggested that the slowing down of water dynamics around hydrophobic groups is the consequence of a steric effect, which prevents the creation of five-coordinated water molecules around these groups. Recently, Laage and Hynes proposed a detailed mechanism for water reorientation involving five-coordinated water molecules.[3] In this mechanism the pathway for reorientation involves a rotating water molecule that concertedly breaks a hydrogen bond with an overcoordinated first-shell neighbor and reforms one with an undercoordinated second-shell neighbor. In another molecular dynamics study by Sharp et al. the effect of hydrophobic solutes on the structure of water was investigated.[4] These researchers observed that hydrophobic solutes tend to preferentially displace water molecules that overcoordinate a second water molecule, providing a rationale for why hydrophobic solutes lower the amount of network defects. These studies together with our results form compelling evidence for the notion that the immobilization of water molecules around a hydrophobic solute arises from a steric effect, in which the hydrophobic group prevents a fifth water molecule from approaching a tetrahedrally coordinated water molecule, and as such prevents the molecule to reorient.

We conclude by returning to the iceberg model of Frank and Evans. Our results provide a molecular picture of these icebergs: they consist of four strongly immobilized water OH groups for every methyl group in solution. They are the consequence of a decrease in the configurational space available to water molecules around hydrophobic solutes. This notion also explains Frank and Evans' original observation of a decreased entropy upon the dissolution of hydrophobic compounds in water. The structure of the iceberg, however, is not the ordered structure observed in ice, but it rather resembles the disordered hydrogen-bond network of bulk water: the icebergs are ice-like from a dynamical perspective but water-like as far as structure is concerned. This provides an explanation for why hydrophobic icebergs were not previously observed using structural methods.

[2] F. Sciortino, A. Geiger, and H. E. Stanley, Nature 354, 218 (1991)
[3] D. Laage and J. T. Hynes, Science 311, 832 (2006)
[4] K. R. Gallagher and K. A. Sharp, J. Am. Chem. Soc. 125, 9853 (2003)

THEORY

Mixed Frequency/Time Domain Coherent Multidimensional Vibrational Spectroscopy and Coherence Transfer Spectroscopy

John Wright, Andrei Pakoulev, Mark Rickard, Kate Kornu, Nathan Mathew

[1]Department of Chemistry, 1101 University Avenue, University of Wisconsin, Madison, WI 53706 (USA). wright@chem.wisc.edu; http://www.chem.wisc.edu/~wright/menu.htm

Our program has been concerned with the development of coherent multidimensional electronic[1-4] and vibrational[5-14] spectroscopies that are based on mixed frequency/time domain measurements. The methods we have developed have been four wave mixing (FWM) spectroscopies but they need not be restricted to FWM. Three tunable excitation beams are focused into a sample at appropriate phase matching angles and FWM creates an output beam at a frequency $\omega_4 = \omega_1 - \omega_2 + \omega_3$. The excitation pulse width is matched to the sample's resonances so there is adequate spectral resolution. It is sufficiently short that there is also adequate temporal resolution of the quantum state dynamics. Multidimensional spectra are obtained by scanning the excitation lasers and monitoring the FWM intensity at the output frequency. The intensity is enhanced when the excitation frequencies match the sample's resonances. The dynamics of all the coherences and populations are measured by scanning the time delays between excitation beams over all possible time orderings of the three excitation pulses.

Our program has developed two multidimensional methods for vibrational spectroscopy-doubly vibrationally enhanced (DOVE) FWM and triply vibrationally enhanced (TRIVE) FWM. DOVE-FWM uses two infrared excitations to excite two vibrational quantum states and a Raman transition between the states to create the FWM output coherence. The cross-peaks between the vibrational modes must be coupled because at least one of the transitions must be a combination band. TRIVE-FWM uses three infrared excitations to excite the vibrational quantum states and the final FWM coherence creates the output signal. The cross-peaks between the vibrational modes require an anharmonicity because coherence pathways involving fundamentals and those involving combination bands would destructively interfere. The long term goal of our program is to develop a new family of coherent multidimensional spectroscopies that are based on measurements in the mixed frequency/time domain and can be used to gain selectivity in measurements of complex systems.

 Experiments based on making measurements in the mixed frequency/time domain offer several important advantages.

- Phase coherence between excitation pulses is required only during excitation period so excitation frequencies can be very different. This advantage removes the difficulties of achieving the long term phase coherence required for 2D time domain methods which scan the delay times to measure the actual temporal oscillations. It also removes the need to phase lock different excitation beams when their frequencies are different.
- FWM has many different coherence pathways through which to reach the final output coherence and these all interfere. By time ordering the excitation pulses and by detecting the output coherence with a monochromator, one selects the specific coherence pathways of interest.
- Scanning the time delays over all possible time orderings allows one to follow the dynamics of all the time ordered pathways and allows one to measure the population relaxation times and the coherence dephasing times.

- By isolating specific pathways and defining all of the coherences involved in the pathway, one can discriminate against other pathways that may be inherently more intense. This advantage allows one to isolate the effects of coherence transfer including those with intermediate populations and multiple quantum coherences

Figure 1 shows a TRIVE-FWM 2D spectrum for a mixture of a nickel dicarbonyl $(Ni(CO)_2)$ and tricarbonyl $(Ni(CO)_3)$ chelates. The TRIVE experiment uses two tunable lasers (ω_1 and ω_2) and a phase matching geometry of $\vec{k}_4 = \vec{k}_1 - \vec{k}_2 + \vec{k}_{2'}$. The spectrum was obtained by scanning ω_1 for successive values of ω_2 while monitoring the output intensity at $\omega_4 = \omega_1$. The time delays were set to provide the time ordering $\vec{k}_1, \vec{k}_2, \vec{k}_{2'}$. The symmetric and antisymmetric modes of $Ni(CO)_2$ have diagonal and cross-peaks at the position of the lower left box and the symmetric and two nearly degenerate antisymmetric modes of $Ni(CO)_3$ appear at the upper right boxes. If the time delays are changed, one finds a temporal splitting along the ω_2 axis in the $Ni(CO)_3$ cross-peak on the lower right. At zero delay, the peak is not split but after a 2.5 ps delay, the splitting is large. After a longer delay, it collapses. This behavior is the manifestation of quantum beating in the frequency domain. It is described more fully in a recent publication.

When the time ordering of the excitation pulses changes, new coherent pathways are created. Figure 2 shows the domains associated with the different time orderings and their relationship to conventional nonlinear experiments. The coherence pathways that correspond to these domains are described elsewhere. As the delays are changed, one passes through different coherence pathways and the changes in the intensities measure how the populations and coherences change in time. Figure 3 shows an example of these changes for a typical TRIVE experiment. By analyzing the temporal behavior, one directly measures the coherence dephasing and population relaxation rates.

This paper has summarized the capabilities of a new family of coherent multidimensional spectroscopies that are based in the mixed frequency/time domain. These new methods will be particularly appropriate for biological problems. Applications of these methods to biological problems has already been demonstrated.
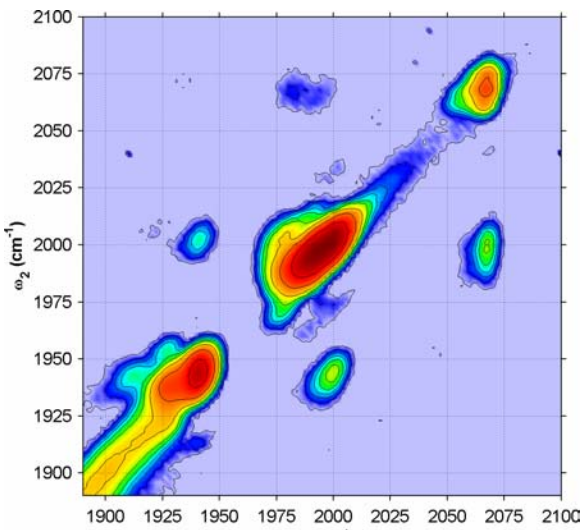

Figure 1- 2D TRIVE spectrum of a $Ni(CO)_2(PPh)_2$ and $Ni(CO)3(PPh)$ mixture.
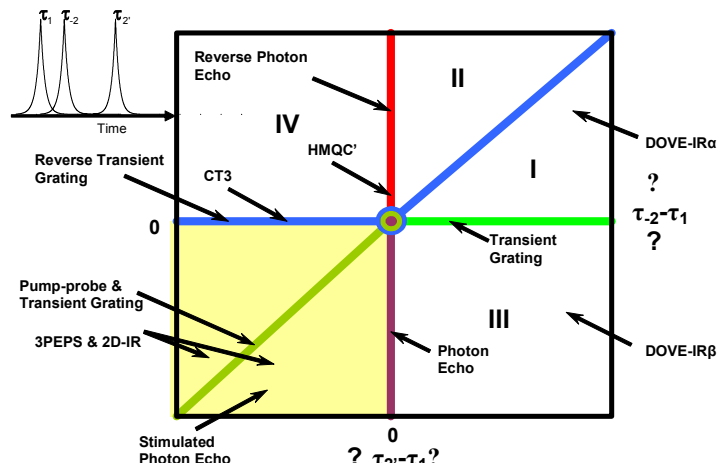

Figure 2- Diagram of the different time orderings that occur when the delays between the three excitation pulses are scanned
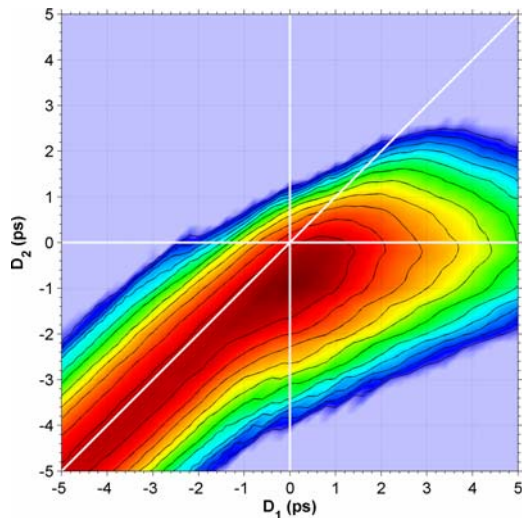
Figure 3- Example experimental 2D dependence of the TRIVE signal as a function of the delay times between each excitation pulse while the excitation pulses are tuned to the lowest cross-peak in Fig. 1.

(1)   Wright, J. C.; Carlson, R. J.; Hurst, G. B.; Steehler, J. K.; Riebe, M. T.; Price, B. B.; Nguyen, D. C.; Lee, S. H. *International Reviews of Physical Chemistry* **1991**, *10*, 349.

(2)   Carlson, R. J.; Wright, J. C. *Journal of Chemical Physics* **1990**, *92*, 5186.

(3)   Riebe, M. T.; Wright, J. C. *Chemical Physics Letters* **1987**, *138*, 565.

(4)   Steehler, J. K.; Wright, J. C. *Journal of Chemical Physics* **1985**, *83*, 3188.

(5)   Rickard, M. A.; Pakoulev, A. V.; Mathew, N. A.; Kornau, K. M.; Wright, J. C. *Journal of Physical Chemistry A* **2007**, *111*, ASAP (Web Release Date: 12.

(6)   Rickard, M. A.; Pakoulev, A. V.; Kornau, K.; Mathew, N. A.; Wright, J. C. *Journal of Physical Chemistry A* **2006**, *110*, 11384.

(7)   Pakoulev, A. V.; Rickard, M. A.; Meyers, K. A.; Kornu, K.; Mathew, N. A.; Thompson, D. C.; Wright, J. C. *Journal of Physical Chemistry A* **2006**, *110*, 3352.

(8)   Murdoch, K. M.; Condon, N. J.; Zhao, W.; Besemann, D. M.; Meyer, K. A.; Wright, J. C. *Chemical Physics Letters* **2001**, *335*, 349.

(9)   Zhao, W.; Wright, J. C. *Physical Review Letters* **2000**, *84*, 1411.

(10)   Zhao, W.; Wright, J. C. *Journal of the American Chemical Society* **1999**, *121*, 10994.

(11)   Zhao, W.; Wright, J. C. *Physical Review Letters* **1999**, *83*, 1950.

(12)   Chen, P. C.; Hamilton, J. P.; Zilian, A.; LaBuda, M. J.; Wright, J. C. *Applied Spectroscopy* **1998**, *52*, 380.

(13)   Wright, J. C.; Labuda, M. J.; Zilian, A.; Chen, P. C.; Hamilton, J. P. *Journal of Luminescence* **1997**, *72-74*, 799.

(14)   Labuda, M. J.; Wright, J. C. *Physical Review Letters* **1997**, *79*, 2446.

Relation between frequency and H bond length in heavy water

Stanislas Pommeret[1], Jean-Claude Leicknam[2] and Savo Bratos[2]

[1] * CEA/Saclay, DSM/DRECAM/SCM URA 331 CNRS, Laboratoire de Radiolyse, F-91191 Gif-sur-Yvette, France [2] Laboratoire de Physique Théorique de la Matière Condensée, Université Pierre et Marie Curie-Paris6, UMR 7600 (CNRS), Paris, France.

The published work on H bond dynamics mainly refers to diluted solutions HDO/D_2O rather than to normal water.[1] The reasons for this choice are both theoretical and experimental. Mechanical isolation of the OH vibrator eliminating the resonant energy transfer makes it a better probe of the local H bond network, while the dilution in heavy water reduces the infrared absorption, which permits the use of thicker experimental cells. The isotopic substitution does not alter crucially the nature of the problem. The water dynamics is still the subject of intense theoretical[2] and experimental[3] studies. The length r of an OH…O group is statistically distributed over a large interval comprised between *2.7* and *3.2 A* with a mean value $r_0 = 2.86$ *A*. Liquid water may thus be viewed as a mixture of hydrogen bonds of different length. Two important characteristics of hydrogen bonding must be mentioned. (i) The OH stretching vibrations are strongly affected by this interaction. The shorter the length r of the hydrogen bond, the strongest the H bond link and the lower is its frequency ω: the covalent OH bond energy is lent to the *OH..O* bond and reinforces the latter. A number of useful relationships between ω and r were published to express this correlation. The one adopted in our previous work is the relationship due to Mikenda[4]. (ii) Not only the OH vibrations, but also the HDO rotations are influenced noticeably by hydrogen bonding. This is due to steric forces that hinder the HDO rotations. As they are stronger in short than in long hydrogen bonds, rotations are slower in the first case than in the second. This effect was only recently discovered, but its existence is hardly to be contested.[5] In the present contribution, we want to revisit the relationship between the frequencyof the OH vibrator and the distance OH..O.

Water molecule has three normal modes $\omega_1, \omega_2, \omega_3$, and the OH stretching frequency of HDO corresponds to ω_3. The quantities examined in what follows are $<\Delta\omega_3(r,t)>$ and $<\Delta\omega_3(r,t) \Delta\omega_3(r,t')>$. In these functions, $\omega_3(r,t)$ indicates the value of the frequency ω_3 at time t given that the OH...O bond length was r at time 0. Moreover, $\Delta\omega_3(r,t) = \omega_3(r,t) - <\omega_3>$. In calculating statistical averages, intramolecular vibrations were treated by quantum mechanics and all remaining variables by classical mechanics. The potential employed was the pair-additive extended-simple-point-charge (SPCE) potential of Berendsen et al.[6] The classical calculations

[1] T. Elsaesser, H.J. Bakker, *Ultrafast Hydrogen Bonding Dynamics and Proton Transfer Processes in the Condensed Phase*, Kluwer, Dordrecht, 2002.

[2] M. Diraison, Y. Guissani, J-Cl. Leicknam, and S. Bratos, Femtosecond solvation dynamics of water: solvent response to vibrational excitation of the solute, *Chem. Phys. Lett.* **258**, 348-351 (1996). C. P. Lawrence and J. L. Skinner, Vibrational spectroscopy of HDO in liquid D2O. III. Spectral diffusion, and hydrogen bonding and rotational dynamics, *J. Chem.Phys.* **118**, 264-272 (2003). S. A. Corcelli, C. P. Lawrence, J. B. Asbury, T. Steinel, M. D. Fayer, and J. L. Skinner, Spectral diffusion in a fluctuating charge model of water, *J. Chem. Phys.* **121**, 8897-8900 (2004).

[3] J. Stenger, D. Madsen, P. Hamm, E. T. J. Nibbeling and T. Elsaesser, Ultrafast vibrational dephasing of liquid water, *Phys.Rev. Lett.* **87**, 027401 1-4 (2001). C. J. Fecko, J. D. Eaves, J. J. Loparo, A. Tokmakoff and P. L. Geissler, Ultrafast hydrogen bond dynamics in the infrared spectroscopy of water, *Science* **302**, 1698-1702 (2003). S.Yeremenko, M. S. Pshenichnikov and D. A. Wiersma, Hydrogen-bond dynamics in water explored by heterodyne-detected photon echo, *Chem.Phys.Lett.* **369**, 107-113 (2003).

[4] W. Mikenda, Stretching frequency versus bond distance correlation of O---D(H)**...**Y (Y = N, O, S, Se, Cl, Br, I) hydrogen bonds in solid hydrates, *J. Mol. Struct.*, **147**, 1-15 (1986).

[5] S. Woutersen, U. Emmerichs, H.J. Bakker, Femtosecond mid-IR pump-probe spectroscopy of liquid water: Evidence for a two-component structure, *Science* **278**, 658-660 (1997). G. Gallot, S. Bratos, S. Pommeret, N. Lascoux, J.-C. Leicknam, M. Kozinski, W. Amir, and G.M. Gale, Coupling Between Molecular Rotations and OH..O Motions in Liquid Water: Theory and Experiment, *J. Chem. Phys.*, **117**, 11301 (2002).

[6] H. J. C. Berendsen, J. R. Grigera and T. P. Straatsma, The missing term in effective pair potentials, *J. Phys. Chem.*, **91**, 6269-6271 (1987).

were performed as follows. The simulation box contained 255 D_2O molecules and one HDO molecule with periodic boundary conditions. The long-range electrostatic interactions were taken into account by calculating the Ewald sum. The equations of motion were integrated with the help of leap frog algorithm. The thermodynamic point considered here corresponds to T=300 K and ρ = 1.09 g/cm3. The statistical quantities were extracted from two independent runs of 5 ns after equilibration; the time step of the simulation was 0.5 fs. The configurations of the system were saved every 5 fs and the frequency of the OH vibrator computed. The O…O distance r_{OO} between the oxygen atom of the HOD molecule and that of a D_2O molecule can be defined in different ways. Some authors assimilated it to the O…O distance between the HDO and the closest D_2O. We preferred to attribute it to D_2O molecule for which the H…O distance is the smallest in the same pair of molecules. Then, using quantum mechanical perturbation theory, one obtained analytical expressions of $\omega_3(r,\tau)$ in terms of the derivatives of the intermolecular potential with respect the internal vibrations.[7]

Once the instantaneous frequency $\omega_3(t)$ and distance $r_{OO}(t)$ have been computed for a large number of steps of molecular dynamics, one can examine some properties of H bonds. As noted earlier[8], the variables ω_3 and r_{OO} are correlated. This correlation is strong enough to exhibit a well defined peak in the (ω_3 , r_{OO}) plane. It is then possible to compute the mean distance r_{OO} at a given frequency ω_3, and the mean frequency ω_3 at a given distance r_{OO}. These two functions are plotted in Figure 1A. It is clear that, even if they are different, the difference between them is small. Comparing them with the Mikenda relation4, one finds a good agreement. Note that the empirical relationship was established for solids.
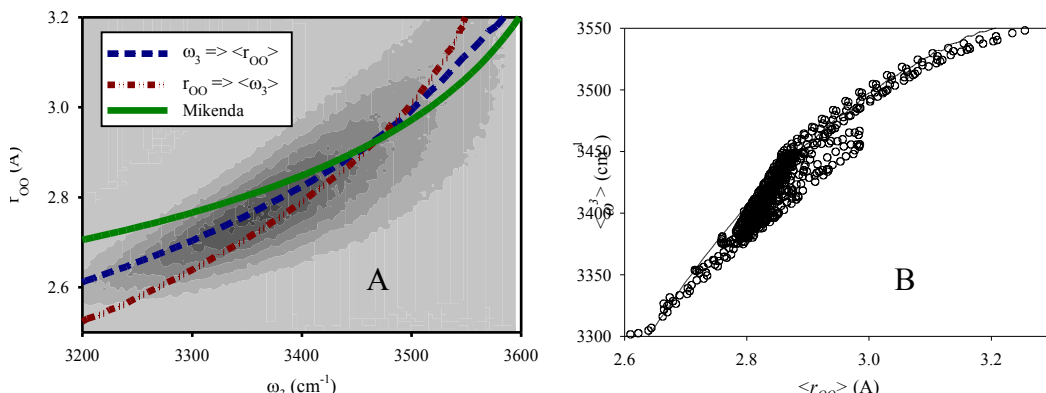

Figure 1: Relationship between the frequency ω_3 of the OH vibrator and the distance r_{OO}. (A) Solid line is the Mikenda relation4; the long dash curve gives the mean distance r_{OO} for a given frequency ω_3; and the dash dot dot curve gives the mean frequency ω_3 at a given distance r_{OO}. (B) Parametric plot of $<\omega_3(r,t)>$ as a function of $<r_{OO}(r,t)>$ for times varying between 0 and 3 ps, and r varying between 2.6 and 3.2 A. The solid line is $<\omega_3(r)>$.

Having established a relationship between the frequency and the distance in static conditions, we re-examined it from dynamical point of view. In order to do it, we have computed the mean distance and the mean frequency for different times t: we extracted from the MD runs the configurations for which the H bond distance was equal to r, and followed the mean frequency $<\omega_3(r,t)>$ and the mean distance $<r_{OO}(r,t)>$ in time. The parametric plot (Figure 1B) shows a strong correlation between these two quantities, whatever the initial value of r.

To go further in the comparison between frequency and distance as a function of time, we have developed a new theory that makes the link between the distance and the frequency, assuming that the initial wavepacket is selected by a femtosecond laser pulse. It is inspired by a recent theory of time resolved X-ray diffraction.[9] This theory requires the knowledge of two time dependent functions: $<\omega_3(r,t)>$ that we presented earlier and

[7] M. Diraison, J-Cl. Leicknam, G. Tarjus, and S. Bratos, Computer simulation study of inelastic neutron scattering from liquid water, Phys. Rev. E 50 2689-2695 (1994).
[8] R. Ray, K. B. Moller and J. T. Hynes, Hydrogen bond dynamics in water and ultrafast infrared spectroscopy, *J. Phys.Chem.A* **106**, 11993-11996 (2002)

$$<\Delta\omega_3(r,t)\ \Delta\omega_3(r,t')>_C = <\omega_3(r,t)\ \omega_3(r,t')> - <\omega_3(r,0)><\omega_3(r,0)> \qquad (2)$$

This function is much alike the standard frequency shift correlation function $<\Delta\omega_3(t)\ \Delta\omega_3,t')>$, but is not identical to it. The frequency shift correlation function is well fitted (Figure 2A) by two exponentials (40 and 625 fs). If t and t' are large with respect to 625 fs, the system has lost the memory of its initial condition and it is easy to show that $<\Delta\omega_3(r,t)\ \Delta\omega_3(r,t')>_C \rightarrow <\Delta\omega_3(t)\ \Delta\omega_3,t')>_C$. In Figure 2B, we illustrated the time dependence of $<\Delta\omega_3(r,t)\ \Delta\omega_3(r,t)>_C$ for $r = 2.86$ A. For long times, this function reaches the value of $<\Delta\omega_3(0)\ \Delta\omega_3(0)>_C = 11780$ cm^{-2}, but at short time its value is only 4000 cm^{-2}. This indicates that when pumping at a given frequency, one selects a narrow range of distances of the H bond network. The evolution of the function toward the asymptotic value is characterized, as in the frequency shift correlation function, by a fast and a slow component.
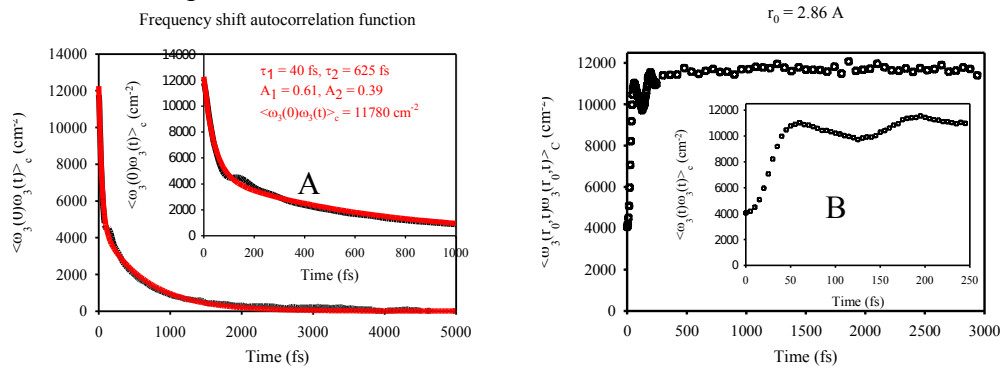

Figure 2: Frequency correlation functions: A) Frequency shift correlation function $<\Delta\omega_3(t)\ \Delta\omega_3(t')>$. B) Function $<\Delta\omega_3(r,t)\ \Delta\omega_3(r,t)>$.

The present study confirms the link between the frequency of an OH vibrator and the H bond network surrounding it. Even so the relation between the distance r_{OO} and ω_3 is statistical in nature; it is sufficiently narrow to affirm that the measurement of the mean frequency ω_3 at a given time is related to the distance r_{OO} at a given time as it was stated earlier.[10]

---

[9] S. Bratos, F. Mirloup, R. Vuilleumier and M. Wulff, Time resolved X-ray diffraction: statistical theory and its application to the photophysics of molecular iodide, *J. Chem. Phys*. **116,** 10615-10625 (2002).

[10] G.M. Gale, G. Gallot, F. Hache, N. Lascoux, S. Bratos, J.-Cl. Leicknam, Femtosecond dynamics of hydrogen bond in liquid water: a real time study, *Phys. Rev. Lett*. **82**, 1068-1071 (1999).

Ultrafast Internal Conversion Processes for Excited Solvated Electrons for Clusters and the Bulk

Sighart F. Fischer,P.O.J.Scherer,W. Dietz, and A.A.Zharikov

[1] Physik-Department T38 Technische Universität München 85748 Garching,Germany

An electron in a polar medium can induce its own potential via polarization of the medium by its charge. At equilibrium the gain in the electronic localization energy and the work performed by the medium to provide the electronic potential reach a minimum. Thus the equilibrium polarization can be expressed by the charge distribution, which can be determined in a self consistent manner by a nonlinear Schrödinger equation[1]

$$(1) \qquad -\frac{\hbar^2}{2m}\Delta\Psi(\vec{r})+U_{eq}(\vec{r})\Psi(\vec{r})=E^{(eq)}\Psi(\vec{r})$$

$$(2) \qquad U_{eq}(\vec{r})=-e^2\left(1/\varepsilon_\infty-1/\varepsilon_s\right)\int\frac{1}{|\vec{r}-\vec{r}\,'|}|\Psi(\vec{r}\,')|^2 d^3r\,'$$

The equilibrium ground state potential is shown in Fig.1a. The eigenvalues are denoted in analogy to the hydrogen atom as 1s, 2p, and 2s etc. It should be noted that the adiabatic ionization potential IP lies below the instant continuum of the equilibrium polarization by an amount equal to the polarization energy of the medium Π.

Excitation of the s-state to the p-state is followed by relaxation to the equilibrium configuration of the p-state in competition with internal conversion to the ground state. To describe this relaxation process we introduce the polarization strength X, which serves as reaction coordinate. The polarization potential $E_i(X)$ can be derived via a recently developed scaling method [1] to yield (Fig.1b)

$$(3) \qquad E_i(X)=\frac{X^2}{2}-\frac{3}{4}X^{4/3}X_{,i2/3}\,.$$

Here X_i refers to the minimum of the potential for the different electronic states i=s,p,... . This analytic expression does not incorporate short range effects. They do not contribute much in the case of a weakly bound electron in the relaxed p configuration.
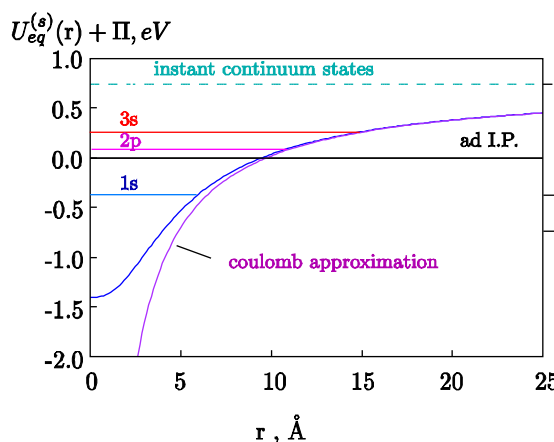

Fig. 1a Equilibrium electronic potential
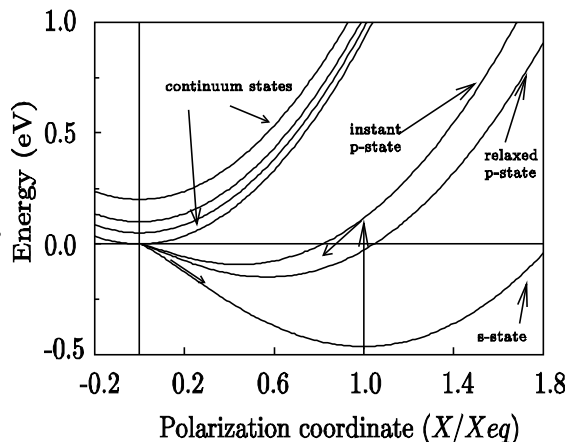
Fig. 1b Adiabatic polarization potentials

For an extended state the detailed structure of the first solvation shell is not important and a simplified continuum approximation can be applied to evaluate the nonadiabatic coupling

between the p-state and the s-state. Recently we have shown , that the nonadiabatic coupling induced by one normal mode k of a water molecule at distance R can be expressed in terms of the electronic and the vibronic transition dipoles μ^e and μ^v respectively as follows [2,3]

$$(4) \quad V^k_{p,0\to s,1}(\vec{R}) = \left[(\vec{\mu}^v_k \vec{\mu}^e - 3\mu^v_{kz}\mu^e_z)f\left(\frac{R}{a}\right) + \mu^v_{kz}\mu^e_z g\left(\frac{R}{a}\right)\right]\frac{1}{R^3} \qquad \text{with}$$

$$(5) \quad f\left(\frac{R}{a}\right) = erf\left(\frac{R}{a}\right) - \frac{R}{\sqrt{\pi}a}e^{-\left(\frac{R}{a}\right)^2} \qquad \text{and} \qquad g\left(\frac{R}{a}\right) = \frac{4R^3}{\sqrt{\pi}a^3}e^{-\left(\frac{R}{a}\right)^2}$$

Taking the angular average of the coupling squared and the sum over all modes as well as all molecules the following simple result evolves

$$(6) \quad \sum_k \langle \left(V^k_{p,0\to s,1}\right)^2\rangle_\infty = \sum_k \frac{4\sqrt{2\pi}\rho}{9}\frac{\mu^2_k\left(\mu^e\right)^2}{a^3}$$

The coupling mechanism can be interpreted as the nonadiabatic generalization of the Förster transition dipole coupling for energy transfer. The radius a corresponds to the radius of the donor molecule. Interestingly the long range character of the coupling can be tested against experiments[4] in which the lifetime of s-p excited anionic water clusters have been measured by photodetachment. Taking the cluster size dependence of the coupling as dominating factor for the size dependence of the lifetime we can evaluate the lifetime analytically for the following simplified coupling model for a cluster with a radius R.

$$(7) \quad \tilde{V}_{k^2}(R) = \frac{2}{3}\frac{\left(\mu^v_k\right)^2\left(\mu^e\right)^2}{\left(a^3\sqrt{2\pi}+R^3\right)^2}$$

Integrating the interaction squared up to R the following dependence of the cluster lifetime results

$$(8) \quad \tau(n) = \tau(\infty)\left(1+\frac{2}{3}(2\pi)^{3/2}\rho a^3\frac{1}{n}\right)$$

Here $\tau(\infty)$ stands for the lifetime of the bulk, ρ is the number density of water and n gives the number of molecules in the cluster. The predictions with regard to the n-dependence and the enhancement by a factor of about 1.4 due to deuteration are experimentally well documented[4].

The dynamics along the reaction coordinate X is dictated by the relaxation function $R(t)$ shown for water and methanol in Fig.2a. It can be seen, that within the first 50 fs the rapid solvation due to librational motion in water is completed. At this point the excitation energy $E_p(t)$ gets in resonance with the OH stretching modes causing the shoulders in the IR spectrum, which presents the first absorption feature of the solvating electron [5].

We can simulate the appearance of shoulders around the OH-stretching band by use of the damping model with V^2 given in Eq. (6) which amounts to $(400 \text{ cm}^{-1})^2$.

$$(9) \quad H = (E_p - i\Gamma_p)|p\rangle\langle p| + (E_L - i\Gamma_L)|L\rangle\langle L| + V(|p\rangle\langle L| + |L\rangle\langle p|)$$

The $s \to p$ excitation energy E_p becomes time dependent reflecting the dynamics of the solvation process. The energy E_L with the half-width Γ_L represents the OH-stretching band, which couples with the coupling constant V to the electronic transition $p \to s$. The time dependent line shape function $L(E, E_p(t))$ follows from the Green's function G_{pp}

$$(10) \quad L(E, E_p(t)) = -\frac{1}{\pi} \operatorname{Im}(G_{pp}) = -\frac{1}{\pi} \operatorname{Im}\left(E - E_p + i\Gamma_p - \frac{V^2}{E - E_L + i\Gamma_L} \right)^{-1},$$

which can be expressed as

$$(11) \quad L(E, E_p(t)) = \frac{1}{\pi} \frac{V^2 \Gamma_L + \Gamma_p (E - E_L)^2 + \Gamma_p \Gamma_L^2}{\left[(E - E_p)(E - E_L) - V^2 - \Gamma_p \Gamma_L \right]^2 + \left[\Gamma_p (E - E_L) + \Gamma_L (E - E_p) \right]^2}.$$

Representative examples for $E_p(t)$ are given in Fig 2b. It shows the splitting of the electronic line shape into two at resonance of $(E_p = E_L)$.
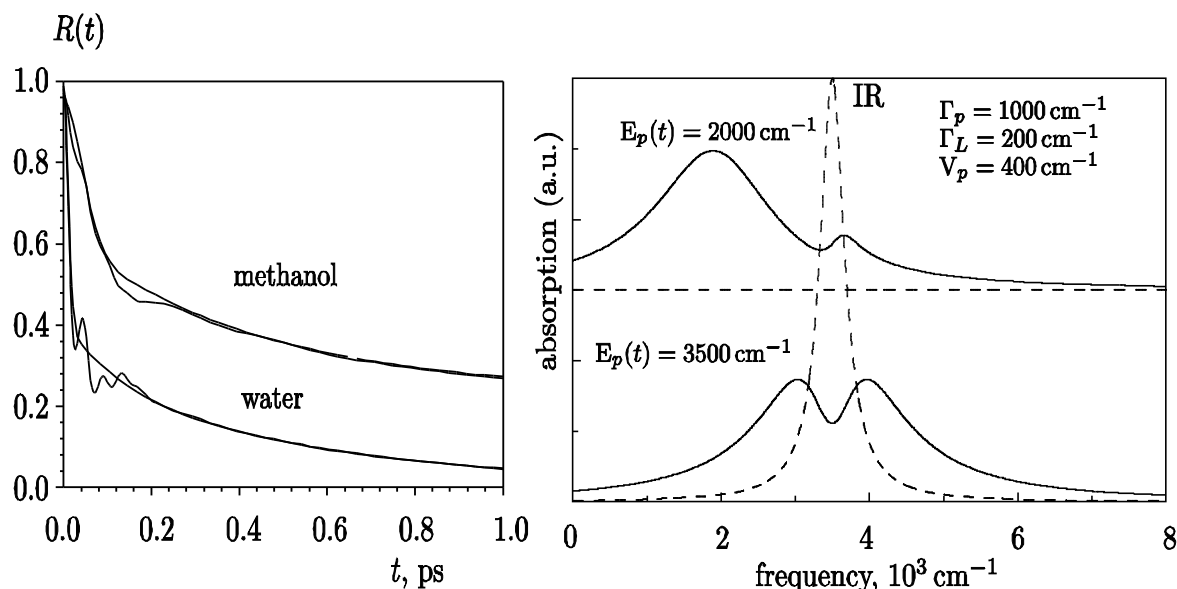

Fig. 2a Relaxation function R(t)   Fig. 2b Time-dependent line-shape functions .

[1] A.A. Zharikov and Sighart Fischer, J. Chem. Phys. **2006**, 124 , 54056

[2] Sighart F. Fischer and W. Dietz , Z. Phys. Chem. **2007**, 221, 585-595

[3] P.O.J. Scherer and Sighart F. Fischer, Chem.Phys.Lett. **2006** , 421, 427

[4] A.E. Bragg, J.R.R. Verlet, A. Kammrath, O. Cheshnovsky and D.M. Neumark, J.Am.Chem.Soc. **2005** 127,127

[5] R. Laenen, T. Roth and A. Laubereau, Phys. Rev. Lett. **2000** 85,50

Fifth-order nonlinear spectroscopy (3D-IR) to probe non-Gaussian stochastic processes

S. Garrett-Roe[1] *and P. Hamm*[1]

[1] Institute of Physical Chemistry, Univeristy of Zurich, Winterthurerstrasse 190, CH-8057 Zurich, Switzerland. s.garrett-roe@pci.unizh.ch, http://www.pci.unizh.ch/

Our understanding of the structural rearrangements of the hydrogen bond network of liquid water on the fastest time-scales – sub-ps – comes primarily from non-linear ultrafast infrared (IR) spectroscopies coupled with molecular dynamics (MD) simulations. The OH stretch of liquid water is sensitive to the local hydrogen bonding environment; as the environment fluctuates so does the OH frequency. The usefulness of the spectroscopy depends sensitively on how the structural coordinate projects onto the spectroscopic one. Here we use MD simulations to show that hydrogen bond rearrangements occur largely perpendicular to the OH stretch frequency-axis and that 3-point frequency joint probability densities are able to probe these dynamics more selectively than 2-point probability-densities, like those underlying recent 2D-IR experiments [1, 2, 3, 4].
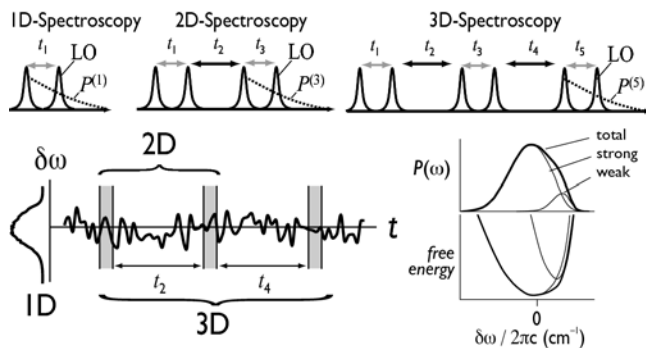

Figure 1: Characteristic frequency trajectory of the OH oscillator in liquid water

The time-series of the OH oscillators's frequencies generate the signals observed in all spectroscopies in a complex manner [5], but we will frame our discussion in the limit of inhomogeneous broadening where motional narrowing is minimal. Here we use molecular dynamics to simulate the frequency trajectories of an ensemble of water molecules using the Gromacs package [6] in the NVT ensemble, with 1019 molecules at 300 K and 1 atm using 2 fs time-steps. Long range electrostatic forces are treated with the PME approximation to the Ewald summation. The OH stretching frequencies are calculated in 2 steps. First, the total mass-weighted intermolcular force is projected on the OH bond axis [7]. Second, the forces are scaled to frequency following the proposal of Oxtoby [8] in which forces on an anharmonic bond change the bond-length and hence the $0 \rightarrow 1$ transition frequency. We use only the cubic anharmonicity which has been shown to be sufficiently accurate [9]. These calculations neglect the effects of resonant energy transfer, so are appropriate to describe the spectroscopy of isotopically substituted water HOD/D_2O. Finally, we use the Condon approximation, which is not strictly valid for water [10] but whose effect is secondary to the approximation of inhomogeneous dynamics.

If the dynamics of a system are Gaussian, then the 2-point correlation function completely describes the dynamics of the system. Higher order correlations are either 0 by symmetry (odd orders) or factorize into products of 2-point correlation functions. Water, however, is markedly non-Gaussian. The linear spectrum is asymmetric, which itself is sufficient to say the dynamics are non-Gaussian; but, moreover, the results of 2D-IR experiments [2, 11, 12]

and MD simulations [9] show that the dynamics of the OH stretch vary with the initial frequency of the oscillator.

The next higher order of correlation function is a 3-point correlation function,

$$c_3(t_2, t_4) = \langle \delta\omega(t_2 + t_4)\delta\omega(t_2)\delta\omega(0)\rangle \tag{1}$$

$$* = \iiint_{-\infty}^{\infty} \mathrm{d}(\delta\omega_1)\mathrm{d}(\delta\omega_3)\mathrm{d}(\delta\omega_5)$$

$$* \times \delta\omega_1 \delta\omega_3 \delta\omega_5 \, p(\delta\omega_5, t_2 + t_4 | \delta\omega_3, t_2 | \delta\omega_1, 0), \tag{2}$$

which correlates the initial frequency $\delta\omega(0)$ with the frequency at two later times $\delta\omega(t_2)$ and $\delta\omega(t_2+t_4)$. In principle, a fifth-order non-linear experiment like 3D-IR should be the lowest order spectroscopy which is sensitive to this correlation function [13].
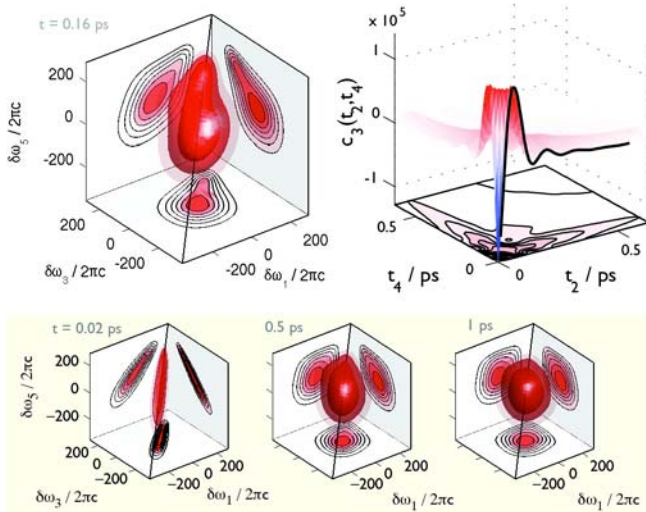

Figure 2: 3-point joint probability distributions of water as a function of $t=t_2+t_4$, and $t_2=t_4$.

The joint probability density is a 3D object (Fig. 2). When t_2 and t_4 are short compared to τ_c, then the distibution is stretched along the body-diagonal of the 3D ω-space (Fig. 2 bottom left); when $t \gg \tau_c$ then the probability density is nearly spherical (Fig. 2 bottom right); in between, the joint probability density shows complicated structure (Fig. 2 top left). Projections of this asymmetric distribution onto any of the cartesian planes, however, produce a symmetric object with no hint of the complex 3D structure. This is the equivalent of a projection slice theorem [13], reducing the 3D experiment to 2D, and the loss of information suggests that the 3D experiment may have novel spectroscopic content.

These 3D joint probability densities could be measured in a 3D-IR experiment, at least in principle. Very similar 3D-IR experiments have recently been demonstrated on model compounds [14]. Measurements on water would provide experimental constraints on the microscopic models proposed from MD simulations, but these experiments must contend with motional narrowing to the full extent. A comparison of the spectra predicted from these simulations calculated with standard response function formalism [5, 13] show that the overall shape of the joint probability density is severely distorted by the time required to

interrogate the system. How much of the shape can be extracted remains to be seen, but we note that the dynamics of hydrogen bond exchange happen on the blue side of the absorption line, where motional narrowing is less severe.

References

[1] Fecko, C. J., Loparo, J. J., Roberts, S. T., and Tokmakoff, A. "Local hydrogen bonding dynamics and collective reorganization in water: Ultrafast infrared spectroscopy of HOD/D2O" *J. Chem. Phys.* **122**, 054506 (2005).

[2] Loparo, J. J., Roberts, S. T., and Tokmakoff, A. "Multidimensional infrared spectroscopy of water. II. Hydrogen bond switching dynamics" *J. Chem. Phys.* **125**, 194522 (2006).

[3] Asbury, J. B., Steinel, T., Stromberg, C., Corcelli, S. A., Lawrence, C. P., Skinner, J. L., and Fayer, M. D. "Water dynamics: Vibrational echo correlation spectroscopy and comparison to molecular dynamics simulations" *J. Phys. Chem. A* **108**, 1107–1119 (2004).

[4] Cowan, M. L., Bruner, B. D., Huse, N., Dwyer, J. R., Chugh, B., Nibbering, E. T. J., Elsaesser, T., and Miller, R. J. D. "Ultrafast memory loss and energy redistribution in the hydrogen bond network of liquid H2O" *Nature* **434**, 199–202 (2005).

[5] Mukamel, S. *Principles of Nonlinear Optical Spectroscopy* Oxford University Press, New York (1995).

[6] Lindahl, E., Hess, B., and van der Speol, D. "GROMACS: A package for molecular simulation and trajectory analysis" *J. Mol. Mod.* **7**, 306–317 (2001).

[7] Eaves, J. D., Tokmakoff, A., and Geissler, P. L. "Electric field fluctuations drive vibrational dephasing in water" *J. Phys. Chem. A* **109**, 9424–9436 (2005).

[8] Oxtoby, D. W., Levesque, D., and Weis, J.-J. "A molecular dynamics simulation of dephasing in liquid nitrogen" *J. Chem. Phys.* **68**, 5528–5533 (1978).

[9] Møller, K. B., Rey, R., and Hynes, J. T. "Hydrogen bond dynamics in water and ultrafast infrared spectroscopy: A theoretical study" *J. Phys. Chem. A* **108**, 1275–1289 (2004).

[10] Schmidt, J. R., Corcelli, S. A., and Skinner, J. L. "Pronounced non-Condon effects in the ultrafast infrared spectroscopy of water" *J. Chem. Phys.* **123**, 044513 (2005).

[11] Steinel, T., Asbury, J. B., Corcelli, S. A., Lawrence, C. P., Skinner, J. L., and Fayer, M. D. "Water dynamics: Dependence on local structure probed with vibrational echo correlation spectroscopy" *Chem. Phys. Lett.* **386**, 295–300 (2004).

[12] Kraemer, D., Cowan, M. L., Paarmann, A., Huse, N., Nibbering, E. T. J., Elsaesser, T., and Miller, R. J. D. "Anomalous temperature dependence of the 2D IR spectrum of liquid water" *TRVS Conference Proceedings* (2007).

[13] Hamm, P. "Three-dimensional-ir spectroscopy: Beyond the two-point frequency fluctuation correlation function" *J. Chem. Phys.* **124**, 124506–124518 (2006).

[14] Ding, F. and Zanni, M. T. "Heterodyned 3D-IR spectroscopy" *Chem. Phys.* **accepted** (2007).

Vibrational Dephasing in Confined Myoglobin

A. Goj[1], R. F. Loring[1]

[1] Department of Chemistry and Chemical Biology, Cornell University, Baker Laboratory, Ithaca, NY 14853-1301 USA. RFL2@cornell.edu.
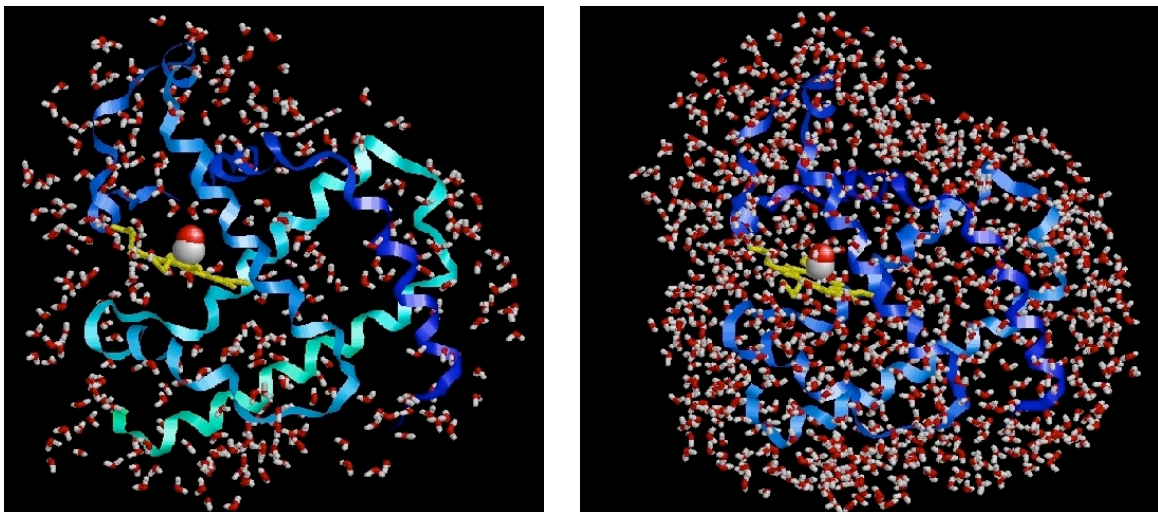
Figure 1 Structural snapshots from molecular dynamics simulations of myoglobin mutant H64V-CO solvated by one (left panel) or two (right panel) hydration layers. In each case, mobile water is surrounded by a static matrix of immobile water molecules, not shown.

The motions of a protein can be controlled by relaxation processes in the molecule's environment.[1] Since multidimensional infrared spectroscopy probes nuclear motions in the electronic ground state, comparing such measurements for a given protein in a variety of solvent environments allows the elucidation of this connection between solvent relaxation and protein dynamics. Fayer and coworkers have carried out frequency-resolved three-pulse vibrational echo studies of the dephasing of the stretching vibration of CO, bound to the active site in wild-type and mutant myoglobin in liquid and glassy solvent environments.[2-5] Vibrational echo measurements[4] of the myoglobin mutant H64V in a trehalose glass at room temperature have shown that CO dephasing is sensitive to the effects of molecular confinement on protein dynamics. In trehalose glass, myoglobin is believed to be surrounded by a thin layer of water, sequestered at the protein-solvent interface.[6] The protein thus interacts directly with water molecules whose motions are doubly constrained by interfaces with the protein and with the glassy matrix.

The infrared absorption spectrum of the CO vibration in wild-type MbCO shows three peaks, associated with spectroscopically distinct protein conformations.[2] These spectroscopic substates are connected to the configuration of the distal histidine, the most polar residue close to the active site. In the mutant protein H64V, the distal histidine is replaced by a nonpolar valine, with the spectroscopic effect that the infrared absorption spectrum of bound CO consists of a single peak. Since vibrational dephasing of CO in the wild-type protein is strongly influenced by motions of the distal histidine, H64V may be viewed as a model system in which CO dephasing reveals other dephasing mechanisms present in the wild-type species, arising from interactions of CO with the rest of the protein and with the solvent.

To investigate the effect on protein dynamics of confining the solvent, we have calculated vibrational echoes for H64V-CO surrounded by a layer of mobile water, which is encapsulated by a matrix of immobile water molecules, a simplified representation of a glass.[7]

We employed a model in which the CO coordinate is treated as a classical dynamical variable with a vibrational frequency containing a time-fluctuating component contributed by the time-varying classical force on this degree of freedom. This model[2-4] includes the effects of electrostatic forces from protein and solvent on the electric dipole moment of the CO. A single molecule of H64V-CO, constructed by attaching a CO ligand to the active site of the mutant sperm whale metmyoglobin with structure 2MGJ in the Protein Data Bank[8], together with a chloride ion for electroneutrality and TIP3P water molecules, was simulated at constant energy and volume with the MOIL force field.[9] Each simulation of confined H64V began with a configuration from a trajectory in an equilibrium simulation of H64V in water at T=300 K. Water molecules with oxygen atoms initially further than a distance R from all protein atoms were held immobile throughout the simulation, while water molecules nearer to the protein were free to move within this static potential. Simulations were performed for R =3 Å, which corresponds to one mobile hydration layer, and for $R = 5$ Å, representing two mobile hydration layers, as shown in Fig. 1.
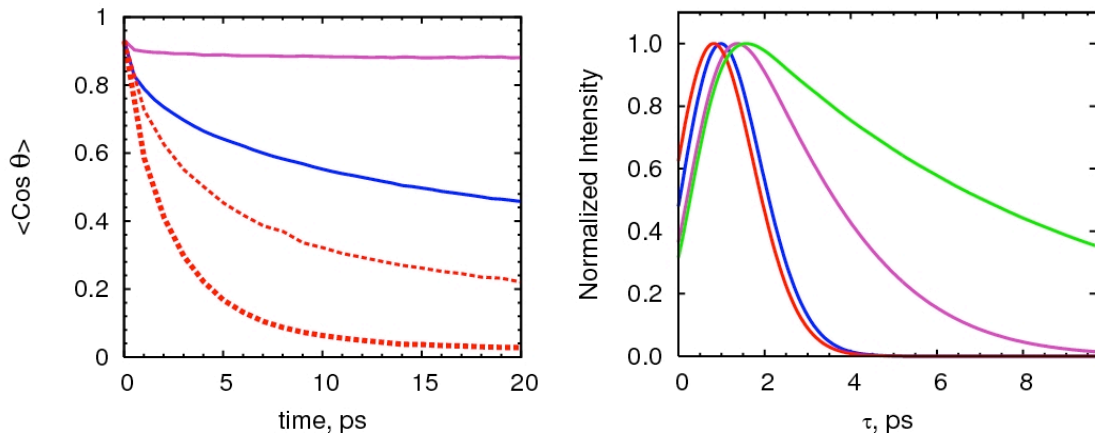

Figure 2 Left panel shows that orientational relaxation of water molecules in the vicinity of the protein varies with degree of confinement, as discussed below. Right panel shows two-pulse vibrational echo signals for H64V-CO under varying degrees of confinement, as discussed below.

On the experimental time scale, the most significant water dynamics are orientational, and the effects of confinement on these dynamics are shown in the left panel of Fig. 2, which plots the averaged scalar product of a water dipole at time t with its initial value. The uppermost pink curve for $R = 3$ Å shows that rotational relaxation is insignificant for a single mobile hydration layer, while the blue curve for $R = 5$ Å shows that orientational relaxation takes place on the experimental time scale for two mobile hydration layers. The thin and thick dashed red curves were computed from simulations[3] of H64V in liquid water for molecules in the first hydration layer and first two hydration layers, respectively. These molecules, whose motions are constrained by the interface with the protein, reorient significantly more rapidly than comparably located molecules whose dynamics are additionally constrained by a static matrix. The right panel of Fig. 2 shows calculated two-pulse vibrational echo signals, plotted versus the delay time between pulses, for completely immobile solvent (green curve), $R = 3$ Å (pink curve), $R = 5$ Å (blue curve), and liquid water (red curve). Surprisingly, the echo decays for $R = 5$ Å and for liquid water are nearly identical, despite the slower orientational dynamics of water molecules in the former case. While the orientational dynamics of water are constrained for the case of two mobile hydration layers, relative to that for liquid water solvating the protein, these motions are evidently sufficient to dephase the CO vibration on the same time scale as for the protein in

liquid solution. This dephasing is caused both by direct electrostatic interactions of water molecules with the CO and by protein dynamics that are facilitated by solvent relaxation.

Three-pulse vibrational echo signals are plotted in Fig. 3 as a function of the delay time between the first pair of excitation pulses τ. The delay time between second and third laser pulses T_w is increased from T_w=0.5 ps on the left, to T_w=8 ps on the right. The red curves show the measured echo signal of H64V in a room temperature trehalose glass[4], the dotted curves show calculated echo signals for H64V in a matrix of immobile water molecules,[4] and the solid curves show calculated echo signals for H64V solvated by one mobile hydration layer (R=3Å), surrounded in turn by a static water matrix.[7]
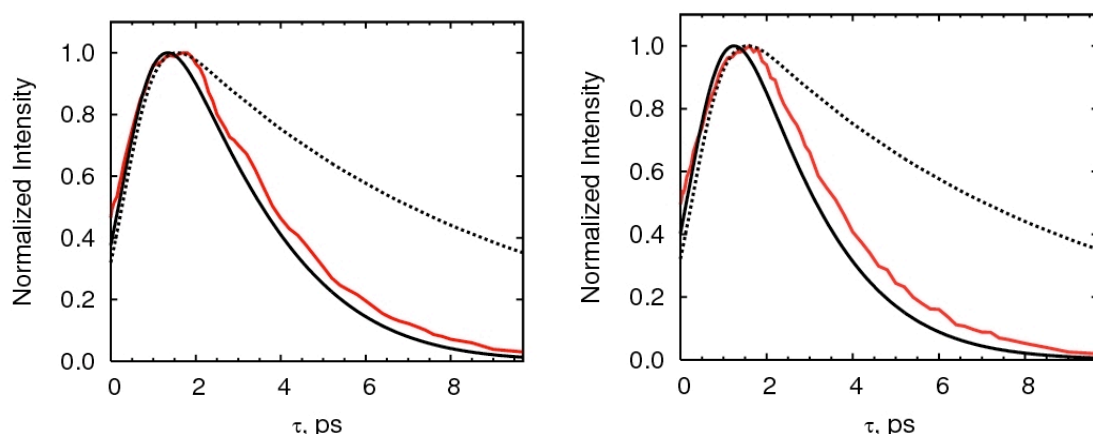

Figure 3 Measured (red) and calculated (black) curves show three-pulse vibrational echo signals for the myoglobin mutant H64V. Red curves show echoes for H64V in trehalose glass at room temperature, dotted curves are calculated for H64V in a matrix of static water molecules, and the solid black curves are calculated for H64V solvated by one mobile hydration layer, surrounded by a static water matrix. The waiting time T_w is increased from 0.5 ps in the left panel to 8 ps in the right panel.

The calculated[7] echo signal for a protein surrounded by a single mobile hydration layer agrees well with the measurement[4] in a trehalose glass, in which the protein is also believed to be surrounded by a mobile water layer,[6] encapsulated in a constraining matrix. These calculations confirm that vibrational echo studies of a ligand in the active site of a globular protein are sensitive to confinement of the protein surface, and demonstrate[2] that classical mechanical simulations using an empirical force field can reproduce the amplitudes and time scales of the protein dynamics that are measured in multidimensional infrared spectroscopy. We acknowledge support from the US National Science Foundation through Grant No. CHE0413992.

1   H. Frauenfelder, B. H. McMahon, P. W. Fenimore, Proc. Nat. Acad. Sci. US **2003**, 100, 8615-8617
2   K. A. Merchant, W. G. Noid, R. Akiyama, I. J. Finkelstein, A. Goun, R. F. Loring, M. D. Fayer, J. Am. Chem. Soc. **2003**, 125, 13804-13818
3   I. J. Finkelstein, A. Goj, B. L. McClain, A. M. Massari, K. A. Merchant, R. F. Loring, M. D. Fayer, J. Phys. Chem. B **2005**, 109, 16959-16966
4   A. M. Massari, I. J. Finkelstein, B. L. McClain, A. Goj, X. Wen, K. L. Bren, R. F. Loring, M. D. Fayer, J. Am. Chem. Soc. **2005**, 127, 14279-14289
5   A. M. Massari, I. J. Finkelstein, M. D. Fayer, J. Am. Chem. Soc. **2006**, 128, 3990-3996
6   G. Cottone, S. Giuffrida, C. Ciccotti, L. Cordone, Proteins: Struct., Funct., Bioinf. **2005**, 59, 291-302
7   A. Goj and R. F. Loring, Chem. Phys. **2007**, in press
8   M. L. Quillin, R. M. Arduini, G. N. Phillips, J. Mol. Biol. **1993**, 234, 140-155
9   R. Elber, A. Roitberg, C. Simmerling, R. Goldstein, H. Li, G. Verkhivker, C. Keasar, J. Zhang, A. Ulitsky, Comput. Phys. Commun. **1995**, 91, 159-189

Nonadiabatic Coupling Mechanism for Ultrafast Electron Transfer in Reaction Centers of Bacterial Photosynthesis

P.O.J. Scherer and S.F. Fischer

Department of Physics T38, Technische Universität München, 85748 Garching

We investigate ultrafast electron transfer as a transition between two adiabatic Born-Oppenheimer states which include the mixing of donor and acceptor orbitals

$$\varphi_i = (c\varphi_D + s\varphi_A) \rightarrow \varphi_f = (-s\varphi_D + c\varphi_A)$$

where the mixing ratio depends on the energy gap ΔE and the resonance integral J according to

$$cs = \frac{J}{\sqrt{\Delta E^2 + 4J^2}}$$

Within the harmonic parallel mode approximation the nonadiabatic matrix element for a transition involving the creation of one quantum of the promoting mode p reads

$$V_{nad,p} = \hbar^2 FCF \quad \frac{1}{2Q_{p,0}} \int \varphi_i(r;R) \bigtriangledown_{Q_p} \varphi_f(r;R) dr$$

where FCF denotes the Franck-Condon factor of the accepting modes ($\neq p$) and $Q_{p,0} = \sqrt{\hbar/2\omega_p}$ is the zero point amplitude of the promoting mode. With the help of the commutator relation

$$[\bigtriangledown_{Q_s}, H]_- = \Delta E \bigtriangledown_{Q_s} V_{pot}$$

we have

$$V_{nad,s} = \hbar^2 FCF \quad \frac{1}{2Q_{p,0}\Delta E} \int \varphi_i(r;R) \left(\bigtriangledown_{Q_p} V_{pot}\right) \varphi_f(r;R) dr$$

The transition occurs essentially at configurations where the energy gap of the electronic wavefunctions equals one quantum of the promoting mode. Therefore we apply the on shell approximation

$$\Delta E = \hbar\omega_p \quad cs = \frac{J}{\sqrt{(\hbar\omega_p)^2 + 4J^2}}$$

to have

$$V_{nad,s} = FCF \quad Q_{0,p} \int \varphi_i(r;R) \left(\bigtriangledown_{Q_p} V_{pot}\right) \varphi_f(r;R) dr$$

inserting the mixed orbitals and neglecting the cross terms we find

$$V_{nad,s} = FCF(\Delta E_{eq} - \hbar\omega_p) \quad \frac{J}{\sqrt{(\hbar\omega_p)^2 + 4J^2}} \times$$

$$\times Q_{0,p} \left(\int \varphi_A(r;R) \left(\bigtriangledown_{Q_p} V_{pot}\right) \varphi_A(r;R) dr - \int \varphi_D(r;R) \left(\bigtriangledown_{Q_p} V_{pot}\right) \varphi_D(r;R) dr \right)$$

We studied model systems of Bacteriochlorophyll and Bacteriopheophytine on the 6-31G/HF level. First normal modes were calculated for each of the molecules and then the partial reorganisation energies were evaluated to obtain the shift of the equilibrium position. Within the displaced harmonic oscillator model the Franck-Condon weighted

density of states was calculated as the Fourier transform of the time correlation function. Typically, we find a broad distribution of accepting modes up to $\approx 1500 cm^{-1}$, as is shown in figure 1.
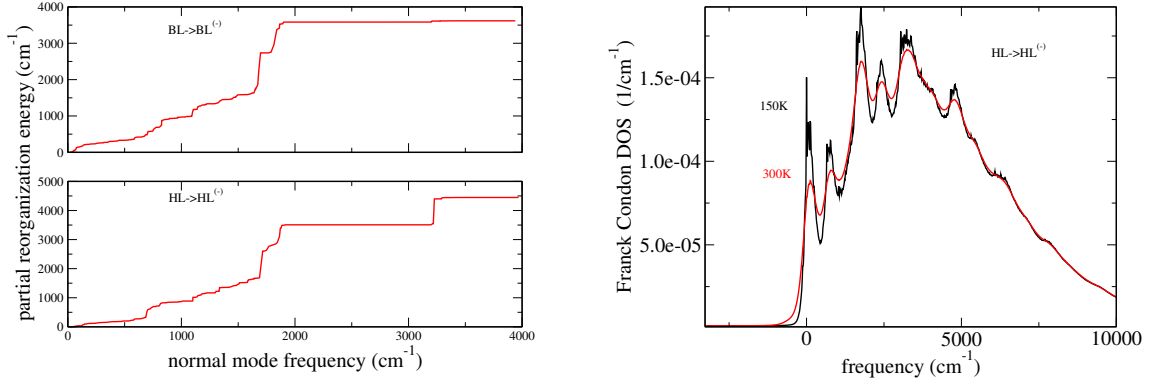

Figure 1: partial reorganization energies (cumulative plot) and Franck-Condon factor

To evaluate the nonadiabatic coupling matrix element we approximated the potential energy by Coulombic interactions with atomic partial (Mulliken type) charges

$$V_{pot}(r,R) = \sum_j \frac{-e\,q_j}{4\pi\varepsilon_0|r-R_j|}$$

end evaluated the integrals at the equilibrium configuration which involves two-and three-center integrals over the 6-31G basis functions. The square of

$$f_p = \left(Q_{0,p}\nabla_{Q_p}\right)\left(\int \varphi_A(r;R_{eq})\sum_j \frac{-e\,q_j}{4\pi\varepsilon_0|r-R_j|}\varphi_A(r;R_{eq})dr- \right.$$

$$\left. -\int \varphi_D(r;R_{eq})\sum_j \frac{-e\,q_j}{4\pi\varepsilon_0|r-R_j|}\varphi_D(r;R_{eq})dr\right)$$

is shown in figure 2 for the first $(P* \to P^+B^-)$ and second $(P^+B^- \to P^+H^-)$ electron transfer step.

For an estimate of the transfer rate we approximate the density weighted factor f^2

$$\int_0^{\hbar\omega} \rho(\hbar\omega_p)f^2(\hbar\omega_p) \approx v^2\hbar\omega \approx 0.01(eV)^2 \frac{\hbar\omega}{1000cm^{-1}}$$

by an average value corresponding to the dashed lines in fig.2. Then the integral over $(cs)^2$ can be performed. The Franck Condon weighted density of states is approximated by an average value of $10^{-4}/cm^{-1}$. For a resonance integral of $10cm^{-1}$ (values of this order have been reported from several authors) the estimated rate is

$$k_{nad} = \frac{2\pi}{\hbar}\frac{\pi}{4}Jv^2FCF \approx 1/ps$$

215
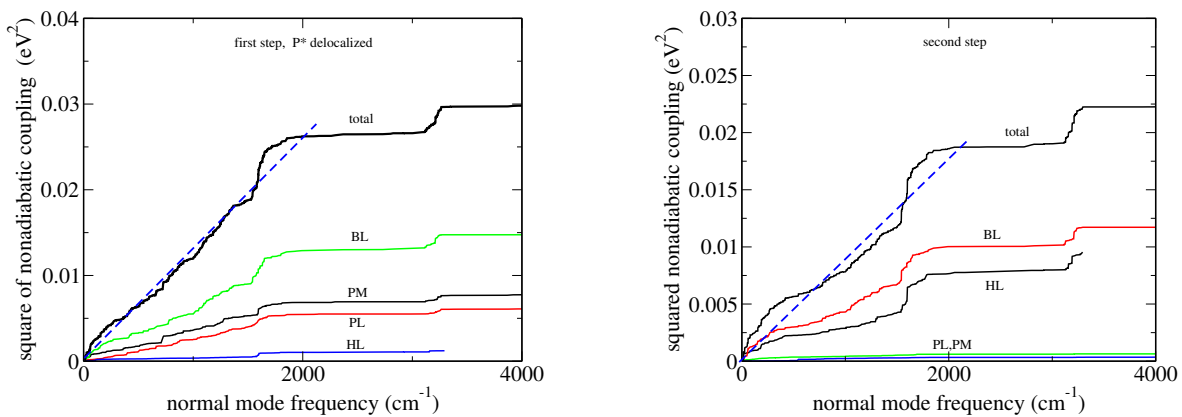
Figure 2: calculated nonadiabatic couplings

whereas the conventional expression for similar parameters gives

$$k_{conv} = \frac{2\pi J^2}{\hbar} FCF \approx 0.01/ps$$

It is well known in the literature that larger values around $J \approx 100cm^{-1}$ are necessary to explain the observed rates in the $1/ps$ regime, however such values are not really understandable on the basis of quantum calculations.

Finally we like to note that the nonadiabatic coupling mechanism can be visualized as a dipole-dipole type coupling between the infrared dipole of the promoting mode and the transition dipole of the electronic transition which is essentially given by cs times the change of the permanent dipole moment. A similar treatment was recently presented for ultrafast internal conversion processes during electron solvation[1].
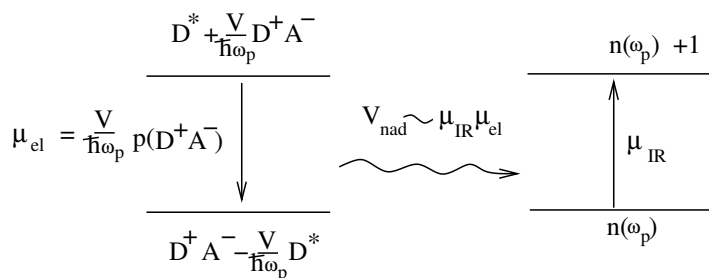

Figure 3: nonadiabatic dipole-dipole coupling mechanism

[1]P.O.J. Scherer and S.F. Fischer, Chem.Phys.Lett.**2006** 421 427